UNIVERSITAT POLITÈCNICA DE CATALUNYA BARCELONATECH

Tesis Doctoral

Departamento de Ingeniería Eléctrica

Caracterización de la electrificación de tormentas para su aplicación en procesos de sistemas de alerta: el caso de aerogeneradores y otras infraestructuras elevadas

Albert Salvador Yuste

Barcelona, julio de 2021

UNIVERSITAT POLITÈCNICA DE CATALUNYA

DEPARTAMENTO DE INGENIERÍA ELÉCTRICA

Tesis Doctoral

Caracterización de la electrificación de tormentas para su aplicación en procesos de sistemas de alerta: el caso de aerogeneradores y otras infraestructuras elevadas

Tesis por compendio de artículos para optar

al grado de Doctor en Ingeniería Eléctrica

Memoria presentada por:

Albert Salvador Yuste

Directores:

Nicolau Pineda Rüegg

Joan Montanyà Puig

Barcelona, julio de 2021

Resumen

En una sociedad cada vez más tecnológica, con una gran dependencia en los sistemas eléctricos, electrónicos y de telecomunicaciones, la vulnerabilidad a los efectos del rayo también va en aumento. La implementación de sistemas de seguimiento y vigilancia en tiempo real de la actividad de rayos atmosféricos puede mejorar enormemente las actuaciones a llevar a cabo durante episodios de tormenta, como puede ser un aislamiento de dispositivos de la red eléctrica, así como la detección de qué puntos han sido afectados y requerirían una intervención. Desde este punto de vista, la industria eléctrica tiene una especial exposición a este tipo de daños, con un especial enfoque hacia los aerogeneradores.

La detección temprana de actividad eléctrica en las tormentas es crucial para la emisión de avisos. Además, cuando la información de sistemas de detección de rayos se combina con otros como el radar meteorológico, imágenes de satélite, radiosondeo, etc., su detección y anticipación crece notoriamente. Por este motivo, esta tesis de investigación aporta conocimiento analizando la información de la morfología de las nubes de tormenta y las intensidades de precipitación con el radar meteorológico, así como las detecciones de las señales eléctricas con los sistemas de localización de rayos. Esto permite detectar cuáles son las condiciones meteorológicas y características más comunes en las nubes de tormenta que permiten su anticipación, la detección del primer rayo y poder generar avisos.

En primer lugar, se realiza una breve introducción para enmarcar la situación y objetivos de esta tesis. Seguidamente se presenta el estado del arte sobre los aspectos necesarios para poder hacer un seguimiento del trabajo realizado. La segunda parte comprende los artículos que integran esta tesis por compendio. En ellos se exponen las principales líneas de investigación que se han seguido a lo largo del desarrollo de la tesis y a qué conclusiones se han llegado.

En el primero de los artículos se establecen unos indicadores meteorológicos para la detección de actividad eléctrica en las tormentas. Con los datos del radiosondeo de Barcelona, se realiza una climatología de las isotermas de $-10°C$ y $-40°C$ (rango de temperaturas donde se estima que existe la región de fase mixta y que separa las distintas regiones de carga dentro de una nube de tormenta) para evaluar su variación estacional. El radar meteorológico, que proporciona la localización e intensidad de precipitación de las nubes de tormenta, traduce la intensidad de precipitación como reflectividad (expresado en dBZ). Los productos TOP-12 y TOP-35 (altura máxima que alcanza el nivel de reflectividad de 12 y 35 dBZ) se postulan como indicadores de presencia de electricidad atmosférica cuando alcanzan las alturas de las isotermas de $-40°C$ y $-10°C$, respectivamente. Finalmente, se evalúa la climatología de la altura de la isoterma de $-10°C$ durante el invierno, destacando la posible implicación con afectaciones a infraestructuras elevadas.

El siguiente artículo analiza qué relaciones se observan entre las posibles estructuras eléctricas de una tormenta con la actividad eléctrica que se deriva de cada una de ellas. Así, con la implementación del *Lightning Mapping Array* en la zona del Delta del Ebro, se establece la estructura eléctrica de la tormenta a partir de la determinación de los inicios de cada rayo. Los rayos se originan generalmente en la interfase de distintas regiones de carga opuesta dentro de la nube de tormenta, y su detección permite determinar las alturas de estas regiones. Las estructuras eléctricas mayoritariamente encontradas han sido la clásica tripolar (con una región de carga negativa central, con dos regiones de carga positivas encima y debajo de esta), una estructura con dipolo superior en que la región de carga positiva inferior no existe o es muy débil, y finalmente una estructura de dipolo inferior, con región positiva inferior dominante. Esta última es la que presenta la menor ratio de descargas nube-tierra, y la clásica estructura tripolar resulta la más favorecedora.

En el último artículo del compendio se evalúan las condiciones meteorológicas en situaciones de descargas en aerogeneradores. Siendo un campo cada vez más emergente, y con planes de incremento de los parques eólicos en Catalunya, este último artículo tiene una voluntad más práctica y aplicada, de especial interés para la industria eólica. Se detecta que la frecuencia de estas afectaciones no va directamente relacionada con la distribución anual de los rayos nube-tierra, mucho más frecuentes en periodos cálidos. El análisis concluye que todas las descargas con afectaciones a aerogeneradores suceden en periodos más fríos, mayormente de noviembre a abril. Se establece la estructura tripolar clásica como la más frecuentemente detectada en estos episodios, con la particularidad de una región de carga positiva inferior cercana a la superficie.

Seguidamente, se presentan unas conclusiones generales del trabajo realizado durante la tesis y unas perspectivas de trabajo futuro. Como último punto, se presentan todos aquellos artículos y presentaciones en congresos que se han derivado del desarrollo de este periodo doctoral. Se concluye la tesis con la presentación de otros trabajos realizados durante la duración de esta tesis doctoral. Finalmente, agradecer y remarcar el Programa de Doctorat Industrial (PDI - Project DI 59/2015) dentro del cual esta tesis ha sido enmarcada, destacando así el enfoque aplicado de esta.

Abstract

In an increasingly technological society, with a great dependence on electrical, electronic and telecommunications systems, vulnerability to the effects of lightning is also increasing. The implementation of monitoring and surveillance systems in real time of lightning activity can greatly improve the actions to be carried out during storm episodes, such as isolation of devices from the electrical network, as well as the detection of affected points that would require intervention. From this point of view, the electric power industry has a special exposure to this type of damage with a special focus on wind turbines.

Early detection of lightning activity in storms is crucial for the issuance of warnings. In addition, when the information from lightning detection systems is combined with others such as meteorological radar, satellite images, radiosonde, etc., its detection and anticipation grow notoriously. For this reason, this research thesis provides knowledge by analysing information on the morphology of storm clouds and precipitation intensities with meteorological radar, as well as the detections of electrical sources with lightning location systems. This makes it possible to detect the most common meteorological conditions and characteristics in storm clouds that allow their anticipation, the detection of the first lightning strike, and the ability to generate warnings.

First, a brief introduction summarises this thesis scope and objectives. Next, it is presented the state of the art on the aspects necessary to be able to monitor the work carried out. The second part includes the articles that make up this thesis by compendium. In them, it is exposed the main lines of research that have been followed throughout the development of the thesis and what conclusions have been reached.

The first article proposes some meteorological indicators for the detection of lightning activity in storms. With the data from the Barcelona radiosonde, a climatology of the isotherms of -10°C and -40°C (temperature range where it is estimated that the mixed phase region exists and that separates the different charge regions within a storm cloud) to evaluate its seasonal variation. The meteorological radar, which provides the location and intensity of precipitation of storm clouds, translates the intensity of precipitation as reflectivity (expressed in dBZ). The TOP-12 and TOP-35 products (maximum height reached by reflectivity levels of 12 and 35 dBZ) are postulated as indicators of the presence of lightning activity when they reach the isotherm heights of -40°C and -10°C, respectively. Finally, the climatology of the height of the -10°C isotherm during the winter is evaluated, highlighting the possible implication with affectations on elevated infrastructures.

The second article analyses what relationships are observed between the possible electrical structures of a storm with the lightning activity derived from each of them. Thus, with the implementation of the Lightning Mapping Array in the Ebro Delta area, the electrical structure of the storm is established by determining the initiations of each flash.

Flashes generally originate at the interface of different regions of opposite charge within the storm cloud, and their detection allows to determine the heights of these regions. The most common electrical structures found are the classic tripolar (with a central negative charge region, with two positive charge regions above and below it), a structure with an upper dipole in which the lower positive charge region does not exist or it is very weak, and finally a lower dipole structure, with a dominant lower positive region. The latter shows the lowest cloud-to-ground discharge ratio, and the classic tripolar structure is the most favorable.

The last article of the compendium evaluates the meteorological conditions in situations of discharges in wind turbines. Being an increasingly emerging field, and with plans to increase wind farms in Catalonia, this last article has a more practical and applied focus, which is of special interest for the wind industry. It is detected that the frequency of these effects is not directly related to the annual distribution of cloud-to-ground activity, which are much more frequent in warm periods. The analysis concludes that all discharges affecting wind turbines occur in colder periods, mostly from November to April. The classic tripolar structure is established as the most frequently detected in these episodes, with the particularity of a lower positive charge region close to the surface.

Next, it is presented some general conclusions of the work carried out during the thesis and some prospects for future work, followed by all articles and conference presentations that have been derived from the development of this doctoral period. The thesis is concluded with the presentation of other related works developed during the extent of this doctoral studies. Finally, acknowledges the Industrial Doctorate Program (PDI - Project DI 59/2015) and its applied approach for supporting this thesis work.

Agraïments

Abans de res voldria agrair als meus directors de tesi, en Joan Montanyà i en Nicolau Pineda, per haver-me ofert la oportunitat de formar part d'aquest projecte de doctorat industrial. Alhora, donar les gràcies per l'acompanyament durant tota aquesta etapa, tot el coneixement que he pogut aprendre d'ells, així com la confiança que m'han transmès i recolzament en els moments més durs. En definitiva, sense la seva tutela aquesta tesi no hagués sigut ni de bon tros la mateixa.

També agrair molt especialment a Fulgura S.L., o en definitiva, a la Glòria Solà, per tot allò que hem pogut compartir, tant professional com interpersonalment, des del primer dia de feina. Part també imprescindible d'aquest projecte, la seva ajuda ha suposat de gran valor per a mi, també a l'hora de tenir en compte les meves opinions i posada en comú.

Vull agrair també a *nowcast GmbH*, i com no pot ser d'altra manera al Prof. Hans-Dieter Betz, en Matthias Möhrlein i la Sofia Riso, amb tota la formació respecte a la xarxa de llamps LINET que em van fer arribar i al tractament de les seves dades. A Ubimet, i en especial a en Manuel Safner i en Christian Aichinger, amb qui he pogut compartir informació d'anàlisis relacionats amb la xarxa LINET durant el projecte i compartir inquietuds sobre el seu funcionament. I per descomptat a Dena Desarrollos S.L., per tota la seva col · laboració durant tot el projecte. Gràcies especialment a la Silvia Alés, l'Angel Illa, en Josep Rico, en Xavier Colom, l'Albert Ramon, en Cristian Bravo, en Ramon Silva, en Víctor Lorenzo, la Irene Martínez i a la Patricia Martínez, per l'experiència professional que m'han transmès, així com pel seu interès i passió en la feina realitzada.

A tots els companys d'investigació amb qui he tingut la infinita sort de poder-hi compartir temps. Als qui m'han acompanyat des de la Universitat Politècnica de Catalunya, en Ferran Fabró, en David Romero i l'Oscar van der Velde, moltes gràcies pel seu valuós temps i la seva assessoria en el coneixement de llamps i el seu tractament. També no puc oblidar-me d'en Jesús López, en Toni Rey i en Michele Urbani, amb qui he pogut compartir tant bones estones com intercanvi de coneixements i experiències, també imprescindibles en aquest projecte. Per descomptat també a l'equip de teledetecció del Servei Meteorològic: la Helen San Segundo, la Patricia Altube, en Tomeu Rigo, l'Oriol Argemí, en Sergio Castillo i en Francesc Roura. A totes elles els agraeixo enormement la seva ajuda i coneixements, que n'han sigut molts, però també pels respirs en què la desconnexió de la feina ha permès conèixer-nos. Molt agraït també a tot l'equip de predicció i vigilància, en especial a la Montse Arán i en Sergio Gallego, amb qui he pogut compartir molts dubtes i inquietuds.

A tots ells, i als qui segurament m'hauré deixat de esmentar inintencionadament, que en tot moment hi han estat, sacrificant el seu temps, gràcies.

Fora del projecte de doctorat, no puc deixar-me als amics i amigues del bar amb qui tantes hores hem compartit i, donades les circumstàncies actuals, no ens hem pogut trobar

tant com voldríem. A tots ells i elles, gràcies per l'interès continuat per l'estat de la feina feta i pels ànims donats. I no em semblaria adequat destacar-ne a ningú en especial, però la situació actual m'impedeix no fer un molt especial agraïment a l'Aleix Alsina i l'Aleix Roca (el guapo i l'altre, no necessàriament en aquest ordre), amb qui portem (quasi) tot els caps de setmana de confinament amb teleconferències maratonianes, cadascú amb les seves cabòries, però compartint temps i recolzament psicològic en les moltes hores de xerrameca i distracció. També a la Victoria Durant, que des de la distància no ha deixat de enviar-me ànims i suport en tot allò que m'he hagut d'enfrontar.

M'agradaria fer un especial agraïment a la meva família, amb els meus pares al capdavant, la Montse i en Xavi, per estimar-me, escoltar-me i recolzar-me en tot allò que m'he anat trobant al llarg de la meva vida. També als meus avis i àvies, que des d'allà on em puguin veure, que sàpiguen que penso molt en ells. És clar també agraïments a la meva cosina Marta i en Víctor, que tot i amb la gestió dels petits sempre poden trobar un moment per interessar-se per mi. I per descomptat, gràcies a l'Àngels i en Joan, pel suport en molts aspectes i l'entusiasme i afany pels temes tractats de la tesi.

Finalment a l'Elena. Per brindar-m'ho tot, aguantar tots els moments d'estrès amb paciència i fer-me somriure. És gràcies al teu suport incondicional que he pogut arribar fins aquí. No puc evitar sentir-me especial estant amb tu.

Aquesta tesi doctoral ha sigut emmarcada dins del Programa de Doctorats Industrial (DI 59/2015) de l'Agència de Gestió d'Ajuts Universitaris i de Recerca (AGAUR) de la Generalitat de Catalunya. També ha estat recolzat per el Ministerio de Economía y Competitividad de España (MINECO) i el Fondo Europeo de Desarrollo Regional (FEDER) amb els projectes ESP2015-69909-C5-5-R, ESP2017-86263-C4-2-R i PID2019-109269RB-C42.

Lista de Acrónimos

AGAUR	Agència de Gestió d'Ajuts Universitaris i de Recerca
AoS	Area de estudio / Area Of Study
ASIM	Atmosphere-Space Interactions Monitor
CAPE	Energía potencial convectiva disponible / Convective Available Potential Energy
CAPPI	Indicador de posición del plan de altitud constante / Constant Altitude Plan Position Indicator
CG	Rayo nube-tierra / Cloud-to-Ground
CGFR	Ratio de rayos nube-tierra / Cloud-to-Ground Flash Rate
ChR	Región de carga / Charge Region
CI	Intervalo de confianza / Confidence Interval
CSI	Índice de éxito crítico / Critical Success Index
ELMA	Ebre Lightning Mapping Array
FAR	Ratio de falsas alarmas / False Alarm Ratio
FEDER	Fondo Europeo de Desarrollo Regional
HF	Alta frecuencia / High Frequency
IC	Rayo nube-nube / Intra-Cloud
ICFR	Ratio de rayos nube-nube / Intra-Cloud Flash Rate
IQR	Rango intercuartil / Interquartile Range
LCL	Nivel de condesación por ascenso / Lifting Condensation Level
LF	Baja Frecuencia / Low Frequency
LINET	LIghtning detection NETwork (nowcast GmbH)
LLS	Sistema de localización de rayos / Lightning Location System
LMA	Lightning Mapping Array
LMA-LIC	Lightning Initiation Centers detected by LMA
LMA-SC	Source count detected by LMA
LRG	Lightning Research Group
LwDip	Lower Dipole thunderstorm structure
MDF	Magnetic Direction Finding
MINECO	Ministerio de Economía y Empresa, de España (a julio de 2021, Ministerio de Asuntos Económicos y Transformación Digital)
MSL	Nivel medio del mar / Mean Sea Level
NIC	Carga no inductiva / Non-Inductive Charging
SMC	Servei Meteorològic de Catalunya
POD	Probabilidad de detección / Probability Of Detection
TFR	Ratio total de rayos / Total lightning Flash Rate
TL	Número total de rayos / Total Lightning
TOA	Time-Of-Arrival

TOP	Producto de altura máxima de un eco radar/ Radar echo top product
TriP	Tripole thunderstorm structure
TRMM	Tropical Rainfall Measuring Mission
TSS	True Skill Statistic
UPC	Universitat Politècnica de Catalunya
UpDip	Upper Dipole thunderstorm structure
UTC	Tiempo universal coordinado / Coordinated Universal Time
VHF	Muy alta frecuencia / Very High Frequency
VLF	Muy baja frecuencia / Very Low Frequency
WRF	Weather Research and Forecast
XDDE	Xarxa de Detecció de Descàrregues Elèctriques (del SMC)
XRAD	Xarxa de RADars Meteorològics (del SMC)

Índice

Índice de Figuras

1 Introducción

En esta tesis se evalúan las condiciones meteorológicas de entorno que favorecen la iniciación de actividad eléctrica dentro de una nube de tormenta. Con un enfoque multi-sensor (radar meteorológico, datos de rayos de nube-nube y nube-tierra, y datos del perfil vertical de la atmósfera derivados de radiosondeo), se procura estudiar este fenómeno atmosférico. A partir de los resultados se evalúan qué parámetros se proponen como indicadores para la detección del inicio de la actividad, análisis y, de ser necesario, la sucesión de avisos y medidas que se tienen que llevar a cabo para prevenir sus posibles efectos adversos.

Al respecto de este último aspecto, se destacan los posibles perjuicios de esta actividad eléctrica, puesto que los rayos son un fenómeno atmosférico que puede causar daños severos a todo tipo de infraestructuras, especialmente vinculadas con componentes eléctricos y electrónicos. Enfocando especialmente en los rayos que descienden de la nube hacia tierra, el impacto de estos puede causar distintos tipos de afectaciones, desde inyecciones de corriente muy elevados a los sistemas eléctricos, a sobretensión a las líneas eléctricas, con posibles desperfectos de distinta consideración.

Es por todos conocido que las tormentas provocan rayos, pues es precisamente la presencia de este meteoro el que define la tormenta y la diferencia de otros tipos de estructura de precipitación, como por ejemplo un chaparrón. Ahora bien, no todas las tormentas tienen la misma intensidad, por ejemplo, tormentas de gran desarrollo vertical que tienen mucha actividad de rayos intra-nube, pero pocos rayos a tierra en comparación con la altura que ha alcanzado. Por el otro lado, hay situaciones de invierno donde, a pesar de no haber condiciones de convección profunda, se producen rayos a tierra que pueden dañar sistema de telecomunicaciones e incluso aerogeneradores de parques eólicos.

Las nubes de tormenta tienen típicamente una estructura eléctrica en que capas de polaridad opuesta se van ordenando horizontalmente unas encimas de la otras. La localización en altura de estas capas tiene una estrecha dependencia con la altura de distintas isotermas, encontrándose de forma frecuente una capa inferior de carga negativa entre los $-10°C$ y $-25°C$ y una capa superior positiva alrededor de los $-40°C$. Además, típicamente se detecta una capa positiva y negativa en la parte inferior y superior de la nube, respectivamente, con un nivel de carga significativamente inferior a las dos primeras. Esta estructura se puede observar esquematizada en la Figura 1.

La microfísica de la región de fase mixta (región dentro de una nube de tormenta, típicamente localizada entre los $-10°C$ y $-25°C$, donde coexisten partículas de agua sobreenfriada y pequeños cristales de hielo) es compleja y los procesos de carga dentro de la nube siguen siendo un campo de investigación abierto, con aún varios interrogantes. No obstante, el enfoque de esta tesis es más práctico, en el sentido de definir parámetros que pueden alertar sobre la intensidad de la tormenta. La actividad nube-tierra cobra un

especial interés, pues es la que tiene mayor afectación en nuestra sociedad, con daños económicos e incluso personales.

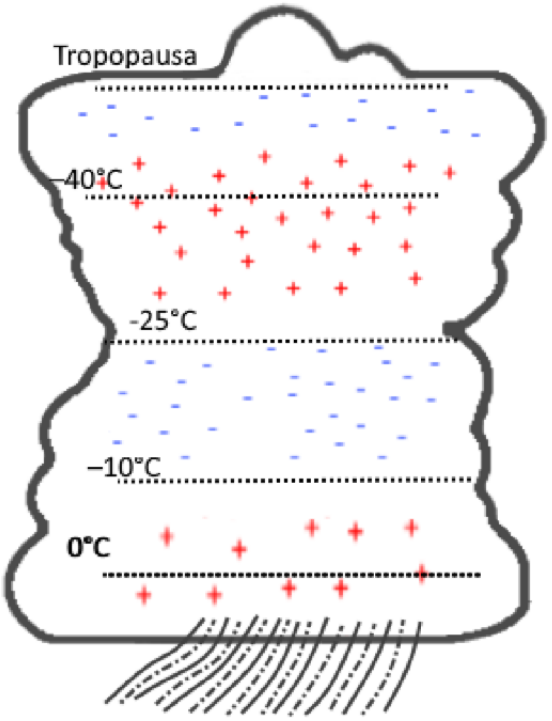

Figura 1. Estructura eléctrica típica de una nube de tormenta. Se representa un posible *overshooting top* por encima de la tropopausa. Entre las isotermas de −10°C y −25°C suele presenciarse una región de carga negativa. Alrededor de la isoterma de −40°C se observaría una región de carga positiva. Adicionalmente se añaden una región de carga positiva y negativa en la parte inferior y superior de la nube, respectivamente, con una carga inferior a las primeras.

Las infraestructuras elevadas como las torres de comunicación y los aerogeneradores son susceptibles de sufrir impactos de rayo bajo condiciones de tormenta. Las condiciones para que un rayo se inicie mantienen un grado de incertidumbre, tal y como se podrá observar en esta tesis, pero es conocido que este tipo de infraestructuras pueden experimentar actividad eléctrica durante todo el año. Por ejemplo, durante las estaciones del año más frías, en condiciones de tormenta parece que las condiciones son más favorables (Montanyà et al., 2012), ya que se considera que la capa negativa inferior de las tormentas durante esta época del año está más baja, favoreciendo la capacidad de las torres elevadas de iniciar rayos ascendentes. Aun así, las tormentas eléctricas más intensas acostumbran a desarrollarse durante las estaciones más cálidas, con las regiones de carga más elevadas. Esto hace que las afectaciones por actividad eléctrica sean, en general, un problema que se extiende durante todo el año.

En el caso particular de los aerogeneradores, los rayos son un fenómeno que frecuentemente han causado daños severos, en los que se puede diferencias daños directos, como daños estructurales de las turbinas, así como daños indirectos, como las afectaciones a las infraestructuras eléctricas del parque eólico (e.g., Braam et al., 2002; Yamamoto et al., 2009; Yasuda et al., 2012; Garolera et al., 2016; March, 2016). Estas afectaciones se

han visto incrementadas debido a la rápida expansión de los parques eólicos en los últimos años que, a su vez, han creado una demanda para avanzar en técnicas de previsión de rayos y de viento, los principales vectores de daños de estas infraestructuras (e.g., Foley et al., 2012). Además, siempre teniendo en cuenta los costes añadidos que conlleva la operación y mantenimiento de cada uno de los elementos de los aerogeneradores, así como el sistema de control general, entre otros elementos (e.g., Madsen, 2017).

Durante las últimas décadas se han ido instalando sistemas de detección y localización de rayos para aumentar la cobertura de detección (e.g., Cummins and Murphy, 2009), así como su eficiencia ha ido mejorando paulatinamente (e.g., Nag et al., 2015). Estos sistemas proporcionan información sobre la actividad eléctrica en tiempo real, y ayudan a tomar decisiones en diferentes ámbitos (e.g., Shindo and Suda, 2008; Clulow et al., 2018; Meng et al., 2019), desde simples desconexiones de componentes eléctricos, deteniendo la actividad de los aerogeneradores, hasta realizando advertencias a las personas que estén realizando actividades al aire libre, como en trabajos de minería, aeropuertos y aeronáutica, transporte, comunicación, agricultura, entre otros (e.g., Zhang et al., 2012; Elsom and Webb, 2014; Tovar et al., 2014). La combinación de los sistemas de localización presenta una gran sinergia con otros sistemas de teledetección meteorológica, entre ellos el radar meteorológico, imágenes de satélite, radiosondeo, etc., la cual aumenta notoriamente la cualidad de la detección (e.g., Montanyà et al., 2008).

Esta tesis se enmarca dentro del Programa de Doctorats Industrials. Esta circunstancia se traduce en el objetivo de, más allá de aportar información a una vertiente más académica, aportar productos que puedan ser de especial interés a los posibles mercados que se derivan de la actividad de rayos desde distintos aspectos. Estas aplicaciones pueden ser enfocadas tanto desde el punto de vista de incorporación en sistemas de avisos, para emisiones de alarmas de cercanía de eventos meteorológicos adversos relacionados con la presencia de actividad eléctrica, como de análisis de zonas con especial afectación, así como de posterior evaluación de los posibles daños relacionados, entre otros.

La dualidad universidad-empresa ha sido clave para el desarrollo del doctorado industrial. Desde el punto de vista universitario y de investigación, el grupo *Lightning Research Group* de la Universitat Politècnica de Catalunya y el Servei Meteorològic de Catalunya han proporcionado un volumen ingente de datos de sistemas de teledetección como el radiosondeo de Barcelona, la Xarxa de Radars Meteorològics, la red de detección de rayos Xarxa de Detecció de Descàrregues Elèctriques, así como la red de detección *Lightning Mapping Array* instalada en el Delta del Ebro. Desde el punto de vista empresarial, se destaca la empresa Fulgura S.L., especializada en la prevención, protección e investigación en el sector del rayo. La colaboración añadida con la empresa *nowcast GmbH* (Múnich, Alemania) ha permitido el uso de los datos de la red de detección de rayos *Lightning Detection Network*, con una amplia distribución en Europa, así como otras zonas del mundo, para poder desarrollar las actividades descritas en esta tesis.

1.1 Objetivos

Esta tesis analiza la actividad eléctrica atmosférica, con un especial enfoque hacia los procesos que se generan dentro de la nube de tormenta y sus posibles descargas hacia tierra, con los respectivos daños que estos pueden provocar.

El objetivo principal de esta tesis es la identificación de las condiciones meteorológicas, que se puedan parametrizar y usar regularmente para generar productos de aviso, que favorecen la presencia de actividad de rayos, las características más comunes detectadas en las nubes de tormenta que provocan estas descargas, diferenciando las descargas internas dentro la misma nube de tormenta con las que tienen llegada u origen a la superficie. Para tal fin, se pone en valor la sinergia de los datos del radar meteorológico, del radiosondeo y de las distintas redes de detección de rayos para realizar un análisis más adecuado de estas situaciones. Finalmente, se propone identificar la incidencia de este tipo de descargas en infraestructuras elevadas, como los aerogeneradores, edificaciones típicamente relacionadas con una afectación elevada frente a este tipo de sucesos. Esto proporcionará una información muy importante para la industria eólica, permitiendo desarrollar sistemas de avisos que gestionen las actuaciones a llevar a cabo, tanto en forma de prevención frente al riesgo como de actuación para reducir sus posibles afectaciones.

Para tal fin, y a partir de las herramientas de las que se disponen para la elaboración de esta investigación, se detallan unos objetivos parciales:

- **Propuesta de indicadores que permitan identificar la actividad de rayos**. Se propone el cruce de información entre las alturas de reflectividad radar con las alturas de isotermas determinadas por radiosondeo o modelo meteorológico como indicador para determinar las condiciones favorables a la presencia de actividad eléctrica atmosférica. Este será validado con sistemas de detección de rayos.
- **Estudio de las intensidades de actividad de rayos con el potencial convectivo de la tormenta.** Tradicionalmente, se ha vinculado la altura máxima de una tormenta con el poder convectivo de esta. Sin embargo, un alto desarrollo vertical no siempre conduce a la separación de cargas, por lo que la relación no es sencilla. Se compararán algunas características de otros estudios en otras zonas de estudio con el área propuesta en esta tesis.
- **Evaluación de los indicadores y potencialidad de actividad de rayos a lo largo del año**. Los indicadores anteriormente propuestos se validarán según la estacionalidad de las condiciones meteorológicas, con un enfoque principal hacia la variación de las alturas de las isotermas, así como la intensidad de descarga. Esto tiene una importante aplicación en los parques eólicos frente a la actividad de rayos en periodos fuera de temporada.
- **Determinar la influencia de la estructura eléctrica de las tormentas en los tipos de rayos detectados.** La incidencia de rayos según si son intra-nube o descargas al suelo difiere durante las fases dentro del ciclo de vida de una tormenta,

así como de la estructura eléctrica que presenta esta en cada instante, facilitando el desarrollo y desplazamiento de distintos tipos de descarga eléctrica. Se analizará la utilidad de la altura de las regiones de carga como variable en este análisis, comparándolas con alturas típicas detectadas en otros estudios.

- **Analizar los niveles de incidencia de actividad de rayos en aerogeneradores.** Típicamente se vinculan los periodos más cálidos con los que más actividad eléctrica atmosférica se detecta. Aun así, se evaluará si este comportamiento estacional tiene relación directa con las descargas con inicio o final en aerogeneradores.
- **Comparar las características comunes de las tormentas y de los rayos en periodos de especial afectación a aerogeneradores.** Del mismo modo que la estructura eléctrica de una tormenta puede tener influencia en sus descargas, se evaluarán las características de estas. Adicionalmente se analizarán las características de los rayos que afecten a los aerogeneradores, tanto descendentes como ascendentes.

1.2 Estructura de la tesis

Compuesta por 6 capítulos, esta tesis ha sido planteada como un compendio de artículos. En el Capítulo 1, se presenta una introducción al trabajo realizado durante la tesis, así como los objetivos principales de esta. En el Capítulo 2 se detalla el estado del arte, donde se señala información relevante para el entendimiento de esta tesis, con conceptos claves de las tormentas, como el ciclo de vida y su estructura eléctrica, así como algunas particularidades de algunas regiones de carga y su incidencia en la actividad de rayos. Para terminar, se detallan los sistemas de detección de descargas eléctricas utilizados durante el proyecto, con especial enfoque al sistema *Lightning Mapping Array*, así como la información de radar meteorológico, ambas imprescindibles en la elaboración de esta tesis.

El Capítulo 3 presenta los tres artículos que componen el compendio. Se presentan cada uno en sus respectivos contextos, se detallan las observaciones que se han realizado, así como las conclusiones que se extraen de cada uno de ellos, respondiendo a los objetivos principales de la tesis anteriormente planteados. Seguidamente, en el Capítulo 4 se presentan las conclusiones finales del trabajo realizado de forma global, y se detallan algunas perspectivas de futuro sobre las que se podría realizar y ampliar el trabajo realizado hasta el momento actual.

Posteriormente, en el Capítulo 5 se detallan aquellas contribuciones, tanto nacidas como artículos como las que han sido propuestas como participaciones en distintos congresos en forma de póster o presentaciones orales, que se han derivado del trabajo realizado durante mi periodo doctoral. Finalmente, y para dar una perspectiva de las tareas realizadas en el marco del doctorado industrial bajo el que esta tesis ha sido elaborada, en el Capítulo 6 se detallan aquellas actividades llevadas a cabo en paralelo al entorno universitario, y que se le han dado un punto de vista más empresarial y práctico.

2 Estado del arte

Los rayos son descargas eléctricas que conectan distintas zonas con carga eléctrica opuesta de la nube de tormenta. Se pueden diferenciar dos tipos de rayos según las zonas que conectan. Por un lado, encontramos los rayos nube-nube (IC, del inglés *Intra-Cloud*), los cuales conectan dos zonas de carga opuesta dentro de una misma nube de tormenta; por el otro los nube-tierra (CG, del inglés *Cloud-to-Ground*), que conectan uno de los estratos de carga de la nube con la superficie terrestre.

Los siguientes apartados detallan los distintos factores que típicamente van ligados a la actividad eléctrica, tanto de formación como tipología. Además, se detallarán qué características presentan algunos tipos de infraestructuras elevadas frente a ellos, algunos sistemas de detección, y que potencialidades presentan algunos de ellos.

2.1 Ciclo de vida de las tormentas

A las tormentas clásicamente se les ha otorgado una fase según su ciclo de vida: la fase de cúmulo o desarrollo, la fase de madurez y por último la fase final o de disipación. Esta clasificación viene definida típicamente por la información de radar (e.g., Doswell, 2001, 2007) En la Figura 2 se puede ver un esquema con las distintas fases típicas de una tormenta.

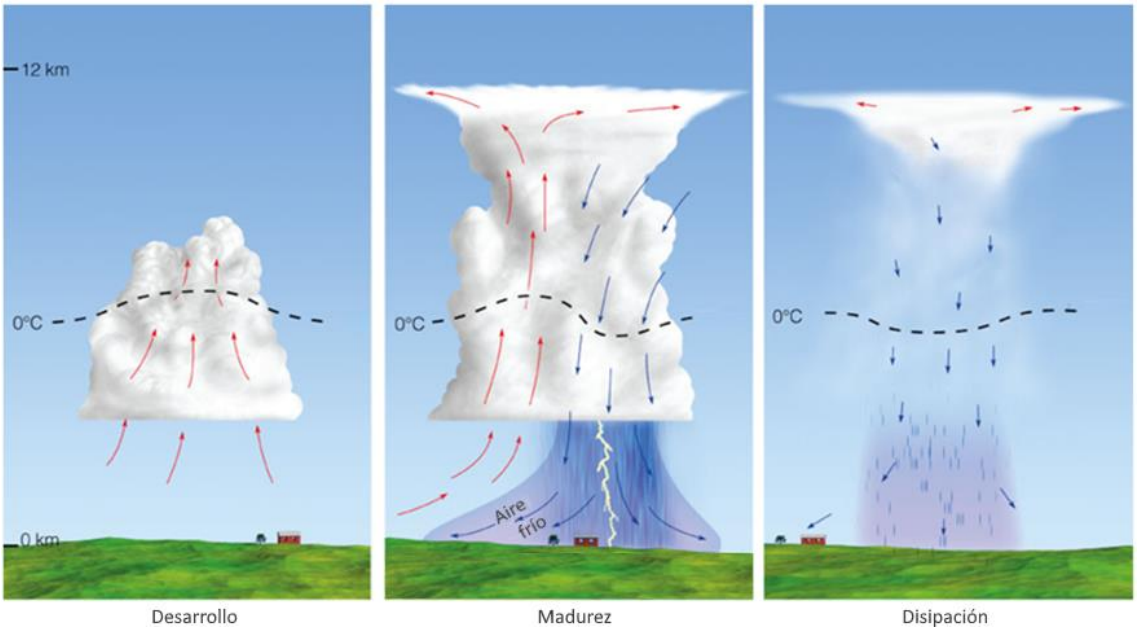

Figura 2. Fases del ciclo de vida de una tormenta. Las flechas indican corrientes de aire, rojo para cálidos y azules para fríos. Imagen adaptada de Ahrens (2008).

La fase de desarrollo de una tormenta está compuesta por un cúmulo de nubes que ascienden debido a una corriente ascendente, típicamente formada por una convergencia de distintas parcelas de aire (e.g., Williams et al., 1989; Rigo et al., 2010). En esta fase

normalmente no se detecta precipitación, o en todo caso de forma muy tenue, aunque no implica que no se puedan empezar a detectar las primeras señales eléctricas, las cuales son mayormente IC.

Estudios anteriores (e.g., Goodman et al., 1988; Williams, 1989; Williams et al., 1989; Carey and Rutledge, 1996) han demostrado que la convección típica de una masa de aire dentro de una tormenta puede llegar a durar aproximadamente una hora. Es durante esta fase cuando se detectan las primeras señales de descargas eléctricas, los cuales acostumbran a ser rayos IC, mientras que los rayos CG suelen alcanzar su frecuencia máxima después de los primeros, ya que el núcleo principal de la celda desciende a altitudes más bajas (Laksen and Stansbury, 1974; Goodman et al., 1988; MacGorman et al., 1989; Williams, 1989; Carey and Rutledge, 1996).

La tormenta entra en fase de madurez cuando ya empieza a presentar precipitación, creando una corriente de aire fría descendente, no sin una mantenida alimentación de la nube por corrientes ascendentes (e.g., MacGorman et al., 1989). Es durante esta fase cuando los procesos de granizo y lluvia intensa pueden ocurrir en mayor medida, además de las detecciones de las primeras descargas CG (e.g., Soula et al., 2004; Wiens et al., 2005). La tormenta también alcanza su altura máxima, típicamente limitada por la altura de la tropopausa, la cual puede provocar una forma de yunque en la parte superior de la nube. En casos de tormentas con fuertes corrientes ascendentes, la nube puede superar el nivel de la tropopausa, causando *overshooting tops* (e.g., Adler et al., 1985; Bedka, 2011).

Por último, la fase de disipación se inicia cuando las corrientes descendentes dominan sobre las ascendentes, y estas van disipando la nube de tormenta (e.g., Doswell, 2001). La intensidad de precipitación disminuye, aunque aún es posible la presencia de rayos, tanto IC como CG.

2.2 Estructura eléctrica de las tormentas

La estructura eléctrica típica de una nube de tormenta se puede observar en la Figura 1 y se describe a continuación destacando los punto claves de esta (e.g., Dotzek et al., 2005; Krehbiel et al., 2008):

- La región inferior de las tormentas acostumbra a tener un estrato de carga negativa, típicamente localizada en un rango de temperaturas comprendido entre los $-10°C$ y $-25°C$.
- Por encima de esta encontraríamos una región de carga positiva, situada aproximadamente a la altura de la isoterma de $-40°C$.
- Una tercera capa, también positiva se encontraría en la base de la nube, pero con un nivel de carga relativamente más débil que la anterior.
- Además, se detecta una capa negativa adicional en la parte más elevada de la nube de tormenta, también llamada *screening layer* (MacGorman and Rust, 1998; Krehbiel et al., 2008).

Tal y como se detalla, las principales regiones de carga se separan en la región de fase mixta (entre −10°C y −25°C), donde coexisten los hidrometeoros tanto en forma líquida como en forma sólida. Además, y como se ha mencionado, este tipo de estructura se complementa por una capa negativa adicional en la parte superior de la nube. No obstante, algunas tormentas que llevan tras de sí tiempo adverso como las supercélulas, pueden presentar estructuras eléctricas anómalas donde, por ejemplo, la estructura tripolar clásica se ve invertida (Bruning et al., 2014).

Existen distintas propuestas de mecanismos de electrificación de una nube de tormenta. El más aceptado en los últimos años es el proceso no inductivo (*Non-Inductive Charging Mechanism*, NIC) (e.g., Takahashi, 1978; Jayaratne et al., 1983; Saunders et al., 2006; MacGorman et al., 2008). Este proceso consiste en que el graupel (granizo) precipitante, que ha capturado en el proceso pequeñas gotas de agua superenfriadas, colisiona con otros cristales de hielo y, en función de la temperatura ambiental, transcurre una transferencia de carga en que el graupel adquiere una carga eléctrica, negativa o positiva, y el cristal de hielo adquiere la carga de polaridad opuesta. Adicionalmente, el tamaño pequeño típico de los cristales de hielo provoca que estos tiendan a adquirir la carga positiva y además son arrastrados verticalmente hacia arriba por las corrientes ascendentes. En su contra, el mayor tamaño del graupel provoca su carga negativa y posición más baja en la nube de la tormenta (Wallace and Hobbs, 2006), creando dos zonas de carga diferenciadas y de polaridad opuesta. Se establece habitual la presencia de una tercera zona de carga positiva en la base de la nube, lo que lleva a hablar de una distribución tripolar clásica (e.g., Krehbiel, 1986; Williams, 1989; Tessendorf et al., 2007; Stolzenburg and Marshall, 2008).

Además, y tal y cómo se ha introducido en la descripción de la estructura eléctrica de la nube de tormenta, este proceso físico de distribución de cargas depende de la temperatura y, por extensión, de la altura de las isotermas (con especial enfoque en la región de fase mixta entre las isotermas de −10°C y −25°C), así como de la altura de la tropopausa (e.g., Krehbiel et al., 2008; Liu et al., 2021). Debido la variabilidad de estas, con especial enfoque hacia la tropopausa (causado mayoritariamente por la estacionalidad y la latitud donde se detecta la tormenta) se entiende que las tormentas tropicales tienen un potencial mayor para alcanzar un desarrollo vertical más elevado en comparación con otras tormentas localizadas en latitudes más elevadas (e.g., Williams et al., 1989). A su vez, las alturas de las distintas isotermas y tropopausa presentan su mayor variabilidad estacional en latitudes medias. Esta característica provoca que las alturas de los niveles de carga en una tormenta de invierno se encuentren más bajas que los que encontraríamos en un periodo más cálido, es decir, más cerca del nivel de superficie. Esto se puede ver esquematizado en la Figura 3.

Aunque esta es la estructura típica de una nube de tormenta, se han observado múltiples situaciones en que la distribución de las cargas se encuentra en un régimen inusual en que las polaridades se invierten o, incluso en algunos episodios mayormente relacionados con tormentas de carácter multicelular, en que la organización de esta estructura eléctrica va variando a lo largo del episodio (Rust et al., 2005).

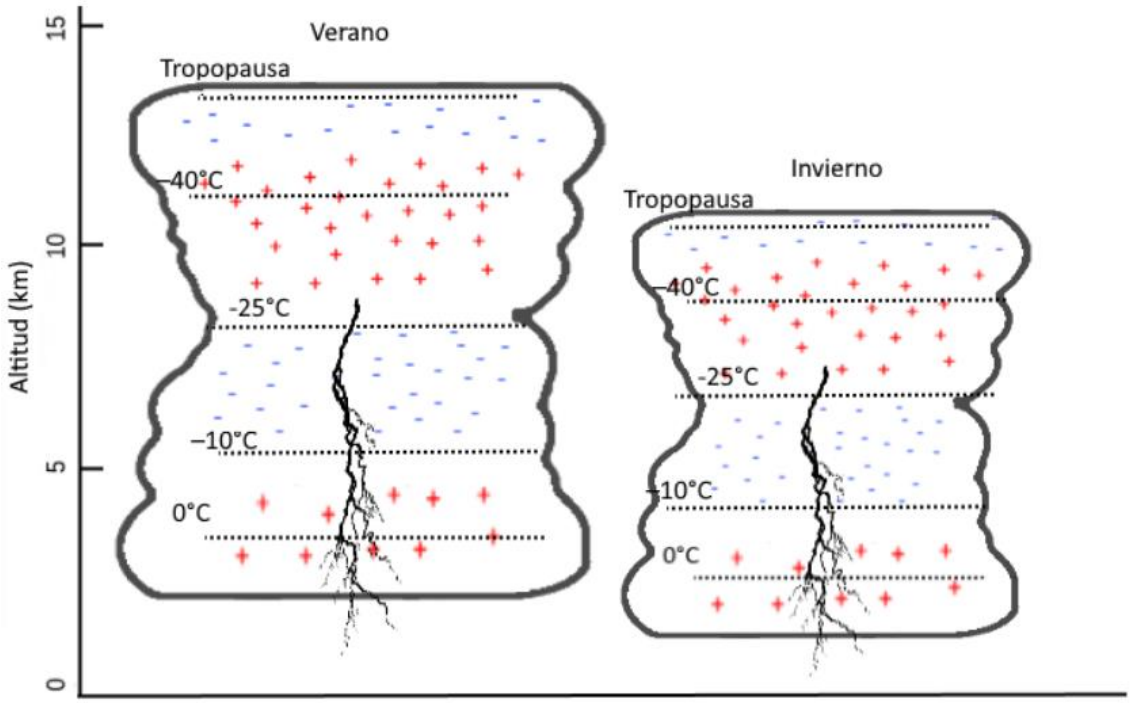

Figura 3. Variación de la localización en altura de los centros de carga para tormentas en verano e invierno en latitudes medias. Adaptado de los resultados de Salvador et al. (2020).

2.3 Lower Positive Charge Region (LPCR)

En una estructura tripolar clásica dentro de una nube de tormenta, la presencia de la región inferior de carga positiva (*Lower Positive Charge Region*, LPCR) aumenta localmente el campo eléctrico, facilitando así la formación de descargas eléctricas que se dirigen hacia tierra (e.g., Wiens et al., 2005; Krehbiel et al., 2008; Cooray et al., 2014). Los primeros trabajos de Clarence and Malan (1957) ya sugirieron que una LPCR es esencial para la iniciación la rayo CG. Además, estudios derivados de modelos numéricos han determinado la importancia que la presencia de la LPCR tiene sobre el desarrollo y presencia de las descargas CG negativas (e.g., Mansell et al., 2002, 2005). En la Figura 4 se puede observar en un esquema de capas las dos principales corrientes eléctricas entre las regiones de carga de polaridad inversa. Debido a la mayor carga de las principales regiones de cargas de polaridad inversa más intensas, la corriente eléctrica entre estas es mayor (I_1) que entre la región de carga negativa inferior y la región inferior de carga positiva (I_2). Aun su menor intensidad, esta última es la que favorecería los rayos CG.

La región de carga negativa se encuentra relacionada con la región de fase mixta (entre $-10°C$ y $-25°C$), mientras que la región de carga positiva más baja se encuentra típicamente justo debajo del nivel de congelación (Nag and Rakov, 2009), donde los hidrometeoros de fase sólida se derriten para convertirse en gotas de lluvia (Marshall and Rust, 1993; Shepherd et al., 1996). Esta región de carga fue confirmada con mediciones de globo y detectores de campo eléctrico en superficie (e.g., Jacobson and Krider, 1976;

Marshall and Winn, 1982; Marshall and Rust, 1991). Rakov and Uman (2003) propusieron cuatro hipótesis diferentes con respecto al origen de esta LPCR. Entre estas, se destacan la asociación a) con el granizo, que se carga positivamente a temperaturas más cálidas que la temperatura de inversión, b) con la carga positiva depositada en la nube por la actividad de los rayos, c) con efectos de corona a nivel de superficie del suelo y d) con una región de carga positiva formada por atracción electrostática en el límite inferior de la nube.

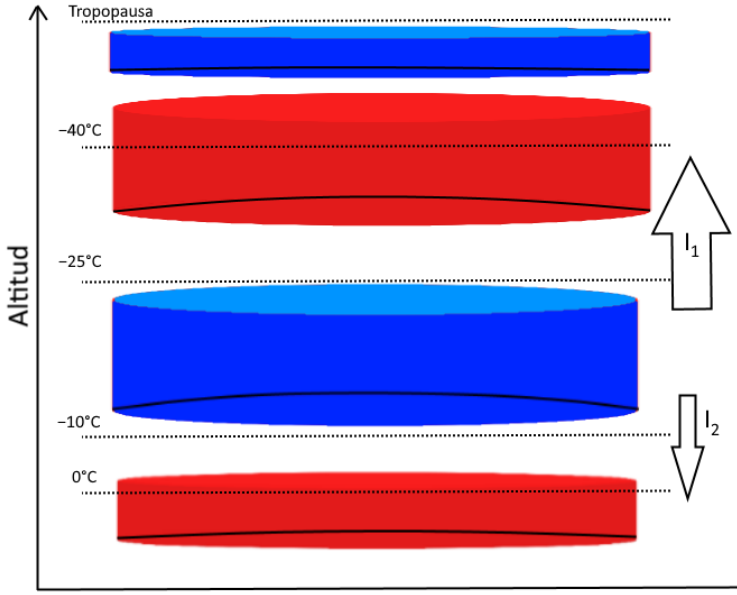

Figura 4. Configuración de capas para una tormenta con estructura eléctrica típica. El grosor de cada capa (rojo para las regiones de carga positiva y azul para las negativas) indica el nivel de carga de cada región. Las flechas indican los principales corrientes eléctricos verticales de las tormentas: I_1 entre la región negativa inferior y la positiva superior, e I_2 entre la región negativa inferior y positiva inferior, siendo la primera típicamente más intensa que la segunda por el mayor potencial eléctrico entre las distintas capas. Adaptado de Krehbiel et al. (2008).

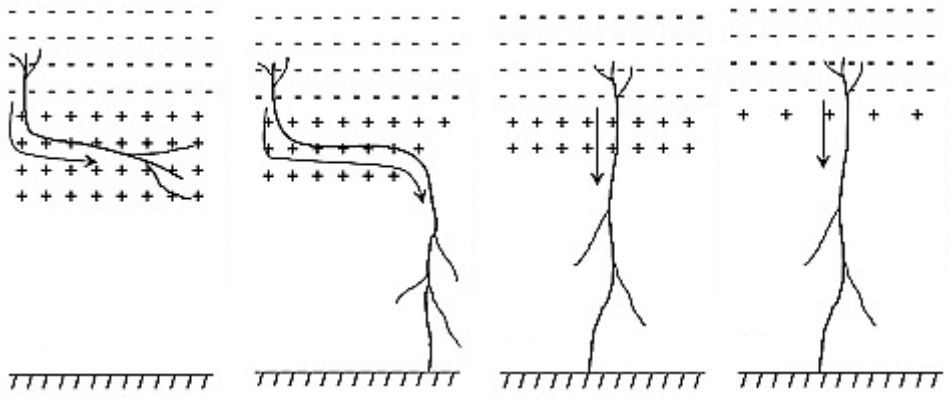

Figura 5. Esquema del perfil vertical en que, de izquierda a derecha, el nivel de carga de la LPCR va disminuyendo, y se observa su influencia en el desplazamiento de un rayo de carga negativa. Las flechas indican la dirección de propagación de esta descarga. Adaptado de Nag and Rakov (2009).

Estudios como Qie et al. (2005), Nag and Rakov (2009) y Iudin et al. (2017) también advierten que el caso de una LPCR con demasiada carga puede provocar el bloqueo de los

líderes negativos hacia la superficie. Nag and Rakov (2009) representaba un esquema para ilustrar esta situación, la cual se ha adaptado en la Figura 5. A la izquierda se puede observar como una LPCR muy dominante impide completamente que una descarga inicialmente orientada hacia la superficie alcanzara su objetivo, viéndose retenida dentro de esta capa positiva, impidiendo la posible detección de un rayo CG. Siguiendo hacia la derecha en la representación, un descenso en la carga de esta región inferior dificulta en menor medida su descenso, manteniéndose momentáneamente en la LPCR para acabar descendiendo hasta el suelo. Finalmente, los dos últimos casos suponen un descenso clásico de un rayo originado en la región negativa de la nube provocado por la diferencia de potencial con la región positiva inferior.

2.4 Tipología del rayo

Planteados brevemente en el inicio de este capítulo, existe la diferenciación de las descargas según si estas alcanzan o no la superficie (CG e IC, respectivamente), así como la aparición de cada tipo de estos según la fase del ciclo de la tormenta en la que se encuentre, donde los IC dominan en el inicio de estas. No es hasta la fase de maduración cuando los CG empiezan a ganar típicamente más protagonismo.

Aun así, se estima que de todas las descargas que ocurren durante una tormenta, el 90% corresponden a descargas IC, frente al 10% restante correspondiente a descargas CG. De estos últimos, se acostumbran a diferenciar cuatro tipos de líderes según su sentido vertical (descendente o ascendente) y según su polaridad (negativa y positiva). Estas distintas tipologías de CG se pueden observar esquematizadas en la Figura 6. El inicio de los rayos IC típicamente es localizado entre las principales regiones de carga de la nube, positiva y negativa, donde el campo eléctrico es más intenso. El punto común entre todos los tipos de rayos es su iniciación, provocada por una descarga preliminar de ruptura (*Preliminary Breakdown*, PB), el cual acostumbra a ser bipolar, provocando dos líderes con diferente polaridad que se trasladan por regiones de carga opuesta (e.g., Montanya et al., 2015).

Las descargas CG son típicamente más conocidas debido a su mayor facilidad para medir corrientes y tomas de fotografías. Las de polaridad negativa son los más comunes, ya que provendrían de la principal región de carga negativa, pasando a través de la inferior positiva más débil, en una estructura tripolar clásica. Para el caso de un CG negativo, la formación de su líder, causada por el PB, procede con un descenso hacia la superficie en un proceso llamado S*tepped Leader* (SL). El proceso termina cuando se inicia la descarga de retorno (*Return Stroke*, RS) en la que se transporta toda la carga del rayo. En cuanto a intensidades se calcula que el valor medio de estos RS es aproximadamente de 30 kA, con casos superiores a los 100 kA. Se puede observar un esquema de este proceso en la Figura 7.

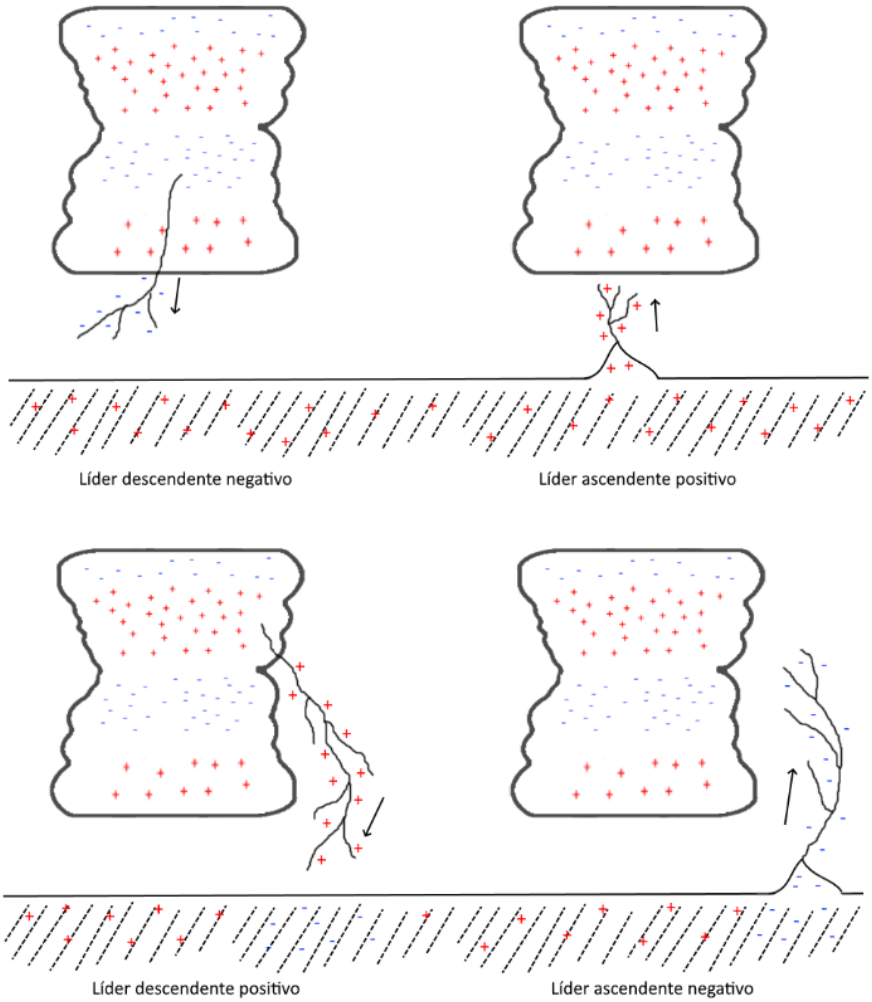

Figura 6. Esquema de las distintas combinaciones de descargas CG según su polaridad y sentido vertical. Adaptado de Dwyer and Uman (2013).

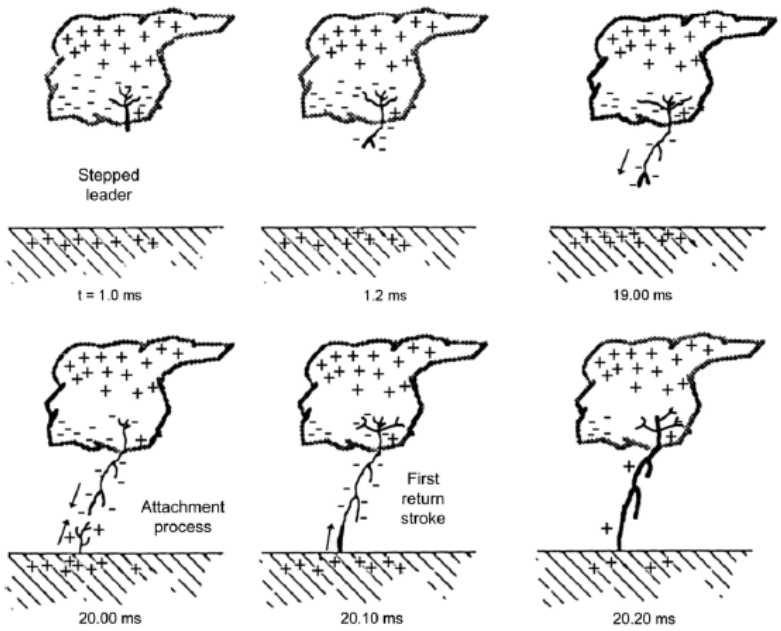

Figura 7. Esquema del proceso de descarga de un CG negativo. Tomado de Dwyer and Uman (2013).

Los rayos CG positivos descendentes son estadísticamente menos frecuentes que los negativos, mayormente detectados en los inicios de la fase de madurez o en su fase de disipación, así como durante tormentas de invierno. Debido a su naturaleza, estas descargas provienen de la parte superior de la nube, donde se sitúa la región de carga positiva en una estructura típica tripolar, tal y como se ha podido observar en la Figura 6. Típicamente no presenta tantas ramificaciones como el anterior, aunque los posteriores procesos de RS tienen naturaleza similar. En cuanto a intensidades suelen alcanzar valores medios parecidos a sus respectivos negativos, pero los más intensos pueden alcanzar los 300 kA, con lo que pueden causar daños mucho más importantes que los primeros.

Los rayos CG ascendentes, tanto positivos como negativos, tienen un comportamiento parecido a sus respectivos descendentes, diferenciándose con qué región de carga de la nube interactúan (la región negativa para los líderes positivos, y la región positiva para los líderes negativos). A diferencia de los descendentes (mucho más frecuentes que los ascendentes), necesitan de una estructura elevada, típicamente con elementos terminados en punta, generando un fuerte campo eléctrico capaz de iniciar un líder estable que se propague hacia la nube. Dado el caso de que alcancen regiones de carga de las nubes, se producirían los procesos de RS antes mencionados.

2.5 Particularidades de las infraestructuras elevadas

Existen distintos tipos de infraestructuras elevadas que son susceptibles de ser afectadas por procesos eléctricos atmosféricos. Esto es debido a que estas están expuestas a campos eléctricos locales muy fuertes, justo debajo de las nubes de tormenta. Así, son más propensos a iniciar líderes de propagación ascendentes (e.g., Berger, 1967; Rachidi et al., 2008; Zhou et al., 2010). Entre estas, encontramos los aerogeneradores en los parques eólicos, así como las antenas de telecomunicaciones, torres elevadas de industrias, etc.

Se pueden observar algunas fotografías de muestra en la Figura 8. Este tipo de infraestructuras son susceptibles de sufrir tanto procesos de líderes descendentes desde la nube de tormenta como ascendentes desde la misma infraestructura. En el caso de las antenas, las cuales suelen localizarse en las zonas más elevadas de la orografía, presentan una especial exposición a rayos de invierno, debido a su mayor cercanía a las regiones de carga más bajas de las nubes.

Los aerogeneradores están localizados alrededor del mundo, y muchas de estas localizaciones tienen características totalmente distintas entre ellas. La posibilidad de caída de un rayo en estos aerogeneradores es difícil de determinar para la industria eólica, ya que entran en juego muchos parámetros (March, 2015).

Figura 8. Fotografías de antenas con afectaciones de rayos. A la izquierda, fotografía con un objetivo ojo de pez de un líder ascendente en el Niu de l'Àliga (Bagà, Barcelona). Créditos a *Lightning Research Group* (UPC). A la derecha, líder ascendente en la torre de comunicaciones de Collserola (Barcelona). Créditos a Carles Castillejo (@Castibalsera).

De forma general, y para cualquier estructura elevada, la exposición al riesgo de caída de rayos (N_d) viene muy vinculado con tres aspectos: la densidad de caída de rayos (N_g, típicamente expresado en número de impactos por km^2 y año), la altura efectiva de la estructura H (entendida como la suma de la altura real más el efecto topográfico), y las condiciones ambientales C_d (International Electrotechnical Commission., 2010). Como se puede deducir, el primer y tercer punto dependen íntegramente de las características de la localización de la edificación, y el segundo además influye la altura de la estructura en sí. El cálculo de esta densidad de caída sigue la siguiente ecuación:

$$N_d = N_g \cdot 9\pi \cdot H^2 \cdot 10^{-6} \cdot C_d \qquad (1)$$

Por ejemplo, en Europa la actividad eléctrica se concentra mayoritariamente durante los meses más cálidos, ya que está directamente relacionado con el calentamiento solar y la disponibilidad de vapor de agua en la atmósfera, resignando solamente el 3% de toda la actividad eléctrica anual a los meses invernales (Poelman et al., 2016). Aun así, y aunque globalmente se pueda observar un comportamiento similar con las tormentas de invierno, este hecho no es contrario a que estas pocas descargas invernales puedan ser muy energéticas y puedan causar grandes daños (Yokoyama et al., 2014). Esto también va ligado al hecho de que durante el invierno se presentan las condiciones más favorables para la iniciación de rayos ascendentes desde infraestructuras elevadas, como por ejemplo los aerogeneradores, debido a la baja altura de la capa de carga negativa principal de las

tormentas (Montanyà et al., 2014). En Montanyà et al. (2016) se presentó un mapa global de la actividad eléctrica atmosférica durante los periodos de invierno, aportando una herramienta para identificar áreas de riesgo de actividad eléctrica invernal cuando se realicen avaluaciones de riesgo para la implementación de infraestructuras elevadas, como los ya nombrados aerogeneradores. Este mapa se puede observar en la Figura 9 (Montanyà et al., 2016).

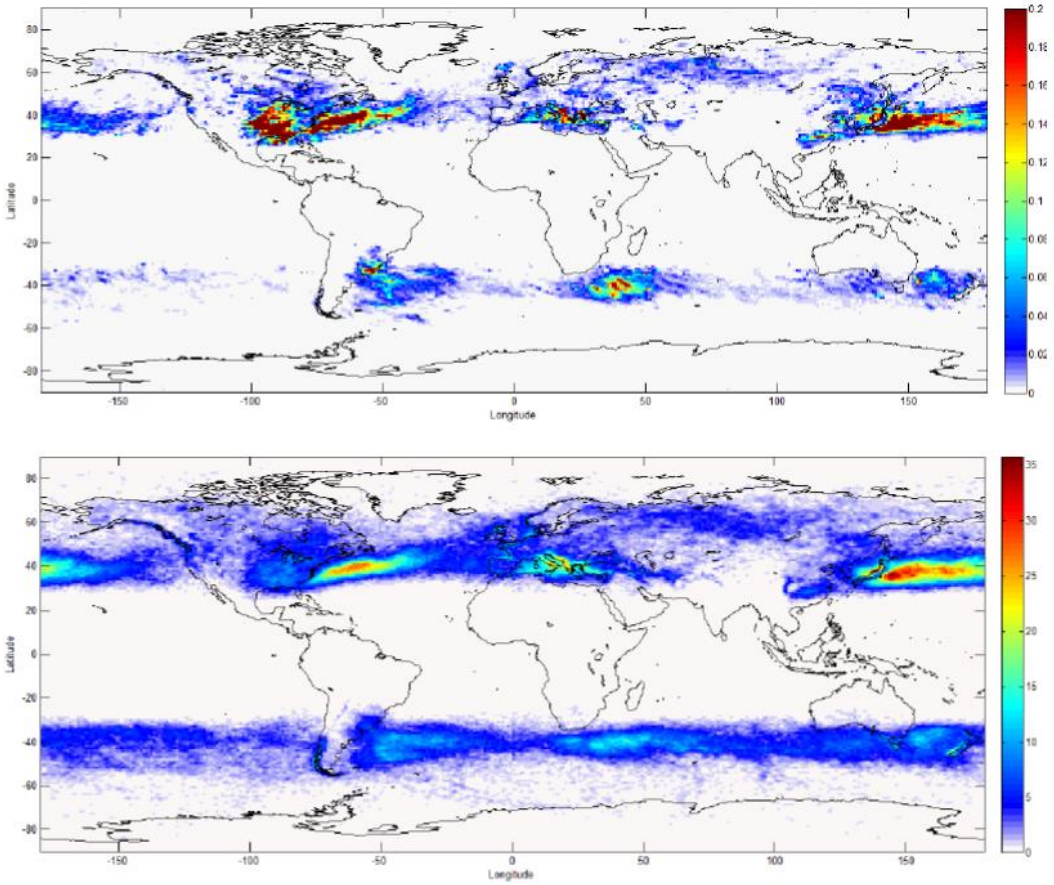

Figura 9. Arriba, la distribución global de densidad de descargas eléctricas de invierno (descargas/km$^2 \cdot$ año). Debajo, número medio de tormentas de invierno por año. Ambas corresponden al periodo de estudio 2009-2013 (Montanyà et al., 2016).

Así, se puede observar como un conjunto de aerogeneradores pueden ser afectados por la actividad eléctrica derivada de una tormenta a lo largo de todo el año, tanto de descargas que provienen de la misma nube de tormenta, como de rayos ascendentes, derivados de la gran diferencia de carga entre la superficie y el nivel de carga inferior negativa de la tormenta. Además, destacando las diferencias de esta última en situaciones de meses más cálidos y meses de invierno, que determinan la altura de este nivel de carga de la tormenta. Estos distintos casos de posibles orígenes de las descargas, así como sus posibles destinos, se pueden ver representados en la Figura 10.

Adicionalmente, en la Figura 11 se puede observar una captura de un video realizado con una cámara de alta velocidad, en el que se pueden observar estos líderes ascendentes provocados por los aerogeneradores. Estas descargas eléctricas acostumbran a producirse a

intervalos regulares, con un periodo estrechamente relacionado con la velocidad de rotación de los mismos aerogeneradores. Es importante notar que algunas palas de los aerogeneradores presentan inicio de líder ascendente, causado por un importante campo eléctrico en el aire, pero no alcanzan el contacto con la nube que provocaría la posterior descarga eléctrica. Además, estas descargas se pueden llegar a producir a decenas de quilómetros respecto a los núcleos más activos de las tormentas. Esto conlleva a que las posibles alertas que se puedan generar a partir de la previsión de episodios de tormenta pueda tener un amplio radio de posible afectación.

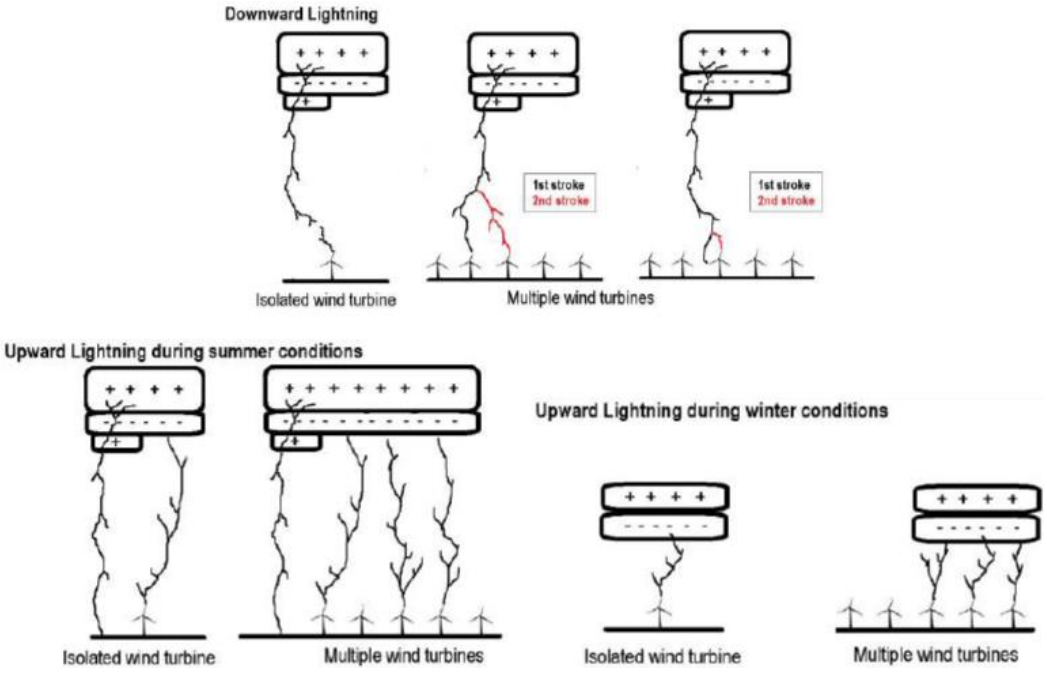

Figura 10. Situaciones en que múltiples descargas pueden impactar a un grupo de aerogeneradores, diferenciando los casos de descargas nube-tierra y descargas ascendentes. De estas últimas, se diferencian las condiciones de meses cálidos y meses de invierno (March, 2016).

Figura 11. Líderes ascendentes provocadas por aerogeneradores (Montanyà et al., 2014).

2.6 Lightning Location Systems (LLS)

En esta tesis se han utilizado tres sistemas distintos de detección de rayos (*Lightning Location Systems*, LLS). Los métodos de detección de estos dependen de las características de emisión electromagnética de cada tipo de rayo, es decir, en qué rango de frecuencia emiten mayoritariamente. Para ello, se diferencian las descargas IC, que emiten principalmente en frecuencias de radio más altas *Very High Frequency* (VHF), y las descargas de retorno en rayos CG, que emiten principalmente en *Low Frequency* (LF) y *Very Low Frequency* (VLF). Conociendo tales características, los principales métodos de detección de los LLS más comunes son los siguientes:

- *Time Of Arrival* (TOA). A partir de la diferencia de tiempos de detección de una misma emisión electromagnética por distintas antenas se determina la localización de la señal.
- *Magnetic Direction Finding* (MDF). Con capacidad de medición del campo magnético a partir de dos antenas ortogonales entre sí, se determina la dirección de la emisión electromagnética.
- Interferometría. De forma parecida al método TOA, pero usando diferencias de fase de longitud de onda entre la detección de cada antena para determinar su localización.

Adicionalmente, existen otros tipos de métodos de detección de rayos. El *Optical Imaging*, por ejemplo, basa la detección de los rayos en la detección óptica de la luz que emiten las descargas. Para más detalles sobre los sistemas y métodos de detección, consultar Nag et al. (2015). Así mismo, la lista siguiente pasa a detallar los sistemas de detección usados durante la tesis, así como sus características principales.

- *Xarxa de Detecció de Descàrregues Elèctriques* (XDDE). Red gestionada por el Servei Meteorològic de Catalunya (SMC), la cual trabaja en el rango del VHF (110 – 118 MHZ) con un antena con cinco dipolos para detectar los IC con interferometría (Lojou and Cummins, 2006), y en LF utilizando una antena de campo eléctrico para la detección de los CG, utiliza una técnica combinada de TOA/MDF (Cummins and Murphy, 2009). Actualmente está formada por cuatro sensores Vaisala LS-8000 (Pineda and Montanyà, 2009; Pineda et al., 2011). Montanyà (2014) evaluó el rendimiento de este sistema, determinando una eficiencia de detección entre el 80-85% para los CG.
- *Lightning Detection Network* (LINET). Desarrollada en la Universidad de Múnich y actualmente gestionada por *nowcast GmbH*, el cual trabaja tanto en LF como VLF, y proporciona información de rayos tanto para proyectos de investigación como para empresas y usuario final (Betz et al., 2009a). Basa su sistema de detección en el método TOA. Para más información pueden consultar Betz et al. (2009) y Höller et al. (2009).

- *Lightning Mapping Array* (LMA). Red de sensores VHF (Rison et al., 1999; Thomas et al., 2001, 2004) que, de forma pasiva, reciben impulsos en un rango de 60 – 66 MHz. Su localización de los rayos mediante técnica TOA le permite reconstruir el canal del rayo de forma tridimensional en el tiempo y espacio gracias a una frecuencia de detección de unos 80 µs. De esta manera, se pueden llegar a ver fácilmente hasta dos o tres mil señales por rayo, las cuales permiten realizar esta reconstrucción.

2.7 Potencialidades del LMA en el análisis de la altura de los estratos de carga.

Existen distintos procesos por el cual se puede determinar la estructura eléctrica de una tormenta, como pueden ser mediciones con globos y detectores de campo eléctrico. También se pueden determinar indirectamente a partir de las detecciones de los líderes con un sistema LMA para la determinación de esta estructura a partir de la localización de las descargas dentro de la nube de tormenta. En la Figura 12 se puede observar un diagrama simplificado de los componentes de un sistema LMA.

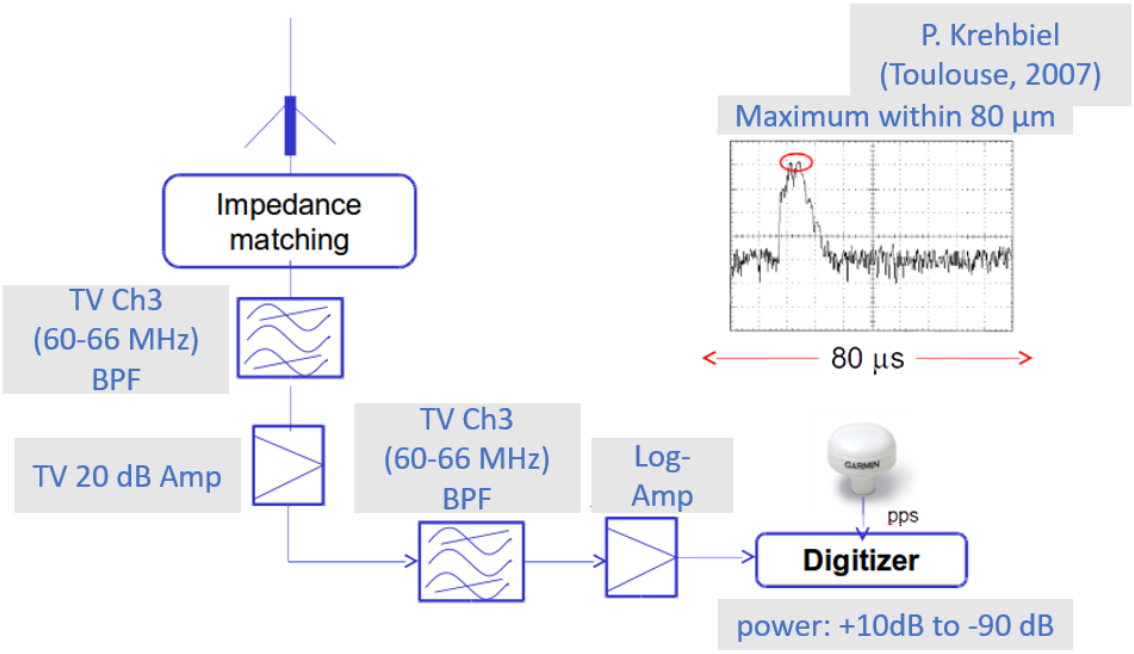

Figura 12. Diagrama de los componentes principales de un sistema LMA (basado en Rison et al. (1999) y Thomas et al. (2004)).

Estas características permiten que, para cada rayo, el sistema LMA detecta e identifica los líderes, pudiendo caracterizar las tormentas a las cuales se asocia actividad eléctrica. También gracias a la capacidad de otorgar un valor de potencia a cada señal, se pueden llegar a diferenciar las distintas polaridades de los estratos de carga, debido a que el conjunto de las señales de polaridad negativa es más fuerte que las de polaridad positiva. Posteriormente, la determinación de los estratos de carga se estima a partir de la altura donde estos líderes se desplazan. Sin embargo, es un aspecto sobre el cual todavía se está

trabajando y no se dispone de mucha observación. Un ejemplo de representación de esta reconstrucción de un rayo a partir de los sensores LMA puede ser el representado en la Figura 13 (Van Der Velde and Montanyà, 2013).

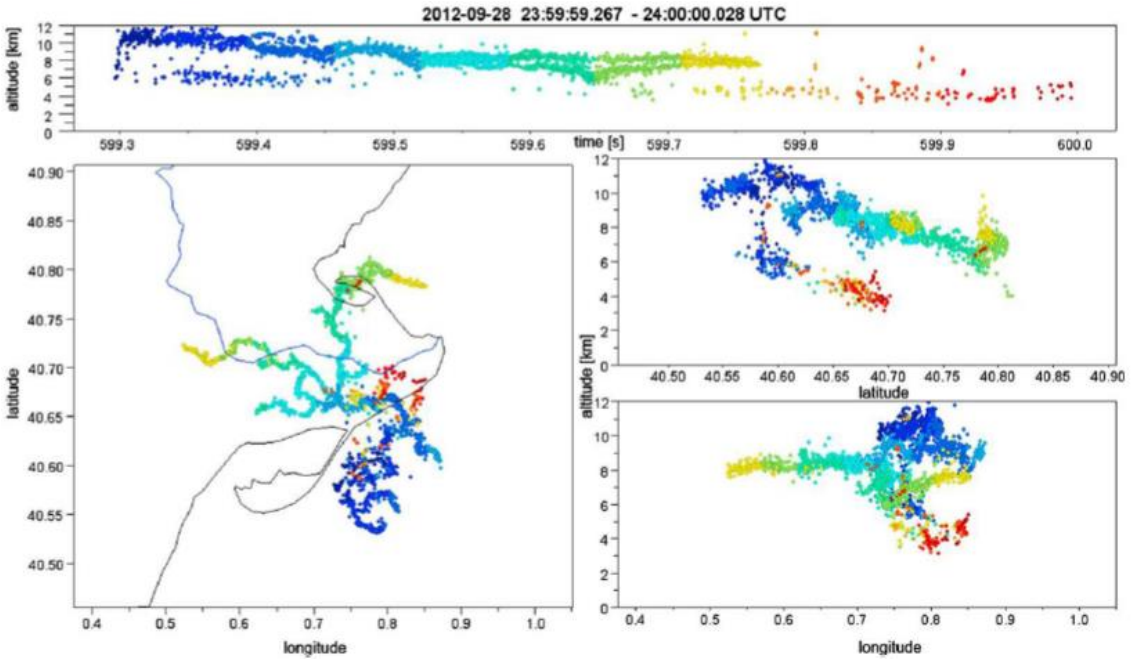

Figura 13. Ejemplo de reconstrucción de una descarga eléctrica IC con los detectores LMA. Arriba se puede observar una representación de estas señales en altura y tiempo, donde cada señal está coloreada según el tiempo desde el inicio del rayo. Abajo a la izquierda se puede observar una representación en planta, y a su derecha la altura frente a la latitud y la longitud (Van Der Velde and Montanyà, 2013).

Gracias a que podemos conocer en un momento puntual la estructura eléctrica de la tormenta y que se conoce que la dinámica eléctrica de una tormenta está fuertemente conectada con su desarrollo microfísico y dinámico, conjuntamente con una fuerte relación entre la convección de una tormenta y su intrínseca actividad eléctrica, se puede llegar a definir la fase actual de una tormenta. Esta se define como la etapa de la tormenta dentro de su ciclo de vida, las cuales han sido detalladas en el apartado 2.1. A partir de esto, se podría proporcionar no solo una previsión de tiempo severo, sino también añadirle otras características, como por ejemplo la duración esperada de este episodio y su intensidad.

En la Figura 14 se puede observar otra representación de una descarga de un rayo con el sistema LMA. A diferencia del anterior, se indican las potencias detectadas por cada señal. Esto permite, debido a la mencionada sensibilidad del sistema por las señales negativas, una identificación aproximada las señales según su polaridad, con las señales negativas indicadas por colores más cálidos y las positivas por colores más fríos. Así, se estructura la tormenta por una región de carga positiva y negativa, respectivamente. Adicionalmente y como ejemplo, en la parte superior de la figura, se observa un descenso vertical desde el nivel positivo de carga cerca del eje temporal horizontal en 447.4 ms, indicando la potencialidad del LMA para la identificación de descargas CG.

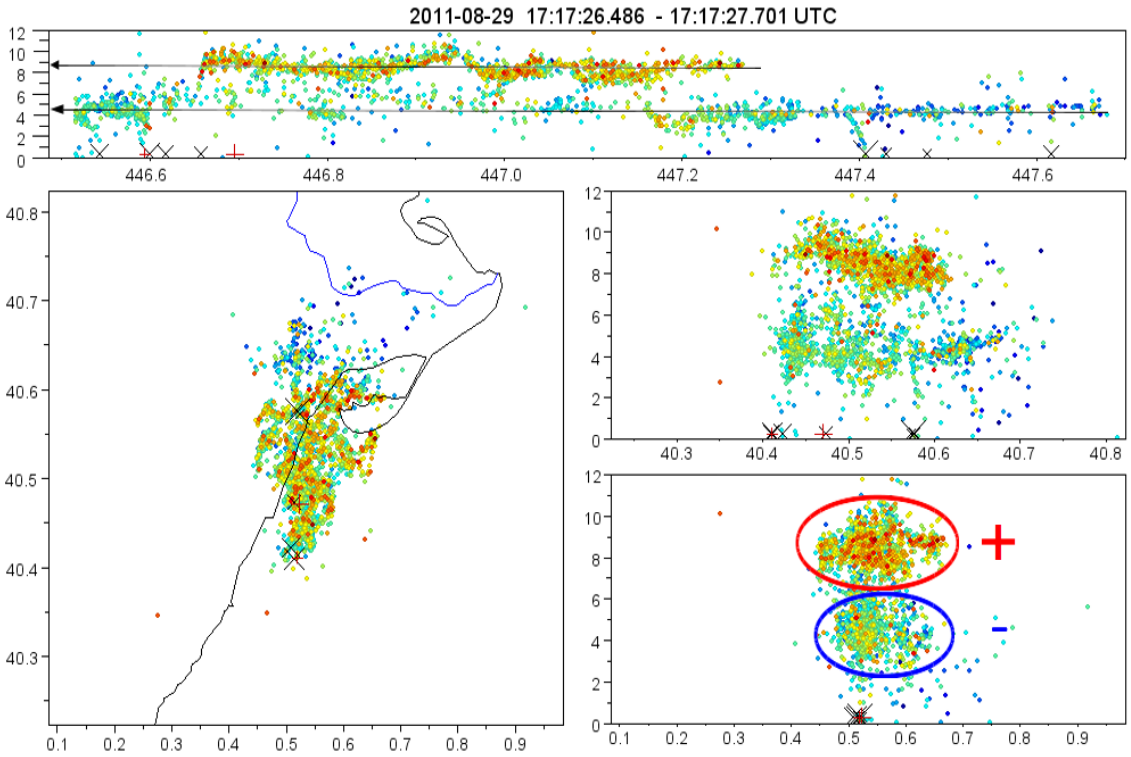

Figura 14. Representación de una descarga eléctrica con los detectores LMA. Igual que la Figura 13, pero en esta ocasión se colorean las señales por su potencia de detección. En la parte superior se añaden unas flechas indicando la posición donde se determinan las alturas de los niveles de carga. Abajo a la derecha se hace una categorización de polaridades de cada región a partir de sus potencias. A modo orientativo, las señales detectadas por el sistema XDDE se añaden con cruces rojas y negras, indicando su polaridad negativo y positivo, respectivamente. Figura adaptada de Van Der Velde and Montanyà (2013).

En julio de 2011, el grupo LRG, del Departament d'Enginyeria Elèctrica de la Universitat Politècnica de Catalunya (UPC), instaló un sistema LMA al Delta del Ebro (ELMA), formado por un conjunto de once estaciones. Este sistema fue implantado dentro del marco del proyecto *Atmosphere-Space Interactions Monitor* (ASIM), gestionado por la *European Space Agency* (ESA), y financiado por el Ministerio de Economía y Competitividad (MINECO), cuyo objetivo es la observación de tormentas eléctricas extremas, el vapor de agua, nubes y aerosoles y su interacción en la atmósfera. A lo largo del 2012, este sistema se fue ampliando gradualmente hasta alcanzar un máximo de once estaciones (Van Der Velde and Montanyà, 2013).

2.8 Radar meteorológico

El radar meteorológico proporciona información sobre las características de las partículas de precipitación, tanto sean gotas de lluvia, como granizo, nieve, etc., aportando datos de localización, intensidad, y velocidad respecto al radar, entre otros. Así, permite identificar los núcleos convectivos de las tormentas, su estructura y, tras un lapso de tiempo, calcular su potencial trayectoria y evolución.

Para el desarrollo de esta tesis ha sido imprescindible la utilización de información de la Xarxa de Radars (XRAD) del SMC. Esta red está formada por cuatro radares: Puig Bernat (PBE), Puig d'Arques (PDA), Creu del Vent (CDV) y La Miranda (LMI). La cobertura de estos radares, así como una fotografía del radar de CDV se pueden observar en la Figura 15. Estos radares operan en la banda C (5,600 – 5,650 MHz) y son del tipo Doppler, es decir, son capaces de detectar la velocidad radial de las señales detectadas.

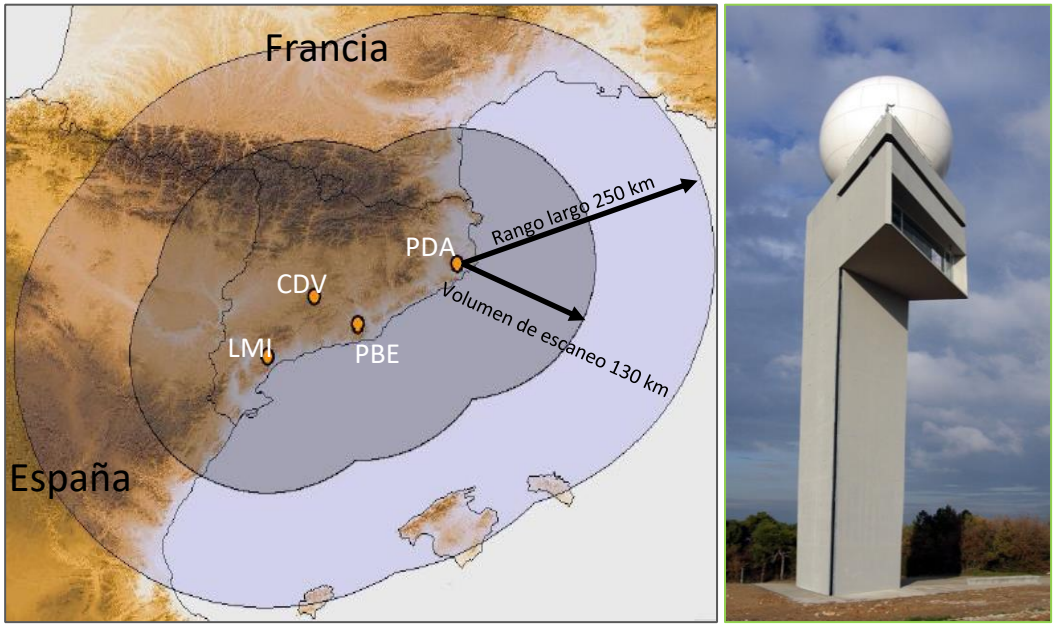

Figura 15. A la izquierda, rango de detección de la red XRAD del SMC, donde se señalan las posiciones de los radares meteorológicos que la conforman. Se diferencian entre los rangos cortos y largos de toda la red. A la derecha una fotografía del radar de CDV.

La red realiza 14 escaneos bidimensionales (llamados PPI – *Plan Position Indicator*) en que se va variando la el ángulo de elevación entre ellos, cada 6 minutos (Altube, 2016). La interpolación de los datos de cada uno de estos escaneos forma volúmenes polares tanto de reflectividad radar como de velocidades radiales, y permiten obtener observaciones a altitud constante (CAPPI – *Constant Altitude PPI*). Ambos son generados a partir de la interacción de los pulsos de las antenas en el rango de las microondas con los blancos interceptados, que típicamente son hidrometeoros en sus distintos estados (lluvia, nieve, granizo, etc.) que son devueltos hacia las antenas con valores distintos de energía dispersada. El tiempo que demoran en volver a la antena define la distancia, y por tanto posición, del blanco interceptado. Las distintas intensidades de energía dispersada que recibe la antena se definen como reflectividad (típicamente expresada en dBZ), que indican la intensidad de precipitación de los distintos tipos de hidrometeoros. En la conversión entre la energía recibida y el valor de reflectividad cabe tener en cuenta la dependencia con el tipo de hidrometeoro detectado (e.g., Kumijan, 2013). Para el caso del radar Doppler, las velocidades radiales son calculadas según la velocidad media de los blancos observados (Altube, 2016). En el caso del rango largo (hasta 250 km) solo se realiza un escaneo en el mismo periodo.

En este estudio se ha trabajado tanto con el producto CAPPI, que permite obtener una aproximación de la morfología de las nubes de tormenta, como el producto TOP. A veces también llamado *echotop*, indica la máxima altura que alcanza un cierto nivel de reflectividad en una zona concreta. Como ejemplo, en la Figura 16 se puede observar como a través de una proyección de un corte sobre el producto MAX (donde se representan los niveles máximos de reflectividad detectados según distintas proyecciones) se puede definir el nivel TOP-35 como la altura máxima alcanzada por el nivel de reflectividad de 35 dBZ.

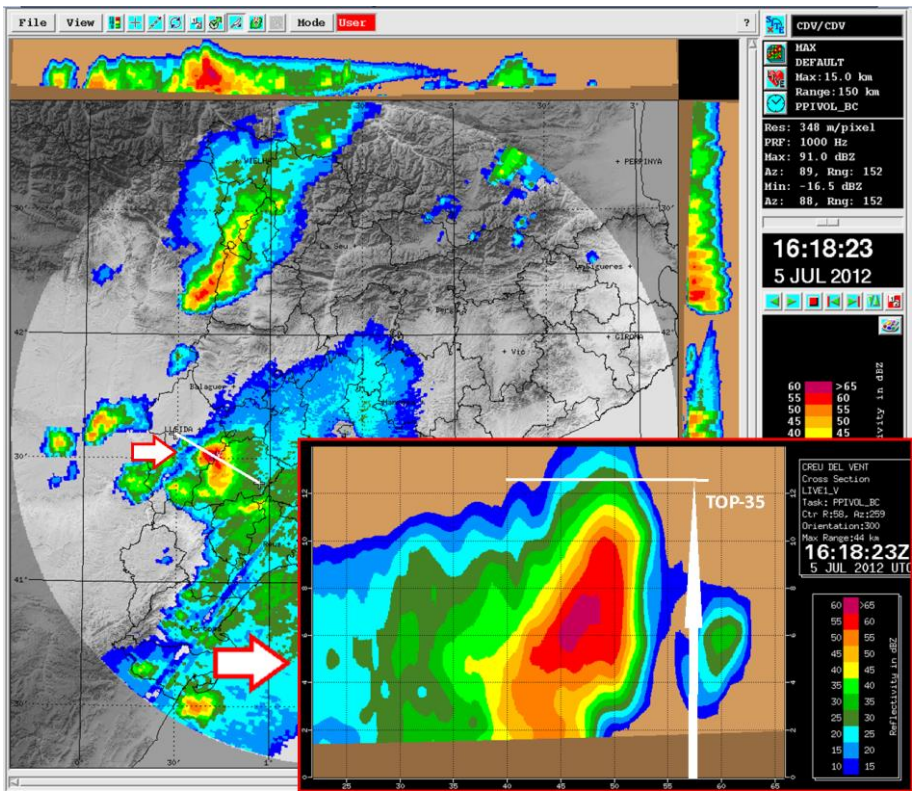

Figura 16. Producto MAX del radar meteorológico CDV. En el centro se representa la reflectividad máxima en proyección LAT vs LON, arriba en proyección LON vs altura y a la derecha LAT vs altura. Se señala con una flecha un corte en el mapa central que se amplía en la figura inferior derecha. A partir de esta, y en este caso, se define la altura TOP-35 como la altura máxima que alcanza el nivel de reflectividad de 35 dBZ, señalada con una flecha blanca vertical.

Este producto TOP puede ser calculado para todos los niveles de reflectividad que detecta el radar meteorológico. De forma operativa, el SMC genera los productos de TOP-12 y TOP-35 (alturas máximas, típicamente en km, alcanzadas por los niveles de reflectividad de 12 y 35 dBZ, respectivamente). Estas alturas son definidas típicamente como la altura que alcanzan las nubes de precipitación y/o tormenta (e.g., Rosenfeld et al., 1993; Yuter and Houze, 1995), y como indicador del nivel de intensidad de precipitación que alcanzan las tormentas (e.g., Vincent et al., 2003; Yang and King, 2010; Liu et al., 2012), respectivamente. En la Figura 17 se puede observar una representación de este producto TOP-12, donde se puede observar con la escala de colores indicada las distintas alturas máximas alcanzadas del nivel de reflectividad de 12 dBZ según la localización de detección.

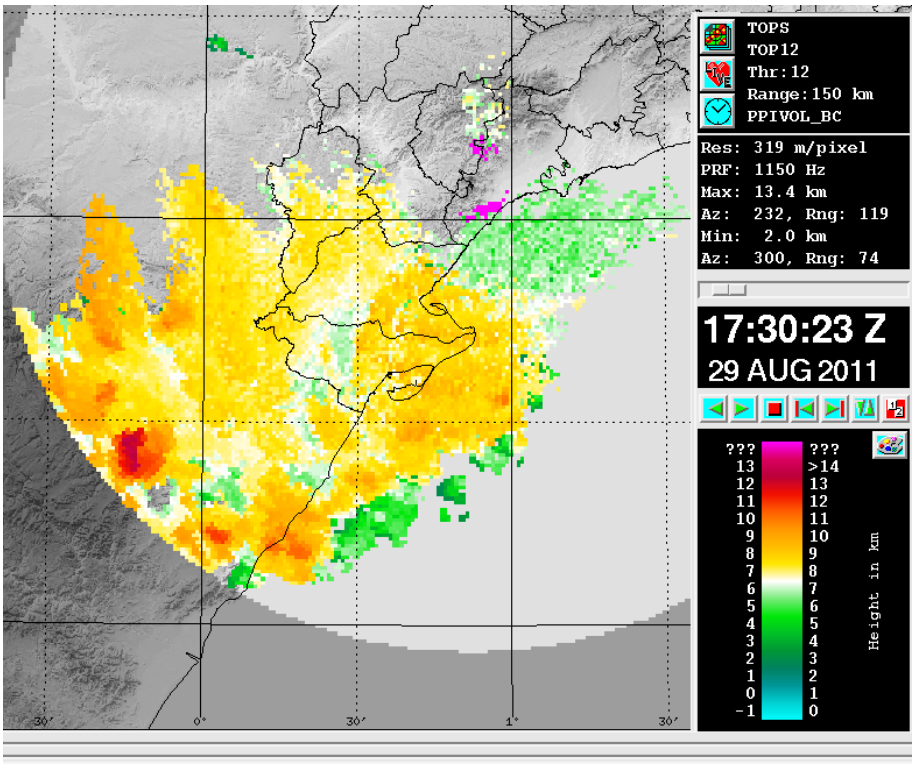

Figura 17. Producto TOP-12 del radar LMI. En él se representan con la escala de colores indicada las alturas máximas que alcanza el nivel de reflectividad de 12 dBZ.

Esta información de los TOP-12 y TOP-35 ha sido combinada con las alturas de las isotermas en las zonas de estudio, obtenidas mayoritariamente con información del radiosondeo de Barcelona o con datos del modelo WRF (*Weather Research and Forecast*) (Mercader-Carbó et al., 2010). Esto ha permitido conocer cuando algunos de estos TOP han superado o no han alcanzado ciertas alturas de isotermas, típicamente vinculadas con las regiones de fase mixta (entre las isotermas de -10°C y -25°C, indicando la localización del dipolo graupel-hielo. Más información en 2.2), o incluso si han alcanzado la altura de la tropopausa.

Las alturas de estos TOP a lo largo del año han permitido definir algunas características de estas alturas frente a la presencia de actividad eléctrica atmosférica en la zona de estudio. Así, se han combinado la información de descargas eléctricas con las alturas de los distintos TOP de referencia. Esto ha permitido, entre otros, poder observar casos de tormentas eléctricas en periodos más fríos que, aunque no alcanzaban alturas muy elevadas debido al menor poder convectivo respecto a periodos más cálidos, presentaban actividad eléctrica e, incluso, descargas hacia tierra, con casos de afectaciones en infraestructuras elevadas como los aerogeneradores.

3 Artículos integrantes del compendio

3.1 Seasonal variations on the conditions required for the lightning production

3.1.1 Introducción y metodología

Tradicionalmente se relaciona la presencia de actividad eléctrica en las nubes de tormenta con el potencial convectivo de estas (e.g., Macgorman et al., 1989; Williams et al., 2005; Deierling and Petersen, 2008). Así mismo, se considera que la altura alcanzada por la tormenta está directamente relacionada con los niveles de convección profunda. Sin embargo, esta relación normalmente se vincula con la altura que consiguen alcanzar ciertos niveles de reflectividad radar, típicamente los comprendidos entre los 30 y 40 dBZ. Por lo tanto, es mejor usar una relación con mayor base física, como las alturas de los niveles de reflectividad radar mencionados, directamente relacionados con los hidrometeoros que participan en el proceso de carga eléctrica. Entre estos, se destaca especialmente que alcancen la región de fase mixta entre las isotermas de -10°C y -25°C. Es en esta región donde se encuentran muchas partículas cargadas debido a procesos NIC, efecto que provoca una alta relación con las intensidades de descargas eléctricas. Este proceso depende mucho de la temperatura, con lo que conviene convertir una dependencia de los niveles de reflectividad con la altura hacia una dependencia con la temperatura, dicho de otro modo, los niveles de las isotermas. Múltiples estudios han establecido relaciones entre estas, observándose relativas invariancias entre distintas regiones climáticas y distintos tipos de tormentas (e.g., Vincent et al., 2003; Shindo et al., 2015). Así, y teniendo en cuenta la alta variabilidad de alturas de distintas isotermas, especialmente en zonas de latitudes medias, se propone evaluar estas alturas para identificar, con extensión a todas las estaciones del año, su posición respecto a la superficie. Esta tendrá especial atención en los periodos menos cálidos, típicamente más olvidados debido a la menor frecuencia de detección de tormentas eléctricas, en comparación con las estaciones más cálidas.

Este estudio surge de la necesidad de buscar unos indicadores meteorológicos simples para todo el año de electrificación de las nubes de tormenta. Debido a la dependencia de los procesos de electrificación con la temperatura, las alturas alcanzadas por el umbral de reflectividad seleccionado no son las mismas según el mes del año. Esto permitiría, solo observando las alturas de ciertos niveles de reflectividad y las de las isotermas del radiosondeo o de predicción de modelo, anticiparse a episodios de tormentas que puedan conllevar actividad eléctrica. Así, la realización de avisos sería lo más pronto posible para tomar las medidas de protección necesarias. A su vez, se pretende observar si relaciones entre las alturas máximas de las tormentas con la intensidad eléctrica de estas, concuerda con la de otras zonas de estudio y, al mismo tiempo, es aplicable a distintas estaciones del año.

La zona de estudio, tal y como se detalla en el artículo, presenta un especial interés para un estudio estacional de la actividad eléctrica, ya que esta es detectada durante todo el año, no solo durante las estaciones cálidas, aunque sí más frecuentes, especialmente durante los meses de junio a octubre. Además, su cercanía al mar Mediterráneo proporciona condiciones favorables para la actividad eléctrica en otoño e invierno, siendo la temperatura del mar un factor determinante.

El anteriormente mencionado radiosondeo de Barcelona proporciona en este artículo una climatología de las isotermas de $-10°C$ y $-40°C$, así como la altura de la tropopausa, por un periodo de 17 años entre 2001 y 2017. Estos datos, con más de 12,000 sondeos en total (dos observaciones diarias, a las 00 y 12 UTC), proporcionan una información robusta respecto a las alturas típicas a las que encontramos los distintos niveles mencionados. Así, en el artículo se representan con sus respectivos rangos intercuartiles diarios para todo el año, permitiendo observar de forma clara su oscilación a lo largo del año. También obtenemos los valores de índice CAPE (*Convective Available Potential Energy*) (Wallace and Hobbs, 2006) derivado de la información del radiosondeo.

La red de radares del SMC participa en este estudio con las alturas máximas alcanzadas de los niveles de reflectividad de 12 y 35 dBZ, mencionadas en el artículo como TOP-12 y TOP-35, para la zona de estudio, con una frecuencia de medición de 6 minutos. En este caso, el periodo de medidas obtenidas comprende los años entre 2013 y 2017.

El último parámetro que analizamos en la zona de estudio es la actividad eléctrica atmosférica a partir del XDDE. Para el mismo periodo de estudio que el de los niveles de reflectividad radar (entre 2013 y 2017), se obtienen los valores de ratio total de rayos TFR (*Total Flash Rate*), así como un indicador binario de presencia / no presencia de descargas eléctricas en la zona.

3.1.2 Conclusiones

Del artículo se extraen distintas conclusiones:

- A comparativa con otros estudios como Williams (1985), se ha encontrado una relación de quinta potencia entre la altura de las tormentas y el ratio de descargas eléctricas en tormenta para todo el año, a excepción del invierno, donde se reduce a una tercera potencia.
- El índice CAPE, útil para la previsión de condiciones favorables a la formación de tormentas, no se postula suficiente para la determinación cuantitativa de las ratios de descargas de nube.
- Se postulan como indicadores los niveles de reflectividad de 12 dBZ y 35 dBZ alcanzando las alturas de las isotermas de $-40°C$ y $-10°C$, respectivamente, como predictores de la iniciación de rayos. Con ellos, los valores de POD están por encima de 60% durante todo el año, aunque con valores FAR ligeramente altos. Para reducir este último, sin reducir significativamente la probabilidad de detección, se

propone el nivel de 35 dBZ alcanzando la isoterma de −10°C como el mejor aplicable durante todo el año.

- La climatología de la isoterma de −10°C en el área de estudio alcanza bajas alturas, hasta 1.5-2.0 km durante el invierno, pudiendo implicar afectaciones a infraestructuras elevadas en superficie causadas por rayos ascendentes, así como sus respectivas descargas de retorno.
- Se destaca la gran potencialidad de uso de estos indicadores que combinan reflectividad radar y altura de las isotermas para la pronta emisión de avisos a múltiples sistemas de alarma y *nowcasting* para que anticipen las posibles tormentas eléctricas con el máximo de anticipación posible. A su vez, destacar nuevamente la problemática de las regiones de carga a baja altura en periodos fuera de temporada que facilitan procesos de rayos ascendentes en múltiples tipos de infraestructuras elevadas.

3.1.3 Artículo y referencia

Salvador, A., Pineda, N., Montanyà, J., Solà, G., 2020. Seasonal variations on the conditions required for the lightning production. *Atmospheric Research*, 243: 104981. doi: 10.1016/j.atmosres.2020.104981.

Seasonal variations on the conditions required for the lightning production

Albert Salvador [a,b], Nicolau Pineda [a,b], Joan Montanyà [b], Gloria Solà[b]

[a] Meteorological Service of Catalonia, Carrer Berlín 38-46, 08029 Barcelona, Spain

[b] Lightning Research Group, Technical University of Catalonia, Carrer Colom 1, 08222 Terrassa, Spain

ABSTRACT

Given the growing concern on lightning threats outside the main warm-season, the objective of this study is to get further insight on the seasonal variations of the necessary conditions required for the production of lightning. In this regard, the study aims to find a basic indicator of cloud electrification that could be useful as an all-year-round robust predictor to warn about lightning threats. To this end, a large dataset of weather radar data products, total lightning observations and radiosounding isotherm heights have been used.

According to previous studies, the radar storm height is tightly correlated with the total lightning flash rate. A fifth order relationship fits from spring to autumn and a third order power law in winter. In spite of the good correlation between the radar storm height and the total lightning flash rate, the vertical development alone may be insufficient as a basic indicator for thunderstorm conditions. Alternatively, two different predictors for the lightning onset have been analysed: 12 dBZ radar reflectivity echoes reaching the –40°C isotherm height and 35 dBZ reflectivity echoes reaching the –10°C. Results show that the most suitable all-year-round predictor is the TOP-35 above –10°C.

KEYWORDS: radar storm height, total lightning flash rate, lightning predictor

1. Introduction

For many years, the relationship between the lightning flash rate and thunderstorm characteristics such as the vertical structure of radar reflectivity in thunderstorms has been a topic of study (e.g., Williams et al., 1989; Carey and Rutledge, 1996; Schultz et al., 2011). Indeed, this is a subject of great interest, not only for understanding thunderstorm electrification, but also for other fields like nowcasting (e.g., Gatlin and Goodman, 2010; Farnell et al., 2017); lightning protection (e.g.,

Rachidi et al., 2008; March, 2017); nitrogen oxide (NOx) concentration modelling (e.g., Mecikalski and Carey, 2017) and lightning parameterization in model convective schemes (e.g., Price and Rind, 1994; Mazarakis et al., 2009; Karagiannidis et al. 2019). Convective updraft is a key component of cloud electrification, since it drives the development of graupel and ice crystals, enhancing particle collision and providing a means to charge separation that ultimately leads to lightning production. Williams (1985) proposed a relationship in which the total lightning flash rate (TFR) increased as the fifth power with the maximum height of the storms. Ushio et al. (2001), Futyan and Del Genio (2007) and Yoshida et al. (2009) reported a similar relationship from satellite data.

The onset of lightning has been typically associated with the exceedance of a certain limit of reflectivity at a given height (e.g., MacGorman and Rust, 1999, Chapt.7). However, a high vertical development is not always related to strong convective currents leading to charge separation, so this relationship is not straightforward. Studies such as MacGorman et al. (1989) and Carey and Rutledge (1996) concluded that the TFR of a storm is correlated with the level of radar reflectivity comprised between 30 and 40 dBZ that reaches the mixed-phase region. This relationship can be explained by the increase of charged particles due to the non-inductive charging mechanism (hereafter, NIC) (Takahashi 1978; MacGorman et al. 2008). The NIC mechanism as a dominant source for lightning production is supported by the strong correlations found between the amount of precipitation ice and the TFR using ground-based radar reflectivity and lightning observations in field campaigns (e.g., Williams et al., 1989; MacGorman and Rust, 1999; Deierling et al., 2008; Liu et al. 2012).

Since the NIC process is temperature sensitive, it is convenient to convert the height dependence of radar reflectivity into temperature dependence. Several studies have analysed the correlation between radar-derived storm characteristics like radar reflectivity and the sufficient heights of the isotherms to reach the conditions required for the lightning production. Among them, Dye (1989) established that the level of reflectivity of 40 dBZ has to reach the isotherm of −10°C to initiate electrification, and others such as Gremillion and Orville (1999), Yang and King (2010) and Wang et al. (2016) used the same criteria for the appearance of cloud-to-ground discharges. Gremillion and Orville (1999) also established a relationship between the height of the −15°C and −20°C isotherms and the reflectivity levels of 30 dBZ and 20 dBZ respectively, to indicate the start of the electrical activity. In addition, Liu et al. (2012) concluded that the flash rate of a storm is well correlated with the volume of high radar reflectivity (35 dBZ) within the mixed phase region (between the −5°C and −35°C isotherms).

Interestingly, it seems that there is a relative invariance of this relationship between different climatic regions and different types of storms (Vincent et al., 2003; Shindo

et al., 2015). For example, Michimoto (1991) found that these isotherm temperature levels are also applicable to winter storms. Keeping in mind the dependence of the electrification processes on temperature, cloud charges are at lower altitudes in winter, favouring interaction with ground structures such as towers and wind turbines. Under these conditions, wind turbines and other tall man-made structures are prone to trigger upward leaders (Wang and Takagi, 2012; Montanyà et al., 2014a; Warner et al., 2014, Pineda et al. 2018) which can be followed by one or more downward-leader-return-stroke sequences, similar to those in downward lightning (Rakov and Uman, 2003 Ch. 4). Kingfield et al. (2017) found a fourfold increase in lightning densities on tower locations during autumn/winter. Additionally, winter storms can produce very energetic lightning events and a large amount of damage (e.g., Yokoyama et al., 2014, Schultz et al. 2018).

To better understand these relationships, it should be further investigated in different kinds of weather regimes and in different seasons, as pointed out by Liu et al (2012).

Bearing in mind the growing concern on lightning threats outside the main warm-season, the objective of this study is to get further insight on the seasonal variations of the conditions required for lightning production. In this regard, the study aimed to find a basic indicator of cloud electrification, which in turn can be useful as an all-year-round robust predictor to warn about lightning threats and to set up lightning parameterizations in model convective schemes. To this end, a large dataset of convective system properties derived from weather radar, total lightning observations and radiosounding isotherm height measurements have been used for the seasonal analysis. Skill scores have been calculated to determine the degree of diagnostic ability of the proposed predictors.

The organization of the paper is as follows: Section 2 describes the studied area, the different data used and the methodology of the analysis; Section 3 presents the main results obtained, Section 4 deals with the discussion of the results and finally section 5 presents the summary and conclusions.

2. Data and Methodology

2.1. Studied Area

The area of study (hereafter AoS) is the Ebro's river mouth region, in the north-eastern part of the Iberian Peninsula (Fig. 1). This area is interesting for a seasonal analysis since lightning activity is present allthroughout the year, not only in the warm season (e.g., Soriano et al., 2001; Montanyà et al., 2016; López et al., 2017; Pineda et al., 2018). Although lightning activity is concentrated during the "warm season" (June to October in the AoS), the proximity to the Mediterranean Sea

provides favourable conditions for autumn and winter activity, the warm waters being the driver for storm development. (e.g., Kotroni and Lagouvardos, 2016; Galanaki et al., 2018; Rigo et al., 2019).

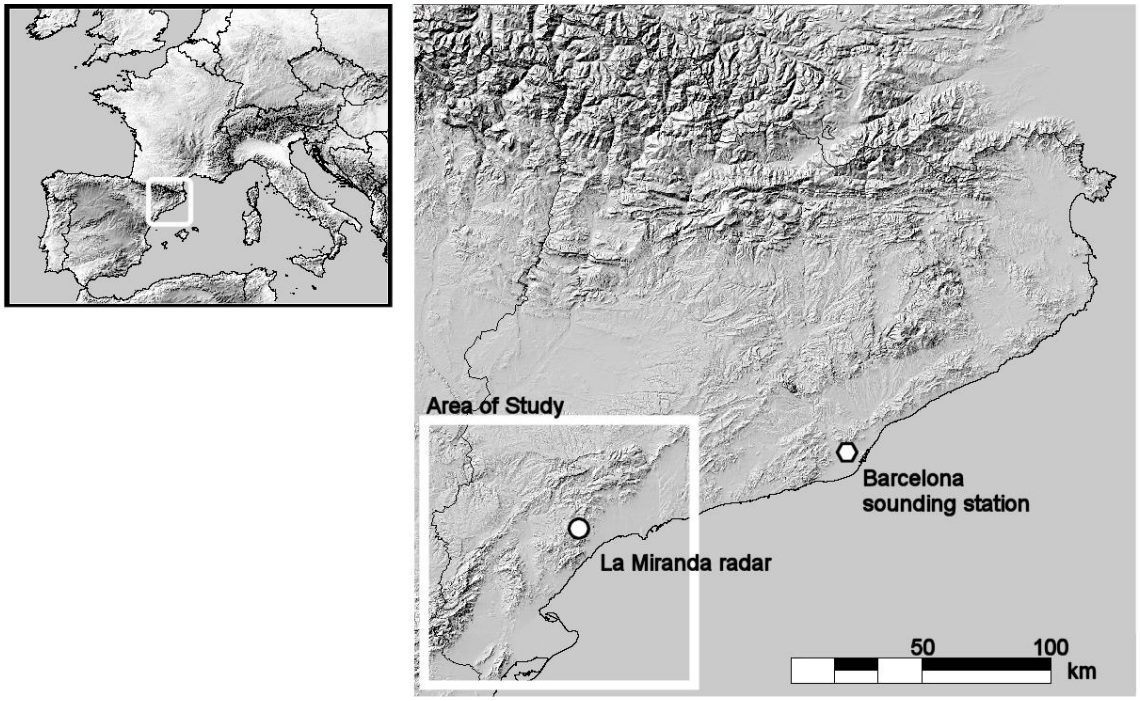

Figure 1. The Area of Study (AoS); Ebro river mouth region, in the north-eastern part of the Iberian Peninsula and in the western Mediterranean basin. The black circle inside the AoS corresponds to "La Miranda" radar (N 41° 05′ 30.24″ E 0° 51′ 48.58″; 950 m above MSL), and the outside one corresponds to Barcelona sounding station (N 41° 23' 4.08" E 2° 7' 3.36" – N° WMO: 08190).

2.2. Data used

Atmospheric Soundings

The heights of the significant isotherms in the current analysis (–10°C, –20°C and –40°C) have been obtained from radiosounding data. The closest sounding station to the AoS is Barcelona (N 41° 23' 4.08" E 2° 7' 3.36" – N° WMO: 08190), which is operated by the Meteorological Service of Catalonia (Servei Meteorològic de Catalunya, hereafter SMC). Since December 2008, the radiosonde of Barcelona belongs to the World Meteorological Network through the GTS (Global Telecommunication System). Daily measurements (every 12h) from the years between 2001 and 2017, resulting in 12410 soundings, have been used to calculate daily averages of the height for the mentioned isotherms, as well as the for tropopause.

In particular, the height of the tropopause has been determined according to the following criteria. By convention, it is defined as the level at which the temperature gradient is below -2°C km^{-1}, also provided that the average gradient between this

level and all higher levels within 2 km does not exceed -2°C km^{-1} (Manual on Codes - International Codes, WMO 2011). In reality, it is possible to find different levels in which these conditions are fulfilled along the vertical profile. The lowest case level is called "first tropopause", and this is the one that will be used in this study. Indeed, the definition allows determining the first tropopause from a single radiosonde ascent (Wilcox et al., 2012).

In addition, the CAPE index (Convective Available Potential Energy, Wallace and Hobbs, 1973) obtained from the Barcelona radiosonde has also been used. The magnitude and vertical distribution of CAPE play an important role in determining the updraft velocity and the size and vertical distribution of the hydrometeors that participate in the charge separation (Williams et al., 2005). The convective updraft must be strong enough to ensure supercooled liquid water is replenished and graupel is lifted above the charge-reversal temperature zone (-15° C to -20° C) (Zipser and Lutz 1994). Most of the studies in the extratropics show good correlation between these two parameters (Carey and Rutledge, 1996; Ushio et al., 2001; Boccipio, 2001; Zhou et al., 2002).

Weather Radar

Weather radar has been used to determine thunderstorm characteristics like the maximum height reached. The SMC operates a weather radar network in the region, consisting on four C-band (5600 to 5650 MHz) Doppler radars. The closest radar to the AoS is “La Miranda” (N 41° 05′ 30.24″ E 0° 51′ 48.58″; 950 m above MSL) (Fig. 1). Polar volumes are acquired every 6 minutes, in a fourteen-elevation scan scheme. Further technical details of the SMC weather radar systems and network characteristics can be found in Bech et al. (2004) and Argemí et al. (2014).

Cloud phase identification using single polarization radar data is challenging in the 0 to −40°C temperature range, where both liquid and ice hydrometeor phases are sustainable. In the absence of dual-pol capabilities, the present work relies on the radar echo top product (TOP) and on the maximum height of radar echoes within an intensity equal or higher than a given reflectivity threshold. In particular, the TOP-12 and TOP-35 dBZ were selected among the operative products generated at the SMC. TOP-12 is a proxy for the maximum height reached by the thunderstorm (Rosenfeld et al., 1993), whereas TOP-35 is a proxy for the maximum convective intensity of precipitation systems (Liu et al., 2012). The analysed period encompassed observations for years from 2013 to 2017.

Lightning detection

Lightning data used in this study was collected by the SMC’s lightning location system (LLS). The SMC-LLS, which covers the Catalonia region (NE Iberian Peninsula), including the AoS, is composed of four total lightning detectors (Vaisala

LS-8000). LS-8000 combines VHF and LF to detect both intra-cloud (IC) and cloud-to-ground (CG) flashes (total lightning). On one hand, IC flashes are detected in the very high frequency (VHF, 110 to 118 MHz) region and located using interferometry (Lojou and Cummins, 2006). On the other hand, CG return strokes are detected by a low frequency (LF) sensor and located using a combination of the TOA/MDF (Time-of-Arrival/Magnetic Direction Finding) technique (Cummins and Murphy, 2009). CG strokes are grouped into CG flashes using an algorithm based on a time and a distance criterion (Cummins et al., 1998). Montanyà (2014b) evaluated the performance of the SMC-LLS, establishing a CG flash detection efficiency of about 80-85%. A detailed report of the SMC-LLS configuration can be found in Pineda and Montanyà (2009). Similar to the radar data, the lightning data used in this study includes the period between 2013 and 2017. At this point, it may be noticed that IC and CG data are combined into total lightning "flashes". That is, IC flashes and CG strokes are grouped by the Vaisala's flash algorithm (Cummins et al., 1998), which relies mainly on the lightning spatial extension and on its duration.

2.3. Methodology

In the present study, the seasonal variations of the necessary conditions for the lightning occurrence are analysed through total lightning data, the radar echo top product, the heights of the significant isotherms and CAPE index derived from radiosounding data.

The identification scheme applied considers two dichotomous categories: thunderstorm conditions and the lack of them. Precipitation structures in the AoS are characterised, on a 6-min basis (the time span of the radar volumes), by the radar TOP products TOP-12 and TOP-35, and binary labelled according to the presence of lightning. Heights of the isotherms and CAPE index associated to each 6-min time bin are derived from the nearest sounding.

Regarding the fifth power relationship between the radar storm height and the total lightning flash rate, the applied methodology follows the one presented in Williams (1985) and Ushio et al. (2001). This way, results can be compared directly. These authors performed a linear regression in a log-log graph using of the median flash in each 1 km interval of the thunderstorm height.

Additionally, a climatological seasonal cycle of the significant isotherms and tropopause heights has been elaborated from the 2001-2017 sounding database. On this basis, monthly averages of the TOP-12 and TOP-35 heights (both with and without lightning) were used to analyse the evolution during the year, as well as the seasonal variations.

Dichotomous (event/non-event) forecasts are often verified by using a 2 by 2 contingency table (Doswell et al., 1990). In the present study, this technique is used

to determine the degree of diagnostic skill of the two proposed metrics for identifying periods of lightning and no-lightning. Different skill scores can be derived from the contingency table. Most common are the Probability of Detection (POD) and False Alarm Ratio (FAR). More sophisticated skill scores are often more useful, as the Critical Success Index (CSI), the True Skill Statistic (TSS) (Murphy and Daan, 1985) or the Heidke skill score (Panofsky and Brier, 1958). For details on contingency tables and skill scores see for example Haklander and Van Delden (2003).

3. Results

3.1. Relation between Lightning Flash Rate and Radar Parameters

The first result presented is the relationship between the total lightning flash rate (TFR) and the thunderstorm maximum height derived from TOP-12. The plot has been split into seasons (Fig. 2), as it was found that this relationship changes throughout the year. A positive logarithmic correlation has been confirmed between the TOP-12 of the storm and its TFR. It applies above the 5 km height, as lightning activity with cloud tops (TOP-12) below 5 km heights is very low, mostly activity below 1 flash·min^{-1}. Interestingly, a correlation is observed for all seasons, even though the majority of events correspond to summer and autumn. Compared to winter and spring, the TFR reaches one order of magnitude higher rates, attaining in some cases 100 flashes per min^{-1}. Contrarily, the few episodes occurring during winter and spring seasons tend to have lower TOP-12 values, with a respective lower TFR. For each season, there is a maximum height that seems the storms cannot overcome, going from the lowest height in winter around 10 km and a maximum between summer and autumn around 15 km. Indeed, this maximum height is related to the tropopause, the height of which varies across the year. This is further discussed in section 3.3.

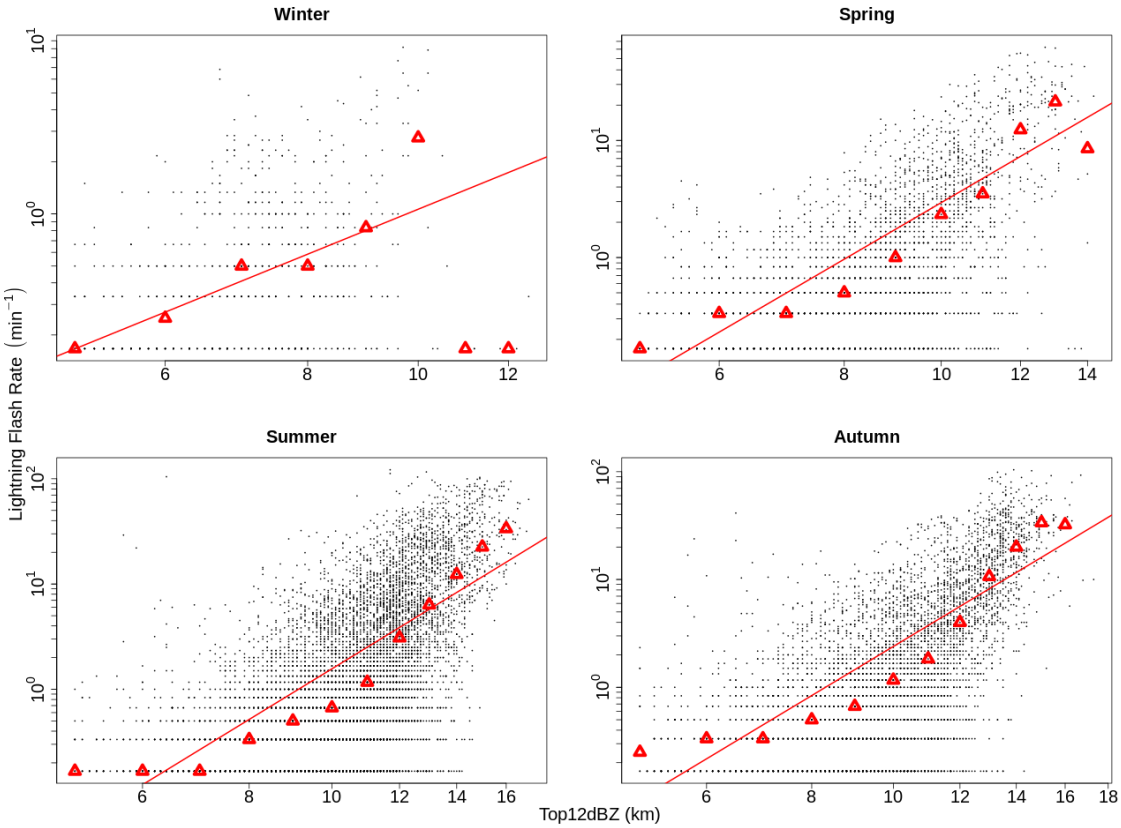

Figure 2. Seasonal scatterplots of the total lightning flash rate per minute as a function of the mean convective radar storm height (TOP-12) on a log-log plot. TOP-12 values have been shifted to 5 km to represent radar only those echoes above the 0°C isotherm. The triangles represent the median of the TFR at each km height (amsl). Least squares fit line to the triangles is shown in red.

Additionally, a trend line has been added to relate TFR with radar storm height (radar echo tops above the 0°C isotherm) in each season. Table 1 summarizes the correlations obtained through equation 1

$$\log(TFR) = \alpha \cdot \log(TOP\text{-}12) - \beta \qquad \text{(eq.1)}$$

Table 1. Estimates of the seasonal correlation parameters corresponding to eq.1

	α	β	R^2 (adjusted)	RMSE
Winter	2.6783±0.3352	2.6511±0.2818	0.9402	0.0523
Spring	4.9836±0.6195	4.5148±0.5850	0.8884	0.2173
Summer	4.9634±0.5599	4.7689±0.5639	0.8758	0.2753
Autumn	4.6966±0.5321	4.3180±0.5359	0.8748	0.2616

Note that the ratio factor between the TFR and the TOP-12 (α) indicates a fifth power relationship, in agreement with Williams (1985), Ushio et al. (2001) and Futyan and Del Genio (2007). Winter is the exception since it is closer to a third power relationship. Adjusted R-squared ranges from a minimum in autumn (R^2=0.87) to a maximum in winter (R^2=0.94) seasons.

3.2. TOP versus CAPE

The relationship between the TOP-12 and the TOP-35 with the CAPE index has been analysed. Figure 3 presents the distance between the TOP-35 height and the -10°C isotherm versus the CAPE. The size of each point corresponds to the average of the TFR. Overall, a direct relationship can be identified between the maximum CAPE values and higher TOP-35 heights. The higher the CAPE, the higher the TOP-35 can reach, allowing a higher TFR. Still, the TOP-35 has a maximum height at the tropopause. However, a high CAPE does not necessarily imply high TOP-12 or TOP-35. Indeed, conditional instability allows for vigorous convective growths, but it is not a sufficient condition for high flash rates, as the number of flashes on days with similar CAPE can differ up to an order of magnitude. Strong updrafts are needed in the mixed phase region (represented here by the TOP-35), where the NIC mechanism is effective (e.g., Deierling and Petersen, 2008; Liu et al., 2012).

Kaltenböck et al. (2009) proposed a threshold CAPE value of 250 J/kg as a discriminator between thunderstorm and non-thunderstorm conditions throughout Europe. From this, Aran and Pineda (2011) carried on a research for a study area more similar to ours, and concluded that a value of 220 J/kg fits better to be used as a dichotomous predictor. This last threshold is also represented in Figure 3 for comparison with the current results.

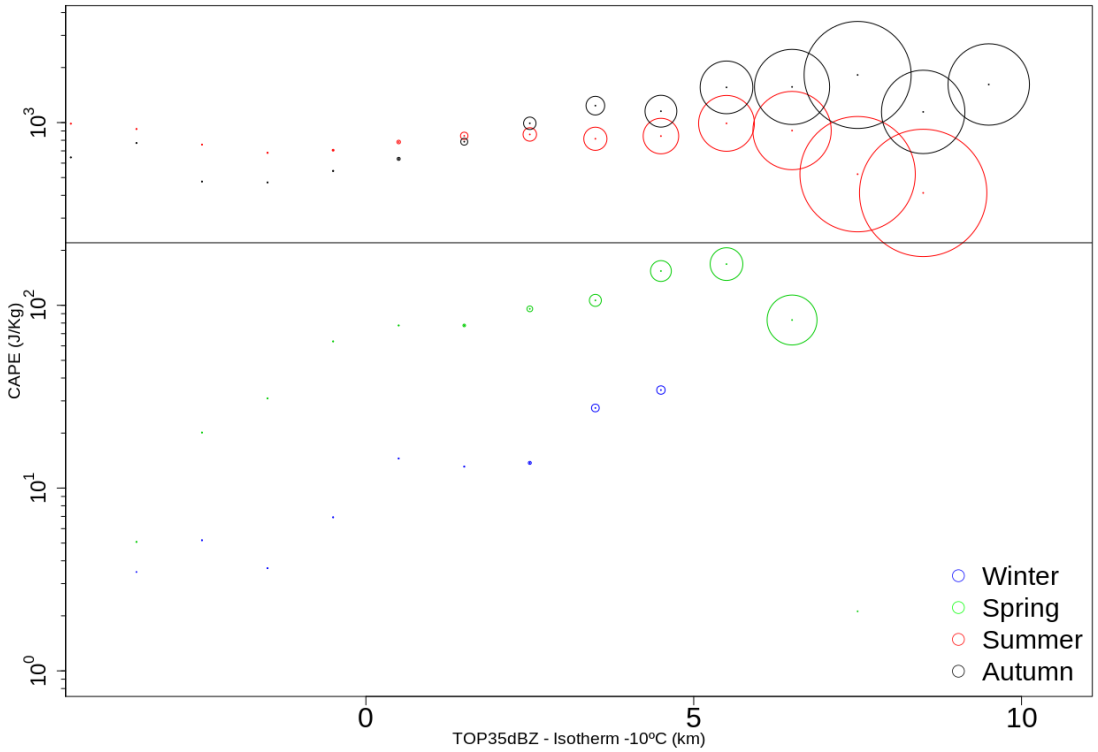

Figure 3. Relation between the TOP-35 (height above -10°C isotherm), the CAPE and the lightning flash rate. The TOP-35 (above -10°C) has been segmented into one-kilometre bins. For each bin, the average of the CAPE is represented. The diameter of each dot is proportional to the average of the TFR. Note that the vertical axis is logarithmic. A horizontal line has been added to CAPE (220 J/kg) for comparison.

Besides, the data is classified by seasons using different colours, and the radius of the circles is proportional to the TFR. Each dot represents the average of the CAPE for each km height (height of the TOP-35 above -10°C isotherm). In general, the higher CAPE values correspond to autumn episodes, followed by summer, spring and winter. So, the logarithmic scale in the CAPE values shows that the heights of TOP-35 (above the -10°C) in the case of winter and spring seasons are mostly lower than those of summer and autumn, as well as their values of TFR, as observed in the previous figure. In addition, during summer and autumn seasons it is likely to find CAPE values much higher than those of the rest of the year, allowing the TOP-35 to reach high altitudes, that in turn will lead to stronger electric fields and ultimately, higher TFR. Also, it is observed that the highest values of lightning activity, especially during summer and autumn, correspond to values higher than the 220 J/kg indicated above for the AoS.

3.3. Radar TOPS vs. Heights of Isotherms and Tropopause

This section introduces the height of the isotherms, to compare the height of the radar reflectivity with the temperature. In addition, the analysis applies a dichotomous classification, treating the two categories "with lightning" and "without lightning" separately. Figure 4 presents, on a monthly basis, the relationship between the tropopause, the –10°C and –40°C isotherms heights and TOP-12 in the AoS. The top panel corresponds to thunderstorm conditions (17,635 cases), whereas the bottom panel is for precipitation structures without lightning (271,106 cases).

The annual cycle of isotherm heights (–10°C and –40°C) has a minimum during the coldest months in the AoS, that is between December and February. They are located around 4 km and 8 km height amsl respectively. On the other hand, they reach 6 km and 10 km respectively between July and August, that is, the warmer months in the AoS. Regarding the tropopause, although it displays a higher short-term variance, it has a long-term trend similar to that of the isotherms, ranging from 10 km in winter to 14 km amsl in summer.

Boxplots for the whole “TOP-12 with thunderstorm” population (Fig. 4a) show higher heights, the median being close to the –40°C isotherm height. The median is slightly above the –40°C isotherm in the warm season months, and slightly below during the winter months. The interquartile range (IQR, the box encompassing values between quantiles 25 and 75) is mainly located between the –40°C and the tropopause heights during the warm-season months. Contrarily, the interquartile range stays below the –40°C during the coldest months. The behaviour of the other category “TOP-12 without lightning” is significantly different (Fig. 4b); the median for stays always below the –10°C height. It should be noted that the third quartile approximately matches the height of the –10°C isotherm all year long.

a)

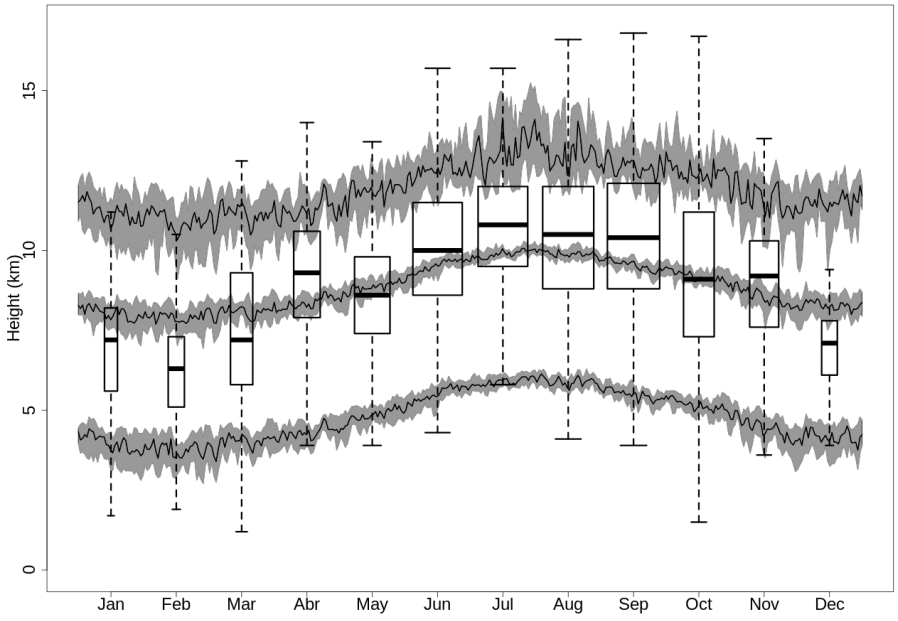

b)

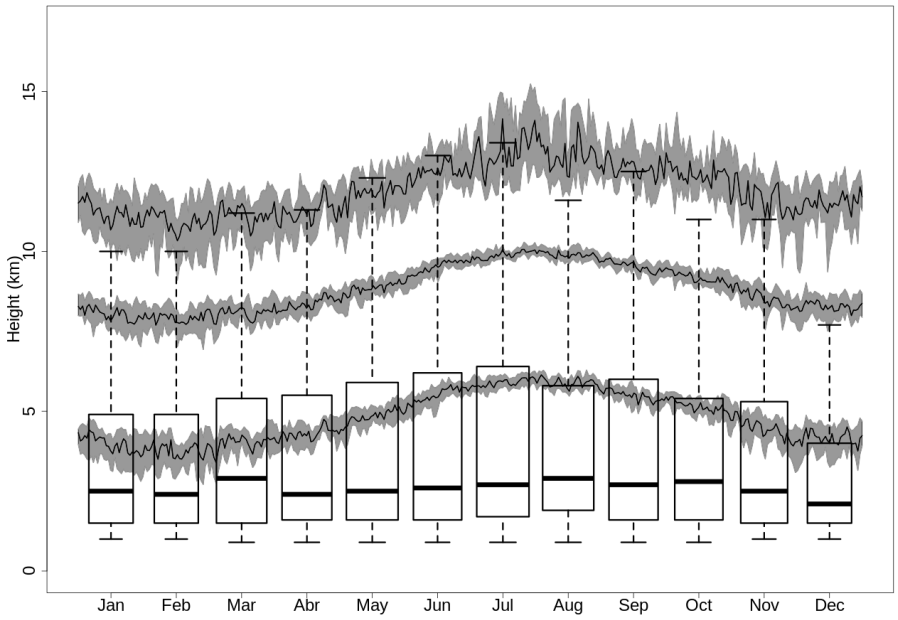

Figure 4. Monthly evolution of the height of significant isotherms (–10°C and –40°C) and of the TOP-12 for the 2001-2017 period. Boxplots correspond to the TOP-12 within the AoS for each month. a) TOP-12 with lightning activity. b) TOP-12 without lightning activity. The boxplots displayed in the figures represent the interquartile range (IQR) of TOP-12 heights (with or without lightning activity), with a solid black line indicating the median value. Whiskers indicate the lower and upper limits of the 1.5 IQR. The altitudes of the –10°C and –40°C isotherms, as well as the height of the tropopause, are represented by a black line that indicates the median value and a grey shadow that delimits the corresponding IQR.

During the cold season, the upper limit of the 1.5 IQR whiskers hardly exceeds the tropopause, and is not until June that the TOP-12 can reach 15 km heights. This overshooting pattern, which is the result of updrafts, associated with strongly convective storms, with enough force to rise above the general equilibrium level in the tropopause (e.g., Bedka, 2011) is an indicator of severe weather (e.g., Brunner et al., 2007) and it is present in the region until October. TFR during periods with overshooting is an order of magnitude higher compared to periods without overshooting, with averages of 47 flash per min^{-1} and 4 flash per min^{-1} respectively.

a)

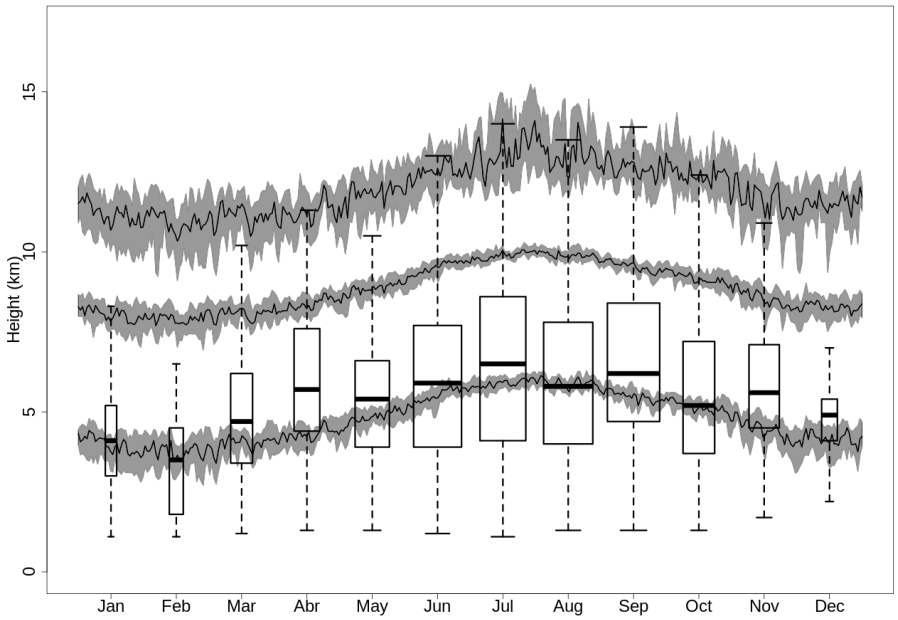

b)

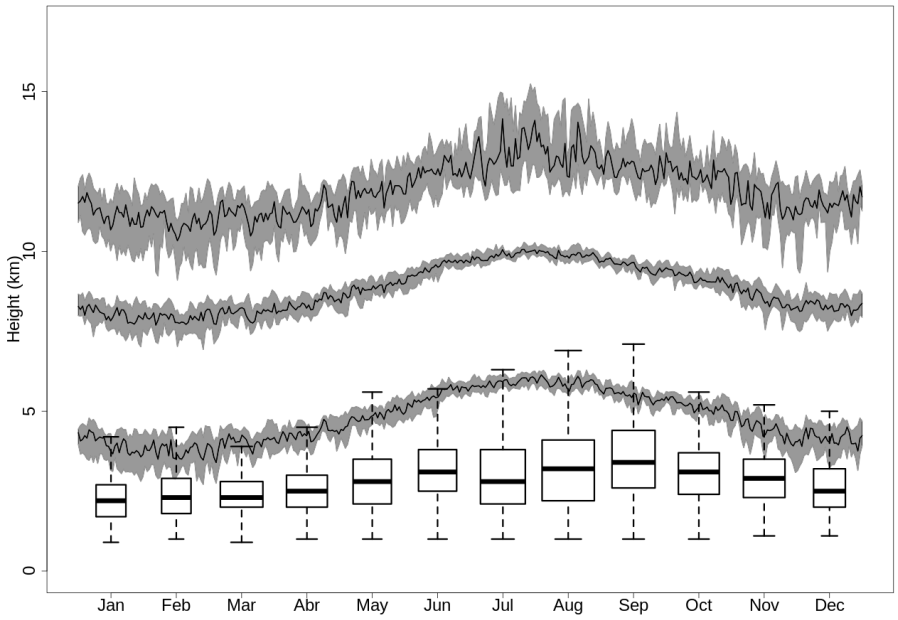

Figure 5. As Fig. 4 but for TOP-35.

Regarding the TOP-35, Fig. 5 shows its evolution along the year, in comparison to the height of the –10°C and –40°C isotherms. For the "TOP-35 with thunderstorm" (14405 cases) category (Fig. 5a) the average height for all months is very close to or higher than the height of the –10°C isotherm. As in the TOP-12 case, it is not until the warm season months that the TOP-35 height reaches the tropopause. In turn, for the "TOP-35 without lightning" (41448 cases) case, neither the median height nor the top 1.5 IQR reach the height of the –10°C isotherm.

While the median for “TOP-12 with thunderstorm” is related to the –40°C (Fig. 4a), the median for the “TOP-35 with thunderstorm” follows the average height of the –10°C isotherm along the year (Fig. 5a). Regarding the “TOP-35 without thunderstorm”, the median hardly reaches 3-4 km. Here, the trend for upper limit of the 1.5 IQR is similar to the –10°C isotherm evolution.

3.4. Contingency tables and skill scores

Contingency tables were used to determine the degree of diagnostic skill of the height of the TOP-12 and TOP-35 as thunderstorm predictors. That is, lightning activity is forecasted in two situations: when the height of the TOP-12 is above the -40°C, or when the height of the TOP-35 is above the -10°C. Additionally, the combination of both was also evaluated (one requiring both conditions and the second requiring at least one of the conditions). Table 2 presents the annual skill scores and by seasons for all the analysed period.

The TOP-12 has a POD of 62% and a FAR of 51%. Assuming a threshold of 50%, for both POD and FAR, to determine whether they are useful or not to predict lightning detection, this predictor would generate too many false alarms. Besides, it has little to no skill during winter. The POD reaches its maximum during summer (66%), with a minimum of 41% of false alarms for the same season. By using the TOP-35 instead, the POD is almost similar (64%). However, the FAR is significantly lower (31%). Still, the condition for the TOP-35 generates too many false alarms during winter (65%).

Contrarily, when a looser criterion is applied (fulfilment of either one of the conditions) the POD values are the highest of any other predictor (74%), but the FAR also increases to its maximum (52%).

The annual CSI, the ratio of hits to the total number of events and false alarms (Donaldson et al., 1975), is highest for TOP-35 and for “TOP-12 and TOP-35” conditions, with values between 50-45%, respectively. Again, a difference is observed between winter and the rest of the seasons, being the first one to obtain the lowest values. A known problem of the CSI is that it doesn’t take into account the correct forecast of null events. In our case, it is also important to correctly forecast that no lightning is going to occur if thunderstorm conditions are not attained.

Table 2. Skill scores for the TOP-12 height (above -40°C) and TOP-35 (above -10°C) as thunderstorm predictors (annual, seasonal) compared with thunderstorm assessment through lightning observations. Probability of Detection (POD), False Alarm Ratio (FAR), Critical Success Index (CSI), True Skill Statistic (TSS) and the Heidke Skill Score.

Index		POD	FAR	CSI	TSS	Heidke
h(TOP12)> h(-40°C)	Annual	0.62	0.51	0.38	0.58	0.52
	Winter	0.31	0.87	0.10	0.28	0.16
	Spring	0.55	0.66	0.26	0.51	0.39
	Summer	0.66	0.41	0.45	0.61	0.58
	Autumn	0.64	0.43	0.43	0.60	0.57
h(TOP35)> h(-10°C)	Annual	0.64	0.31	0.50	0.54	0.55
	Winter	0.67	0.65	0.30	0.55	0.39
	Spring	0.72	0.42	0.47	0.61	0.55
	Summer	0.59	0.22	0.50	0.50	0.54
	Autumn	0.68	0.26	0.54	0.58	0.59
h(TOP12)> h(-40°C) AND h(TOP35)> h(-10°C)	Annual	0.49	0.15	0.45	0.46	0.54
	Winter	0.25	0.50	0.20	0.23	0.29
	Spring	0.49	0.23	0.43	0.46	0.54
	Summer	0.48	0.11	0.46	0.45	0.51
	Autumn	0.54	0.13	0.50	0.51	0.57
h(TOP12)> h(-40°C) OR h(TOP35)> h(-10°C)	Annual	0.74	0.52	0.41	0.69	0.55
	Winter	0.61	0.82	0.16	0.57	0.26
	Spring	0.73	0.65	0.31	0.68	0.60
	Summer	0.75	0.42	0.48	0.68	0.60
	Autumn	0.76	0.45	0.47	0.71	0.60

If both TOP-12 and TOP-35 conditions are required, the FAR is significantly reduced (15%). However, these more restrictive conditions also lower the POD (49%). Again, this combination is not useful during winter, as the FAR is still too high (50%).

In this regard, the True Skill Statistic, TSS, does take the quiescent cases into account. The values of the TSS are lower than the corresponding POD, but the behaviour is similar for the two scores. The frequency distribution has a lot of quiescent cases, so the difference between POD and TSS remains quite low in all cases, especially with TOP-12, and TOP-12 or TOP-35. However, according to Doswell et al. (1990), the TSS fails to deal effectively when the correct forecasts of non-occurrence dominate the contingency table, which is our case. Instead, the Heidke skill score (Panfosky and Brier, 1958; Von Storch and Zwiers, 1999) is better suited. As presented in Table 2, all predictors present annual Heidke values above 50%. The lowest value

corresponds to winter, with a minimum of 39% for TOP-35. For the rest of the seasons, "TOP-12 or TOP-35" is the best predictor with values of 60%.

4. DISCUSSION

4.1. Lightning flash rate and radar storm height

Radar storm height is a basic indicator of cloud electrification and lightning activity (e.g., Zipser and Lutz, 1994; Petersen et al., 1996; Nesbitt et al., 2000). The link between both is the strength of vertical air motion, which plays a fundamental role in the charge separation, which in turn will determine the flash rate. This relates lightning production to fundamental meteorological aspects of thunderstorms like the height of the cloud tops, measurements that can be estimated from weather radar or meteorological satellites (e.g., Ushio et al., 2001; Pessi and Businger, 2009; Karagiannidis et al., 2015). Note that radar measurements provide a better estimate of the height to which large particles are lifted by the convective updraft. Therefore, radar echo tops are more directly related to the intensity of convection than cloud top height measured by meteorological satellites, since the latter may be substantially higher than the height to which significant radar signal extends (e.g., Liu et al., 2007).

As found in previous studies, the radar storm height is well-correlated with the lightning flash rate. Williams (1985) stated a fifth order relationship between both. Ushio et al. (2001) further quantified this relationship using TRMM (Tropical Rainfall Measuring Mission) and lightning imaging sensor (LIS) data, reproducing Williams' fifth order relationship over the US, although with some variation in the power law slope. The present results bring more evidence to this power law relationship. Current results correspond to a long series and are from a different mid-latitude region of the world, compared to previous studies. Interestingly, spring to autumn data roughly follow the same power law relationship, suggesting that it may be possible to use a single fit in all three seasons (Table 1).

Contrarily, winter shows some variation in the power law slope. From these results for winter, the following question arises: Why is it harder, for winter thunderstorms, to reach high flash rates? As pointed out by Williams (2018), water vapour concentration, the fuel for moist convection, has an exponential dependence on temperature (according to the Clausius-Clapeyron relationship). This relationship states an exponential dependence on temperature, with a rough doubling of water vapour concentration for every 10°C of temperature increase. In the AoS, the contrast between winter, with surface temperatures of 0°C or less, and summer, with temperatures around 30°C, is nearly an order of magnitude. This suggests a 6-fold increase in water vapour concentration in summer compared to winter. On the

basis of the NIC mechanism, this increase provides at least partial explanation for the large contrast in lightning activity between summer and winter. Another difference between seasons is the Convective Available Potential Energy.

4.2. TOP-35 versus CAPE

The CAPE index is useful for forecasting favourable conditions for thunderstorm formation, through the assessment of vertical air motions in moist convection; perhaps the most important variable linking surface air temperature and lightning activity (Williams et al., 2005). A high CAPE value translates as a high convective power. This will allow TOP-35 to reach high altitudes, that in turn will lead to stronger electric fields and ultimately, higher TFR. As shown in Fig. 3, high TFR are related to high TOP-35 (above the -10°C isotherm), which usually occurs in high CAPE conditions. However, this index could not be used to make quantitative estimates of lightning flash rates within storms. A high CAPE is a favourable condition to allow the TOP-35 to reach height, but is not a sufficient condition for a high TFR. In addition to high CAPE value, availability of moisture and certain triggering mechanisms are necessary for initiation and maintenance of convection.

Thunderstorm activity in Europe occurs under a wide range of CAPE values (Kaltenböck et al., 2009). These authors suggested a threshold of CAPE 250 J/kg to distinguish between thunderstorm and non-thunderstorm conditions; and a threshold of 400 J/kg to discriminate between ordinary thunderstorms and severe events. Another study, which better fits our region of study, suggests a threshold of 220 J/kg for a dichotomous predictor (Aran and Pineda, 2011).

In general, CAPE values are an order of magnitude less in winter than in summer (e.g., Schultz, 1999; Market et al., 2007; Rauber et al., 2014). As shown in Figure 3, the CAPE hardly reaches the 200 J/kg threshold during winter and spring. In winter, CAPE is often produced by warmer, moister air sliding under cold air. Indeed, in winter, it is more difficult for sunlight to warm the surface to destabilize the atmosphere in the manner that is common in summer. Nevertheless, TFRs during the cold season are not negligible (the median values per season are 0.33 flash min^{-1} in winter, 0.83 flash min^{-1} in spring, 1 flash min^{-1} in summer and 1.17 flash min^{-1} during autumn), as they can still cause storms with sufficiently high electrical activity too produce discharges and impacts on various types of exposed elevated structures.

4.3. Relation between Radar Reflectivity and Heights of Isotherms

In spite of the existing relationship between radar storm height and lightning flash rate, the vertical development alone may be insufficient as a basic indicator for thunderstorm conditions. A more reliable predictor would be the attainment of a certain level of reflectivity (e.g., 35 dBZ) above the height of a given isotherm (e.g., –

10°C). On the basis of the NIC mechanism, the detection of a 30-40 dBZ or greater radar echo at heights above the –10°C isotherm is indicative of the presence of a sufficient quantity of hydrometeors in the mixed phase region for electrical charging, because the NIC mechanism requires precipitation-size ice particles and super-cooled liquid water to coexist between about –10°C and –20°C (Takahashi, 1978; Saunders et al., 2006; Lang and Rutledge, 2011).

Based on this premise, different predictors can be found in literature. For example, Dye (1989) required that the radar reflectivity of 40 dBZ reached the –10°C isotherm. Gremillion and Orville (2009) required the reflectivity levels of 30 dBZ and 20 dBZ to reach, respectively, the –15°C and –20°C isotherms. From the results of the present study, two different predictors are proposed: lightning production can be expected in radar structures where the height of the echo-tops (TOP-12 product) exceeds the –40°C height. Similarly, the TOP-35 reaching the –10°C is indicative of electrification. Both predictors have a POD above 60%. However, the FAR is also high. False alarms can be diminished combining both predictors, despite losing some prediction efficiency. For maximizing the POD, the best predictor is requiring that either "TOP-12 or TOP-35" reach the isotherms heights of -40°C and –10°C, respectively. All in all, these predictors are useful from spring to autumn. In winter the best predictor is a TOP-35 above –10°C, despite it also has a high FAR.

Focusing on the -10°C isotherm, Fig.6 presents the monthly evolution of its height in the AoS throughout the year. The monthly averages for a 17-year period indicates that the –10°C isotherm is between 5.5 and 6 km amsl during the thunderstorm season (June-September) and around 4 km amsl in winter (December to March). Therefore, in the transition from summer to winter, the mixed phase region (i.e., the region between 0°C and the –10°C isotherm) descends around 1.5-2.0 km. The practical implication of this downward shift is that ground infrastructures (power lines, wind turbines, telecomm towers, etc.) are subjected to stronger electric fields and are therefore exposed to upward lightning (e.g., Wang and Takagi, 2012; Warner et al., 2012; Bruning et al., 2014; Montanyà et al., 2016). Pineda et al. (2018) brought evidence on the higher incidence of lightning on wind turbines during transitional periods (spring and autumn), even though the main thunderstorm season in the AoS is concentrated on the summer months.

Adler et al. (1985) showed that the location of the overshooting tops approximately locates the updraft area of a storm and is often indicative of the intensity of the storm. Considering that the TFRs during periods with overshooting (here understood as TOP-12 above the tropopause) have been found to be an order of magnitude higher compared to periods without overshooting, this pattern seems relevant to warn about high TFR cores.

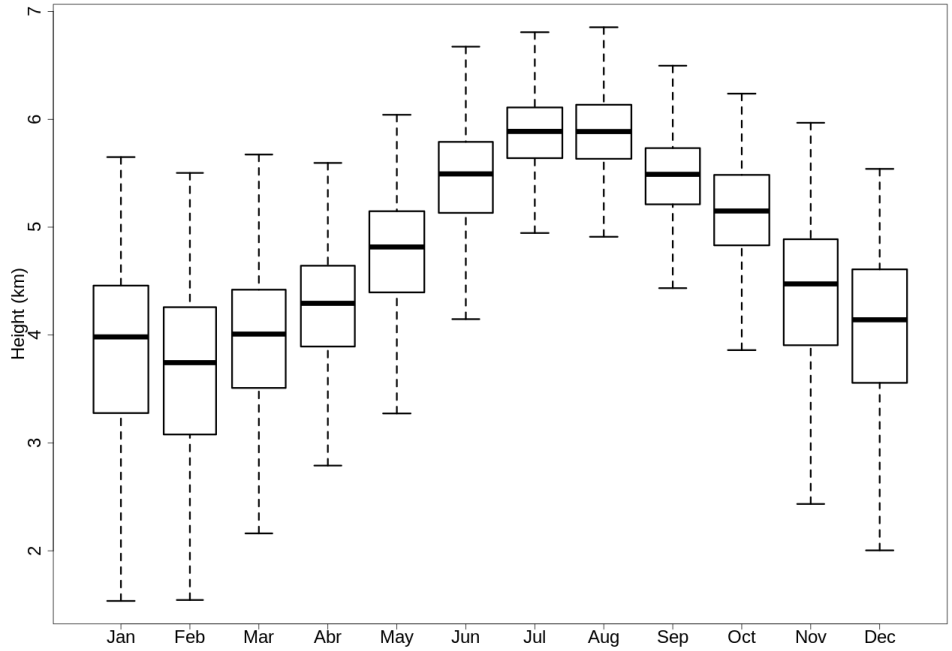

Figure 6. Boxplots of the monthly evolution of the –10°C isotherm within the AoS (2001-2017).

5. Summary and conclusions

A large dataset of weather radar echo tops, total lightning observations and radiosounde derived isotherm height have been used as proxies of the convective system properties in order to investigate relationships between storm intensity and lightning activity.

As found in previous studies, the radar storm height is tightly correlated with the total lightning flash rate. The fifth order relationship proposed by Williams (1985) fits for the AoS from spring to autumn, whereas the power law growth decreases in winter to the third power.

The CAPE index is useful for forecasting favourable conditions for thunderstorm formation. However, a high CAPE is not a sufficient condition for high TFR and cannot be used to make quantitative estimates of lightning flash rates.

In spite of the good correlation between the radar storm height and the total lightning flash rate, the vertical development alone may be insufficient as a basic indicator for thunderstorm conditions. A more reliable predictor would be the presence of a certain level of reflectivity above the height of a given isotherm, as it takes into account the dependence of the electrification processes on the temperature.

From the results of the present study, two different predictors for the lightning onset are proposed: 12 dBZ radar reflectivity echoes (TOP-12 product) reaching the –40°C

height (particles lifted by the convective updraft); and 35 dBZ reflectivity echoes (TOP-35 product) reaching the –10°C (sufficient quantity of hydrometeors in the mixed phase region). The skill scores of the two predictors have been calculated, as well as their combinations. For both predictors, POD values are above 60% all throughout the year but FAR values are slightly high. False alarms can be reduced combining the two predictors, while losing some POD. All in all, the most suitable all-year-round predictor is the TOP-35 above -10°C.

The climatology of the –10°C isotherm in the AoS (2001-2017), shows a downward shift of about 1.5-2.0 km during winter (December to March). Practical implication of this descent is that infrastructure on the ground is subject to stronger electric fields and is therefore prone to upward discharges and more exposed to return-stroke impact.

Acknowledgments

This study was co-funded by the autonomous Government of Catalonia, the Meteorological Service of Catalonia and Fulgura S.L., under the framework of the Industrial Doctorate Programme (Project DI 59/2015).

References

Adler, R.F, Markus, M.J., Fenn, D.D., 1985. Detection of severe Midwest thunderstorms using geosynchronous satellite data. Monthly Weather Review, 113, 769-781.

Aran M., Pineda, N., 2011. Convective instability indexes as thunderstorm predictors for Catalonia, proceedings of the 6th European Conference on Severe Storms (ECSS), Palma de Mallorca, Spain, 3-7 October 2011

Argemí, O., Altube, P., Rigo, T., Ortiga, X., Pineda, N., Bech, J., 2014. Towards the improvement of monitoring and data quality assessment in the weather radar network of the Meteorological Service of Catalonia, 8th European Conference on Radar in Meteorology and Hydrology (ERAD), Garmisch-Partenkirchen, Germany, Sept. 2014

Bech, J., Vilaclara, E., Pineda, N., Rigo, T., López, J., O'Hora, F., Lorente, J., Sempere, D., Fàbregas, F.X., 2004. The weather radar network of the Catalan Meteorological Service: description and applications. Proceedings of the 3rd European Conference on Radar (ERAD 2004), Copernicus GmbH.

Bedka, K.M., 2011. Overshooting cloud top detections using MSG SEVIRI Infrared brightness temperatures and their relationship to severe weather over Europe, Atmospheric Research, Volume 99, Issue 2, 2011, Pages 175-189, https://doi.org/10.1016/j.atmosres.2010.10.001.

Boccipio, D.J., 2001. Lightning scaling relations revisited. J. Atmos. Sci. 59, 1086–1104.

Bruning, E. C., Weiss, S. A., Calhoun, K. M., 2014. Continuous variability in thunderstorm primary electrification and an evaluation of inverted-polarity terminology. Atmospheric Research (135–136): 274-284.

3.1 SEASONAL VARIATIONS ON THE CONDITIONS REQUIRED FOR THE LIGHTNING PRODUCTION

Brunner, J.C., Ackerman, S., Bachmeier, A.S., Rabin, R.M., 2007. A Quantitative Analysis of the Enhanced-V Feature in Relation to Severe Weather. Weather and Forecasting - WEATHER FORECAST. 22. 10.1175/WAF1022.1.

Carey, L. D., Rutledge, S.A., 1996. A multiparameter radar case study of the microphysical and kinematic evolution of a lightning producing storm. Meteor. Atmos. Phys., 59, 33–64, doi: https://doi.org/10.1007/BF01032000.

Cummins, K. L., Murphy, M. J., Bardo, E. A., Hiscox, W. L., Pyle, R. B., Pifer, A. E., 1998. A Combined TOA/MDF Technology Upgrade of the U.S. National Lightning Detection Network, J. Geophys. Res., 103, 9035–9044.

Cummins, K., Murphy, M., 2009. An Overview of Lightning Locating Systems: History, Techniques, and Data Uses, With an In-Depth Look at the U.S. NLDN, IEEE Transactions on Electromagnetic Compatibility, Vol. 51 (3), pp. 499-518

Deierling, W., Petersen, W. A., 2008. Total lightning activity as an indicator of updraft characteristics, J. Geophys. Res., 113, D16210, doi:10.1029/2007JD009598.

Deierling, W., Petersen, W. A., Latham, J., Ellis, S., Christian, H. J., 2008. The relationship between lightning activity and ice fluxes in thunderstorms, J. Geophys. Res., 113, D15210, doi:10.1029/2007JD009700.

Donaldson, R.J., Dyer, R.M., Krauss, M.J., 1975. An objective evaluator of techniques for predicting severe weather events. Preprints, 9th Conf. on Severe Local Storms. Amer. Meteor., Norman, OK, pp. 321–326.

Doswell III, C.A., Davies-Jones, R., Keller, D.L., 1990. On summary measures of skill in rare event forecasting based on contingency tables. Weather Forecast. 5, 576– 585.

Dye, J. E., Winn, W. P., Jones, J. J., Breed, D. W., 1989. The electrification of New Mexico thunderstorms: 1. Relationship between precipitation development and the onset of electrification, J. Geophys. Res., 94(D6), 8643–8656, doi:10.1029/JD094iD06p08643.

Farnell, C., Rigo, T., Pineda, N., 2017. Lightning jump as a nowcast predictor: Application to severe weather events in Catalonia. Atmospheric Research. 183. 130-141. 10.1016/j.atmosres.2016.08.021.

Futyan, J. M., Del Genio, A. D., 2007. Relationships between lightning and properties of convective cloud clusters, Geophys. Res. Lett., 34, L15705, doi:10.1029/2007GL030227.

Galanaki, E., Lagouvardos, K., Kotroni, V., Flaounas, E., Argiriou, A., 2018. Thunderstorm climatology in the Mediterranean using cloud-to-ground lightning observations, Atmos. Res., 207: 136-144

Gatlin, P.N., Goodman, S.J., 2010. A total lightning trending algorithm to identify severe thunderstorms. J. Atmos. Ocean. Technol. 27 (1), 3–22.

Gremillion, M., Orville, R., 1999. Thunderstorm Characteristics of Cloud-to-Ground Lightning at the Kennedy Space Center, Florida: A Study of Lightning Initiation Signatures as Indicated by the WSR-88D. Amer. Meteor. Soc., 14, 640-649.

Haklander, A.J., Van Delden, A., 2003. Thunderstorm predictors and their forecast skill for the Netherlands. Atmospheric Research 67– 68 (2003) 273– 299.

Kaltenböck, R., Diendorfer, G., Dotzek, N., 2009. Evaluation of thunderstorm indices from ECMWF analyses, lightning data and severe storm reports, Atmos. Res., 93: 381-396, https://doi.org/10.1016/j.atmosres.2008.11.005

Karagiannidis A., Lagouvardos, K., Kotroni, V., 2015. The use of lightning data and Meteosat Infrared imagery for the nowcasting of lightning activity. Atmospheric Research, 168 (2016) 57–69, doi: 10.1016/j.atmosres.2015.08.011.

Karagiannidis A, Lagouvardos, K., Lykoudis, S., Kotroni, V., Giannaros, C., Betz, H.D., 2019. Modeling lightning density using cloud-top parameters. Atmospheric Research, 222, 163-171.

Kingfield, D. M., Calhoun, K. M., de Beurs, K. M., 2017. Antenna structures and cloud-to-ground lightning location: 1995–2015, Geophys. Res. Lett., 44, 5203–5212, doi:10.1002/2017GL073449.

Kotroni, V., Lagouvardos, K., 2016. Lightning in the Mediterranean and its relation with sea-surface temperature. Environ. Res. Lett. 11, 034006. http://dx.doi.org/10.1002/asl.685.

Liu, C., Zipser, E. J., Nesbitt, S. W., 2007. Global distribution of tropical deep convection: Different perspectives from TRMM infrared and radar data, J. Clim., 20(3), 489–503, doi:10.1175/JCLI4023.1.

Liu, C., Cecil, D. J., Zipser, E. J., Kronfeld, K., Robertson, R., 2012. Relationships between lightning flash rates and radar reflectivity vertical structures in thunderstorms over the tropics and subtropics, J. Geophys. Res., 117, D06212, doi:10.1029/2011JD017123.

Lojou, J.Y., Cummins, K. L., 2006. Total lightning mapping using both VHF interferometry and time-of-arrival techniques. In International Conference on Lightning Protection, Kanazawa, Japan, 391-396.

López, J.A, Pineda, N., Montanyà, J., van der Velde, O.A., Fabró, F., Romero. D, 2017. Spatio-temporal dimension of lightning flashes based on three-dimensional Lightning Mapping Array. Atmospheric Research 197: 255-264

Nesbitt, S.W., Zipser, E. J., Cecil, D. J., 2000. A census of precipitation features in the tropics using TRMM: Radar, ice scattering, and lightning observations. J. Climate, 13, 4087–4106.

MacGorman, D. R., Burgess, D. W., Mazur, V., Rust, W. D., Taylor, W. L., Johnson, B. C., 1989. Lightning rates relative to tornadic storm evolution on 22 May 1981. Journal of the Atmospheric Sciences, 46, 221–250. https://doi.org/10.1175/1520-0469(1989)046<0221:LRRTTS>2.0.CO;2

MacGorman, D.R., Rust, W.D., Williams, E.R., 1999. The Electrical Nature of Storms. Physics Today - PHYS TODAY. 52. 10.1063/1.882670.

MacGorman, D.R., Rust, W.D., Schuur, T.J., Biggerstaff, M.I., Straka, J.M., Ziegler, C.L., Mansell, E.R., Bruning, E.C., Kuhlman, K.M., Lund, N.R., Biermann, N.S., Payne, C., Carey, L.D., Krehbiel, P.R., Rison, W., Eack, K.B., Beasley, W.H., 2008. TELEX The Thunderstorm Electrification and Lightning Experiment. Bull. Amer. Meteor. Soc., 89, 997–1014, https://doi.org/10.1175/2007BAMS2352.1

Manual on Codes - International Codes, Volume I.1, Annex II to the WMO Technical Regulations: part A- Alphanumeric Codes (Edition 2011 updated in 2018) ISBN: 978-92-63-10306-2

March, V., 2017. Key issues to define a method of lightning risk assessment for wind farms, Electr. Power Syst. Res., doi: 10.1016/j.epsr.2017.08.020

Market, P., Ebert-Cripe, R.L., Bodner, M., 2007. Case study of a longlived thundersnow event. Natl. Weather Dig. 31. 103-119.

Mazarakis, N., Kotroni, V., Lagouvardos, K., Argiriou, A.A., 2009. The sensitivity of numerical forecasts to convective parameterization during the warm period and the use of lightning data as an indicator for convective occurrence, Atmospheric Research 94 (2009) 704–714

Mecikalski, R.M., Carey, L.D., 2017. Lightning characteristics relative to radar, altitude and temperature for a multicell, MCS and supercell over northern Alabama. Atmospheric Research 191 (2017) 128–140

Michimoto, K., 1991. A study of radar echoes and their relation to lightning discharge of thunderclouds in the Hokuriku district, Part 1: Observation and analysis of thunderclouds in summer and winter. J. Meteor. Soc. Japan, 69, 327–335.

Montanyà, J., van der Velde, O., Williams, E. R., 2014a. Lightning discharges produced by wind turbines. J. Geophys. Res. Atmos., 119, 1455–1462, doi:10.1002/ 2013JD020225.

Montanyà, J., 2014b. Annual Report on the Performance of the Lightning Location System Operated by the Meteorological Service of Catalonia, Internal Technical Report, not published.

Montanyà, J., Fabró, F., Van der Velde, O., March, V., Williams, E., Pineda, N., Romero, D., Solà, G., Freijo, M., 2016. Global distribution of winter lightning: A threat to wind turbines and aircraft. Natural Hazards and Earth System Sciences. 16. 1465-1472. 10.5194/nhess-16-1465-2016.

Murphy, A.H., Daan, H., 1985. Forecast evaluation, in: Allan H. Murphy and Richard W. Katz, eds., Probability, statistics, and decision making in the atmospheric sciences (Westview Press, Boulder, CO) 379-437.

Panofsky, H.A., Brier, G.W., 1958. Some Applications of statistics to meteorology, Philadelphia: the Pennsylvania State University.

Pessi, A.T., Businger, S., 2009. Relationships among Lightning, Precipitation, and Hydrometeor Characteristics over the North Pacific Ocean. J. Appl. Meteor. Climatol., 48, 833–848, https://doi.org/10.1175/2008JAMC1817.1

Petersen, W. A., Rutledge, S. A., Orville, R. E., 1996. Cloud-to-ground lightning observations from TOGA COARE: Selected results and lightning location algorithms. Mon. Wea. Rev., 124, 602–620.

Pineda, N., Montanyà, J., 2009. Lightning Detection in Spain: The Particular Case of Catalonia. 10.1007/978-1-4020-9079-0_7.

Pineda, N., Montanyà, J., Salvador, A., Van der Velde, O., López, J., 2018. Thunderstorm characteristics favouring downward and upward lightning to wind turbines. Atmospheric Research. 214. 10.1016/j.atmosres.2018.07.012.

Price, C., Rind, D., 1994. Modeling global lightning distributions in general circulation model, Monthly weather review, 122: 1930-1939

Rachidi, F., Rubinstein, M., Montanyà, J., Bermudez, J.L., Rodriguez, R., Solà, G., Korovkin, N., 2008. A review of current issues in lightning protection of new generation wind turbine blades, IEEE Trans. Ind. Electron., vol. 55, no. 6, pp. 2489–2496, doi:10.1109/TIE.2007.896443.

Rakov V.A., Uman, M.A., 2003. Lightning: Physics and effects. Cambridge University Press, 2003. 687 p. ISBN 05215832766.

Rauber, R. M., Wegman, J., Plummer, D. M., Rosenow, A. A., Peterson, M., McFarquhar, G. M., Jewett, B. F., Leon, D., Market, P. S., Knupp, K. R., Keeler, J. M., Battaglia, S., 2014. Stability and charging characteristics of the comma head region of continental winter cyclones, J. Atmos. Sci., Vol.71, pp.1559-1582

Rigo, T., Berenguer, M., Llasat, M.C., 2019. An improved analysis of mesoscale convective systems in the western. Mediterranean using weather radar, Atm. Res. 227: 147–156

Rosenfeld, D., Wolff, D.B., Atlas, D., 1993. General Probability-matched Relations between Radar Reflectivity and Rain Rate. J. Appl. Meteor., 32, 50–72, https://doi.org/10.1175/1520-0450(1993)032<0050:GPMRBR>2.0.CO;2

Saunders, C. P. R., Bax-Norman, H., Emersic, C., Avila, E. E., Castellano, N. E., 2006. Laboratory studies of the effect of cloud conditions on graupel/crystal charge transfer in thunderstorm electrification. Quart. J. Roy. Meteor. Soc., 132, 2653-2673.

Schultz, D.M., 1999. Lake-effect snowstorms in northern Utah and western New York with and without lightning, Wea. Forecasting, Vol.14, No.6, pp.1023–1031

Schultz, C.J., Petersen, W.A., Carey, L.D., 2011. Lightning and Severe Weather: A Comparison between Total and Cloud-to-Ground Lightning Trends. Wea. Forecasting, 26, 744–755, https://doi.org/10.1175/WAF-D-10-05026.1

Schultz, C. J., Lang, T. J., Bruning, E. C., Calhoun, K. M., Harkema, S., Curtis, N., 2018. Characteristics of lightning within electrified snowfall events using lightning mapping arrays. J. Geophys. Res. Atmos., 123. https://doi.org/10.1002/2017JD027821

Shindo, T., Miki, T., Saito, M., Asakawa, A., Motoyama, H., Ishii, M., Fujisawa, A., 2015. Meteorological conditions and occurrence of upward lightning at high structures. IEEJ Trans. Power Energy 135(6), 417–418. https://doi.org/10.1541/ieejpes.135.417

Soriano, L.R., de Pablo, F., Díez, E.G., 2001. Relationship between Convective Precipitation and Cloud-to-Ground Lightning in the Iberian Peninsula. Mon. Wea. Rev., 129, 2998–3003, https://doi.org/10.1175/1520-0493(2001)129<2998:RBCPAC>2.0.CO;2

Takahashi, T., 1978. Riming electrification as a charge generation mechanism in thunderstorms. J. Atmos. Sci., 35, 1536-1548.

Ushio, T., Heckman, S. J., Boccippio, D. J., Christian, H. J., Kawasaki, Z.I., 2001. A survey of thunderstorm flash rates compared to cloud top height using TRMM satellite data, J. Geophys. Res., 106(D20), 24089–24095, doi:10.1029/2001JD900233.

Von Storch, H., Zwiers, F.W., 1999. Statistical Analysis in Climate Research. Cambridge Univ. Press, Cambridge. 484 pp.

Vincent, B. R., Carey, L., Schneider, D., Keeter, K., Gonski, R., 2003. Using WSR-88D reflectivity data for the prediction of cloud-to-ground lightning: a North Carolina study. National Weather Digest. 27.

Wallace, J. M., Hobbs, P. V., 1973. Atmospheric Science, An Introductory Survey, International Geophysics, vol. 92, 2nd ed., 504 pp., Academic Press, New York.

Wang, D., Takagi, N., 2012. Characteristics of winter lightning that occurred on a windmill and its lightning protection tower in Japan, IEEJ Trans. Power Energy, 132(6), 568–572, doi:10.1541/ieejpes.132.568.

Wang, F., Zhang, Y., Liu, H., Yao, W., Meng, Q., 2016. Characteristics of cloud-to-ground lightning strikes in the stratiform regions of mesoscale convective systems. Atmospheric Research, 178-179, 207–216. doi: 10.1016/j.atmosres.2016.03.021

Warner, T. A., Cummins, K. L., Orville, R. E., 2012. Upward lightning observations from towers in Rapid City, South Dakota and comparison with National Lightning Detection Network data, 2004–2010, J. Geophys. Res., 117, D19109, doi:10.1029/2012JD018346.

Warner, T. A., Lang, T. J., Lyons, W. A., 2014. Synoptic scale outbreak of self-initiated upward lightning (SIUL) from tall structures during the central U.S. blizzard of 1–2 February 2011, J. Geophys. Res. Atmos., 119, 9530–9548, doi:10.1002/2014JD02169

Wilcox, L. J., Hoskins, B. J., Shine, K. P., 2012. A global blended tropopause based on ERA data. Part I: Climatology. Q.J.R. Meteorol. Soc., 138: 561-575. doi:10.1002/qj.951

Williams, E. R., 1985. Large-scale charge separation in thunderclouds, J. Geophys. Res., 90(D4), 6013–6025, doi:10.1029/JD090iD04p06013.

Williams, E., Weber, M. E., Orville, R.E., 1989. The relationship between lightning type and convective state of thunderclouds. J. Geophys. Res., 94, 13 213-13 220.

Williams, E., Mushtak, V., Rosenfeld, D., Goodman, S., Boccippio, D., 2005. Thermodynamic conditions favorable to superlative thunderstorm updraft, mixed phase microphysics and lightning flash rate. Atmos. Res. 76, 288–306.

Williams, E., 2018. Lightning Activity in Winter Storms: A Meteorological and Cloud Microphysical Perspective, IEEJ Transactions on Power and Energy. Volume 138, Issue 5, Pages 364-373, Released May 01, 2018, Online ISSN 1348-8147, Print ISSN 0385-4213, https://doi.org/10.1541/ieejpes.138.364

Yang, Y.H., King, P., 2010. Investigating the potential of using radar echo reflectivity to nowcast cloud-to-ground lightning initiation over southern Ontario. Weather Forecast. 25 (4), 1235–1248.

Yokoyama, Y., Hermoso, B., Cooray, V., D'Alessandro, F., Diendorfer, G., Duquerroy, P., Engmann, G., Erichsen, H., Galvan, A., Gockenbach, E., Havelka, M., Ishii, M., Kanashiro, A., Méndez, M., Montanya, J., Paolone, M., Rachidi, F., Rousseau, A., Sekioka, S., Shindo, T., Torres, H., Tudor, L., Yamamoto, K., Yasuda, Y., 2014. Lightning protection of wind turbine blades. Electra 274, 43–45.

Yoshida, S., Morimoto, T., Ushio, T., Kawasaki, Z., 2009, A fifth-power relationship for lightning activity from Tropical Rainfall Measuring Mission satellite observations, J. Geophys. Res., 114, D09104, doi:10.1029/2008JD010370.

Zhou, Y., Qie, X., Soula, S., 2002. A study of the relationship between cloud-to-ground lightning and precipitation in the convective weather system in China. Annales Geophysicae. 20. 10.5194/angeo-20-107-2002.

Zipser, E. J., Lutz, K. R., 1994. The vertical profile of radar reflectivity of convective cells: A strong indicator of storm intensity and lightning probability? Mon. Wea. Rev., 122, 1751–1759.

3.2 Thunderstom charge structures favouring cloud-to-ground lightning

3.2.1 Introducción y metodología

Cuando el campo eléctrico entre las distintas regiones de carga opuesta alcanza cierto umbral, ocurre una descarga, que típicamente sucede entre las dos regiones de carga más intensas, la negativa principal y la positiva justo por encima de esta, no alcanzando el suelo. Para producir una descarga a tierra, además, se requiere que la iniciación se realice de forma que el rayo pueda propagarse hacia el suelo. Por ello, es sabido que la presencia de una región de carga por debajo de la región de carga dominante (de polaridad contraria a la primera) en una estructura clásica tripolar aumenta el campo eléctrico, promoviendo un CG desde la región de carga dominante (+CG si la región de carga inferior es negativa, y viceversa). Contrariamente, si se da la presencia de una región de carga positiva inferior excesivamente cargada, esta puede prevenir el descenso de los CG bloqueando su progresión (e.g., Qie et al., 2005; Nag and Rakov, 2009; Iudin et al., 2017). A su vez, esto se traduce en un aumento de los IC entre estas dos regiones de carga.

Los sistemas de avisos de descargas eléctricas están diseñados para alertar sobre las posibles incidencias relacionadas con las descargas nube-tierra, de modo que se pueda actuar de la forma más rápido posible. Así, este artículo plantea establecer qué estructuras eléctricas dentro de una tormenta favorecen la producción de descargas eléctricas, con un especial enfoque hacia las descargas CG, su ratio de descarga y polaridad. Además, se ilustra la identificación de estas estructuras a lo largo del ciclo vital de las tormentas, así como su localización en altitud y temperatura con la ayuda de la determinación de los inicios de las descargas.

Nuevamente se propuso el estudio de la zona del Delta del Ebro y sus inmediaciones por la presencia tanto de la red ELMA, que proporcionará la localización tridimensional y en el tiempo de todas las señales que conforman la descarga del rayo, como del radar meteorológico LMI del SMC. Este último vuelve a aportar información sobre las alturas máximas que alcanzan los niveles de reflectividad de 12 y 35 dBZ (TOP-12 y TOP-35, respectivamente), para la zona de estudio, con una frecuencia de mapeo de 6 minutos. Esta frecuencia es además la que marcará la frecuencia de evaluación de las distintas variables en este estudio.

El LMA permitirá determinar, a partir de las primeras señales de cada rayo, la altura de iniciación para poder establecer la estructura eléctrica de la nube de tormenta en cada instante, diferenciando situaciones en que la tormenta presenta una situación tripolar clásica (TriP), en la que solo se detecta un dipolo inferior (LwDip) o en la que solo se detecta un dipolo superior (UpDip).

Con el objetivo de encontrar una relación entre las estructuras eléctricas y la actividad de descargas en superficie que se pueda extrapolar a distintas zonas, se usa la red de

detección de rayos LINET (información subministrada a partir de la colaboración de Fulgura S.L. y *nowcast GmbH*) para la localización de las descargas CG. Esta red, la cual trabaja en el rango de frecuencia VLF con la técnica TOA, con una precisión aproximada de su localización de unos 150 m, tiene una amplia distribución a lo largo de Europa, con lo que se podrían extrapolar los resultados a zonas con características similares. Finalmente, se propone la salida del modelo WRF para determinar la altura de las isotermas de 0°C, −10°C y −40°C.

Así, para unos episodios de interés, este estudio avalúa, para las distintas estructuras de tormenta determinadas con los inicios de las descargas detectados por el LMA, las alturas donde se encuentran las distintas regiones de carga (tanto en altura como en temperatura) y los compara con otros estudios, los ratios de descarga CG e IC (y de estos últimos, el número de señales por rayo), el ratio IC:CG, así como la polaridad de estas descargas y la anomalía positiva encontrada (periodos con más CG positivos que negativos). Además, también se observa como varía la ratio de descarga CG según la altura de la región de carga superior en una estructura UpDip, y según la diferencia de alturas entre la región de carga inferior y superior cuando se presenta una situación de estructura TriP.

3.2.2 Conclusiones

Del artículo se pueden deducen las siguientes conclusiones:

- La ratio de CG presenta sus valores más altos cuando hay una situación de estructura TriP e inferior en una situación de UpDip. Cuando hay una región de carga inferior muy intensa (LwDip) se alcanza su valor más bajo.
- Las alturas y temperaturas de las regiones de carga determinadas con el LMA presentan acuerdo con otros estudios, con la altura de la región de carga positiva inferior cerca de los 4,730 m y la superior en los 9,150 m. No hay diferencias destacadas entre las distintas estructuras.
- Los picos de corriente más elevados de los CG, en ambas polaridades, se detectan especialmente en situaciones de LwDip.
- La ratio de CG presenta una gran influencia con la altura de las distintas regiones de carga. En el caso de una región de carga positiva muy elevada, debido a una fuerte corriente ascendente, es cuando se observan las mayores ratios de CG.

3.2.3 Artículo y referencia

Salvador, A., Pineda, N., Montanyà, J., López, J. A., Solà, G., 2021. Thunderstorm charge structures favouring cloud-to-ground lightning. *Atmospheric Research*, 105577. doi: 10.1016/j.atmosres.2021.105577.

Thunderstorm charge structures favouring cloud-to-ground lightning

Albert Salvador[1,2], Nicolau Pineda[1,2], Joan Montanyà[2], Jesús A. López[2] and Gloria Solà[2]

[1]Meteorological Service of Catalonia, Carrer Berlín 38-46 08029 Barcelona, Spain

[2]Lightning Research Group, Technical University of Catalonia, Campus de Terrassa, Edifici TR1, Carrer Colom, 1 08222 Terrassa, Spain

ABSTRACT

Thunderstorm electrical structures favouring cloud-to-ground lightning were investigated through a Lightning Mapping Array (LMA), an accurate three-dimensional lightning location system that allows inferring the heights of the regions of charge. The present study focused on classical, convective-scale thunderstorms, aiming to shed new light on how the charge structure affects lightning production, especially the cloud-to-ground fraction, including flash rate and polarity. Results showed that lightning flashes mainly initiate at two levels, around −41 °C (9,150 m MSL) and around −7 °C height (4,730 m MSL). These initiation levels, located between the dominant positive and negative charge regions, allowed to define three main charge structures: an upper dipole (positive above negative), a classical tripole and a lower dipole (negative above positive). Several differences were found between the three categories in terms of the cloud-to-ground lightning production: (i) the classical tripole structure is the one presenting a higher cloud-to-ground flash rate (5.2 flashes·min^{-1}); (ii) in terms of intensity, the presence of an upper positive charge region is more relevant than a lower positive below the main mid negative; (iii) conversely, the lower positive favours higher cloud-to-ground peak currents; (iv) A higher upper positive charge region favours a higher cloud-to-ground rate.

KEYWORDS: atmospheric electricity, Lightning Mapping Array, Cloud-to-ground flash rate, electrification, thunderstorm electrical structure

1. INTRODUCTION

The electrical structure of a classical, convective-scale thunderstorm, where the ascent is provided by conditional instability and the release of convective available potential energy, consists of a vertical tripole, with a dominant middle negative charge region (−ChR) and positive charge regions (+ChR) at the top and below (Krehbiel, 1986; Williams et al., 1989). As a thunderstorm develops, strong updrafts in the convective region favour interactions between graupel and ice crystals (e.g., Zipser and Lutz, 1994, Deierling and Petersen, 2008). In presence of supercooled water, rebounding collisions between ice hydrometeors result in the charging of graupel with negative charge and ice crystals with positive charge (e.g., Saunders and Peck, 1998; Mansell et al., 2005). This charging

mechanism, known as the non-inductive charging mechanism (NIC, Takahashi, 1978; Jayaratne et al., 1983) appears to be the primary source of thunderstorm electrification. All these processes are carried out mainly in the mixed-phase region, typically located in the cloud layer between −10 °C and −40 °C (MacGorman and Rust, 1998). Subsequent differential separation of particles under gravity is then assumed to cause the creation of layers or regions of opposite charge (Bruning et al., 2010, 2014). Temperature appears to be the most important single parameter in controlling the polarity of charge acquired by the cloud particles in the mixed-phase region (e.g., Takahashi and Miyawaki, 2002; Saunders et al., 2006). As a result, this charge structure would consist of a negative charge on graupel (−10 °C to −25 °C), with a positive charge on cloud ice above (−25 °C to −40 °C), and an additional positive charge below, near the 0 °C level (Williams 1989, 2001).

The tripolar structure of thunderstorms is supported by a wide variety of observations (e.g., Williams et al., 1989; Tessendorf et al., 2007; Stolzenburg and Marshall, 2008). Based on measurements made from balloon-borne and ground-based electric field meters, the existence of the lower +ChR was confirmed (Jacobson and Krider, 1976; Marshall and Winn, 1982; Marshall and Rust, 1991). These observations typically found a sharp charge in the dielectric constant around the 0 °C isotherm, associated with the melting level, where ice phase hydrometeors melt to become raindrops (e.g., Marshall and Rust, 1993; Shepherd et al., 1996). Still, the relative amounts of charge in this tripole can vary significantly; leading to top-heavy or bottom-heavy tripole structures (e.g., Mansell et al., 2010). This basic structure has been complemented with a fourth and uppermost region, a negative shallow screening charge at the upper cloud boundary (MacGorman and Rust, 1998; Krehbiel et al., 2008). Of course, this three/four charge region model will not fit in all situations: more complex thunderstorm structures, with up to six charge layers, have been observed in mesoscale convective systems (e.g., Stolzenburg et al., 1998).

On the other hand, severe weather-related storms like supercells can present anomalously electrified structures, where the tripolar structure presents an inverted sequence (e.g., Krehbiel et al., 2000; Rust et al., 2005; Wiens et al., 2005), resulting from unusually large liquid water contents that make graupel to gain a positive charge during rebounding collisions with cloud ice (e.g., Takahashi and Miyawaki, 2002; Saunders et al., 2006).

During charge separation and layering, an electric field builds between ChRs. Once the electric field reaches a critical strength, a discharge occurs. Such breakdowns are mainly triggered between the two strongest ChRs during the storm's convective stages because the majority of lightning typically do not reach the ground. Therefore, it is not sufficient for a storm to be highly electrified to produce cloud-to-ground (CG) flashes. Producing a CG flash requires not only that the electric field must become large enough somewhere in a storm to initiate a flash, but that initiation must be done in such a way that one end of the flash propagates to the ground (Brown et al., 2002).

When channel development begins within the cloud, the polarity of CGs is often controlled by the polarity of the first two ChRs near the earth's surface (Bruning et al., 2014). In most cases, negative charge is lowered to the ground by negative CG (−CG) (when the lowest

ChR is positive), and positive charge is lowered by positive CG (+CG) (when the lowest ChR is negative). Whatever the origin, it is generally thought that the lower +ChR facilitates the launching of a negatively charged leader toward the ground (e.g., Clarence and Malan, 1957; Pawar and Kamra, 2004; Wiens et al., 2005; Krehbiel et al., 2008; Nag and Rakov, 2009; Cooray et al., 2014). The presence of positive charge below the main −ChR increases the electric field at the bottom of this −ChR, promoting electrical breakdown at its lower edge. Numerical modelling (e.g., Mansell et al., 2002, 2005) indicates that lower +ChR is critical for the development of −CG flashes. Moreover, the CG flash rate (CGFR) is controlled primarily by the amount of lower storm charge (Krehbiel et al., 2008).

Contrarily, the presence of excessive charge in the lower +ChR may prevent the occurrence of −CG by "blocking" the progression of descending negative leaders from reaching the ground (e.g., Qie et al., 2005; Nag and Rakov, 2009; Iudin et al., 2017). Additionally, modelling by Iudin et al. (2017) showed that significant reduction or absence of lower +ChR can also prevent the occurrence of −CG. Qie et al. (2005) reported, on the central Tibetan Plateau, that the presence of excessive lower positive charge prevented the occurrence of −CG flashes, which in turn favoured the inception of intracloud (IC) flashes between the main negative and the lower +ChR. VHF imaging presented by Tessendorf et al. (2007) indicates that the lower +ChR appears to be vertically deeper and to have a larger horizontal extent when such ICs are more energetically favourable than −CG flashes.

All in all, thunderstorms will display different intensities on the CGFR along their life-cycle. A fundamental question — which cloud parameters determine the lightning rate in thunderstorms — has not satisfactorily been answered yet (e.g., Boccippio, 2002; Yoshida et al., 2009; Dahl et al., 2011). MacGorman et al. (2011) suggested that most of the variation in the timing (and perhaps amount) of CG lightning is caused by variations in the timing and amount of the lower +ChR. With this paper, we intend to contribute to answering this question.

Approach of the Study

The uninterrupted performance of an LMA system in the Ebre's Delta region (north-eastern coast of the Iberian Peninsula) since its deployment in 2011, allowed gathering large amounts of 3D lightning measurements on different kinds of storms in the region. The present study takes advantage of this large database to focus on classical, normally electrified thunderstorms, aiming to shed new light on how the thunderstorm charge structure affects lightning production, especially the cloud-to-ground fraction, including flash rate, type, and polarity. Indeed, besides severe weather-related damage on the ground, lightning hazard poses a threat to human activity, disrupting economic and social activities. Lightning causes a significant number of deaths, injuries, and property damage reports annually (e.g., Curran et al., 2000; Holle, 2016); causes faults and outages in electric power transmission and electronic systems (e.g., Cummins et al., 1998); and causes accidents to chemical facilities and critical infrastructures like oil and gas refineries and pipelines (e.g., Krausmann et al., 2011).

The organization of the paper is as follows: Section 2 describes the area of study, the instrumentation and data used; Section 3 deals with the methodology; Section 4 presents the results; Section 5 discusses the results and finally section 6 summarises the key findings of the study.

2. INSTRUMENTATION AND DATA

The area of study (hereafter, AoS) of the present study (Fig. 1) was determined by the area of coverage of the so-called Ebre Lightning Mapping Array (ELMA). This LMA system, deployed in the Ebre river delta region within the framework of the Atmosphere-Space Interactions Monitor (ASIM) mission (Neubert et al., 2006; Neubert et al., 2019), consists of eleven stations. This region presents lightning activity throughout the year, the proximity of the Mediterranean Sea still provides favourable conditions for autumn and winter activity in the coastal area, its warm waters being the main driver for storm development after the summer inland thunderstorm season (e.g., Pablo and Soriano, 2002; Montanyà et al., 2016; Pineda et al., 2018).

2.1. Intracloud lightning

The LMA system uses a time-of-arrival (TOA) technique to locate, in three dimensions, lightning radio emissions in the very high-frequency range (VHF, 60–66 MHz) (Rison et al., 1999; Thomas et al., 2004). Each station samples, over 80 μs intervals, the maximum signal amplitude and its GPS-derived precise time, allowing it to detect 2,000 to 3,000 sources per second. To find a solution, a source must be retrieved by at least five LMA stations. The ELMA network sensitivity, estimated through the minimum source power detected (Thomas et al., 2001) is consistent throughout the whole AoS (Fig. 1). Regarding accuracy, the method by Thomas et al. (2004) showed typical horizontal and vertical spatial location errors of the ELMA sources ranging from 10 m to 300 m within the AoS.

The advent of systems capable of mapping IC lightning in 3D like the LMA made possible to determine (i) total lightning flash rates (McCaul et al., 2009; van der Velde and Montanyà, 2013); (ii) typical spatio-temporal lightning dimensions (e.g., Bruning and MacGorman, 2013; López et al., 2017; San Segundo et al., 2020) and (iii) thunderstorm charge structures (e.g., Wiens et al., 2005; Tessendorf et al., 2007; Lund et al., 2009; Biggerstaff et al., 2017; Pineda et al., 2018). To these ends, a flash sorting algorithm is needed, to identify which sources are likely to be part of any given flash. In the present study, the LMA flash algorithm developed by van der Velde and Montanyà (2013) was used. In brief, the algorithm performs VHF source clustering by using a specific time separation between each consecutive source (see San Segundo et al., 2020 for details). The final step to validate a flash is a minimum-source filter, intended to filter noisy sources not related to lightning. This minimum-source filter is set here to 10 sources per flash, like in Schultz et al. (2015) and Carey et al. (2019), among others.

2.2. Cloud to ground lightning

Cloud-to-Ground lightning data from the European LINET network was used to calculate the CG flash rate. LINET employs the TOA technique to locate CG lightning strokes detected in the very-low-frequency range, with a location accuracy of around ~150 m (Betz et al., 2009a). More details about the LINET system can be found in Betz et al. (2009b) and Höller et al. (2009).

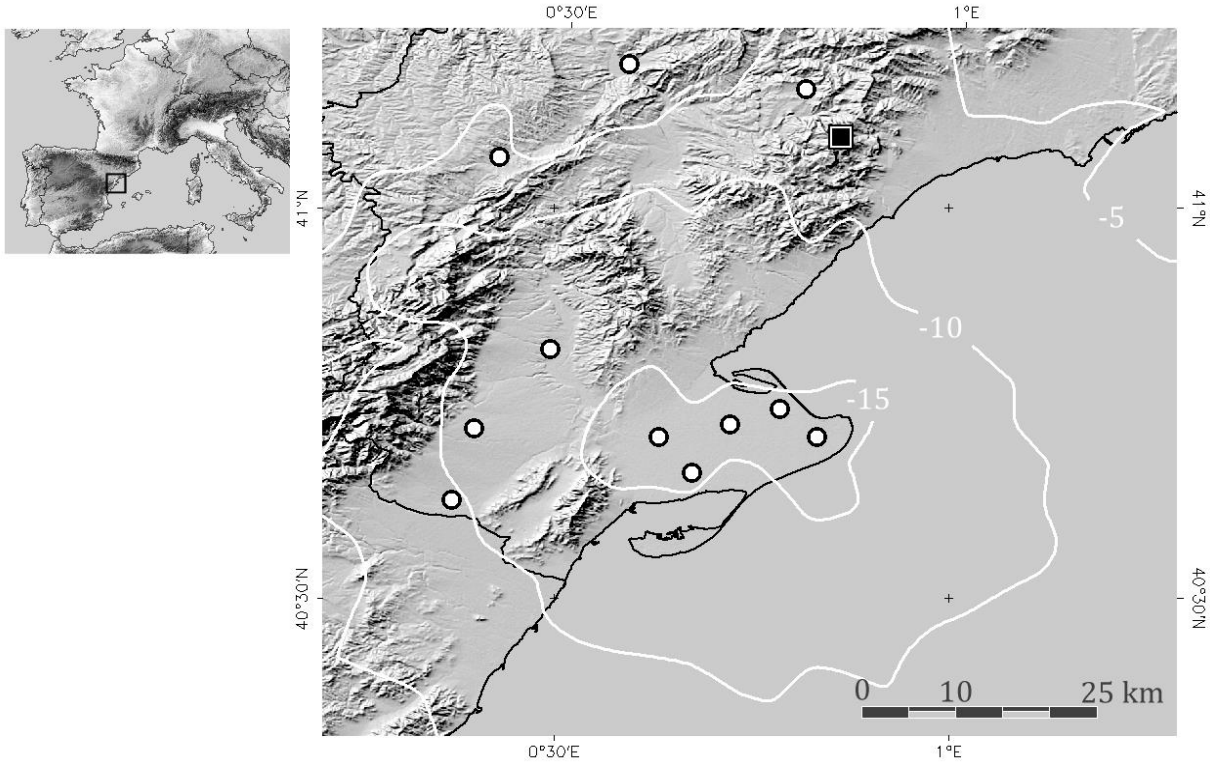

Fig. 1. Area of study (AoS), nearby the Ebre's river Delta, south Catalonia, in the Mediterranean coast at the NE of the Iberian Peninsula. Circles correspond to the locations of the eleven stations that constitute the Ebre Lightning Mapping Array. The black square indicates "La Miranda" weather radar site. White isolines indicate the LMA sensitivity (dBW) across the AoS.

2.3. Meteorological data

The Meteorological Service of Catalonia (*Servei Meteorològic de Catalunya,* hereafter SMC) operates a weather radar network in the region. In particular, "La Miranda" radar (N 41° 05′ 30.24″ E 0° 51′ 48.58″; 950 m MSL) (Fig. 1) is the C-band Doppler radar (5,600 to 5,650 MHz) that covers the AoS. Radar volumes are acquired every 6 minutes, through a fourteen-elevation scan scheme. Further technical details of the SMC weather radar and network characteristics can be found in Argemí et al. (2014) and Altube et al. (2015). The present work mainly relies on the echo top product (TOP), the maximum height of radar echoes within an intensity equal or higher than a given reflectivity, which is used on the analysis of the evolution of the vertical structure of the storms. To this end, 12 and 35 dBZ thresholds were selected among the TOP operative products generated at the SMC. The

TOP−12 product is a proxy for the altitude of the thunderstorm top boundary (e.g., Rosenfeld et al., 1993; Yuter and Houze, 1995), whereas TOP−35 is a proxy for the maximum convective intensity of precipitation systems (e.g., Vincent et al., 2003; Yang and King, 2010; Liu et al., 2012), as it is indicative of the maximum altitude reached by graupel (Straka et al., 2000). Previous studies on the current AoS (Pineda et al., 2018; Salvador et al., 2020) had established that lightning activity can be expected when the radar TOP−12 is above the −40 °C height. Moreover, it intensifies as the TOP−35 remains above the −10 °C isotherm height. Besides, the TOP−35 reaching the −40 °C is indicative of deep convection and large lightning intensities will follow. Similarly, lightning activity stops occurring as these conditions are no longer fulfilled.

Relying on the NIC mechanism to explain cloud electrification (e.g., Takahashi, 1978; MacGorman and Rust, 1998), the environmental temperatures selected in this study were 0 °C, −10 °C, and −40 °C, aiming to delimit the mixed-phase cloud region, where the main −ChR resides (MacGorman and Rust, 1998); as well as the melting level, related to the lower +ChR (Stolzenburg et al., 1994). Heights for these significant isotherms and thermodynamic conditions relative to the analysed episodes were obtained with the Weather Research and Forecast (WRF) model (version 3.1.1; Skamarock et al., 2008). See Mercader et al. (2010) for the details on the parameterization.

3. METHOD

3.1. Inferred charge structure from LMA

Charge structure analysis of LMA data is an interpretative process guided by a realistic physical model of the lightning discharge (Wiens et al., 2005). According to the bi-directional model (Kasemir, 1960; Mazur and Ruhnke, 1993), the lightning discharge initiates in the strong electric field between regions of net positive and negative charge and propagates in opposite directions from the discharge origin (Mazur, 1989; Shao and Krehbiel, 1996; Montanyà et al., 2015). As lightning approaches regions of net charge opposite the leader polarity, the leaders spread outward into these regions (Williams et al., 1985; Coleman et al., 2003). Negative polarity breakdown is inherently more powerful than positive polarity breakdown at the radio frequencies used by the LMA (Rison et al., 1999), resulting in far more LMA sources mapping the negative breakdown than the positive breakdown. Consequently, the majority of sources in a typical flash are interpreted as negative breakdown through a region of positive charge. This way, the horizontal propagation of the lightning channels indicates the existence of vertically stacked horizontal regions of charge (e.g., Shao and Krehbiel, 1996; van der Velde and Montanyà, 2013). Using balloon soundings to measure the electric field, Coleman et al. (2003) found a good agreement between the maximum electric fields and the LMA inferred flash initiations.

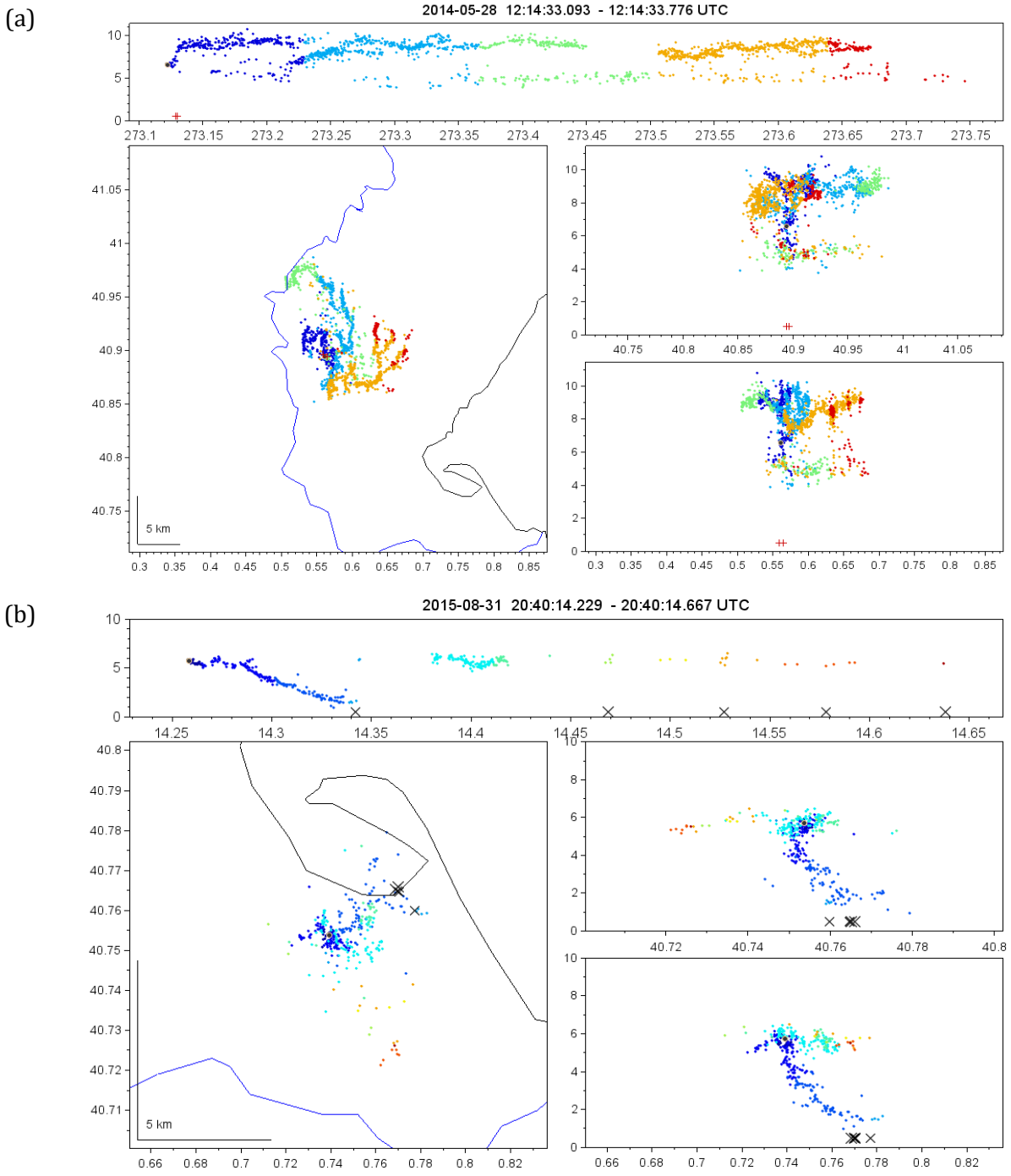

Fig. 2. Multipanel display of (a) intracloud lightning flash and (b) cloud-to-ground flash detected by the Ebre Delta lightning mapping array. LMA sources are coloured with time. Crosses indicate time-position of LINET CG detections. The top panel is the altitude above mean sea level (km) versus time (seconds). The left panel is a plan view map (0.1° latitude equals 11.1 km) with contours of the coastline (black) and Ebro river (blue) as background. The panels at the right show altitude (km) by latitude and longitude.

Fig. 2a shows an example of a typical IC flash as detected by the LMA, from the 28th May 2014 episode. The initial breakdown occurred at 6,000 m MSL, with a negative leader climbing to 9,000-10,000 m MSL, spreading horizontally into the upper half of the +ChR.

As is typical for negative leaders, it is well mapped by the LMA. At the same time, but much less densely mapped, VHF sources at 5,000-6,000 m MSL correspond to the positive leader moving into the upper half of the −ChR (Coleman et al., 2003). Fig. 2a side projections clearly show horizontal regions where lightning channels propagate, indicating the height of the horizontal ChR. Fig. 2b shows a descending negative stepped leader, that culminates with a CG stroke reported by LINET (−7 kA). The leader breakdown is between 5,000-6,000 m MSL. After this first return stroke, LINET reported four more strokes (−12 kA, −9 kA, −7 kA and −14 kA respectively). However, fast dart leaders are not well detected by the LMA. Unlike the stepped leader, the dart leader travels in a more continuous fashion and roughly 2 orders of magnitude faster (Rakov and Uman, 2003).

3.2. Charge regions through Lightning initiations

The first VHF radiation source that is detected by the LMA during a lightning flash provides a good indication of the flash initiation location in space and time. Once individual flashes are obtained with the flash sorting algorithm (section 2.1), its first sources will give information about the lightning initiation location within a few tens of meters or less (Maggio et al., 2005). Breakdown in IC flashes was found to be at the same altitudes as the potential wells associated with a dominant positive charge in the upper part of a storm and with the positive charge in the lower part of the storm. (e.g., Coleman et al., 2003): This way, vertical distributions of flash initiations are used to infer the height of the ChRs.

Whereas a flash-by-flash analysis would be the best way to determine thunderstorm ChRs, an automated method is needed. The method used is developed in the following. For each LMA flash, the three-dimensional position of its initiations (latitude, longitude, altitude) is determined using a method similar to Lund et al. (2009) and Caicedo et al. (2018). First, only flashes with more than 10 sources are selected to avoid noisy sources or partially detected flashes. Average longitudes ($\bar{\lambda}$), latitudes ($\bar{\phi}$) (in radians) and altitudes ($\bar{z}$) (equations 1 to 3 respectively) are then calculated for the first 10 sources to identify the flash initiation.

$$\bar{\lambda} = \frac{\pi}{180}\frac{1}{n}\sum_{i=1}^{n}\lambda_i \qquad (1)$$

$$\bar{\phi} = \frac{\pi}{180}\frac{1}{n}\sum_{i=1}^{n}\phi_i \qquad (2)$$

$$\bar{z} = \frac{1}{n}\sum_{i=1}^{n} z_i \qquad (3)$$

where n is the number of sources; and λ_i, ϕ_i and z_i are the latitude, longitude (in degrees) and altitude of each i source. Then the standard deviation (σ) of these first 10 sources is given by equation 4

$$\sigma = \sqrt{\frac{1}{n-1}\sum_{i=1}^{n} R_e^2(\bar{\phi}-\phi_i)^2\cos^2\bar{\lambda} + R_e^2\left(\bar{\lambda}-\lambda_i\right)^2 + (\bar{z}-z_i)^2} \qquad (4)$$

where the R_e is the radius of the Earth, and $\lambda_i$and ϕ_i are transformed to radians. If the standard deviation is greater than 500 m, the average locations of 10 subsets containing

9 from the original 10 sources are recalculated, that is, for each subset a source is discarded. The standard deviations for each subset are calculated and the smallest and its corresponding subset are selected, discarding the rest. The process is repeated until $\sigma <$ 500 m or only 5 sources remain in the last subset. Finally, the height of the flash initiation is determined as the $\bar{z}$ of the last subset. All these flash initiations are accumulated in a histogram, on a 6-min time bin framework, which is the time span of the radar volumes.

A density function is derived from this histogram to detect the heights where breakdowns accumulate. To improve the self-detection of these maxima, the following requirements were applied to the density function (for each 6-min bin): i) a variable wavelength is used to avoid close maxima (less than 3 km in altitude), ii) only those heights that have a minimum of initiations greater than 30% relative to the mode of vertical distribution (or have at least 5 initiations), will participate in the density function calculation.

LMA-derived lightning initiation centres (LMA-LIC) obtained through this method correspond approximately to either the lower part of the upper +ChR or to the upper part of the lower +ChR. To finally classify the LMA-LIC as an upper +ChR or a lower +ChR, a threshold around a maximum of 1 km above the −10 °C isotherm was used. Finally, in the case that multiple maxima classified in the same category were detected (upper or lower +ChR separately) for the same 6-minute bin, only one maximum height value was kept for each category, corresponding to the height where a greater number of initiations were detected.

After validating the different +ChR, 6-min bins are classified into three different categories: an “Upper” dipole (hereafter UpDip) or “Lower” dipole (LwDip), and a “Tripole” (TriP) when both Upper and Lower +ChR are present, as schematically represented in Fig. 3. To ensure that only favourable lightning activity situations are evaluated, those periods in which the TOP−35 is below the −10 °C isotherm are discarded from the study, as well as the periods with a significant increase in TOP−35 due to strong convection, which would cause the ChR to be not clearly stratified. Additionally, after the automated categories classification, those maximums (and their respective 6-min time bins) that present an anomalous height concerning the rest of the heights of the same category are categorized as "Unclassified". As an example, the results of the whole procedure are shown for one of the case studies in Fig. 4.

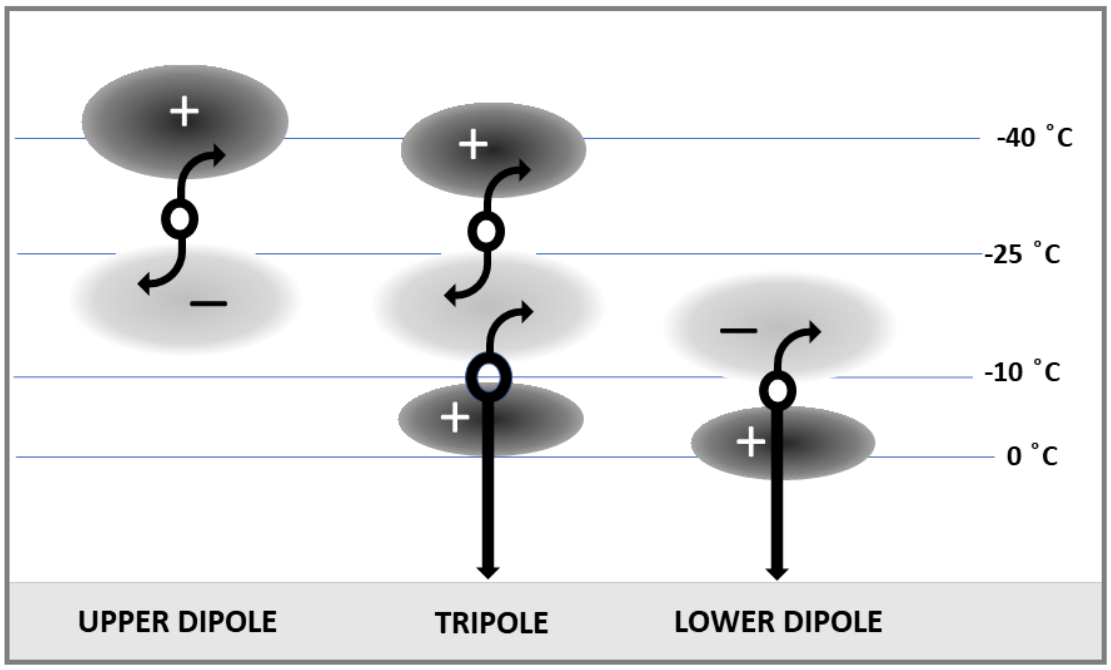

Fig. 3. Idealized scheme of the three main charge structures in thunderstorms. From left to right: Upper Dipole (UpDip), Classic Tripole (TriP) and Lower Dipole (LwDip). The dark grey and light grey circles indicate the position of the main positive and negative charge regions, respectively. The black circles show the position of the initiations of the flashes, and the arrows point out the most typical channel spread of these flashes, going towards the main positive or negative charge regions depending on whether the channels are negative or positive (bi-directional model). Isotherms where the main charge regions are typically found, are also added.

4. RESULTS

4.1. Overview

The following results rely on a set of approximately 95,000 LMA flashes and 31,000 CG flashes from 13 episodes that took place in the AoS, during the warm season between October 2013 and October 2018. Environmental conditions and characteristics of the 13 episodes are summarized in Table 1. Within these episodes, the working unit is the radar-derived 6-min time interval. Recall that each time bin with LMA activity was classified into one of the three categories previously described (or flagged as unclassified). Table 2 presents a summary of the working units per episode and category. A total of 764 6-min time bins were analysed, 13% corresponded to the LwDip category, 38% to the TriP and 44% to UpDip. The remaining 5% was "Unclassified".

Table 1. Summary of case studies. Information on each episode includes Instability indices (e.g, Convective Available Potential Energy, CAPE; Lifting Condensation Level, LCL) and isotherm heights (0 °C, −10 °C, −40 °C and tropopause) derived from the WRF model. Lightning CG flash rates are obtained from LINET data.

Episode		20131004	20140528	20140701	20140802	20150731	20150831	20171018	20171104	20180720	20180809	20180905	20180917	20181019
Radiosounding time (UTC)		12:00	12:00	12:00	12:00	12:00	12:00	12:00	12:00	12:00	12:00	12:00	18:00	12:00
Instability indices	CAPE (J kg^{-1})	2,400	975	1,360	1,925	1,240	1,655	1,425	765	925	2,375	1,500	1,525	690
	Normalized CAPE (NCAPE)	0.18	0.11	0.13	0.19	-	0.20	0.13	0.10	0.15	0.22	0.15	0.14	0.07
	Lifted Index (°C)	-6.5	-3.5	-4.9	-6.6	-4.2	-5.8	-4.9	-3.2	-4.7	-7.6	-4.8	-5.6	-2.3
	Thompson Index (°C)	42	34	24	38	36	36	36	36	20	44	33	33	35
	Total Totals Index (°C)	50.8	53.1	47.1	51.8	51.3	48.4	51.0	54.0	48.9	52.3	48.9	51.1	48.5
	Wet Bulb Zero height (ft. AGL)	12,449	8,120	9,235	10,390	10,840	12,970	9,675	8,590	9,800	12,233	10,756	10,880	10,372
Level of Free Convection, LFC (m AMSL)		367	916	927	908	1,395	720	562	1542.6	3,438	1,100	852	529	736
Lifting Condensation Level, LCL (m AMSL)		367	783	890	828	1,395	881	496	596	1,420	981	852	333	673
Warm Cloud Depth (m)		3,833	1,817	2,810	2,972	2,805	3,369	2,804	2,254	2,880	3,120	3,098	3,617	2,727
Isotherm Heights (m AMSL)	0°C	4,200	2,600	3,700	3,800	4,200	4,250	3,300	2,850	4,300	4,100	3,950	3,950	3,400
	-10°C	5,550	4,100	5,400	5,250	5,600	5,750	4,800	4,350	5,600	5,600	5,550	5,450	5,100
	-40°C	9,600	8,100	9,600	9,500	9,900	8,500	8,800	8,300	9,750	9,550	9,400	9,750	9,100
Tropopause Height (m AMSL)		12,750	10,000	12,000	12,400	11,340	12,550	11,120	10,050	--	11,310	--	12,375	--
LMA Average Flash Rate (min^{-1})		13.5	3,7	18,1	7,9	9,3	35,9	9,9	5,3	11,9	17,9	23,7	11,3	7,6
LMA Maximum Flash Rate (min^{-1})		50,5	27,0	42,3	47,7	49,7	59,0	47,3	38,3	52,7	61,0	64,8	52,3	28,5
Average CG Flash Rate (min^{-1})		11,3	2,4	1,8	2,2	7,9	7,6	5,2	1,9	0,6	3,8	6,6	3,5	4,9
Maximum CG Flash Rate (min^{-1})		32,8	9,2	5,7	14,3	28,8	21,5	24,2	11,7	3,8	13,8	36,7	12,8	19,7

Table 2. Summary of case studies regarding their lightning activity. For each day of study, the number of samples is indicated as the number of 6-min intervals, which correspond to each radar volume time, and they differ according to the electrical structure at that time between Lower (LwDip), Tripole (TriP), Upper (UpDip) and Unclassified. The last two columns correspond to LMA Flash counts and LINET CG Flash counts for each episode.

Episode	*Samples*	*Lower Dipole*	*Classic Tripole*	*Upper Dipole*	*Unclassified*	*#Flash LMA*	*#CG Flash LINET*
20131004	24	0	5	17	2	2,587	2,164
20140528	73	41	24	7	1	2,602	1,464
20140701	62	1	28	29	4	8,055	782
20140802	62	2	17	38	5	4,951	1,349
20150731	34	0	8	23	3	4,516	3,844
20150831	41	1	19	19	2	13,156	2,771
20171018	68	17	34	10	7	6,373	3,334
20171104	49	13	27	6	3	3,535	1,290
20180720	44	2	7	27	8	4,014	197
20180809	88	1	22	63	2	14,389	3,080
20180905	75	0	10	61	4	20,760	5,738
20180918	45	1	31	13	0	4,464	1,405
20181019	99	18	61	20	0	5,732	3,655
TOTAL	**764**	**97**	**293**	**333**	**41**	**95,134**	**31,073**
%		13%	38%	44%	5%		

4.2. Case overview

Before the statistics, two of the case studies are presented, to illustrate the evolution of the lightning activity of storms, the heights where the different ChRs were detected, as well as the radar echo tops trends along the whole life-cycle.

1st July 2014

On that day, convective indices presented moderate conditions of instability, i.e., CAPE 1360 J·kg^{-1}, Lifted Index −4.9 (Table 1). Thunderstorms started to develop in the mountainous region west of the AoS, moving northeast while crossing it. Initially isolated cells evolved into a broken line, oriented in the direction of the predominant SW-NE flow. Over time, the flow rotated to a west-east pattern. New growing cells kept clustering but in a less organized manner until the decay of the whole system between 18:00 and 19:00 UTC. Fig. 4 shows the evolution of the vertical structure of the convective system. After some initially isolated cells, the system intensified between 12:00 UTC and 13:00 UTC, as indicated by an increase in the height of the TOP−35 as well as on the density of LMA sources. The seesaw trend of the TOP−35 in the following hours suggests a sequential development of pulse-type convection. The high LMA source count (hereafter LMA-SC, understood as the number of sources in a 6-min period and in a height interval of 500 m) at higher levels lasted while the TOP−35 remained around the −40 °C. The abrupt decay of the TOP−35 by 18:30 UTC

led to the termination of the lightning activity. LMA-LIC are plotted with blue dots (upper), red dots (lower) and black dots (unclassified).

a)

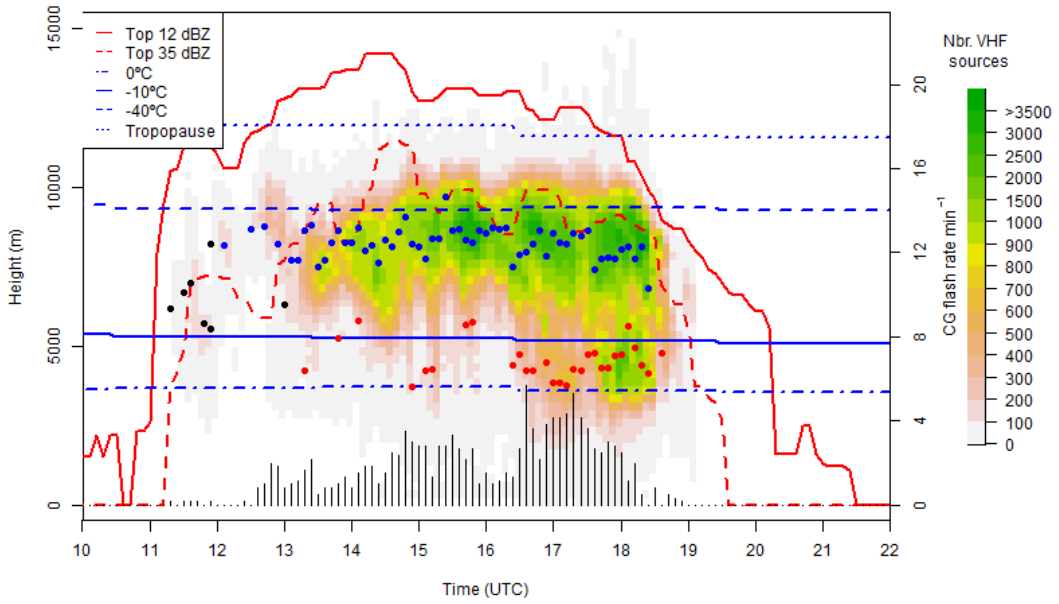

b)

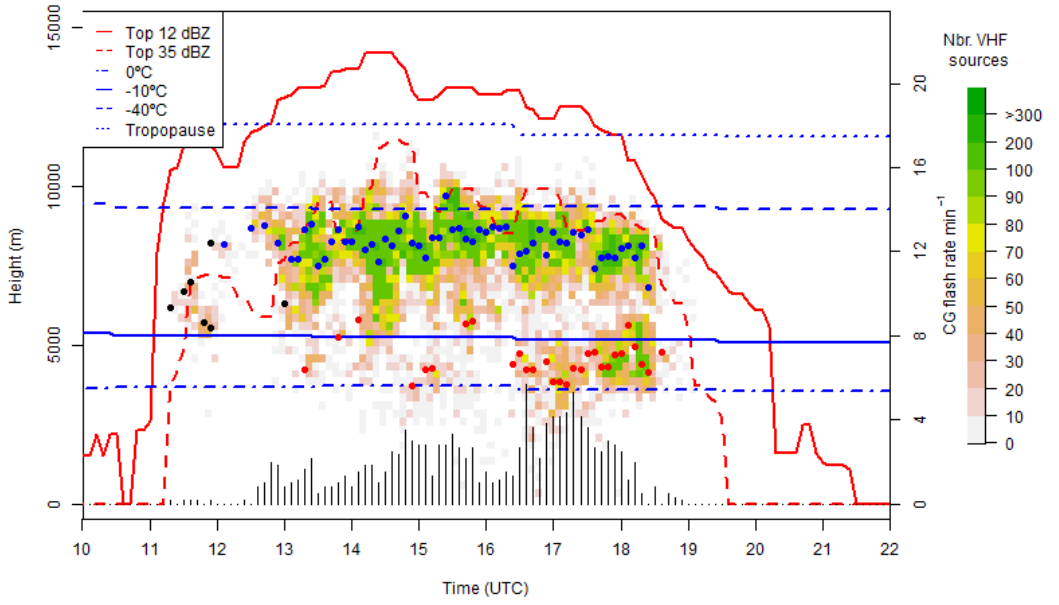

Fig. 4. (a) Evolution of the vertical structure of the storms occurring in the area of study on the 1st July 2014. Time–height LMA source count plot. Colour indicates the relative number of sources according to a pink-yellow-green colour scheme. Red lines correspond to the height of the TOP–12 (solid) and TOP–35 (dashed) products. Barlines indicate the CG flash rate (min^{-1}). Finally, blue lines correspond to the representative environmental temperature values obtained from the vertical sounding profiles (0 °C, −10 °C, −40 °C and tropopause heights in m MSL). (b) only the ten first LMA sources are represented on the density plot. LMA-derived lightning initiation centres are plotted with blue dots (upper), red dots (lower) and black dots (unclassified), on each 6-min time bin.

Early stages began with only IC flashes between mid-level −ChR and upper +ChR, with few −CG flashes. As the storms developed further and precipitation grew and descended, a lower +ChR formed within the strongest precipitation, thus completing the tripole charge archetype (as indicated by the initiation regions in Fig. 4). The CGFR increased after the formation of this lower positive charge, and −CG flashes originated between the mid-level −ChR and lower +ChR, tapping the mid-level negative charge. The high LMA-SC at the lower +ChR at the end of the episode (after 18:00 UTC) may denote an excessive charge in the lower +ChR, preventing the occurrence of −CG by "blocking" the progression of downward negative leaders (Nag and Rakov, 2009).

In this particular case, the main −ChR is delimited between those initiation regions and can be located approximately between 6,000 and 8,000 m MSL. +ChRs being above the upper initiations (9,000-11,000 m MSL) and below the lower initiations (4,000-5,000 m MSL). These three charge regions relate to the typical tripole structure. It is worth noticing the increase in the CGFR on the latest hours, coinciding with the presence of a steady lower +ChR (16:30-18:00 UTC approx.).

28th May 2014

On this day, convective indices indicated weak to moderate conditions of instability, with a weak CAPE of 980 $J \cdot kg^{-1}$ and moderate Lifted Index −3.5 (Table 1). Two differentiated periods can be observed during this day. From 06:00 to 10:00 UTC, the CAPPI sequence analysis showed isolated cells developing along the morning here and there. Fig. 5 shows moderate lightning activity during this period, the LMA-SC being rather low, the CG rate hardly reaching 10 $CG \cdot min^{-1}$. Despite the moderate activity, the LMA-SC allows to clearly identify two mains +ChRs (where the negative leaders propagate), one between 0 °C and the −10 °C heights, the upper one around the −40 °C height. An increase in the LMA-SC from 80 to 100, especially in the lower region, coincides with an increase in the CG rate.

In contrast, and according to the CAPPI analysis, the second part is characterized by a broken line of storms, moving west-east through the AoS (11:00-15:00 UTC). Although LMA-SC intensified in this second period (11-14:00 UTC) (Fig. 5), LMA-LIC remained at similar heights. Contrary to the 1st July 2014 episode, the stronger ChR was the lowermost layer. This situation led to a sudden increase in the CG rate, especially in the moments when the lower +ChR was more intense according to the LMA-SC. Finally, as the TOP−35 decreased to heights below the −40 °C, the upper +ChR weakened, and so did the CG lightning rate until the end of the storm.

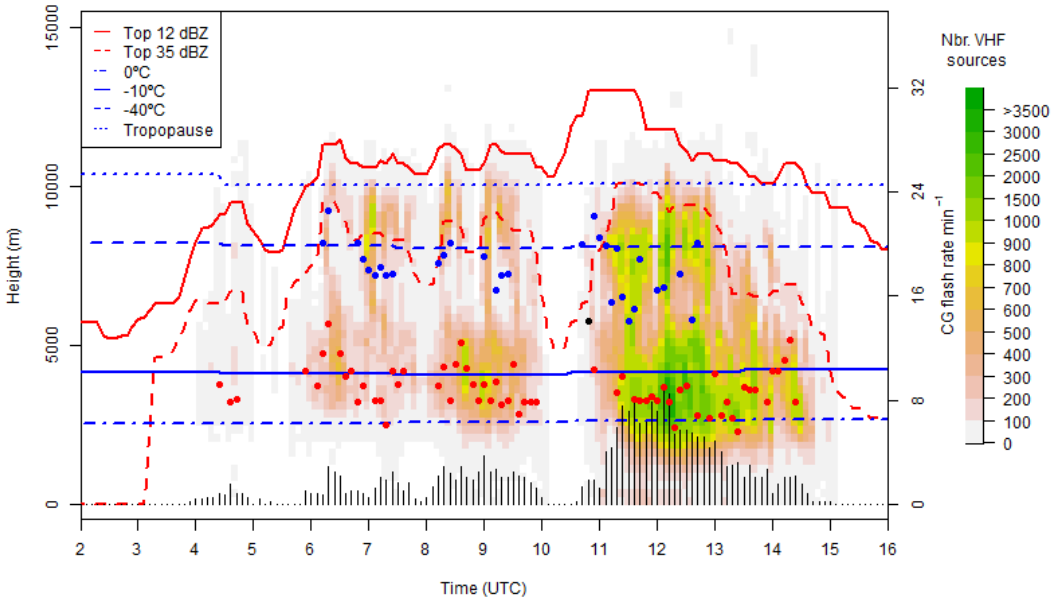

Fig. 5. As to Fig. 4a but for 28th May 2014.

4.3. Charge structure vs Height (Temperature)

Lightning initiations (LMA-LIC) are shown in Fig. 6 for the three categories (LwDip, TriP, UpDip). Relying on the median values of each boxplot, the heights (and environmental temperatures) of the ChRs can be established. The upper +ChR for the tripole is above −40.8 °C (9,150 m MSL). The lower +ChR is below the −7.1 °C height (4,730 m MSL). Interestingly, +ChR are at similar positions on both the UpDip and Trip categories.

As highlighted by Coleman et al. (2003), these LMA-LIC in the upper and lower levels establish the heights of the potential wells between the dominant positive and negative charge in the upper and middle regions of a storm, respectively. Furthermore, Coleman et al. (2003) reported that most CG flashes had a breakdown at lower altitudes, mostly correlated to +ChR in the lower part of the storm.

Table 3 summarizes results from previous studies. Regarding the upper +ChR, most of them showed similar heights, around 8,000-9,000 m MSL, with a minimum of 7,000 m in the northernmost study (Figueras i Ventura et al., 2019). However, others showed a wider range, with heights from 5,200 and 6,000 m according to Caicedo et al. (2018) and Bruning et al. (2007), respectively, to a maximum of 14,500 m MSL in the tropics (López et al., 2019). For those who in turn provided environmental temperatures for this ChR, they also coincide at a temperature close to −40 °C. There is also a consensus for the height of the lower +ChR, being detected at heights around 4,000-6,000 m MSL, and temperatures between 5 °C and −15 °C. Results from the present study located these +ChR at similar heights and temperature ranges, compared to other studies at similar latitudes.

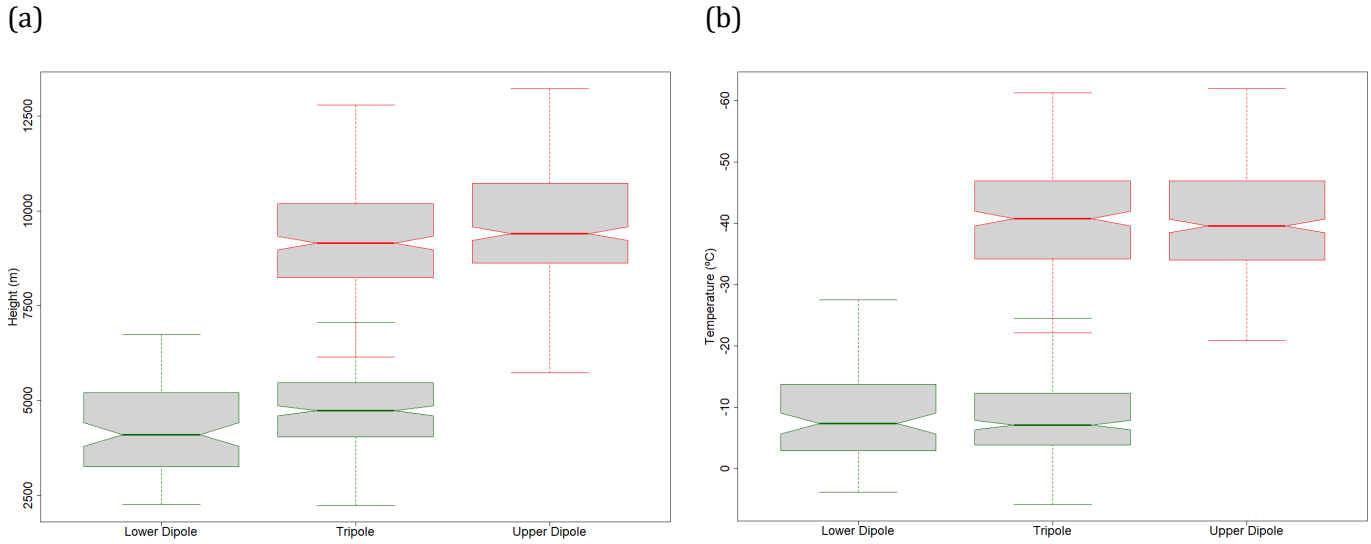

Fig. 6. Boxplot representation of the position of the LMA lightning initiations centres (LMA-LIC) for the three electrical structure categories (LwDip, TriP and UpDip). Centres are both represented by (a) height and (b) temperature. Boxes represent the interquartile range between Q25 and Q75, with a solid line indicating the median value. Whiskers indicate the lower and upper limits of the 1.5 interquartile range. The width of each box indicates the number of samples in each one, and the notch represents the 95% confidence interval of the median.

Table 3. Summary of studies that derived charge region heights (and temperature ranges) from lightning observations.

Study	System	Area of Study	Latitude	Height m MSL (temperature) Upper positive charge region	Height m MSL (temperature) Lower positive charge region
Dotzek et al. (2005)	LDAR II	Texas, U.S.	33°	10,000 m (−45 °C)	4,500 m (−5 °C)
Wiens et al. (2005)	LMA	New Mexico, U.S.	36°	8,000 - 10,000 m	4,000 - 5,000 m
Bruning et al. (2007)	LMA-EFM	Oklahoma, U.S.	35°	6,000 - 8,000 m (−6.5 °C - −19 °C)	4,000 m (2 °C)
Wu et al. (2015)	BOLT	Osaka Bay, Japan	35°	9,000 - 10,000 m	4,000 - 5,500 m
Mecikalski et al. (2015)	LMA	North Alabama, U.S.	34°	8,000 - 10,000 m (−35 °C)	3,500 - 4,000 m (0 °C)
Mecikalski and Carey (2017)	LMA	North Alabama, U.S.	34°	8,000 - 9,000 m (−28.3 °C - −36.2 °C) for a multicell-type storm	3,000 - 4,000 m (3.8 °C - −2.0 °C) for a multicell-type storm
Caicedo et al. (2018)	LMA	North-Central Florida, U.S.	30°	5,200 - 9,800 m (−22.3 °C - −38.2 °C)	2,300 - 5,100 m (10.9 °C - −5.8 °C)
Fuchs and Rutledge (2018)	LMA	Alabama, Washington, D.C., Oklahoma, Colorado, U.S.	32° - 40°	8,700 m (−15 °C - −30 °C)	6,000 m (0 °C - −15 °C)
Pineda et al. (2018)	LMA	Catalonia, Spain	40°	10,000 - 11,000 m (−40 °C)	a lower positive below −10 °C
López et al. (2019)	LMA	Santa Marta, Colombia	11°	11,000 - 14,500 m (−42 °C - −70 °C)	4,000 - 6,000 m (6 °C - −5 °C)
Figueras i Ventura et al. (2019)	LMA	Switzerland	47°	7,000 - 9,000 m	4,000 m
Current Study	LMA	Catalonia, Spain	40°	9,150 m (−40.8 °C)	4,730 m (−7.1 °C)

4.4. Charge structure vs IC rate

Intracloud flash rates (ICFR), calculated once VHF sources are grouped into flashes (section 2.1), were analysed for the three categories. Fig. 7a shows that IC flash rates were similar for the TriP and UpDip categories (median 13.2 and 15.5 flashes·min^{-1}, with a confidence interval (CI) between 11.3 and 15.0 for the first, and 13.5 and 17.5 for the second) but was five times lower for the LwDip (median 3.0 flashes·min^{-1}, with a CI between 2.4 and 3.6). Conversely, VHF sources per flash (Fig. 7b) were

higher for the LwDip category (353 sources per flash, CI between 339 and 367) and diminished to 177 (CI between 173 and 181) for TriP and to 79 (CI between 77 and 81) for the UpDip. This would relate categories TriP and UpDip to convective updrafts where flashes are generally smaller in size, and category LwDip to stratiform or cloud base where flashes tend to have large extents (Carey et al., 2005; Kuhlman et al., 2009; Weiss et al., 2012; Bruning and MacGorman, 2013).

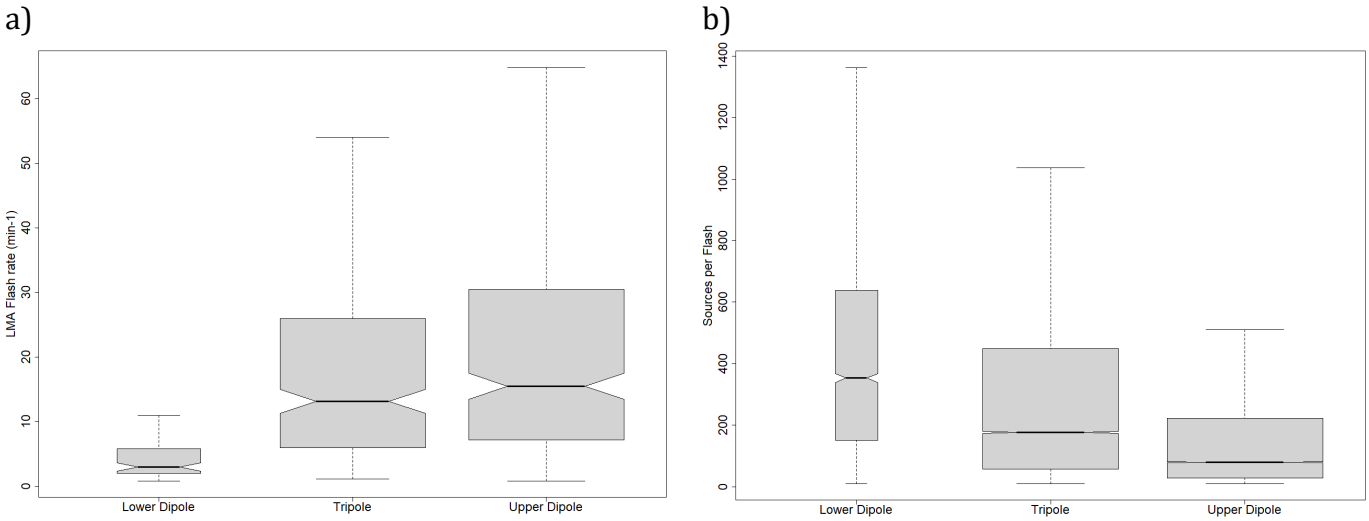

Fig. 7. Boxplot representation according to the different electrical structure categories (LwDip, TriP and UpDip) for (a) LMA Flash rate and (b) number of sources for each LMA Flash.

4.5. Charge structure vs CG rate

The CGFR was found to be different for the three categories (Fig. 8). The flash rate reached higher values when the TriP was present, with a median of around 5.2 flashes·min^{-1}, with an interquartile range between 2.7 and 8.7 flashes·min^{-1}. Contrarily, during phases of the thunderstorm when a dipole category was dominant, the CGFR was lower. In the case of the LwDip, the median CGFR was approximately 2.0 flashes·min^{-1}, with a narrow interquartile range between 1.2 and 3.2 flashes·min^{-1}. The UpDip presented a median value of 3.8 flashes·min^{-1} and a larger interquartile range, with lower and upper limits of 1.3 and 7.8 flashes·min^{-1}, respectively. For both UpDip and TriP categories, the maximum values were close to 17 flashes·min^{-1}, rates never seen in the LwDip category, which had an approximate maximum value of 5.7 flashes·min^{-1}. Notched boxplots show significative differences between categories, as the upper and lower limits do not overlap with each other, with CI lower and upper values of 1.7 and 2.3, 3.3 and 4.4, 4.6 and 5.7 flashes·min^{-1}, for LwDip, UpDip and TriP situations, respectively.

Focusing on the TriP category, where both upper and lower +ChRs are present, Fig. 9a shows the relation of the height difference between the two +ChRs and the CGFR. As the distance between ChR increased, so did the CGFR, from a median value of 3.5 flashes·min^{-1} for the shortest difference (3,000 m) up to a median value of 7.0 flashes·min^{-1} for the largest (6,000 m). A relationship was also found between the height of the UpDip and the CGFR. Similar to the previous one, the higher the upper

+ChR, the higher the CGFR: from a CGFR of 0.8 flash·min^{-1} at 7,000 m MSL, the flash rate steadily increases to reach a median value of 8.8 flashes·min^{-1} for a height of 12,000 m MSL.

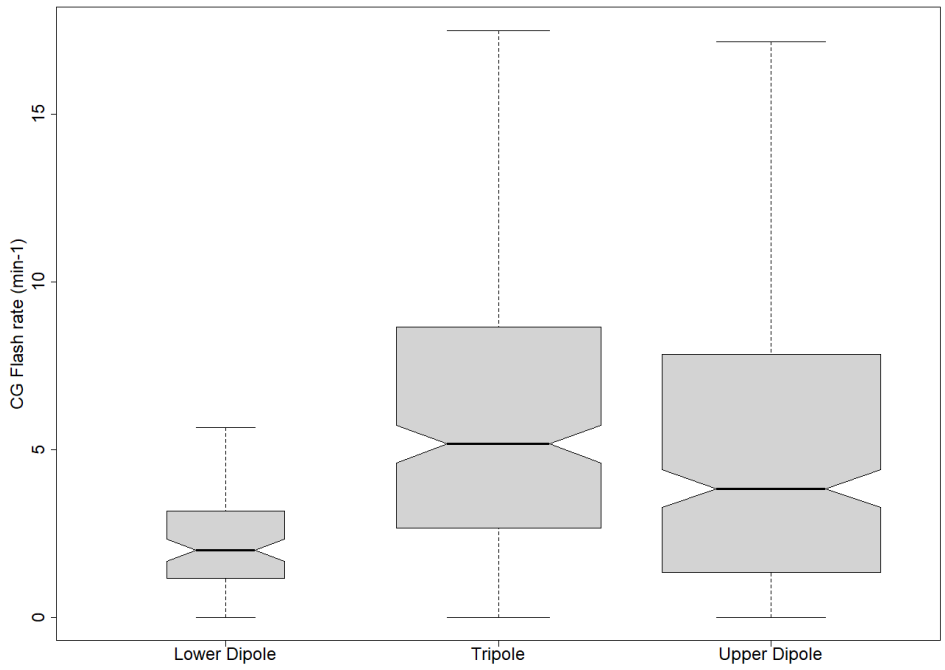

Fig. 8. Boxplots for CG flash rate for the three charge layer categories (LwDip, TriP and UpDip).

a) b)

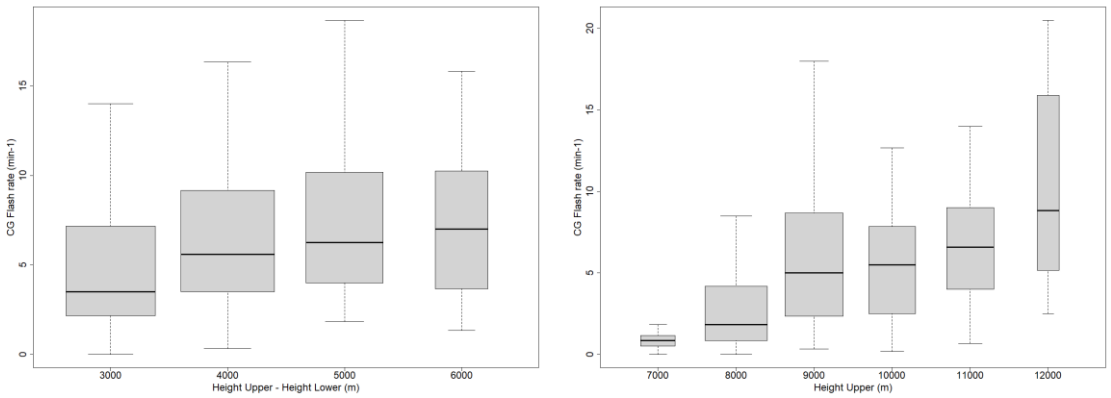

Fig. 9. Boxplots on the ratio of CG flash rate for the three charge layer categories, (a) TriP and (b) UpDip. In the case of TriP, the abscissa axis represents the height difference between the two positive charge regions. In the case of LwDip and UpDip, this represents the absolute value concerning the MSL.

The increase in the CGFR as the UpDip gets higher (Fig. 9b) can be related to vertical air motions, as stronger updrafts typically produce larger CGFR (Williams, 1985; Deierling and Petersen, 2008; Salvador et al., 2020). Strong updrafts tend to produce large ice fluxes which, along with the presence of supercooled liquid water,

promotes charge separating collisions and charge transfer (Williams et al., 1991; Saunders et al., 1991; Saunders and Peck, 1998).

Along with the height of the UpDip, a higher separation between +ChR in the TriP also increased the CGFR (Fig. 9a). A larger separation between ChR can be related to a larger volume for substantial mixed-phase graupel and ice concentrations, which was found to correlate with storm total flash rate (Petersen et al., 2005; Deierling et al., 2005; Liu et al., 2012; Carey et al., 2019).

4.6. Charge structure vs IC:CG ratio

Relatively few studies have examined concurrent trends in both IC and CG lightning within the same thunderstorm. Data available on the current study allows to compare both types of lightning, through the IC:CG ratio, also denoted as Z (Prentice and Mackerras, 1977). Z was found to be different in the three categories (Fig. 10). The highest value was observed for the UpDip, with a median value of 3.33 and a CI between 2.90 and 3.76. Z values above 10 were only detected for the UpDip, with a maximum slightly above 13. The lowest Z corresponds to the LwDip, with a median of 0.30 (with a CI between 0.08 and 0.52). The TriP presented values in between, with a Z of 1.50 (CI between 1.24 and 1.76). In general, in the LwDip category, no ratios greater than 5 were detected, due to a higher number of CGs compared to ICs, compared to the rest of the categories.

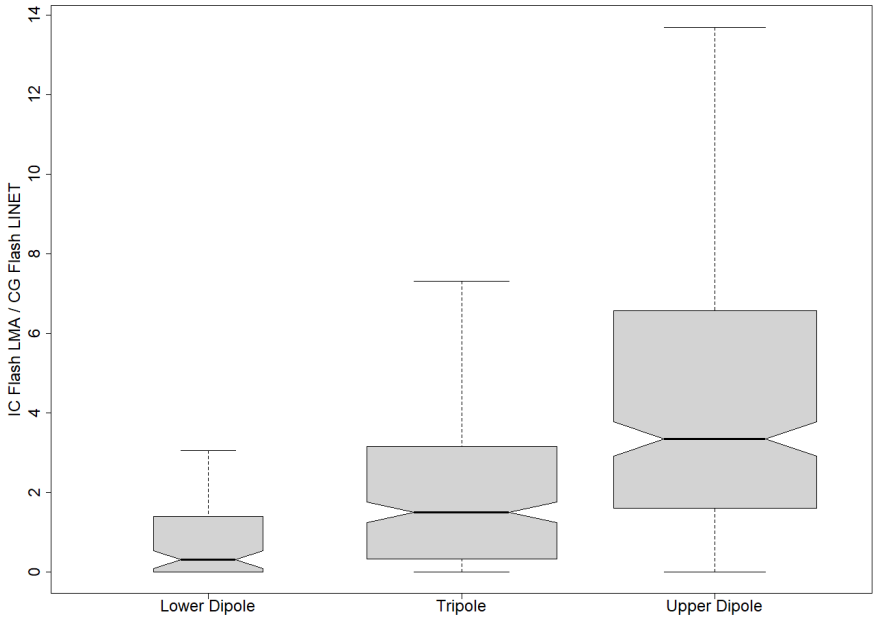

Fig. 10. Boxplots on the ratio IC:CG ratio (Z) for the three charge layer categories (LwDip, TriP and UpDip).

4.7. Charge structure vs CG polarity and multiplicity

Fig. 11 presents the fraction of +CG in each of the three categories. The dashed line indicates one-tenth of the total CG flashes, which was taken as the climatological

reference for positive CGs in the AoS (e.g., Rivas Soriano et al., 2005; Poelman et al., 2016). In particular, the per cent of positives in the total amount of CG in the present study was 9%, similar to the climatological reference. Keeping in mind this 10%, Fig. 11 shows that the median of positives was slightly above the reference for the LwDip category (median of 0.12 with a CI between 0.09 and 0.14). The detailed analysis on the episodes showed few 6-min time bins with positive anomaly (more +CG than −CG), generally occurring at the beginning or at the end of some episodes when the CG rate is below 0.6 CG·min^{-1} (i.e., 1st July 2014, 31st August 2015, 18th September 2018, 19th October 2018).

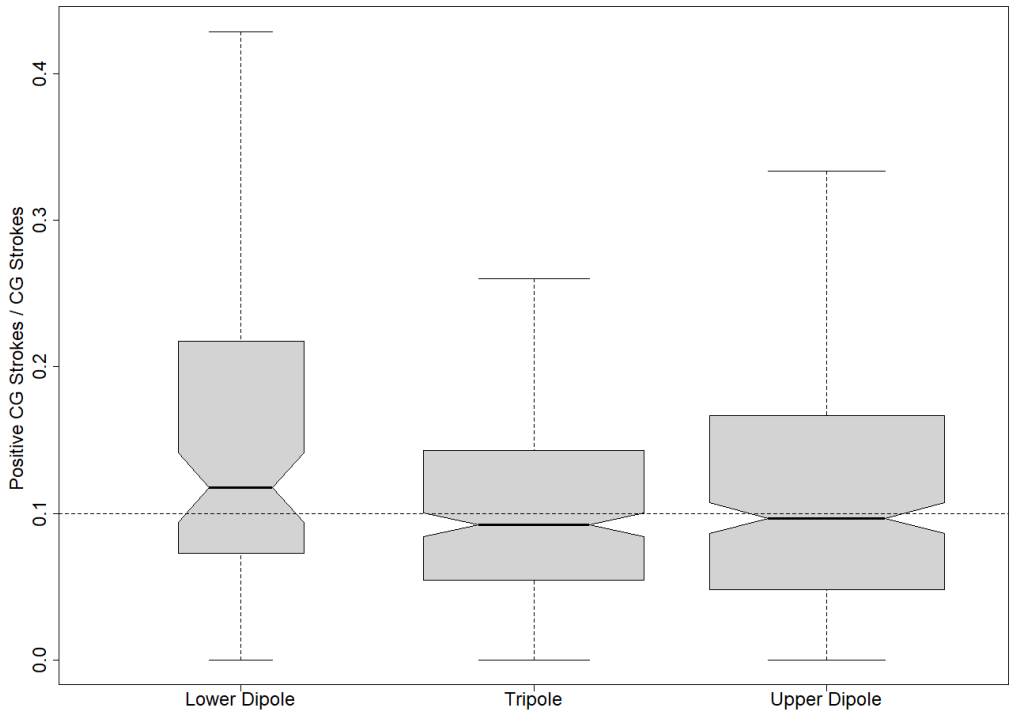

Fig. 11. Boxplots on the ratio of positive CG strokes for the three charge layer categories (LwDip, TriP, UpDip). A horizontal dashed line at 10%, indicates the AoS climatological reference.

CG stroke peak currents also presented some variation between categories (Fig. 12). CG strokes on the LwDip category had higher peak currents on both polarities, with a more pronounced difference on the positive CG strokes, with a median of 15.8 kA (CI between 14.9 and 16.7 kA) for LwDip in front of 13.3 kA (CI between 13.1 and 13.5 kA) for TriP and 12.6 kA (CI between 12.4 and 12.8 kA) for UpDip. Besides, CG strokes above 30 kA hardly occurred in the TriP and UpDip categories. Regarding the negative CG strokes, the median was of −13.6 kA (CI between −13.9 and −13.3 kA), −11.2 kA (CI between −11.3 and −11.1 kA) and −10.4 kA (CI between −10.5 and −10.3 kA) for LwDip, TriP and UpDip respectively. In both cases, it can be observed that in the LwDip category the peak current was statistically significantly higher than the rest.

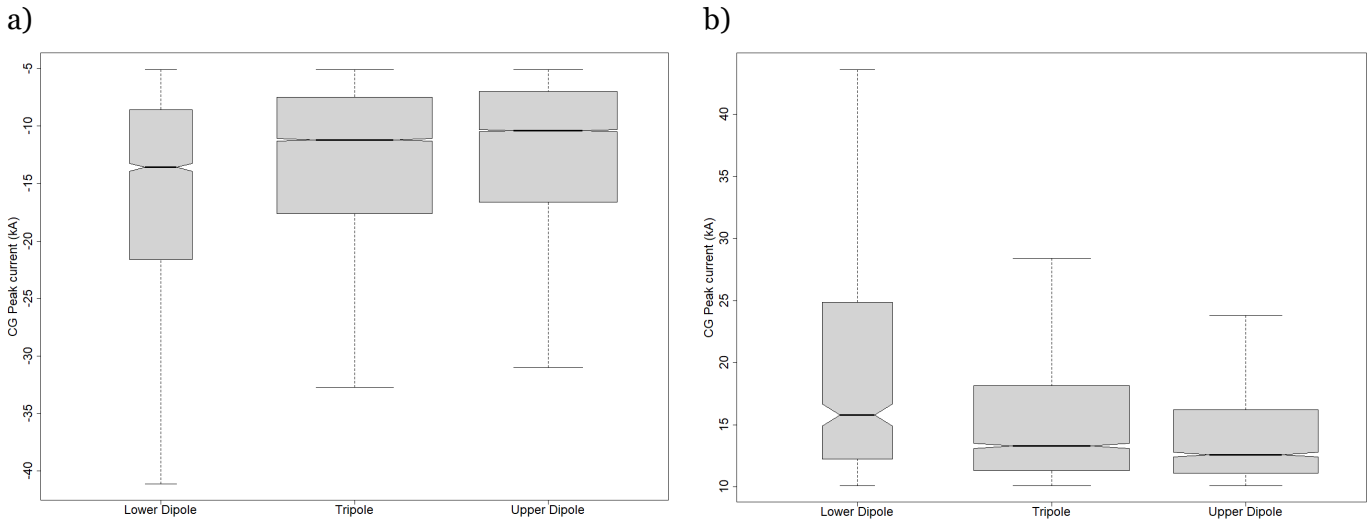

Fig. 12. Boxplots on the (a) negative and (b) positive CG strokes peak current for the three charge layer categories (LwDip, TriP, UpDip).

The multiplicity values were evaluated for the three categories and for each polarity. For LwDip cases, a median multiplicity of 2.42 was observed for +CG flashes and 2.68 for −CG flashes. For the TriP structure, the median multiply values were 2.19 and 2.66 for the +CGs and −CGs, respectively. For UpDip cases, the lowest median values were found, with values of 1.72 for +CG flashes and 2.00 for the −CG flashes.

5. DISCUSSION

5.1. Charge structure vs Height and Temperature

As pointed out by Lund et al. (2009), charge structure analysis relying on LMA observations is limited to the charge layers that participate in lightning production. Thus, LMA observations tend to represent broader regions, compared to results obtained through balloon observations which allow a more specific set of locations for the charge regions (e.g., Coleman et al., 2003, 2008; Rust et al., 2005).

Some studies assume that these broad regions of VHF source density correspond to the regions of positive charge (e.g., Rison et al., 1999; Rust et al., 2005; MacGorman et al., 2008), and therefore lightning initiations will take place near the top or bottom edges of these maxima. On the other hand, other research relies on the location where lightning initiates to infer the charge structure (e.g., Lund et al., 2009; Caicedo et al., 2018). Taking the bidirectional model as a basis for physical interpretation, lightning initiates in the strong electric field between regions of net positive and negative charge, and after short vertical propagation, the following horizontal channel propagation is indicative of the height of the regions of charge (example in Fig. 2). For example, Mecikalski and Carey (2017) showed that peaks in the profiles of VHF sources occur at different altitudes compared to those corresponding only to flash initiations. In the present case studies, such a difference can be seen in Fig. 4a

and Fig. 5 where lightning initiations are combined with the vertical distribution of all sources. Given the leaders grow simultaneously in opposite direction after the initial breakdown (e.g., Montanyà et al., 2015), and recalling that negative leaders spreading on the +ChR tend to emit more VHF radiation (Rison et al., 1999), LMA sources tend to be more numerous and to be distributed more densely in positive charge than in negative charge.

Results found on the present study are not far from idealized positive charge regions on numerical models on vertical charge structure (e.g., Mansell et al., 2005, 2010; Krehbiel et al., 2008; Tao et al., 2009; Tan et al., 2014; Wang et al., 2016; Iudin et al., 2017). The relative minimum in between (−15 °C to −35 °C, ~5,500 to 8,000 m MSL) is consistent with the main midlevel negative charge region, which is not a likely initiation point for lightning flashes (e.g., MacGorman et al., 2001; Fuchs et al., 2015). Results from the present study (Fig. 6) mainly locate lightning initiations in two regions, a higher around −40 °C (~9,000 m MSL), and a lower around −6.0 °C height (~4,500 m MSL).

5.2. Charge structure vs IC rate

Lightning flash rates are directly linked to vertical air motions (e.g., Williams, 1985; Deierling and Petersen, 2008), as stronger updrafts typically produce larger lightning flash rates (e.g., Rutledge et al., 1992; Salvador et al., 2020), which is the case for the upper dipole (Fig. 7a). Indeed, strong vertical motions tend to produce large ice fluxes that promote charge separating collisions along with supercooled liquid water that increases charge transfer per collision (Williams et al., 1991; Saunders and Peck, 1998). Besides, turbulence in strong updrafts results in smaller, more numerous adjacent regions of high charge densities and alternating sign that produce compact flashes (Williams, 1985; Bruning and MacGorman, 2013; Zhang et al., 2017; Zheng et al., 2018). Fig. 7b shows that the sources per flash for the upper dipole is of 79 per flash, compared to the 353 sources in the lower dipole. Figures for this last category can be related to flashes in stratiform regions or to the cloud base, which tend to have larger extents (Carey et al., 2005; Kuhlman et al., 2009; Weiss et al., 2012). These results add further evidence to the prediction from electrostatics that frequent breakdown and large flash extents are opposed (Bruning and MacGorman, 2013).

5.3. Charge structure vs CG rate

The occurrence of −CG lightning indicates a sufficient imbalance in the electric potential between the positive and negative ChRs, allowing the lightning channel to maintain a sufficiently negative potential to propagate to the ground (Krehbiel et al., 2008, Mansell et al., 2010). According to Mansell et al. (2005), at least two mechanisms could reasonably be at work to cause such imbalance: (i) charge separation in the upper part enhances the −ChR while also creating an upper +ChR (ii) a lower positive charge is created by the sedimentation of positively charged

graupel and liquid precipitation. Because the lower ChR often contains less charge than the mid-level ChR and so produces a shallower potential well, the downward propagation of lightning may not stop in the lower charge but may continue to the ground (MacGorman et al., 1989, 2001; MacGorman and Rust, 1998; Coleman et al., 2008). Current results (Fig. 8) show significant differences in the flash rate for the TriP (5.2 CG flashes·min^{-1}) and LwDip (2.0 CG flashes·min^{-1}) even though both categories present a midlevel ChR above a lower ChR of opposite polarity. Therefore, the presence of a significant upper ChR above the mid-level ChR seems to have a bearing on the CG formation. Moreover, the distance between those layers has also shown to influence the CGFR (Fig. 9). Strong vertical motions would favour large ice flows and graupel volumes, increasing charge separation and the storm total flash rate (Petersen et al., 2005; Deierling et al., 2005). The increasing distance between the lower and upper +ChRs allows for a wider mixed-phase region, where these collisions occur, with a consequent increase in CGFR.

Significant differences in the IC:CG ratio (Z, Fig. 10) spotlight the influence of the charge structure on the type of lightning produced. A significant reduction or even absence of a lower +ChR reduces the occurrence of CG, the median for Z on the UpDip category being around 3. Contrarily, a dominant lower dipole (negative over positive) with scare activity above the main −ChR reduces Z to a median around 0.3 for the LwDip, which means almost all IC flashes that initiate in this category has a ramification to the ground (the IC and CG components of the same lightning event are detected by the LMA and LINET respectively).

5.4. Peak current and polarity

The polarity of ground strikes is often controlled by the polarity of the first two charges layers near the earth's surface (Mansell et al., 2002; Wiens et al., 2005; Kuhlman et al., 2006; Tessendorf, 2009), though Krehbiel et al. (2008) discuss several other discharge modes that do not fit this pattern. In most cases, negative charge will be lowered from cloud to ground (as −CG) where the lowest ChR is positive, and the positive charge will be lowered (as +CG) where the lowest ChR is negative. Whether or not a flash comes to the ground is determined by the net energetics of the charge configuration (Krehbiel et al., 2008; Mansell et al., 2010). The local charge layer disposition provides a strong constraint on the local ground strike polarity, since a ChR with polarity opposite to that of the eventual ground strike is required to bring the leader sufficiently close to the surface. In our case, keeping in mind the case study selection focused on regular storms having a classic distribution of charge levels, a predominance of −CGs could be expected, with a 10% per cent of +CG close to the climatological reference.

Interestingly, peak currents on CG strokes were higher in the lower dipole category for both polarities (Fig. 12). There is a negative correlation between the flash rate and the peak current since the lower dipole presents lower flash rates and higher peak currents (Fig. 8). In contrast, the two categories with an upper +ChR had higher

flash rates but lower peak currents, bearing similarity with the negative correlation between IC size and rate previously noted. As pointed out by Zhang et al. (2017), the periods or regions of strong convection tend to have frequent small flashes. In contrast, periods or regions of weak convection tend to have layered distributions of large charge regions, which results in more intense but infrequent flashes.

6. SUMMARY AND KEY FINDINGS

In situ measurements of storms' electrical and thermodynamic properties are scarce, as they are difficult to obtain (i.e., balloon and aircraft-borne instruments). Alternatively, Lightning Mapping Array systems provide information on the three-dimensional and temporal structures of in-cloud lightning during a storm's lifetime. LMA data, although it does not provide quantitative information about charge magnitudes, it can fairly reveal about electrically active regions. Despite this limitation, the LMA provides a fully three-dimensional qualitative picture of the charge structure throughout the evolution of the storm.

Relatively few studies have investigated the relationship between the layered charge structure of the storm and the CG flash rate. Previous case studies based on LMA data mainly focused on severe storms, whereas the present study deals with the electrical structure of classical, normally electrified thunderstorms. Combined with weather radar data, these comprehensive and rather unique datasets in Europe allowed exploring the relationship between a representative sampling of different CG flash rates and the three main charge structures found on these storms: the classical tripole, an upper dipole (positive above negative) and a lower dipole (negative above positive).

A summary of the key findings are as follows:

- The classical tripole structure is the one presenting a higher CG flash rate (5.2 flashes·min^{-1}). The upper dipole follows, with a slightly lower flash rate (3.8 flashes·min^{-1}). Contrarily, the lower dipole has a lower CG flash rate (2.0 flashes·min^{-1}).
- Charge region heights (and temperatures) derived from LMA show good agreement with other studies. The heights of the initiations of the flashes, both of the lower positive (4,730 m MSL, −7.1 °C) and of the upper positive (9,150 m MSL, −40.8 °C), do not show great variation regardless of which of the three main charge structures is detected.
- In terms of CG peak current, the presence of an upper positive charge region is more relevant than a lower positive charge region below the main mid negative. Conversely, the lower positive favours higher CG peak currents on both polarities.
- The height of the different charge regions also has a strong influence on the CG rate. In the case of a very high upper positive charge region, related to a strong updraft, a higher CG rate is observed.

Credit authorship contribution statement

Albert Salvador: Data curation, Methodology, Software, Validation, Writing - original draft. Nicolau Pineda: Conceptualization, Supervision, Writing - review & editing, Funding acquisition, Project administration. Joan Montanyà: Conceptualization, Supervision, Writing - review & editing, Funding acquisition. Jesús A. López: Methodology, Software, Conceptualization. Gloria Solà: Project administration, Funding acquisition, Supervision.

Acknowledgements

This study was co-funded by the autonomous Government of Catalonia, Spain, the Meteorological Service of Catalonia and Fulgura S.L., under the framework of the Industrial Doctorate Projects (Project DI 59/2015) of the AGAUR, Government of Catalonia. This work was also supported by the research grants from the Spanish Ministry of Economy and Competitiveness (MINECO) and the European Regional Development Fund (FEDER): ESP2015-69909-C5-5-R and ESP2017-86263-C4-2-R.

Declaration of competing interest

The authors declare that they have no known competing financial interests or personal relationships that could have appeared to influence the work reported in this paper.

References

Altube, P., Bech, J., Argemí, O., Rigo, T., 2015. Quality Control of Antenna Alignment and Receiver Calibration Using the Sun: Adaptation to Midrange Weather Radar Observations at Low Elevation Angles. J. Atmos. Oceanic Technol., 32, 927–942, https://doi.org/10.1175/JTECH-D-14-00116.1.

Argemí, O., Altube, P., Rigo, T., Ortiga, X., Pineda, N., Bech, J., 2014. Towards the improvement of monitoring and data quality assessment in the weather radar network of the Meteorological Service of Catalonia. In: 8th European Conference on Radar in Meteorology and Hydrology (ERAD), Garmisch-Partenkirchen, Germany, Sept. 2014.

Betz, H.D., Schmidt, K., Laroche, P., Blanchet, P., Oettinger, W.P., Defer, E., Dziewit, Z., Konarski, J., 2009a. Linet—an international lightning detection network in Europe. Atmos. Res. 91, 564–573. https://doi.org/10.1016/j.atmosres.2008.06.012.

Betz, H.D., Schmidt, K., Oettinger, W.P., 2009b. LINET: An international VLF/LF lightning detection network in Europe. Springer, 2009b. In: Betz, H.-D., Schumann, U., Laroche, P. (Eds.), Lightning: Principles, Instruments and Applications. Springer, Netherlands, pp. 115–140.

Biggerstaff, M. I., Zounes, Z., Alford, A. A., Carrie, G. D., Pilkey, J. T., Uman, M. A., Jordan, D. M., 2017. Flash propagation and inferred charge structure relative to radar-observed ice alignment signatures in a small Florida mesoscale convective system, Geophys. Res. Lett., 44, 8027–8036, doi:10.1002/2017GL074610

Boccippio, D.J., 2002. Lightning Scaling Relations Revisited. Journal of the Atmospheric Sciences, 59(6), 1086–1104. doi:10.1175/1520-0469(2002)059<1086:lsrr>2.0.co;2.

3.2 THUNDERSTOM CHARGE STRUCTURES FAVOURING CLOUD-TO-GROUND LIGHTNING

Brown, R.A., Kaufman, C.A., MacGorman, D.R., 2002. Cloud-to-ground lightning associated with the evolution of a multicell storm, J. Geophys. Res., 107(D19), 4397, doi:10.1029/2001JD000968.

Bruning, E.C., Rust, W.D., Schuur, T.J., MacGorman, D.R., Krehbiel, P.R., Rison, W., 2007. Electrical and Polarimetric Radar Observations of a Multicell Storm in TELEX. Monthly Weather Review 135, 2525-2544. https://doi.org/10.1175/MWR3421.1

Bruning, E.C., Rust, W.D., MacGorman, D.R., Biggerstaff, M.I., Schuur, T.J., 2010. Formation of charge structures in a supercell. Mon. Weather Rev. 138, 3740–3761.

Bruning, E.C., MacGorman, D.R., 2013. Theory and observations of controls on lightning flash size spectra. J. Atmos. Sci. 70 (12), 4012–4029. http://dx.doi.org/10.1175/JAS-D-12-0289.1.

Bruning, E.C., Weiss, S.A., Calhoun, K.M., 2014. Continuous variability in thunderstorm primary electrification and an evaluation of inverted-polarity terminology. Atmos.Res. 135–136, 274–284.

Caicedo, J.A., Uman, M.A., Pilkey, J. T., 2018. Lightning evolution in two North Central Florida summer multicell storms and three winter/spring frontal storms. Journal of Geophysical Research: Atmospheres, 123, 1155–1178. https://doi.org/10.1002/2017JD026536.

Carey, L.D., Murphy, M.J., McCormick, T.L., Demetriades, N.W., 2005. Lightning location relative to storm structure in a leading-line trailing stratiform mesoscale convective system. J. Geophys. Res. 110.

Carey, L.D., Schultz, E.V., Schultz, C.J., Deierling, W., Petersen, W.A., Bain, A.L., Pickering, K.E., 2019. An Evaluation of Relationships between Radar-Inferred Kinematic and Microphysical Parameters and Lightning Flash Rates in Alabama Storms. Atmosphere 2019, 10, 796.

Clarence, N.D., Malan, D.J., 1957. Preliminary discharge processes in lightning flashes to ground. Q. J. R. Meteorol. Soc. 83, 161–172.

Coleman, L.M., Marshall, T.C., Stolzenburg, M., Hamlin, T., Krehbiel, P.R., Rison, W., Thomas, R.J., 2003. Effects of charge and electrostatic potential on lightning propagation. J. Geophys. Res. 108.

Coleman, L.M., Stolzenburg, M., Marshall, T.C., Stanley, M., 2008. Horizontal lightning propagation, preliminary breakdown, and electric potential in New Mexico thunderstorms, J. Geophys. Res., 113, D09208, https://doi:10.1029/2007JD009459.

Cooray, V., Cooray, G., Marshall, T., Arabshahi, S., Dwyer, J., Rassoul, H., 2014. Electromagnetic fields of a relativistic electron avalanche with special attention to the origin of lightning signatures known as narrow bipolar pulses. Atmospheric Research, 149, 346–358. doi: 10.1016/j.atmosres.2013.12.011.

Cummins, K. L., Krider, E. P., Malone, M. D., 1998. The U.S. National Lightning Detection Network and Applications of Cloud-to-Ground Lightning Data by Electric Power Utilities, IEEE Transactions on Electromagnetic Compatibility, 40(4): 465

Curran, E. B., Holle, R. L., López, R. E., 2000. Lightning Casualties and Damages in the United States from 1959 to 1994. J. Climate, 13, 3448–3464, https://doi.org/10.1175/1520-0442(2000)013<3448:LCADIT>2.0.CO;2

Dahl, J.M.L., Höller, H., Schumann, U., 2011. Modeling the Flash Rate of Thunderstorms. Part I: Framework. Mon. Wea. Rev., 139, 3093–3111, https://doi.org/10.1175/MWR-D-10-05031.1.

Deierling, W., Latham, J., Petersen, W.A., Ellis, S.M., Christian Jr., H.J., 2005. On the relationship of thunderstorm ice hydrometeor characteristics and total lightning measurements, Atmos. Res., 76(1), 114–126.

Deierling, W., Petersen, W.A., 2008. Total lightning activity as an indicator of updraft characteristics. J. Geophys. Res., 113, D16210.

Dotzek, N., Rabin, R.M., Carey, L.D., MacGorman, D.R., McCormaic, T.L., Demetriades, N.W., Murphy, M.J., Holle, R.L., 2005. Lightning activity related to satellite and radar observations of a mesoscale convective system over Texas on 7–8 April 2002, Atmos. Res., 76, 127–166.

Figueras i Ventura, J., Pineda, N., Besic, N., Grazioli, J., Hering, A., van der Velde, O.A., Romero, D., Sunjerga, A., Mostajabi, A., Azadifar, M., Rubinstein, M., Montanyà, J., Germann, U., Rachidi, F., 2019. Polarimetric radar characteristics of lightning initiation and propagating channels, Atmos. Meas. Tech., 12, 2881–2911, https://doi.org/10.5194/amt-12-2881-2019.

Fuchs, B.R., Rutledge, S.A., Bruning, E.C., Pierce, J.R., Kodros, J.K., Lang, T.J., MacGorman, D.R., Krehbiel, P.R., Rison, W., 2015. Environmental controls on storm intensity and charge structure in multiple regions of the continental United States, J. Geophys. Res. Atmos., 120, 6575–6596, doi:10.1002/2015JD023271.

Fuchs, B.R., Rutledge, S.A., 2018. Investigation of lightning flash locations in isolated convection using LMA observations. Journal of Geophysical Research: Atmospheres, 123, 6158–6174. https://doi.org/10.1002/2017JD027569.

Holle, R. L., 2016. A summary of recent national scale lightning fatality studies Wea. Climate Soc. (2016) 8 (1): 35–42. https://doi.org/10.1175/WCAS-D-15-0032.1

Höller, H., Betz, H.-D., Schmidt, K., Calheiros, R.V., May, P., Houngninou, E., Scialom, G., 2009. Lightning characteristics observed by a VLF/LF lightning detection network (LINET) in Brazil, Australia, Africa and Germany. Atmospheric Chemistry and Physics, 9 (22), pp. 7795-7824.

Iudin, D., Rakov, V., Mareev, E., Iudin, F., Syssoev, A., Davydenko, S., 2017. Advanced numerical model of lightning development: Application to studying the role of LPCR in determining lightning type. Journal of Geophysical Research: Atmospheres, 122, 6416-6430. https://doi.org/10.1002/2016JD026261.

Jacobson, E.A., Krider, E.P., 1976. Electrostatic field changes produced by Florida lightning. J. Atmos. Sci. 33, 103–117.

Jayaratne, E.R., Saunders, C.P.R., Hallett, J., 1983. Laboratory studies of the charging of soft-hail during ice crystal interactions, Q. J. R. Meteorol. Soc., 109, 609630.

Kasemir, H.W., 1960. A contribution to the electrostatic theory of lightning discharge. J. Geophys. Res. 65, 1873–1878.

Krausmann, E., Cozzani, V., Salzano, E., Renni, E., 2011. Industrial accidents triggered by natural hazards: an emerging risk issue. Nat. Hazards Earth Syst. Sci., 11, 921–929.

Krehbiel, P.R., 1986. The electrical structure of thunderstorms. In: The Earth's Electrical Environment. National Academies Press, pp. 90–113.

Krehbiel, P.R., Thomas, R.J., Rison, W., Hamlin, T., Harlin, J., Davis, M., 2000. GPS-based mapping system reveals lightning inside storms. Eos. Trans. AGU 81, 21–25.

Krehbiel, P.R., Riousset, J.A., Pasko, V.P., Thomas, R.J., Rison, W., Stanley, M.A., Edens, H.E., 2008. Upward electrical discharges from thunderstorms. Nat. Geosci. 1, 233–237. https://doi.org/10.1038/ngeo162.

Kuhlman, K.M., Ziegler, C.L., Mansell, E.R., MacGorman, D.R., Straka, J.M., 2006. Numerically simulated electrification and lightning of the 29 June 2000 STEPS supercell storm. Mon. Weather Rev. 134, 2734–2757.

Kuhlman, K.M., MacGorman, D.R., Biggerstaff, M.I., Krehbiel, P.R., 2009. Lightning initiation in the anvils of two supercell storms. Geophys. Res. Lett. 36.

Liu, C., Cecil, D.J., Zipser, E.J., Kronfeld, K., Robertson, R., 2012. Relationships between lightning flash rates and radar reflectivity vertical structures in thunderstorms over the tropics and subtropics. J. Geophys. Res., 117, D06212.

López, J.A., Pineda, N., Montanyà, J., van der Velde, O., Fabró, F., Romero, D., 2017. Spatio-temporal dimension of lightning flashes based on three-dimensional Lightning Mapping Array. Atmos. Res. 197, 255–264. https://doi.org/10.1016/j.atmosres. 2017.06.030.

López, J.A., Montanyà, J., van der Velde, O.A., Pineda, N., Salvador, A., Romero, D., Aranguren, D., Taborda, J., 2019. Charge structure of two tropical thunderstorms in Colombia. Journal of Geophysical Research: Atmospheres, 124, 5503–5515. https://doi.org/10.1029/2018JD029188.

Lund, N.R., MacGorman, D.R., Schuur, T.J., Biggerstaff, M.I., Rust, W.D., 2009. Relationships between lightning location and polarimetric radar signatures in a small mesoscale convective system. Mon. Weather Rev. 137, 4151–4170.

MacGorman, D.R., Burgess, D.W., Mazur, V., Rust, W.D., Taylor, W.L., Johnson, B.C., 1989. Lightning rates relative to tornadic storm evolution on 22 May 1981. J. Atmos. Sci. 46, 221–250.

MacGorman, D.R., Rust, W.D., 1998. The Electrical Nature of Storms. Oxford Univ. Press, Oxford, pp. 422.

MacGorman, D.R., Straka, J.M., Ziegler, C.L., 2001. A lightning parameterization for numerical cloud models. J. Appl. Meteor., 40, 459–478.

MacGorman, D. R., Rust, W. D., Schuur, T. J., Biggerstaff, M. I., Straka, J. M., Ziegler, C. L., Mansell, E. R., Bruning, E. C., Kuhlman, K. M., Lund, N. R., Biermann, N. S., Payne, C., Carey, L. D., Krehbiel, P. R., Rison, W., Eack, K. B., & Beasley, W. H., 2008. TELEX The Thunderstorm Electrification and Lightning Experiment, Bulletin of the American Meteorological Society, 89(7), 997-1014. https://doi.org/10.1175/2007BAMS2352.1

MacGorman, D.R., Apostolakopoulos, I.R., Lund, N.R., Demetriades, N.W.S., Murphy, M.J., Krehbiel, P.R., 2011. The timing of cloud-to-ground lightning relative to total lightning activity. Mon. Wea. Rev., 139, 3871–3886, doi:10.1175/MWR-D-11-00047.1.

Maggio, C., Coleman, L., Marshall, T., Stolzenburg, M., Stanley, M., Hamlin, T., Krehbiel, P., Rison, W., Thomas, R., 2005. Lightning-Initiation Locations as a Remote Sensing Tool of Large Thunderstorm Electric Field Vectors, Journal of Atmospheric and Oceanic Technology, 22(7), 1059-1068. https://doi.org/10.1175/JTECH1750.1

Mansell, E.R., MacGorman, D.R., Ziegler, C.L., Straka, J.M., 2002. Simulated three-dimensional branched lightning in a numerical thunderstorm model. J. Geophys. Res. 107.

Mansell, E.R., MacGorman, D.R., Ziegler, C.L., Straka, J.M., 2005. Charge structure and lightning sensitivity in a simulated multicell thunderstorm. J. Geophys. Res. 110, D12101. http://dx.doi.org/10.1029/2004JD005287.

Mansell, E.R., Ziegler, C.L., Bruning, E.C., 2010. Simulated electrification of a small thunderstorm with two-moment bulk microphysics. J. Atmos. Sci. 67, 171–194.

Marshall, T.C., Winn, W.P., 1982. Measurement of charged precipitation in a New Mexico thunderstorm: lower positive charge centers. J. Geophys. Res. 87, 7141–7157.

Marshall, T.C., Rust, W. D., 1991. Electric field soundings through thunderstorms, J. Geophys. Res., 96, 22,297-22,309.

Marshall, T.C., Rust, W.D., 1993. Two types of vertical electrical structures in stratiform precipitation regions of mesoscale convective systems, Bull. Am. Meteorol. Soc., 74, 2159–2170.

Mazur, V., 1989. Physical model of lightning initiation on aircraft in thunderstorms. J. Geophys. Res. 94, 3326–3340.

Mazur, V., Ruhnke, L.H., 1993. Common physical processes in natural and artificially triggered lightning. J. Geophys. Res. 98, 12,913–12,930. http://dx.doi.org/10.1029/93JD00626.

McCaul Jr, E.W., Goodman, S.J., LaCasse, K.M., Cecil, D.J., 2009. Forecasting lightning threat using cloud-resolving model simulations. Weather Forecast. 24 (3), 709–729.

Mecikalski, R.M., Bain, A.L., Carey, L.D., 2015. Radar and Lightning Observations of Deep Moist Convection across Northern Alabama during DC3: 21 May 2012. Monthly Weather Review 143, 2774-2794. https://doi.org/10.1175/MWR-D-14-00250.1.

Mecikalski, R.M., Carey, L.D., 2017. Lightning characteristics relative to radar, altitude and temperature for a multicell, MCS and supercell over northern Alabama. Atmospheric Research, 191, 128–140. doi: 10.1016/j.atmosres.2017.03.001.

Mercader, J., Codina, B., Sairouni, A., Cunillera, J., 2010. Results of the meteorological model WRF-ARW over Catalonia, using different parameterizations of convection and cloud microphysics. Tethys, 7, 75–86. DOI:10.3369/tethys.2010.7.07.

Montanyà, J., van der Velde, O.A., Williams, E., 2015. The start of lightning: Evidence of bidirectional lightning initiation. Sci Rep 5, 15180. https://doi.org/10.1038/srep15180.

Montanyà, J., Fabró, F., van der Velde, O.A., March, V., Williams, E.R., Pineda, N., Romero, D., Solà, G., Freijo, M., 2016. Global distribution of winter lightning: a threat to wind turbines and aircraft. Nat. Hazards Earth Syst. Sci.16(6), 1465–1472. http://dx.doi.org/10.5194/nhess-16-1465-2016.

Nag, A., Rakov, V.A., 2009. Some inferences on the role of lower positive charge region in facilitating different types of lightning. Geophys. Res. Lett. 36, L05815. https://doi.org/10.1029/2008GL036783.

Neubert, T., Kuvvetli, I., Budtz-Jørgensen, C., Østgaard, N., Reglero, V., Arnold, N., 2006. The atmosphere-space interactions monitor (ASIM) for the international space station. ILWS Workshop 2006. In: GOA, February 19-24, 2006.

Neubert, T., Østgaard, N., Reglero, V., Blanc, E., Chanrion, O., Oxborrow, C.A, Orr, A., Tacconi, M., 2019. The ASIM mission on the International Space Station. Space Sci. Rev. 215, 26. https://doi.org/10.1007/s11214-019-0592-z

Pablo, F.D., Soriano, L.R., 2002. Relationship between cloud-to-ground lightning flashes over the Iberian Peninsula and sea surface temperature. Q.J.R. Meteorol. Soc., 128: 173-183. doi:10.1256/00359000260498842.

Pawar, S.D., Kamra, A.K., 2004. Evolution of lightning and the possible initiation/triggering of lightning discharges by the lower positive charge center in an isolated thundercloud in the tropics. J. Geophys. Res. 109, D02205. https://doi.org/10.1029/203JD003735.

Petersen, W. A., Christian, H.J., Rutledge, S.A., 2005. TRMM observations of the global relationship between ice water content and lightning, Geophys. Res. Lett., 32, L1481, doi:10.1029/2005GL023236.

Pineda, N., Montanyà, J., Salvador, A., van der Velde, O.A., López, J., 2018. Thunderstorm Characteristics favouring downward and upward lightning to wind turbines. Atmos. Res. 214. https://doi.org/10.1016/j.atmosres.2018.07.012.

Poelman, D.R., Schulz, W., Diendorfer, G., Bernardi, M., 2016. The European lightning location system EUCLID – part 2: observations. Nat. Hazards Earth Syst. Sci. 16 (607–616), 2016. https://doi.org/10.5194/nhess-16-607-2016.

Prentice, S. A., Mackerras, D., 1977. The Ratio of Cloud to Cloud-Ground Lightning Flashes in Thunderstorms. Journal of Applied Meteorology, 16(5), 545–550. doi:10.1175/1520-0450(1977)016<0545:troctc>2.0.co;2

Qie, X., Zhang, T., Chen, C., Zhang, G., Zhang, T., Wei, W., 2005. The lower positive charge center and its effect on lightning discharges on the Tibetan Plateau. Geophys.Res. Lett. 32, L05814. https://doi.org/10.1029/2004GL022162.

Rakov, V.A., Uman, M.A., 2003. Lightning: Physics and Effects. Cambridge University Press (2003. 687 p. ISBN 05215832766).

Rison, W., Thomas, R.J., Krehbiel, P.R., Hamlin, T., Harlin, J., 1999. A GPS-based three-dimensional lightning mapping system: initial observations in central New Mexico. J. Geophys. Res. 26, 3573–3576.

Rivas Soriano, L., de Pablo, F., Tomas, C., 2005. Ten-year study of cloud-to-ground lightning activity in the Iberian Peninsula. J. Atmos. and Sol-Terr. Phys. 67 (16), 1632–1639.

Rosenfeld, D., Wolff, D.B., Atlas, D., 1993. General Probability-matched Relations between Radar Reflectivity and rain Rate. J. Appl. Meteorol. 32, 50–72. https://doi.org/10.1175/1520-0450(1993)032<0050:GPMRBR>2.0.CO;2.

Rust, W.D., MacGorman, D., Bruning, E., Weiss, S., Krehbiel, P., Thomas, R., Rison, W., Hamlin, T., Harlin, J., 2005. Inverted-polarity electrical structures in thunderstorms in the Severe Thunderstorm Electrification and Precipitation Study (STEPS). Atmospheric Research. 76. 247-271. 10.1016/j.atmosres.2004.11.029

Rutledge, S., Williams, E., Keenan, T., 1992. The Down Under Doppler and Electricity Experiment (DUNDEE): Overview and preliminary results. Bull. Am. Meteorol. Soc. 73, 3 – 16.

Salvador, A., Pineda, N., Montanyà, J., Solà, G., 2020. Seasonal variations on the conditions required for the lightning production. Atmospheric Research, 104981. doi: 10.1016/j.atmosres.2020.104981.

San Segundo, H., López, J.A., Pineda, N., Altube, P., Montanyà, J., 2020. Sensitivity analysis of lightning stroke-to-flash grouping criteria. Atmospheric Research, 242, 105023. doi: 10.1016/j.atmosres.2020.105023.

Saunders, C.P.R., Keith, W.D., Mitzeva, R.P., 1991. The effect of liquid water content on thunderstorm charging. J. Geophys. Res. 96, 11007–11017.

Saunders, C.P.R., Peck, S.L., 1998. Laboratory studies of the influence of the rime accretion rate on charge transfer during crystal/graupel collisions.J. Geophys. Res. 103, 13,949–13,956.

Saunders, C.P.R., Bax-Norman, H., Emersic, C., Avila, E.E., Castellano, N.E., 2006. Laboratory studies of the effect of cloud conditions on graupel/crystal charge transfer in thunderstorm electrification. Q. J. R. Meteorol. Soc. 132, 2653–2673. http://dx.doi.org/10.1256/qj.05.218.

Schultz, C.J., Carey, L.D., Schultz, E.V., Blakeslee, R.J., 2015. Insight into the Kinematic and Microphysical Processes that Control Lightning Jumps. Weather Forecast. 2015, 30, 1591–1621.

Shao, X., Krehbiel, P., 1996. The spatial and temporal development of intracloud lightning. J. Geophys. Res. 101, 26,641–26,668. https://doi.org/10.1029/96JD01803.

Shepherd, T.R., Rust, W., Marshall, T., 1996. Electric fields and charges near 08C in stratiform clouds. Mon. Weather Rev. 124, 919–938.

Skamarock, W. C., Klemp, J. B., Dudhia, J., Gill, D.O., Barker, D.M., Wang, W., Powers, J.G., 2008. A description of the Advanced Research WRF Version 3. NCAR Tech. Note NCAR/TN-465+STR. [Available online at http://www2.mmm.ucar.edu/ wrf/users/docs/arw_v3.pdf.]

Straka, J. M., Zrnic, D. S., Ryzhkov, A. V., 2000. Bulk hydrometeor classification and quantification using polarimetric radar data: Synthesis of relations. J. Appl. Meteor., 39, 1341–1372

Stolzenburg, M., Marshall, T.C., Rust, W.D., Smull, B.F., 1994. Horizontal distribution of electrical and meteorological conditions across the stratiform region of a mesoscale convective system. Mon. Weather Rev. 122, 1777–1797.

Stolzenburg, M., Rust, W. D., Smull, B. F., Marshall, T. C., 1998. Electrical structure in thunderstorm convective regions: 1. Mesoscale convective systems, J. Geophys. Res., 103 (D12), 14059–14078, doi:10.1029/97JD03546.

Stolzenburg, M., Marshall, T.C., 2008. Charge Structure and Dynamics in Thunderstorms, Space Sci Rev, doi:10.1007/s11214-008-9338-z.

Takahashi, T., 1978. Riming electrification as a charge generation mechanism in thunderstorms. J. Atmos. Sci. 35, 1536–1548.

Takahashi, T., Miyawaki, K., 2002. Reexamination of riming electrification in a wind tunnel. J. Atmos. Sci., 59, 1018–1025, doi:https://doi.org/10.1175/1520-0469(2002)059<1018:ROREIA>2.0.CO;2.

Tao, S., Tan, Y., Zhu, B., Ma, M., Lu, W., 2009. Fine-resolution simulation of cloud-to-ground lightning and thundercloud charge transfer, Atmospheric Research, Volume 91, Issues 2–4, 2009, Pages 360-370, https://doi.org/10.1016/j.atmosres.2008.05.012

Tan, Y., Tao, S., Liang, Z., Zhu, B., 2014. Numerical study on relationship between lightning types and distribution of space charge and electric potential, J. Geophys. Res. Atmos., 119, 1003–1014, doi:10.1002/2013JD019983.

Tessendorf, S.A., Rutledge, S.A., Wiens, K.C., 2007. Radar and lightning observations of normal and inverted polarity multicellular storms from steps. Mon. Weather Rev. 135 (11), 3682–3706.

Tessendorf, S.A., 2009. Lightning: Principles, Instruments and Applications. (Chapter 4) Characteristics of Lightning in Supercells. Springer, pp. 83–114.

Thomas, R. J., Krehbiel, P. R., Rison, W., Hamlin, T., Harlin, J., Shown, D., 2001. Observations of VHF source powers radiated by lightning, Geophys. Res. Lett., 28(1), 143–146, doi:10.1029/2000GL011464.

Thomas, R., Krehbiel, P.R., Rison, W., Hunyady, S.J., Winn, W.P., Hamlin, T., Harlin, J., 2004. Accuracy of the lightning mapping array. J. Geophys. Res. 109, D14207. https://doi.org/10.1029/2004JD004549.

van der Velde, O.A., Montanyà, J., 2013. Asymmetries in bidirectional leader development of lightning flashes. J. Geophys. Res. Atmos. 118, 13504–13519.

Vincent, B.R., Carey, L.D., Schneider, D., Keeter, K., Gonski, R., 2003. Using WSR-88D reflectivity data for the prediction of cloud-to-ground lightning: a North Carolina study. Nat. Wea. Digest 27, 35–44.

Wang, H., Guo, F., Zhao, T., Qin, M., Zhang, L., 2016. A numerical study of the positive cloud-to-ground flash from the forward flank of normal polarity thunderstorm, Atmos. Res., 169, 183–190.

Weiss, S.A., MacGorman, D.R., Calhoun, K.M., 2012. Lightning in the anvils of supercell thunderstorms. Mon. Weather Rev. 140, 2064–2079.

Wiens, K.C., Rutledge, S.A., Tessendorf, S.A., 2005. The 29 June 2000 supercell observed during steps. Part II: lightning and charge structure. J. Atmos. Sci. 62 (12), 4151–4177.

Williams, E.R., 1985. Large-scale charge separation in thunderclouds. J. Geophys. Res. 90 (D4), 6013–6025. https://doi.org/10.1029/JD090iD04p06013.

Williams, E.R., Cooke, C.M., Wright, K.A., 1985. Electrical discharge propagation in and around space charge clouds. J. Geophys. Res. 90, 6059–6070.

Williams, E. R., 1989. The tripole structure of thunderstorms. J. Geophys. Res., 94, 13 151–13 167.

Williams, E., Weber, M.E., Orville, R.E., 1989. The relationship between lightning type and convective state of thunderclouds. J. Geophys. Res. 94 (13) (213–13 220).

Williams, E.R., Zhang, R., Rydock, J., 1991. Mixed-phase microphysics and cloud electrification, 48,2195–2203.

Williams, E. R., 2001. The electrification of severe storms. Severe Convective Storms, Meteor. Monogr., No. 50, Amer. Meteor. Soc., 527–561.

Wu, T., Yoshida, S., Akiyama, Y., Stock, M., Ushio, T., & Kawasaki, Z., 2015. Preliminary breakdown of intracloud lightning: Initiation altitude, propagation speed, pulse train characteristics, and step length estimation. Journal of Geophysical Research: Atmospheres, 120, 9071–9086. https://doi.org/10.1002/2015JD023546.

Yang, Y.H., King, P., 2010. Investigating the potential of using radar echo reflectivity to nowcast cloud-to-ground lightning initiation over southern Ontario. Weather Forecast. 25 (4), 1235–1248.

Yoshida, S., Morimoto, T., Ushio, T., Kawasaki, Z., 2009. A fifth-power relationship for lightning activity from tropical rainfall measuring Mission satellite observations. J. Geophys. Res. 114, D09104. https://doi.org/10.1029/2008JD010370.

Yuter, S.E., Houze, R.A., 1995. Three-Dimensional Kinematic and Microphysical Evolution of Florida Cumulonimbus. Part II: Frequency Distributions of Vertical Velocity, Reflectivity, and Differential Reflectivity. Mon. Wea. Rev., 123, 1941–1963, https://doi.org/10.1175/1520-0493(1995)123<1941:TDKAME>2.0.CO;2.

Zhang, Z., Zheng, D., Zhang, Y., Lu, G., 2017. Spatial–temporal characteristics of lightning flash size in a supercell storm. Atmos. Res. 197, 201 – 210. https://doi.org/10.1016/j.atmosres.2017.06.029.

Zheng, D., Zhang, Y., Meng, Q., 2018. Properties of negative initial leaders and lightning flash size in a cluster of supercells. Journal of Geophysical Research: Atmospheres, 123, 12,857–12,876. https://doi.org/10.1029/2018JD028824

Zipser, E.J., Lutz, K.R., 1994. The vertical profile of radar reflectivity of convective cells: a strong indicator of storm intensity and lightning probability? Mon. Wea. Rev. 122,1751–1759.

3.3 Thunderstorm characteristics favouring downward and upward lightning to wind turbines

3.3.1 Introducción y metodología

Este artículo evalúa las condiciones meteorológicas que se detectan en situaciones de descargas verticales desde y hacia infraestructuras elevadas, con especial enfoque hacia los aerogeneradores. A su vez, detectar las características más frecuentes de las tormentas que los provoquen después de una inspección manual de episodios con esta afectación. A modo comparativo, también se analizan dos episodios de verano como referencia de una estructura vertical típica de una tormenta en periodo cálido.

La industria eólica, como se ha mencionado anteriormente, tiene una especial afectación frente a estos tipos de descarga, especialmente durante los periodos fuera de temporada como el invierno. Así, poder determinar las condiciones meteorológicas que las provocan con la mayor antelación posible, y que sean aplicables a distintas épocas del año, tiene un gran potencial para los sistemas de alarmas, con especial enfoque a esta industria.

El delta del Ebro es propuesto como zona de estudio debido a distintos factores. El primero, e imprescindible, es la presencia de parques eólicos en la zona, los cuales se han ido instalando de forma progresiva desde 1995. Otro es la instalación en la zona de la red ELMA, la cual permitirá representar la distribución en altura de las distintas descargas dentro de la nube, accediendo a interpretar la estructura vertical de la tormenta, y al mismo tiempo observar las descargas ascendentes desde los aerogeneradores.

La fracción de descargas CG requerirá otro sistema de detección de rayos, por lo que se propone utilizar los datos de la XDDE del SMC, el cual trabaja para la detección de estos en el LF. De forma complementaria también se utilizará la red LINET, la cual trabaja en el VLF para la detección de los CG, debido a la alta precisión en la localización de las descargas, con una precisión de alrededor de los 150 m (Betz et al., 2009b), lo que permitirá identificar las descargas cercanas a los aerogeneradores.

Además, la información derivada de radar del SMC, como las alturas máximas que alcanzan los niveles de reflectividad de 12 y 35 dBZ, así como las imágenes CAPPI a 1,000 m, permitirá identificar tanto la intensidad de las tormentas en distintos instantes, qué alturas alcanza, así como la identificación de su morfología. Finalmente, el radiosondeo de Barcelona proporcionará la altura de las isotermas de -10°C y -40°C, permitiendo delimitar la región de fase mixta dentro de la nube, y dos índices de inestabilidad (CAPE y LCL (*Lifting Condensation Level*)) derivados de este, que ayudará a caracterizar las condiciones ambientales de las tormentas analizadas

3.3.2 Conclusiones

El análisis de los distintos episodios permite determinar las siguientes conclusiones:

- Se establece que la altura del nivel de reflectividad de 12 dBZ por encima de la isoterma de $-10°C$ identifica la posible actividad eléctrica en la zona, y el nivel de reflectividad de 35 dBZ alcanzando la altura de la $-40°C$ se traduce en una fuerte convección con altas intensidades de descargas eléctricas. Esto podría permitir identificar condiciones de descargas a aerogeneradores fuera de las estaciones con tormentas más frecuentes.
- Aunque el 85% de las descargas CG anuales en el área de estudio suceden de junio a octubre (con especial intensidad de agosto a septiembre con un 57%), todas las descargas con final o inicio en los aerogeneradores han sucedido de noviembre a abril, periodo que solo comprende el 9% de toda la actividad eléctrica anual en la zona.
- La estructura vertical de la tormenta más frecuentemente detectada cuando los rayos han sido descendentes ha sido la clásica tripolar, pero con una región de carga positiva inferior dominante, además de muy cercana a la superficie. Además, las descargas CG que han afectado a aerogeneradores han tenido mayoritariamente polaridad negativa y con picos de corriente superiores a la media.
- Los rayos ascendentes han ocurrido mayormente en regiones estratiformes, con una región positiva dominante superior por encima de la negativa. Características similares a las encontradas en otros estudios de tormentas de invierno en Japón y EEUU.
- Las tormentas que han comportado incidencias de rayos no presentan ninguna estructura en particular, pero las descargas hacia los aerogeneradores se han podido relacionar con núcleos convectivos en regiones estratiformes dominantes. Si esta crece suficientemente, podría permitir que la diferencia de carga active la descarga ascendente desde la estructura elevada.

3.3.3 Aplicaciones prácticas

Muchos tipos de industrias sufren daños causados por el rayo, especialmente con los que se producen en episodios fuera de temporada, tal y como se ha podido observar en el artículo. Aun con el enfoque especial de los aerogeneradores en este artículo, la información aquí expuesta también presenta un importante interés para infraestructuras elevadas como las antenas de telecomunicación. Aunque las actuaciones a llevar a cabo para su protección sean distintas, poder prever cuando pueden ocurrir estos sucesos puede aportar un beneficio para aplicar medidas necesarias o, por otro lado, poder llevar a término actuaciones de prevención.

Concluyendo, y debido a las importantes aplicaciones prácticas de este estudio, se proponen que estas características se tengan en cuenta en los estándares de protección frente al rayo, los cuales parecen subestimar la cantidad de descargas que sufren, especialmente en episodios de pocas descargas o poca intensidad de precipitación, típicamente ligado a episodios de invierno y de fuera de temporada.

3.3.4 Artículo y referencia

Pineda, N., Montanyà, J, Salvador, A., van der Velde, O., López, J. A., 2018. Thunderstorm characteristics favouring downward and upward lightning to wind turbines. *Atmospheric Research*, 214, 46-63. doi: 10.1016/j.atmosres.2018.07.012.

Thunderstorm characteristics favouring downward and upward lightning to wind turbines

Nicolau Pineda [a,b], Joan Montanyà [b], Albert Salvador [a,b], Oscar A. van der Velde [b], Jesús A. López [b]

[a] Meteorological Service of Catalonia, Carrer Berlín 38-46, 08029 Barcelona, Spain

[b] Lightning Research Group, Technical University of Catalonia, Carrer Colom 1, 08222 Terrassa, Spain

Corresponding author at: Meteorological Service of Catalonia, Carrer Berlín 38-46, 08029 Barcelona, Spain

ABSTRACT

Meteorological conditions and thunderstorm characteristics related to lightning threats to wind turbines are discussed in this paper. Due to the rotating blades, wind turbines may be regarded peculiar tall objects, more susceptible to lightning strikes than other tall man-made structures. In the present study, Lightning Mapping Array and weather radar observations allowed to draw a clear picture of the thunderstorm characteristics leading to lightning strokes to wind turbines, in a coastal area of the Mediterranean basin. Results showed that lightning threats to wind turbines tend to occur during transitional periods (spring and autumn), although the main thunderstorm activity concentrates in the warm summer months. Thunderstorms with downward strokes to wind turbines presented particular features, like a limited vertical development and a dominant lower positive charge layer. Downward cloud-to-ground strokes hitting wind turbines were mainly of negative polarity and with peak currents above the average. On the other hand, conditions for self-initiated upwards from wind turbines resemble those reported in Japan and the U.S winter thunderstorms, with low-cloud based large electrified stratiform regions. These particular conditions, leading to lightning threats to wind turbines, should be properly included in lightning protection standards.

KEY WORDS: lightning mapping array, thunderstorm charge structure, downward and upward lightning, wind turbines

1. INTRODUCTION

The observations of lightning strokes to tall objects have been extensively reported in the literature (e.g., McEachron, 1939; Berger, 1967; Eriksson, 1978). A summary of the research efforts on this subject can be found in Rakov and Uman (2003). Interest in lightning to tall structures has grown in recent years, in particular due to the rapid expansion of wind energy globally (e.g., Rachidi et al., 2008; Foley et al., 2012).

Structures of limited height (below 100 m) will suffer from downward strikes whereas tall structures like wind turbines (hereafter, WT) are more prone to initiate upward lightning (e.g., Rachidi et al., 2008; Zhou et al., 2010). High towers (>100 m height) are exposed to strong local electric fields under thunderclouds, being prone to initiate upward propagating leaders (Berger, 1967). Besides, local topography plays a role on the effective height of the structure. Towers on mountain tops are said to have an effective height that is considerably larger than the physical height of the tower (e.g., Risk 1990; Rachidi et al., 2008; Zhou et al., 2010). The concept of effective height is used to account for the additional field distortion (enhancement) due to the presence of the mountain on which the structure is located (e.g., Pierce, 1971; Eriksson, 1978; Risk, 1994; Zhou et al., 2010).

In addition, rotating blades make WT peculiar tall objects (almost 40% of the total turbine height is in rotation). In this regard, a growing number of studies speculate whether a rotating WT is more susceptible to lightning strikes than stationary turbines (e.g., Rachidi et al., 2008; Wang et al., 2008; Radicevic et al., 2012; Wang and Takagi, 2012; Montanyà et al., 2014). According to Montanyà et al. (2014) the effect of rotation induces an electric field growth rate, necessary for the initiation of stable leaders.

All in all, tall structures like multi-megawatt WT have a higher probability of being struck by lightning, compared to their surroundings (e.g., Rachidi et al., 2008; Wang and Takagi, 2012). Indeed, lightning is one of the major causes of severe damage to WT and add a significant cost to their operation and maintenance (e.g., Braam et al., 2002; Minowa et al., 2006; Yasuda et al., 2012; Candela et al., 2014).

1.1. Type of lightning to tall structures

Lightning strikes can be divided into several categories, where the ones relevant to WT mainly concern lightning polarity and the direction of initiation. Downward lightning occurs mainly under deep convection (e.g., warm-season thunderstorms) and the threat to WT calculated in relation to the regional lightning density (Ng). Downward discharges are predominantly of negative polarity, in correspondence with lightning climatology (Rivas-Soriano et al., 2005; Pineda et al., 2011; Poelman et al., 2016).

As mentioned previously, tall structures above a certain height are prone to initiate upward lightning (UL). Leaders may originate from WT due to locally strong electric fields (self-initiated upward lightning, SIUL) or may be triggered by prior lightning discharges in the vicinity, which can provide the necessary electric fields for the inception of an upward leader (lightning-triggered upward lightning, LTUL). Regarding WT, Wang and Takagi (2012) noted that self-initiation occurred more frequently with higher observed wind speeds (or a rotating windmill) compared

with LTUL. It should be added here that upward propagating leaders not followed by return stroke sequences can go unnoticed by conventional Lightning Location Systems (LLS), and therefore the number of upward leaders from WT will be underestimated (e.g., March, 2017).

Despite the modest occurrence of winter lightning, compared to lightning activity associated to deep convection, winter thunderstorms can produce very energetic lightning events (Zhou et al., 2012a; 2012b), and a large amount of damage to sensitive tall structures such as WT (e.g., Shindo et al., 2012; Wang and Takagi, 2012; Yokoyama, 2013; Honjo, 2015). The underlying reason is the low altitude of the cloud charge, as well as the reduced or even absent lower positive charge region (Murphy et al., 1996; Montanyà et al., 2007; Nag and Rakov, 2009; Williams, 2018). Although the highest winter lightning activity is reported in Japan, Montanyà et al. (2016a) identified other areas prone to winter lightning such as parts of the Mediterranean basin, the eastern coast of the US or in the Southern Hemisphere, Uruguay and its surroundings. For example, Levin et al. (1996), Yair et al. (1998) and Altaratz et al. (1999) have reviewed the meteorological conditions favouring lightning in the eastern Mediterranean. There, winter lightning activity concentrates between December and February. Thunderclouds develop at the cold front or, within the cold air mass, just immediately after passing through the "Cyprus lows" (Altaratz et al., 2001). This type of storm is very similar to winter thunderstorms in western Japan (Michimoto, 1991; 1993), and is different from the summertime, continental, mesoscale convective system type thunderclouds.

1.2. Lightning risk assessment

Current lightning protection standards for WT (e.g., IEC 61400-24, 2010) rely on three main parameters: (i) the lightning density (Ng) of the region where the wind farm is to be installed; (ii) the height of the wind turbine itself and (iii) the environmental factor (Cd). Downward lightning is the most frequent type of lightning and its incidence on a particular wind farm is related to the local Ng. Conversely, UL is only considered in the standard within the environmental factor, among other factors like the complexity of local terrain and the height above sea level. According to different authors (e.g., Rachidi et al., 2008; March 2017) the majority of the strikes to modern turbines are expected to come from UL, and therefore a more realistic approach to calculate its contribution is suggested (e.g., Chan et al., 2018). A proposal on how to account for UL in protection standards is beyond the scope of this paper, but the aforementioned issues emphasise the importance of expanding the knowledge on this topic.

1.3. Objectives

There has been very little study of the in-cloud components of UL from man-made structures. In recent years, the use of high-resolution lightning mapping systems and high-speed video have provided relevant information about lightning occurrence on WT. Observations of lightning initiated by WT with a Lightning Mapping Array (LMA) system (Van der Velde et al., 2011; Schultz et al., 2011; Montanyà et al., 2014; Wang et al. 2017), as well as of direct impacts from downward strokes (Montanyà et al., 2016b) have been recently presented. Bearing in mind the growing concern on the lightning impact on the wind power sector as the wind farm deployment grows around the globe, it is of interest to analyse the meteorological context that favours lightning to/from WT. In particular, our objective in the present study was to identify the characteristics and common features of the thunderstorms that produced flashes striking WT in a coastal area of the western Mediterranean basin. To this end, the analysis mainly relied on LMA, weather radar volumetric data and temperature vertical profiles, to characterise thunderstorms that pose a threat to WT, with special emphasis on the vertical charge structure.

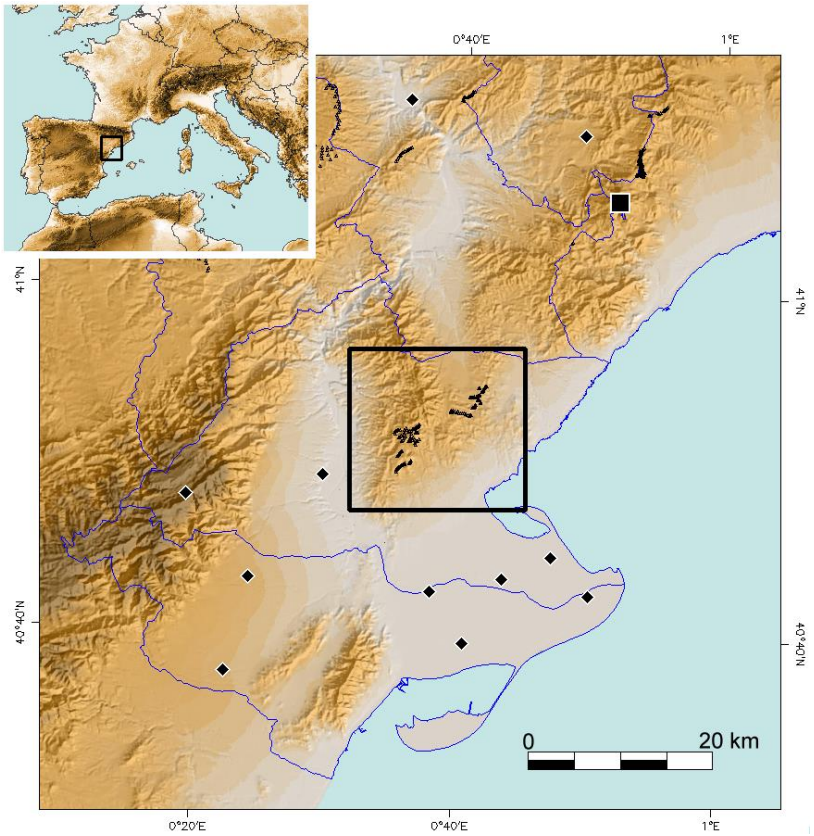

Fig 1. Area of study (AoS), nearby the Ebre's river Delta, south Catalonia, in the Mediterranean coast at the NE of the Iberian Pensinsula . Black diamonds correspond to locations of the *Ebre Lightning Mapping Array* sensors. The black square corresponds to *La Miranda* weather radar site. The highlighted area ecompasses the wind turbines (black triangles) analyzed.

The area of study (hereafter, AoS) is a hilly area in south Catalonia, near the river Ebre's Delta, not far from the coast on the western Mediterranean Sea (Fig. 1). Wind farms have been progressively deployed in the AoS since 1995. Roughly speaking, wind farms consist of 25 to 50 small WT (40-80 m height), with a baseline ranging from 150 to 250 m and produce from 5 to 50 MW. The AoS is an area largely covered by meteorological observation systems, as it has been designed to cover the post launch Cal/Val field campaign of the ASIM project (Neubert et al., 2006). The organization of the paper is as follows: Section 2 describes the instrumentation and analysis technique; Section 3 collects the results; Section 4 deals with the discussion of the results and finally section 5 presents the concluding remarks.

2. INSTRUMENTATION AND ANALYSIS TECHNIQUES

2.1. Intra-cloud lightning

Intra-cloud (IC) lightning was measured with a LMA (Rison et al., 1999; Thomas et al., 2004) deployed in the Ebre's Delta during the summer of 2011 (Fig. 1). The LMA system detects lightning radio emissions in the very high frequency range (VHF, 60–66 MHz) and locates them in three dimensions by a time-of-arrival (TOA) technique. Each station samples, over 80 μs intervals, the maximum signal amplitude and its GPS-derived precise time, allowing to locate 2000 to 3000 sources per second coming from lightning channels inside the cloud. The accuracy of the mapped source locations is expected to be within 10 m in the horizontal dimension, 30 m in the vertical dimension and 40 ns in time (Thomas et al., 2004). This level of accuracy allows identifying the upward leaders associated with a WT.

The so called Ebre Lightning Mapping Array (ELMA) is operated by the Lightning Research Group of the Technical University of Catalonia (http://lrg.upc.edu/en). The initial six-station ELMA was expanded to 11 stations during 2012, enlarging the area of coverage. Details on the ELMA can be found in Van der Velde and Montanyà (2013).

2.2. Cloud to ground lightning

Cloud-to-ground (CG) data is needed to complement the LMA, since the LMA only detects the cloud phase of lightning. CG stroke information used in the current study was obtained from the LLS operated by the Meteorological Service of Catalonia (SMC), composed by four VAISALA LS8000 stations covering the region of Catalonia (NE Iberian Peninsula) including the AoS. CG return strokes are detected by a low frequency (LF) sensor and located using a combination of TOA and Magnetic Direction Finding (MDF) technique (Cummins and Murphy, 2009). Throughout the years of operation, the SMC-LLS performance has been experimentally evaluated by

means of electromagnetic field measurements and video recordings of natural lightning in successive campaigns (Montanyà et al., 2006, 2012; Pineda and Montanyà, 2009). The analysis of the 2013-campaign (Montanyà, 2014) establishes a CG flash detection efficiency for the SMC-LLS around 80–85%.

Additionally, CG data from the European LINET network was available for the analysed events. LINET employs TOA to detect CG lightning strokes in the very low frequency range Betz et al. (2009a). LINET offers a location accuracy reaching an average value of around ~150 m, as verified by CG strokes to towers of known position (Betz et al. 2009a). More details about the LINET system can be found in Betz et al. (2009b).

2.3. Weather Radar

In this work, we also took advantage of weather radar products. The SMC operates a weather radar network in the Catalonia region, with "La Miranda" radar (N 41° 05′ 30.24″ E 0° 51′ 48.58″; 950 m above MSL) located at 40–50 km of the AoS (Fig. 1). The SMC radars operate in C-band (5.600 to 5.650 MHz) and are Doppler type. Polar volumes (radar reflectivity and radial velocity) are acquired every 6 min. Further technical details of the SMC weather radars and network characteristics can be found in Bech et al. (2004) and Argemí et al. (2014).

Since the introduction of weather radar, many studies have dealt with the necessary conditions for the initiation of lightning (e.g., Workman and Reynolds, 1949; Reynolds and Brook, 1956; Larsen and Stansbury, 1974; Dye et al. 1989; Buechler and Goodman, 1990; Hondl and Eilts, 1994). All in all, the onset of significant electrification is associated with a rapid vertical development of convection, which allows the presence of precipitation in the mixed phase region (i.e., the presence of small ice crystals and super-cooled cloud water) above the height of the –10°C isotherm. Therefore, the appearance of a 30–40 dBZ or greater radar echo at heights above the –10°C isotherm indicates the presence of a large enough quantity of hydrometeors in the mixed phase region for electrical charging, and ultimately, lightning.

To account for the thunderstorm vertical development, we worked with the radar echo top product, with 12 and 35 dBZ thresholds (that is, the maximum height reached by the 12/35 dBZ reflectivity echoes). Besides, constant-altitude plan position indicator (CAPPI) at 1000 m AGL images, were used to analyse the storm morphology.

2.4. Sounding vertical profiles

Reviews of charge structure (e.g., Khrehbiel, 1986; Williams, 1989) illustrate a relationship between the height of electrical charge centres and the temperature

profile. In this regard, the heights of the representative environmental temperature values selected were obtained from the Barcelona radiosonde data (Abellán et al., 2011). The Barcelona station (N 41º 23' 4.08" E 2º 7' 3.36") takes part on the Global Telecommunications Service (GTS) observations from 2008, with the code 08190.

Relying on the graupel–ice mechanism conceptual model to explain cloud electrification (e.g., Takahashi, 1978; MacGorman and Rust, 1998), the environmental temperatures selected in this study were –10°C and –40°C, aiming to delimit the mixed-phase cloud region, where the main negative charge region resides (MacGorman and Rust, 1998). In fact, many studies have reported a strong correlation between lightning initiation and radar echoes at –10°C to –20°C levels (e.g., Krehbiel et al. 1984; Buechler and Goodman, 1990; Gremillion and Orville, 1999; Vincent et al., 2003; Yeung et al., 2007). Krehbiel et al. (1984) has noted that this main negative charge region remains at fairly constant altitudes as the storm evolves. Moreover, Tomine et al. (1986) and Michimoto (1991) have stated that these environmental temperatures also apply to winter storms, despite taking place at rather low altitudes.

On the other hand, two instability indices derived from the Barcelona sounding were used to briefly characterise the environment of the analysed thunderstorms: the CAPE (Convective Available Potential Energy, Wallace and Hobbs, 1973), a common metric for the energy available in the environment for thunderstorm growth; and the Lifting Condensation Level (LCL), used to estimate boundary layer cloud heights (e.g., Stackpole, 1967).

2.5. Case study selection

Episodes with lightning flashes involving WT in the AoS were primarily identified by means of LINET CG data. Since clusters of CG are often observed around tall structures (e.g., Betz et al., 2004; Diendorfer et al 2014, Nag et al 2015), the area with wind farms within the LMA coverage was systematically monitored, looking for clusters of strokes in a buffer of 150 m around WT. Data from this first selection was manually inspected using LMA data, searching for leaders ending or starting on WT. This exercise resulted in 5 case studies. Besides, two summer thunderstorm episodes are included in the analysis, in order to have a reference on the typical warm-season vertical charge structure for comparison.

2.6. Analysis technique

The analysis of the evolution of the vertical structure of the storm relied mainly on the evolution of the LMA source density, two radar echo top products (12 and 35 dBZ) and temperature vertical profiles (–10°C and –40°C). Besides, the vertical charge structure was inferred from the LMA observations for the periods when lightning to/from WT occurred. In particular, we used the method developed by van

der Velde and Montanyà (2013), which uses a time-distance-altitude projection to identify the polarity of each IC leader process from the inferred velocity of lightning channels. The LMA predominantly locates sources coming from negative leaders moving through regions of positively charged cloud particles, with propagation speeds of $1–2{\cdot}10^5$ ms^{-1}. Weaker sources from positive leader traces inside the negative charge region are often detected as well, caused generally by recoil leaders (e.g., Mazur, 2002; van der Velde and Montanyà, 2013). Compared to negative leaders, the propagation speed of positive channels is almost an order of magnitude lower, with velocities around $2–3{\cdot}10^4$ ms^{-1} (e.g., Mazur et al., 1998; Shao and Krehbiel, 1996). The majority of these sources typically cluster over a shallow range of altitude, creating regions of net positive and negative charge. LMA observations have also shown that the lightning discharge tend to initiate in-between these opposite charge layers (van der Velde and Montanyà, 2013).

Finally, to account for the horizontal dimensions of the storm system, storm morphology analysis was carried out using the classifications by Parker and Johnson (2000) and Duda and Gallus (2010). All systems were classified using visual inspection of radar CAPPI sequences.

3 RESULTS

The case studies with lightning strokes to WT are summarized in Table 1, which includes both downward and upward lightning events. The selection of case studies includes also includes two summer thunderstorm episodes, to be used as a reference for typical warm season thunderstorms in the analysis and discussion of the charge structure.

3.1. Lightning activity in the region of interest

The first thing to stress about Table 1 is that the episodes involving lightning strokes to WT correspond usually to months with low lightning activity in the AoS, such as April and November. Therefore, before the case overview, lightning patterns throughout the year in the AoS were analysed, using data from the SMC-LLS (12–year period, 2005–2016). The average CG flash density in the AoS is of 2.8 CG flashes km^2 $year^{-1}$, 0.8 above the average density of the whole Catalonia. On the one hand, nearly 87% of the annual CG flashes occur between June and October, with a peak at the end of summer (24% in August and 33% in September). Conversely, months from November to April account for only 9% of the observed lightning activity. Indeed, the seasonal cycle in the AoS is driven by two main factors: the solar heating which peaks in summer and favours the onset of convective storms, and the proximity to the Mediterranean Sea conditioning the autumn and winter activity. From the late summer on, lightning activity moves gradually to the coast and

offshore, where the activity is dominant in autumn. This change is related to the average land/sea temperature difference, the average sea surface temperature being warmer during autumn compared to land (Kotroni and Lagouvardos, 2016; Galanaki et al., 2018).

3.2. Typical summer thunderstorms. Case overview

1st JULY 2014

On that day, convective indices presented moderate conditions of instability (see Table 1). Convection started to develop in the mountainous region west of the Ebre's Delta, traveling to the Northeast afterwards. The initial cells began to cluster in a line, oriented in the direction of the predominant SW-NE flow. Over time, the flow rotated to a West-East pattern. New growing cells kept clustering but in a less organized manner. The cluster of cells crossed the AoS between 17:00 and 18:00 UTC and promptly decayed soon after. Fig. 2 shows the evolution of the vertical structure of the storm occurring in the AoS. Thunderstorms in this episode began to grow rapidly around 11:00 UTC, and continued intensifying until 15:00 UTC, as indicated by increases both in the density of VHF sources. The seesaw trend of the TOP–35 in the following hours suggests a sequential development of pulse-type convection. High IC activity was reported by the LMA as the TOP–35 remained around the –40°C. The abrupt decay of the TOP–35 by 18:30 UTC led to the termination of the lightning activity. It is worth noticing the increase in the CG lightning flash rate (hereafter LFR) on the latest hours, as the VHF burst density showed activity in the lower positive layer (16:30 – 18:00 UTC approx.).

2nd AUGUST 2014

Convection initiated around 11:00 UTC with diverse cells that progressively clustered SW of the Delta, to finally form a non-linear convective system with a large area of reflectivity above 45 dBZ (CAPPI 1km 13:00 UTC) in what looks like the period of maximum development. After that, while moving to the Ebre's Delta from West to East, the complex split into different cells, to finally dissipate around 14:00 UTC. In the meantime, new cells appeared in the radar coverage coming from SW, this time showing a leading stratiform pattern. Subsequent cells continued in the same SW-NE flow over the Delta. The 35–dBZ echo tops (Fig. 3), growing rapidly to reach first the –10°C (4.5 km AMSL approx.) and shortly after the –40°C (9 km AMSL approx.), spanning the mixed-phase region, suggested the presence of graupel and an environment conductive to active charge separation. The LMA density bursted shortly after, showing a high activity between 12:00 and 14:00 UTC, related to negative channels at heights between 9–11 km ASML. Negative channels in the lower layer also became apparent from 12:00 to 13:00 UTC, coinciding with the period of maximum LFR (15 CG min^{-1}). Between 13:00 and 14:00 UTC the TOP–35 almost lost half of its height, and so did the VHF source density and the CG activity.

In the following hours the TOP–35 stayed around the -10°C with a moderate lightning activity until a rapid decline around 20:00 UTC.

Table 1. Summary of case studies. Information on each episode includes: Instability indices (Convective Available Potential Energy, CAPE; Lifting Condensation Level, LCL) and isotherm heights (–10ºC, –40ºC and tropopause) derived from radiosounding. Storm system morphology and area (continuous area above 12 dBZ) are derived from radar imagery. Lightning flash rates (CG) are derived from the SMC-LLS. Finally, the time and type of lightning strokes to wind turbines mapped with the LMA are listed (with maximum peak current per CG flash)

		TYPICAL SUMMER CASES			LIGHTNING TO WT				
Episode		02/08/2014	01/07/2014	20/11/2011	03/04/2012	17/11/2012	16/11/2013	18/01/2014
Radiosounding time (UTC)		12:00	12:00	0:00	12:00	0:00	0:00	0:00
Instability indices	CAPE (J kg^{-1})	2,350	1,350	--	390	113	--	--
	LCL (m AMSL)	890	890	--	100	340	430	750
Tropopause Height (m AMSL)		11,000	12,000	--	11,000	11,650	8,500	10,250
Isotherm Heights (m AMSL)	-10°C	4,550	5,400	3,000	3,900	4,500	3,100	3,800
	-40°C	8,700	9,600	7,100	7,900	8,700	7,100	7,600
Radar Morphology		cluster	cluster	parallel	broken line/	parallel	non-linear	leading
		of cells	of cells	stratiform	trailing str.	startiform	conv.syst.	stratiform
Storm system area (km^2) (>12 dBZ)		2,415	1,905	4,450	5,365	11,485	31,050	10,275
Lightning flash rate (LFR) (CG min^{-1})		4-5	2-3	2-3	1-2	1-2	1-2	3-4
	Maximum LFR	15	8	8	8	4.5	3	11.5
	LFR during strikes to WT	-	-	7	2	3	1.5	4
Lightning to Wind-Turbines		-	-	DW 04:29 (-12)	DW 18:38 (-18)	DW 16:06 (-23)	SIUL 08:13 (-13)	DW 08:40 (-36)
				DW 04:37 (-98)	DW 18:44 (-28)	DW 16:08 (-77)	SIUL 08:37 (+113)	LTUL 09:00 (-24)
	time in UTC			DW 04:39 (-135)	DW 19:33 (-103)	DW 16:24 (-35)	SIUL 08:41 (-39)	DW 09:05 (-19)
	Downward (DW)			DW 04:45 (-53)	DW 19:40 (-12)	DW 17:10 (-15)		DW 09:37 (-106)
	Lightning-triggered upward (LTUL)			DW 06:55 (-31)		DW 17:34 (-138)		DW 09:39 (-127)
	Self-initiated upward (SIUL)			DW 06:57 (-14)		DW 17:59 (+12)		
Maximum Peak current (kA) per CG flash				DW 07:11 (-9)				
				DW 07:15 (-24)				

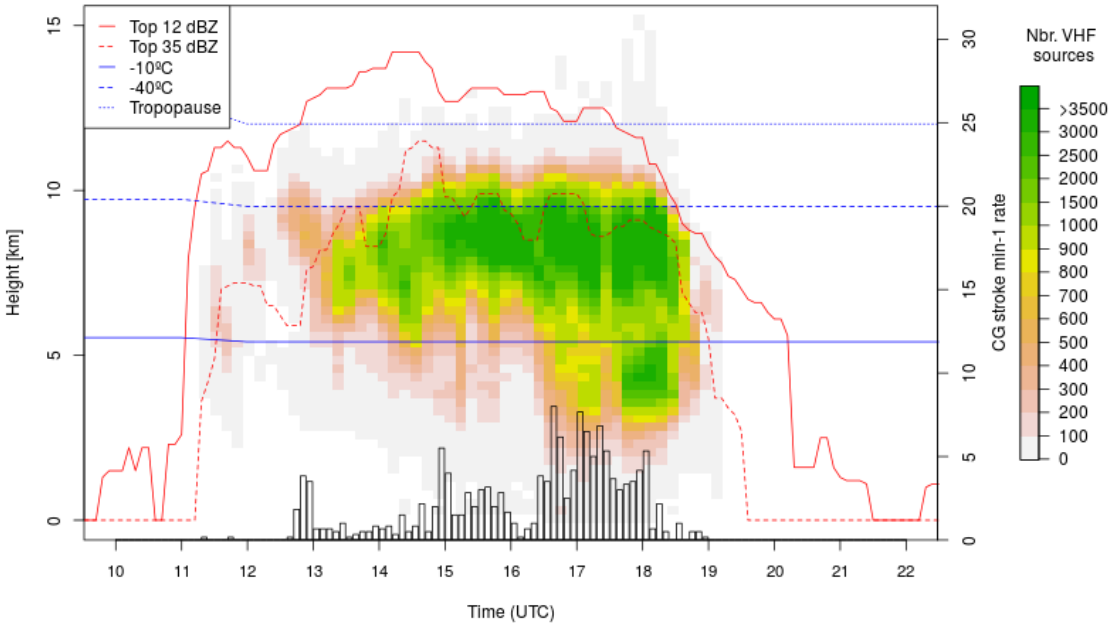

Fig 2. Evolution of the vertical structure of the storms occurring in the area of study on the 1st July 2014. Time–height LMA source density plot. Colour indicates relative density of sources according to a pink-yellow-green colour scheme. The largest source densities are in green. Red lines correspond to the height of the TOP–12 (dashed) and TOP–35 (solid) products. Bar lines indicate the CG flash rate in a 10–min timestamp. Finally, blue lines correspond to the representative environmental temperature values obtained from the vertical sounding profiles (–10°C, –40°C and tropopause heights in km).

3.3. Case studies involving lightning to wind-turbines

The cases listed in Table 1, involving lightning strokes to WT, showed modestly unstable environments with 400 J kg^{-1} of CAPE at most, –10°C levels below 4500m AMSL, nearly saturated vertical profiles and the tropopause at around 10–11 km AMSL or lower. Accordingly, the resulting storm systems were not particularly vigorous. Weather radar sequences showed that thunderstorms favouring lightning strokes to WT did not have any particular precipitation configuration. Besides, they all showed a weak LFR, with lightning to WT occurring around the maximum LFR period.

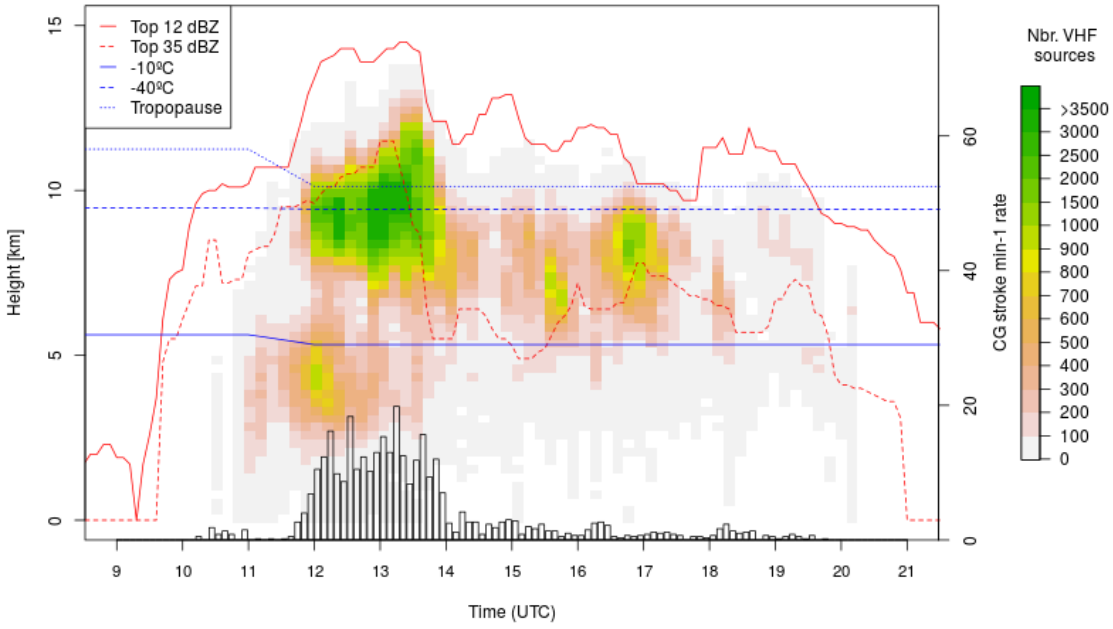

Fig. 3. Analogous to Fig. 2, but showing the evolution of the vertical structure of the storms occurring in the area of study on the 2nd August 2014.

20th NOVEMBER 2011

For this episode, radar imagery showed a stationary thunderstorm system with a parallel-stratiform precipitation configuration, moving SE-NW, with weak convective cells at its southernmost end. The VHF source density (Fig. 4) shows two periods of maximum activity, the first around 04:30 UTC and the second at 07:30 UTC, with a strong lower positive layer at 3–4 km ASML and a weaker upper positive layer between 7 and 9 km ASML. These two periods of maximum activity are delimited by TOP–35 above the –10°C height, and the moments of maximum LFR (7–8 CG min^{-1}) are collocated with the maximum TOP–35 heights. Downward lightning to WT (04:29, 04:37, 04:39, 04:45 UTC) were observed during the first period of maximum activity. At that time, 1-km CAPPI imagery showed a rainfall field extension (>12 dBZ) at that time of about 100 x 40 km. Another series of downwards to WT was observed between 06:55 and 07:15 UTC (06:55, 06:57, 06:58, 07:11, 07:15 UTC), coinciding with high VHF source densities in the low charge layer.

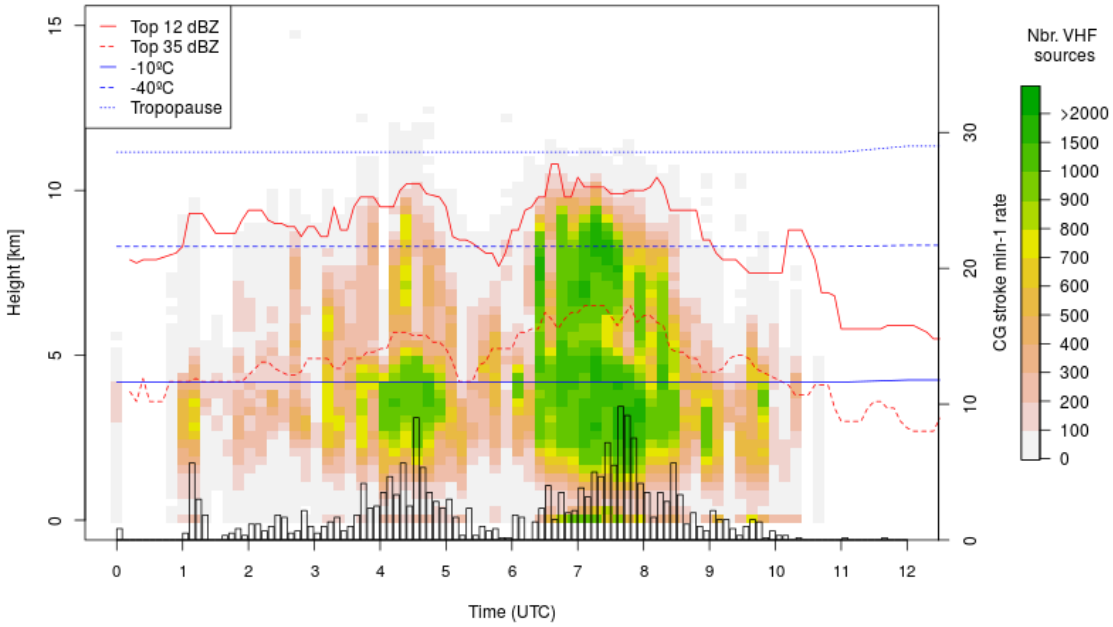

Fig. 4 Analogous to Fig. 2, but showing the evolution on the 20th November 2011. Downward flashes striking WT occurred in two periods, from 04:30 to 04:45 UTC and from 06:55 to 07:15 UTC.

As an example, the LMA plot of the 04:37 UTC flash is shown in Fig. 5. The flash started immediately above a wind turbine with a fast negative downward leader originated at around 3 km altitude, producing two CG strokes to a WT. The first CG stroke produced a current of –98 kA, the second stroke was of –7 kA and occurred 23 ms after. The flash had a low altitude positive leader development with negative leader activity above. No leader activity was observed above 6 km during this lightning event. The plain view panel shows radial channels spreading simultaneously in various directions, all starting from the lightning initiation region. Regarding to the precipitation structure, Fig. 6 shows the 04:39 UTC flash in combination with the radar reflectivity. Similar to the 04:37 UTC flash (Fig.5), this flash also started on the perimeter of a convective core, with a downward channel right after the breakdown, and cloud channels spreading radially to the stratiform precipitation region after the CG return stroke. The second series of lightning to WT had a similar pattern, with the CG flashes to WT starting in the vicinity of convective cores, showing first CG strokes followed afterwards by cloud channels spreading away.

3rd APRIL 2012

At the time of the first downward flashes to WT (18:38, 18:44 UTC), the north-eastward moving thunderstorms looked like a trailing-stratiform system with embedded weak convective cores above the AoS. Two periods of IC activity were observed above the AoS, the first one starting around 13:00 UTC when the TOP–35

reached the –40°C height (the evolution is not shown). After a short period of inactivity, activity restarted between 18:00 and 19:30 UTC approx. The sequence of the LMA source density indicates a progressive decrease in the height of the low charge layer. The downward stroke to a WT occurred during this later period.

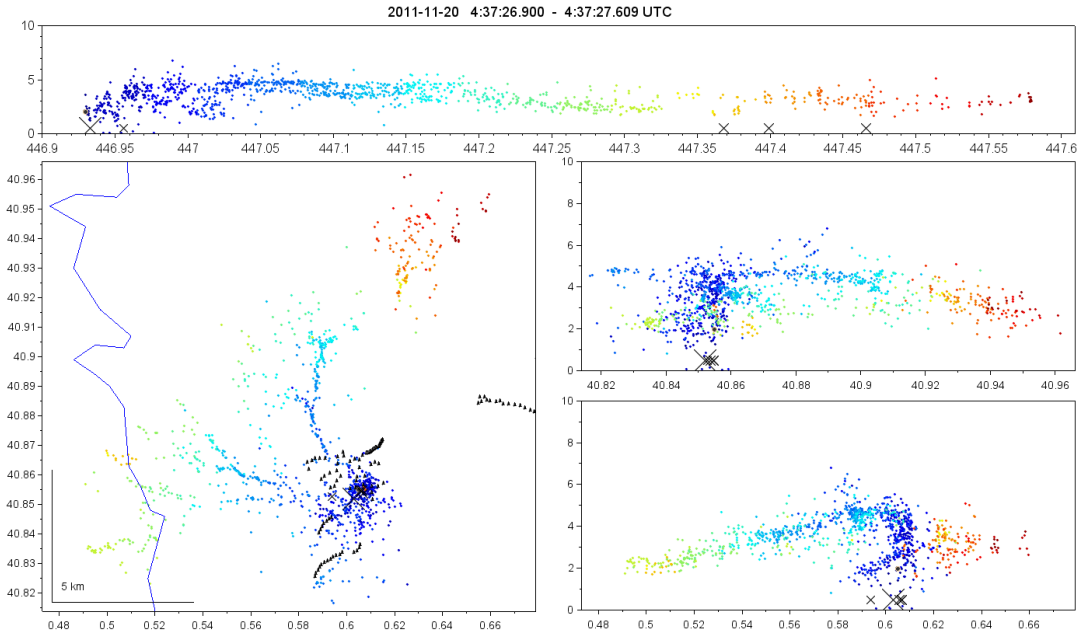

Fig. 5 Multi-panel display of a lightning flash detected by the LMA on the 20th November 2011 at 04:37:26 UTC. VHF sources are coloured as a function of time. The top panel is altitude AMSL (km) versus time (seconds). The left panel is a plan view map (0.1° latitude equals 11.1 km) with contours of the Ebre river (blue) and WT (black triangles) as background. The panels at the right show altitude (km) as a function of latitude and longitude respectively. LINET strokes are displayed with symbols X for negative and +for positive.

Fig. 7 shows the LMA detection of the downward stroke that impacted a WT during this episode. Note that the leader activity stayed below 6 km a with remarkable positive leader development. A negative leader to ground started at the beginning of the flash and ended with a –18 kA stroke to a turbine located on one of the wind farms in the AoS (≈640 m AMSL). According to the radar imagery analysis (not shown), in this case the leader initiated in the rear edge of a convective cell and hit a turbine which was under the same cell at that moment. Compared to precedent case, maximum reflectivity was slightly higher, but the vertical development was similar, with the Top–35 reaching 6.0 to 7.0 km.

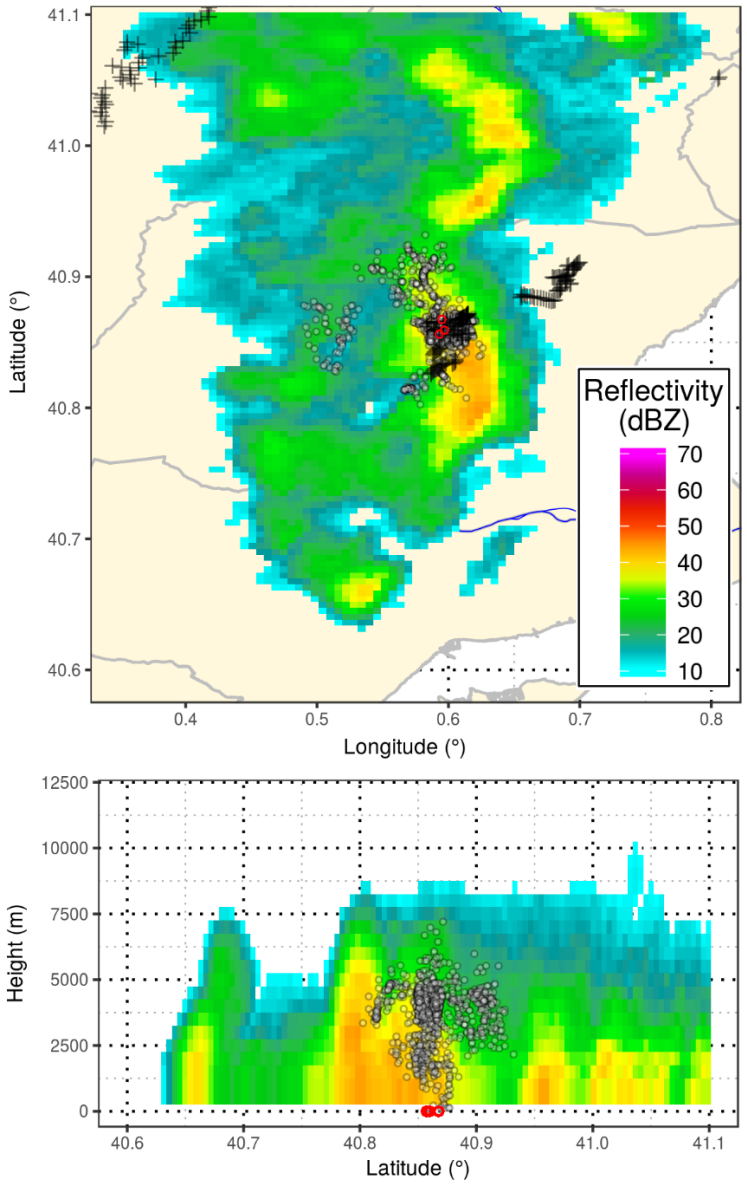

Fig. 6. Radar and LMA lightning data overlay showing the lighting flash to a wind turbine on the 20th November 2011 at 04:39:25 UTC. The LMA sources of a single flash (dots) are combined with the 6–min radar reflectivity volume (04:36-04:42 UTC). LINET CG strokes are represented with red dots. The top panel shows a plain view of the maximum reflectivity (dBZ), while the bottom panel shows the altitude (km) of the LMA sources in the South-North projection of the radar volumetric data. Wind turbines are represented with black crosses.

17th NOVEMBER 2012

Around 11:00 UTC, a broken line of cells crossed the AoS South to North, progressively transforming into a parallel stratiform precipitation structure. From 13:00 UTC some of the cores intensified to reach 50 dBZ. Around 17:30 UTC the storm intensity decreased still, the system remained active and intensified again by 22:00 UTC. However, by that time the main cells were leaving the area of coverage

of the LMA and were not well represented in Fig. 8. VHF source density detected by the LMA shows a bimodal distribution with maximums at 3–4 km and 6–7 km height (similar to the precedent cases). A downward lightning flash to a WT was identified at 17:34 UTC (see Fig. 9). This case corresponds to a complex flash originated about 50 km away from the WT. Before striking the turbine, an intense +CG stroke (+52 kA) triggered a sprite (see van der Velde et al. 2014). After the long negative leader had passed near the WT, positive breakdown occurred and suddenly a negative leader was directed towards a WT, producing 9 strokes. The leader sequence suggests that the first leader development related to the intense +CG flash initiated a new leader breakdown in the wind turbine area. Radar reflectivity in Fig 9 helps locating the negative leader which starts at the border of a convective cell with maximum reflectivity around 45 dBZ. The cloud channel crossed a stratiform area with lower reflectivity, to finally reach a WT which was close to a smaller convective core.

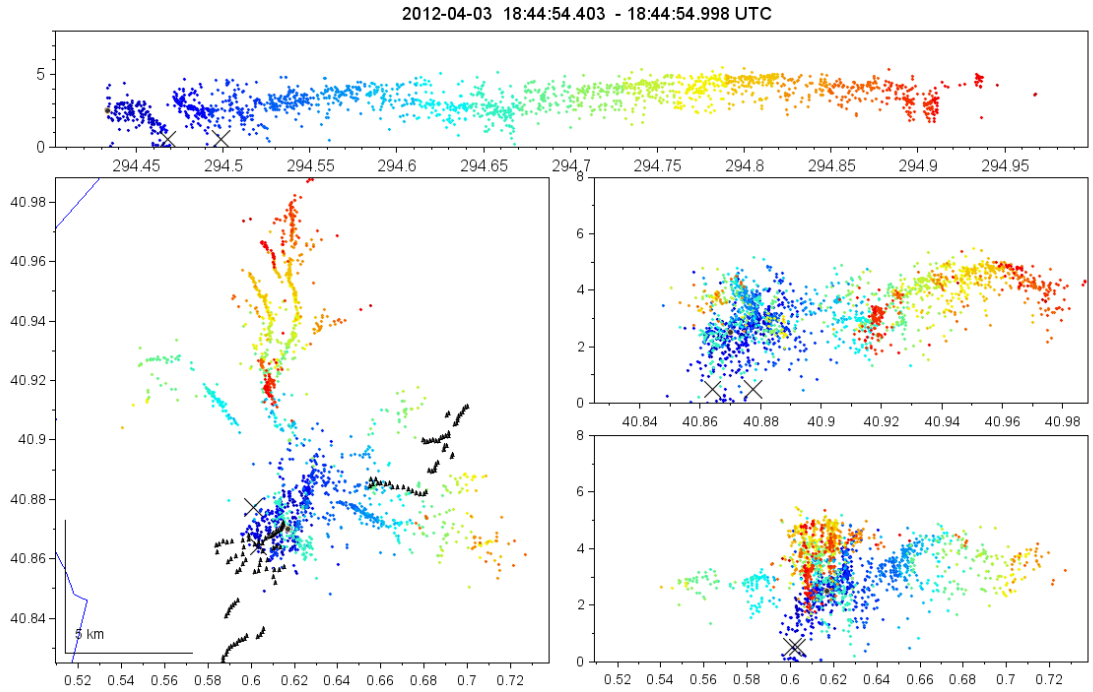

Fig. 7 Analogous to Fig. 5, but for the downward lightning flash to a wind turbine detected by the LMA on the 3rd April 2012 at 184454 UTC.

16th NOVEMBER 2013

On that day, radar imagery showed a leading stratiform precipitation structure, with a large area of moderate reflectivity reaching the AoS around 05:30 UTC. Lightning activity in the AoS was mainly related to embedded convection cores that formed offshore. Ground temperature was about 8°C with a cold air mass from the North and a flow from the Mediterranean due to a low. In this case, the storm was close to the threshold for being considered a winter thunderstorm according to Montanyà et al (2016a) criteria. The evolution of the vertical structure of the storms occurring in

the AoS for this episode (not shown) limits the presence of lightning to a narrow timespan of one hour between 08:15 and 09:15 UTC approximately. This is the only period where the TOP–35 was above the –10°C level (3,100 m AMSL). It is during this period that the upward flashes were detected by the LMA (08:13, 08:37, 08:41 UTC). Fig. 10 reveals pulses related to an upward positive leader, starting close to the ground. After 400 ms approx., a very well resolved negative leader rapidly accelerated upwards into a layer of positive charge. The right panel of Fig. 10 shows leader speeds (van der Velde and Montanyà 2013). In this case, the likely source of the UL was a WT. The flash grew to a size of 65 by 40 km. There seem to be two other upward leaders in the figure (435.6 s and 435.85 s), but not as well resolved by the LMA as the first one.

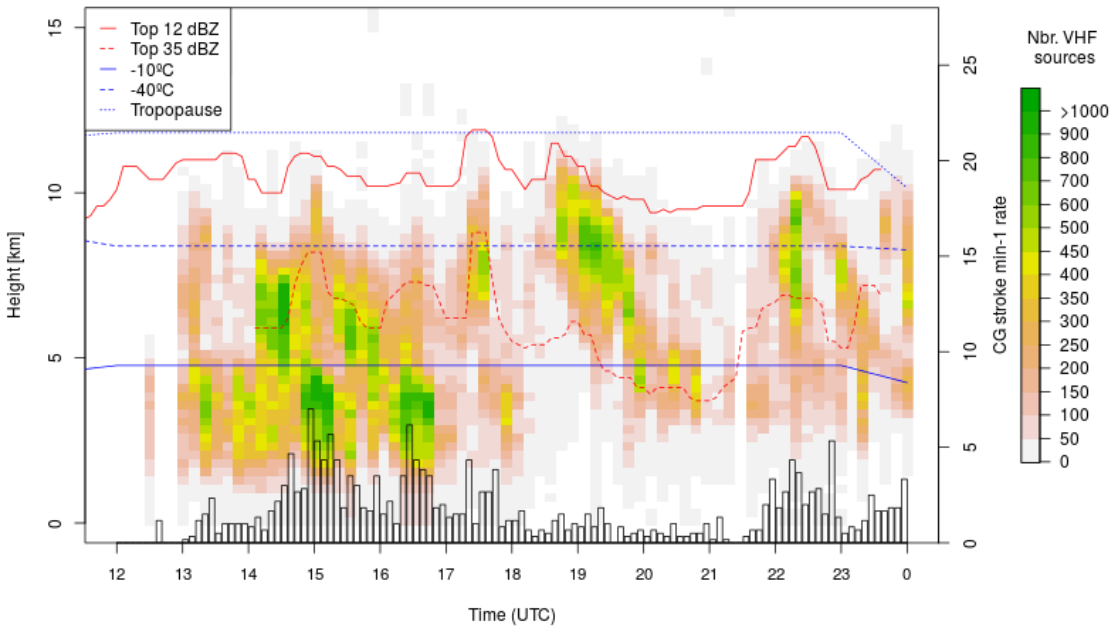

Fig 8. Analogous to Fig. 2, but showing the evolution of the vertical structure of the storms occurring in the area of study on the 17th November 2012.

18TH JANUARY 2014

In the AoS, thunderstorms occurring in winter months like the present case study are usually associated with fronts moving northward along the Spanish east coast, or with Mediterranean humid, unstable air lifted over the elevated terrain near the coast. According to the radar sequence of that day (not shown), around 05:00 UTC some weak cells started crossing the AoS, South to North. From 06:30 UTC, some organisation became apparent, which can be described as a weak leading stratiform precipitation system. It produced lightning between 08:00 and 10:00 UTC aprox. During that period, the evolution of the vertical structure of the storm (not shown) depicted negative channels at two different layers, the upper corresponding to positive charge level between 7 to 9 km, with the low positive layer around 4–5 km.

Four downward CG strokes to WT were observed between 08:40 and 09:37 UTC. As an example, Figure 11 presents the flash to a WT that occurred at 08:40:18 UTC. Like in the 20th November 2011 episode (Fig.6), the flash initiated in the vicinity of a convective core. The LMA depicts a flash starting at 3 km height with a stepped leader that produced three CG strokes to WT (–36, –13, –9 kA). However, this time, the following cloud channels stayed around the core and did not spread to the stratiform region.

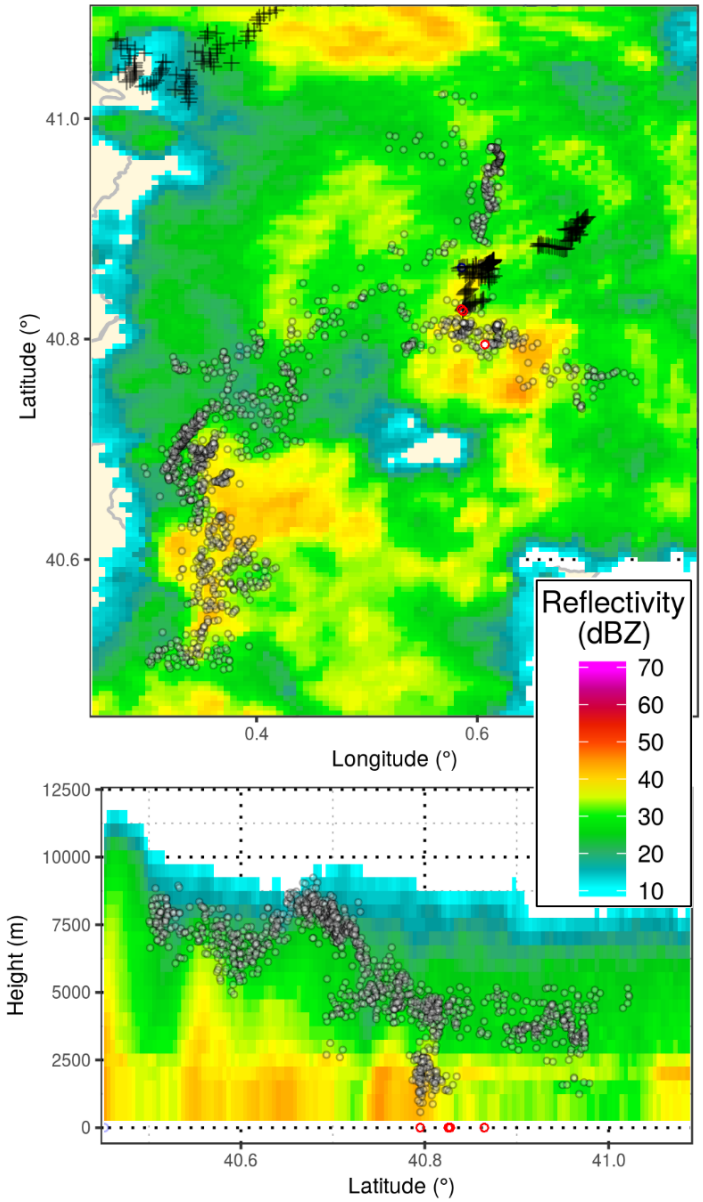

Fig. 9. Analogous to Fig. 6, but showing the 17:34:23 UTC lightning flash to a wind turbine on the 17th November 2012.

Besides, a lightning triggered upward flash was reported at 09:00 by the ELMA (see Fig 12) Although the leader trail was not as well-defined as in the upward flashes detected on the 16th November 2013, it seemed to initiate from a WT. The flash started with a negative CG, followed by cloud positive leader at 4–5 km height. Half

a second after the beginning of the event, negative strokes reported by LINET were followed by negative leaders, spreading at 8–9 km height, before the negative leader from a WT accelerated upwards to reach the negative layer at 6–7 km height. No other strokes where recorded by LINET after the upward leader.

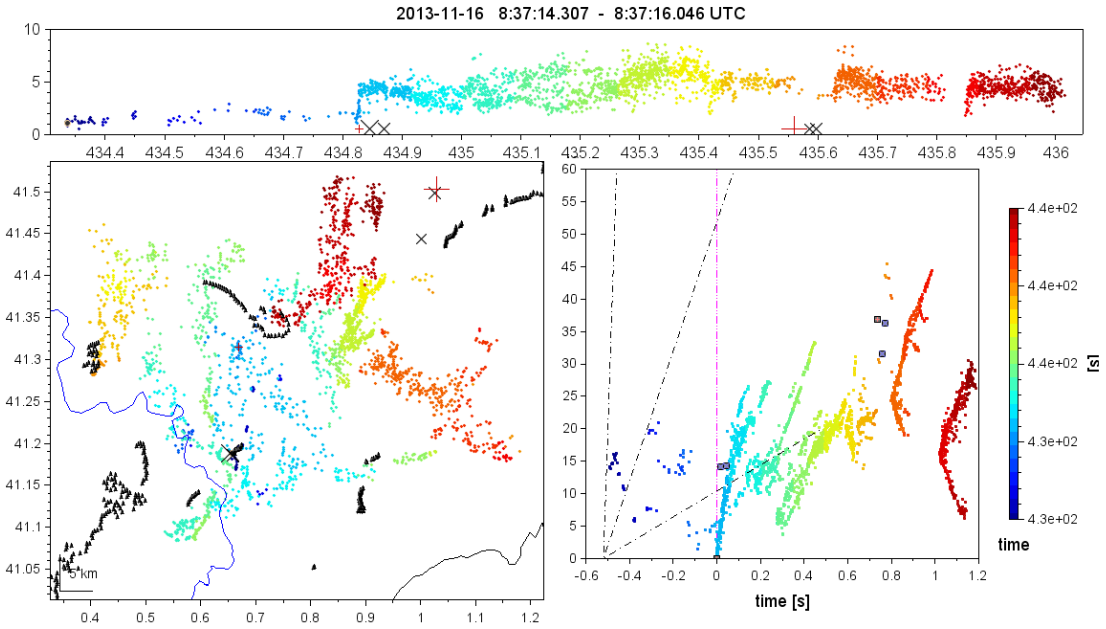

Fig. 10 Multi-panel display of a downward lightning flash to a wind turbine detected by the LMA on the 16th November 2013 at 08:37:14 UTC. For top and left panels see legend in Fig. 5. Unlike the previous LMA figures, here the right panels show the time-distance graph. The dashed reference lines indicate slopes corresponding to speeds of $2 \cdot 10^4$ ms^{-1}, 10^5 ms^{-1}, and 10^6 ms^{-1}. The reference location for the distance is the initiation point of each flash or a cloud-to-ground stroke (at t=0). Black square marks are low-frequency sources detected by LINET (intra-cloud or cloud-to-ground strokes).

3.4. Inferred charge structure

As seen throughout this study, the LMA system depicts the height of the localised VHF sources, predominantly coming from negative leaders moving through positively charged regions. Therefore, the relative density of sources can be used to infer the charge structure inside the thunderstorm cells. Indeed, the majority of these sources typically cluster over a shallow range of altitude, as shown in the previous evolution figures. However, we do not intend here to do a complete characterization of thunderstorms charge structure. Instead, our focus lies on the period with lightning activity concerning WT. Hence, vertical profiles of the charge layer structure have been inferred for the periods in which lightning to/from WT occurred (Fig. 13). While the relative density of LMA sources helps locating the charge layer altitudes, the dominant polarity on each layer was confirmed through the inferred velocity of lightning channels, using the aforementioned method by van der Velde and Montanyà (2013).

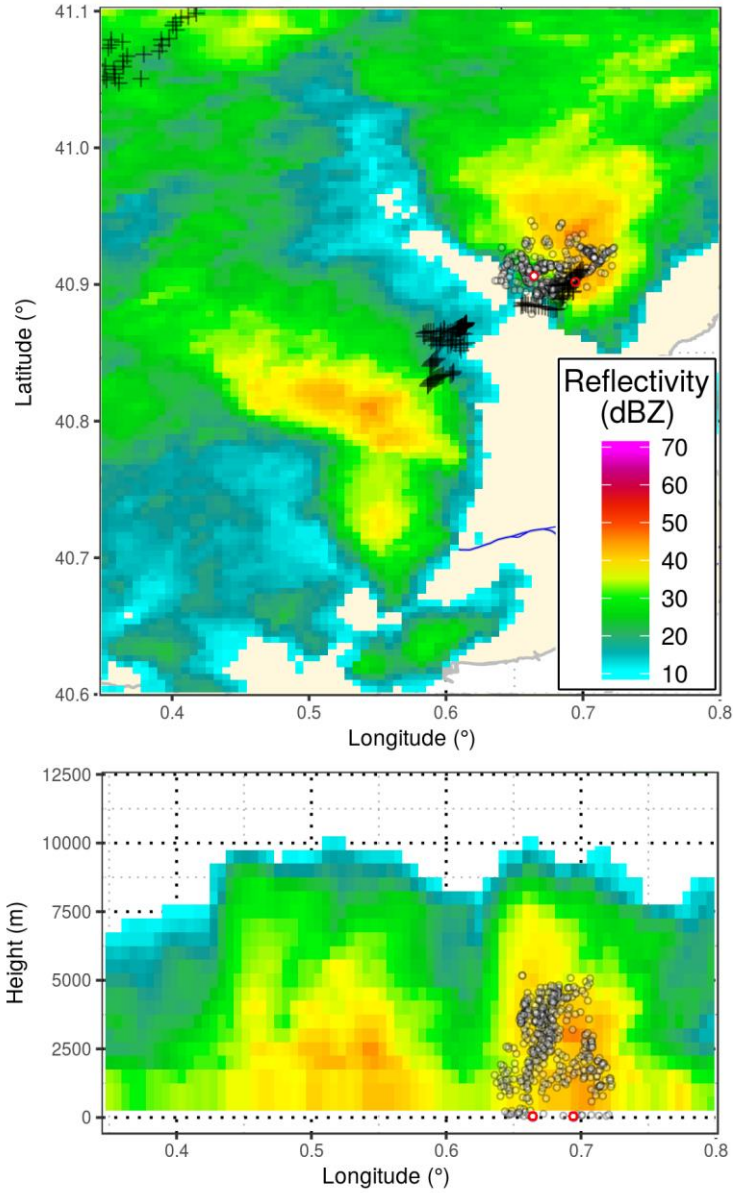

Fig. 11. Analogous to Fig. 6, but showing the 08:40:18 UTC lighting flash to a wind turbine on the 18th January 2014.

As expected, typical summer storms display the basic tripole structure (Williams, 1989, 2001). After a rapid vertical growth (Fig 2, 3) a dipole developed, the upper positive charge layer reaching 10–11 km height (–40°C). The negative charge region below, related to the mixed phase region (e.g., Williams et al 1991), is located between the 5 and 8 km height (–10°C to –25°C). Figs. 2 and 3 also show, at certain stages, the development of a lower positive charge layer, constituting the classical tripole structure.

Interestingly, apart from the 16th November episode, all the other cases analysed showed the same basic tripole structure, the difference being the vertical development they reached. Whereas the upper positive layer reached the 10 km AMSL in the warm season episodes, the cases with downward lightning to WT, only

reached 8–9 km height. On the other hand, it is worth noticing that the lower charge positive region is closer to the surface in all the lightning to WT related episodes. Besides, higher LMA source densities were found on the upper positive layer in the summer reference cases, while LMA source activity dominates in the lowest positive charge layer in the WT related cases.

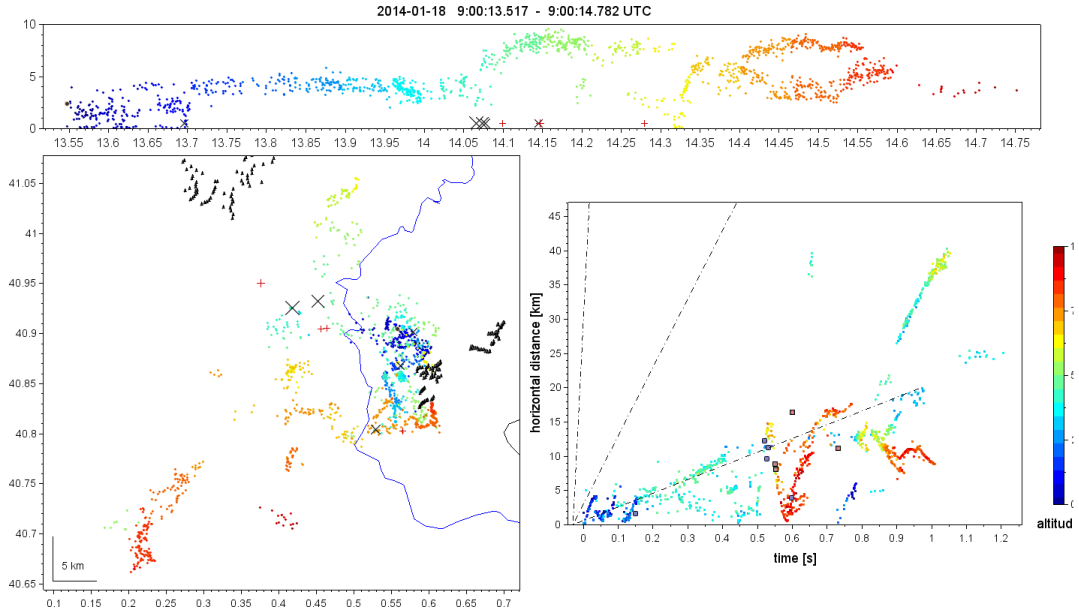

Fig. 12 Analogous to Fig. 10, but for the lightning-triggered upward lightning flash from a wind turbine detected by the LMA on the 18th January 2014 at 09:00:13 UTC.

4. DISCUSSION

4.1. Charge Structure

Results showed charge structures that can be compatible with the tripole produced by the non-inductive charge mechanism (NIC, e.g., Takahashi, 1978; Williams, 1989; Saunders et al., 2006). The LMA inferred charge layers shown in Fig 13 suggest three different types of structure. Firstly, the LMA source density in the warm-season convection episodes (Figs. 2 and 3) shows the maximum activity concentrated in the upper positive charge layer. Deep-convection results in elevated charge structures, with large total LFR but low ground LFR. The CG LFR increases only when a low charge layer is apparent (see Figs. 2 and 3).

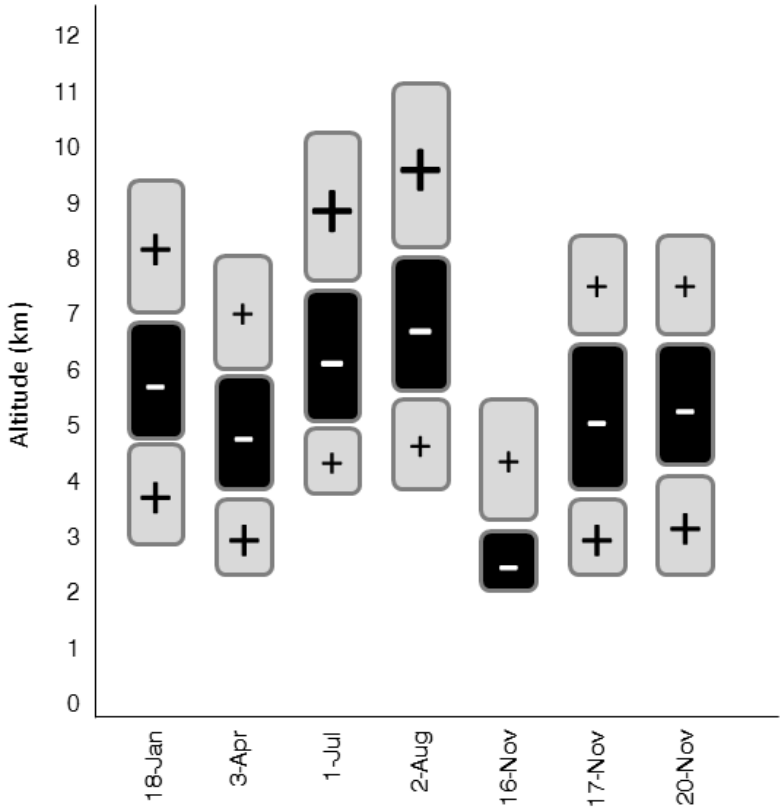

Fig. 13 Charge structure in a vertical profile during the periods for which lightning to/from WT were recorded. The charge structure is inferred from the Lightning Mapping Array (LMA) data analysis, the size of the symbols (+/-) being proportinonal to VHF source density (approximation, not to scale).

Secondly, spring and autumn episodes (e.g., 3rd April, 17th Nov., 20th Nov, Figs. 4 and 8), also having a tripole structure, share another common feature: the lower positive charge layer is the dominant (contrary to warm-season convection where the upper level dominates). This particularity will result in an enhancement of the electric field at the bottom of the negative charge region, providing the means to discharges to propagate to ground as CG flashes (e.g., Jacobson and Krider 1976, Williams 2001, Marshall and Stolzenburg 2002, Pawar and Kamra 2004). Early works by Clarence and Malan (1957) already suggested that lower positive charge centre (LPCC) is essential for the initiation of CG lightning. On the other hand, an excessive LPCC may prevent the occurrence of CG flashes by "blocking" the progression of descending negative leaders from reaching ground (Qie et al 2005, Nag and Rakov, 2009). In this regard, it is worth noting certain differences between the analysed episodes. Lighting to WT on the 20th November, 18th January and 3rd April episodes correspond mainly to CG flashes starting with negative leaders vertically descending to ground. According to the CG classification based on the magnitude of the LPCC by Nag and Rakov (2009), this behaviour suggests a relatively thin LPCC, where the descending negative leader would traverse the positive charge region keeping a predominantly vertical propagation direction towards the ground. Regarding

precipitation structure, this "vertical" negative CG flashes tended to have their origin on the periphery of convective cores. Studies like Carey et al. (2003), Lund et al. (2007) and Akita et al. (2011) pointed out these areas along the perimeter of updrafts as prone to originate CG lightning. Contrarily, lightning strokes to WT on the 17th November show significant horizontal propagation before reaching ground, suggesting a larger LPCC compared to the precedent cases. According to the Nag and Rakov (2009) classification, in this scenario, a negatively-charged leader channel originated in the base of the main negative charge region would travel predominantly horizontally because of the blocking LPCC effect, eventually making a termination to ground.

Thirdly, the 16th November 2013 episode presented a particular structure, with two layers of opposite polarity and no apparent lower positive layer. The structure on that day had common features with what has been observed, also with an LMA, by Wang et al. (2017) in winter thunderstorms in Japan: (i) an horizontal extension much larger than the vertical extension (a large-scale stratiform cloud with relatively weak echo intensity and low cloud top height (ii) the charge regions enclosed between the –10ºC and –20ºC isotherms, in agreement with the NIC, and (iii) a low altitude of the whole cloud, with positive charge over negative charge. This particular charge distribution has also been reported by Schultz et al. (2011) for upwards from high towers during electrified snowfall events. All in all, this particular scenario featured favourable conditions for the self-initiation of UL. Finally, it is worth mentioning that the LMA system can infer the charge structure only when lightning occurs. In this particular case, the lightning rate was very small, so the charge structure inferred from LMA sources cannot be seen as the complete picture of the thunderstorm charge structure.

4.2. Transition season thunderstorms

Results presented bring new evidence on the low correlation existing between lightning incidence on WT and the month average lightning density for the region surrounding the wind farm. Results point out that lightning activity in the AoS concentrates between June and October (85% of the year-round CGs) and especially during August and September (57% of CGs). However, all the analysed episodes with lightning from/to WT occurred between November and April, months that account only for nine percent of the year-round lightning activity.

Other studies on lightning incidence to tall structures have shown a similar pattern. For instance, studies at the Gaisberg Tower (Montanyà et al., 2007; Diendorfer, 2009) have shown that although the thunderstorm season in Austria is between April and August, actually the months with the highest numbers of recorded flashes at the Gaisberg tower are March and November, respectively, which are definitely months outside the convective season and generally with very little thunderstorm

activity in Austria (Diendorfer, 2017). Other studies in towers around Europe also registered a majority of self-initiated flashes during the winter period, such as the Peissenberg Tower (Manhardt et al., 2012). On the contrary, the majority of upward flashes at the Säntis Tower occur during summer (Romero et al., 2013; Smorgonskiy et al., 2015) like in Rapid City (Warner et al., 2012a, b). According to Smorgonskiy et al. (2015) seasonal variations could be attributed to the differences in the tower effective height, although they pointed out that further research is needed to validate this hypothesis.

Going back to the present results, with the exception of the January case, the rest occurred during the transition from summer to winter and vice versa. During these transition periods, at most mid-latitude locations, like the AoS, the lower boundary of the mixed phase region (i.e., the –10°C isotherm) suffers a sudden change of height. Fig.14 shows the average evolution of the height of the –10 °C isotherm throughout the year near the AoS (calculated from the Barcelona radiosounding database). The average over a 10–year period (2006–2015) indicates that the –10°C isotherm is between 5.5 and 6 km height during the thunderstorm season (June-September) and around 4 km height in winter (December to March). Interestingly, most of the episodes with lightning to WT have been observed during the transitional season, when the isotherm –10°C is approximately 1.5 km below the typical thunderstorm season and therefore closer to ground.

4.3. Morphology and Size of the storm

Results showed that the storms involved in lightning strokes to WT had no particular precipitation structure, developed in a weak convective environment and had modest amounts of lightning. Recently, Wang et al. (2017) pointed out the preference of CG lightning for regions with weak updraft and downdraft. In the present case study, the majority of downward lightning striking WTs are linked to weak convective cores embedded into stratiform dominant systems.

Interestingly, some of the analysed case studies also produced sprites, episodes which are analysed in detail in Van de Velde et al. (2014). There are other studies that reported sprite-parent +CGs involved also in UL (Warner et al., 2011; Lyons et al., 2011 and 2014). High peak current +CGs are followed by long continuing currents, thus resulting in large charge moment changes (CMC) capable of producing transient luminous events (TLE) (e.g., sprites, elves, halos) as documented in different studies (Takahashi et al., 2003; Suzuki et al., 2006; Matsudo et al., 2007; Van de Velde et al., 2014). It is worth stressing out that in our cases most storm systems were relatively small (see dimensions in Table 1) compared to other TLE-related systems like those documented in the central United States (e.g., Lyons, 1996; Lyons et al., 2003; Lang et al., 2010, 2011; Lu et al., 2013). Thunderstorms like 20th November, 3rd April and 17th November exhibited slow storm motion and weak

organization in the absence of a strong cold pool, having only weak updrafts in the humid, low energy environment (van der Velde et al 2014). In any case, the stratiform region of these thunderstorms may grow large enough to allow the necessary charge moment change to trigger a sprite. Regarding the SIUL episode, the 16th November 2013, the storm system area is significantly larger than the rest of episodes.

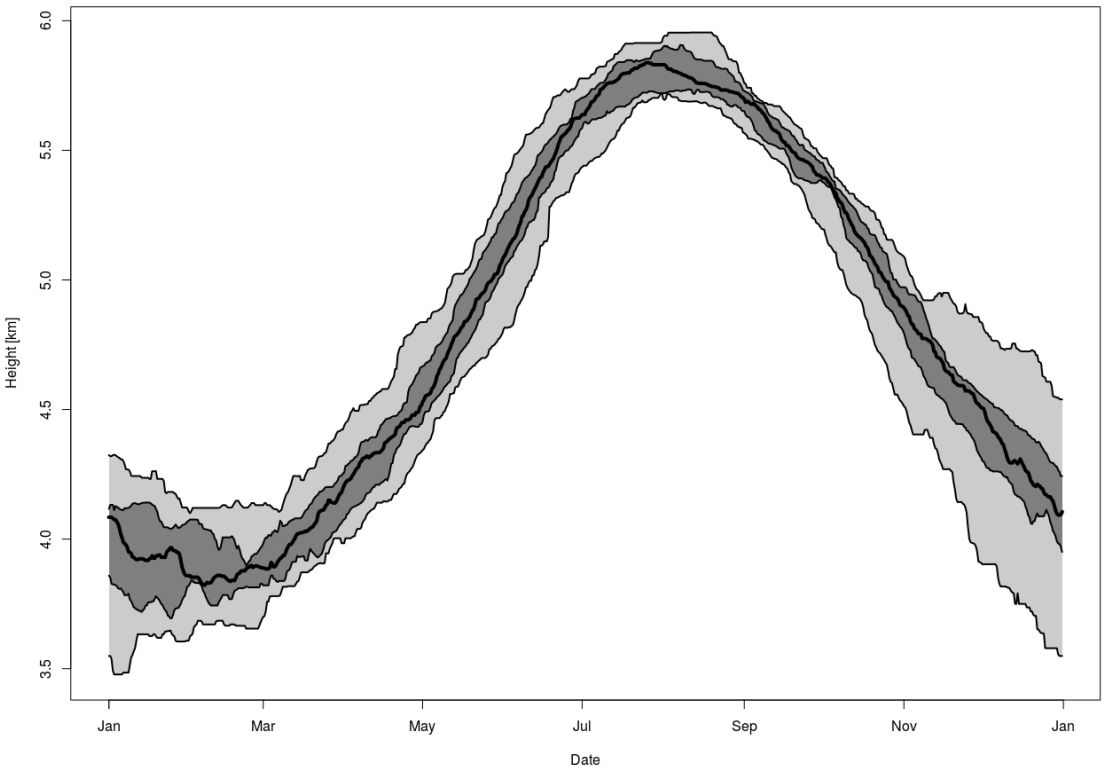

Fig. 14 Annual evolution of the −10°C isotherm height over a 10-year period (2006–2015). Median (bold line), area between percent 25 and 75 (dark grey) and area between min and max (light grey) AMGL Source: Barcelona radiosonde data

4.4. Peak current and polarity

CG peak current and polarity reported on Table 1 corresponding to the CGs to WT show that almost all downward strokes had negative polarity (only one positive case), with rather high peak currents. According to the SMC-LLS records, the average (and median) for Catalonia over the last 7 years (2010–2016) for negative CG strokes is of −18.2 kA (−12.9 kA). In the present study, fifteen of the twenty-two negative downwards to WT had peak currents above the average, and furthermore, in 8 cases the peak current is extremely high (above the 95 percentile, −48 kA). These figures suggest that the peak current plays a role on the attachment process to WT. The distance between the tips of the negative downward leaders and the grounded structure (striking distance, Golde 1945), can be estimated using expressions that relate this distance and the peak current (Love 1973, Cooray et al.

2007) The striking distance increases with increasing peak current (Love 1973, Wang et al. 2013, Tran and Rakov 2015, Visacro et al. 2016), thus favouring the attachment to salient objects like WT.

4.5. Self-initiated and Lightning-triggered upwards

As stated in the introduction, upward lightning (UL) may originate from WT due to locally strong electric fields (self-initiated upward lightning, SIUL) or may be triggered by prior lightning discharges (lightning-triggered upward lightning, LTUL). In our case study, all SIUL cases were reported during a single episode, the 16th November 2013. Complementary data from LMA and LINET allows to confirm the absence of a pre-existing lightning (IC or CG) in the vicinity that may have triggered those upwards. Vertical trails of the SIUL flashes detected on that day (Fig. 10) are similar to LMA observations reported by Schultz et al (2011) during a thundersnow. In both cases, upward flashes start with a series of very low altitude pulses, followed by a upward negative leader that reaches the upper positive layer. This sequence may be repeated in time, starting from other turbines of the wind farm. The 16th November 2013 episode has very low cloud bases, low freezing levels and a considerable stratiform region (more than 30,000 km^2, 2 to 7 times more than the "downward" cases). Under these conditions, the electric field above the WT may become large enough to initiate breakdown, and an upward leader may initiate even without additional transient enhancement from a nearby CG or IC lightning discharge. According to Yuan et al. (2017), the relatively low lightning frequency may have facilitated the efficient charge accumulation in the stratiform cloud, favouring the upward leader inception.

On the other hand, Warner et al. 2014 pointed out that strong ambient winds may not be essential for the triggering as SIULs could originate from rotating turbine blade tips at almost any ambient wind velocity. Wang and Takagi (2012) also noted that self-initiation occurred with higher observed wind speeds (or a rotating windmill) compared with other-triggered upward flashes. The underlying reason would be the wind removal of the screening layer present near the tip of the tower that acts as an inhibitor of the upward leader initiation. Unfortunately, for our case studies we do not have wind records from the windfarms to analyse the possible influence of the wind speed.

In Wang and Takagi (2012), LTUL flashes occurred during taller and more active storms, whereas the majority of SIUL took place when there was not significant lightning activity. In our cases studies, Fig.13 shows a thinner and lower charge structure for the SIUL triggering episode, as well as intermediate conditions for the downward/LTUL episodes, compared to the higher typical summer charge structure. On the other hand, LFR in the AoS were similar in both SIUL and LTUL episodes, the difference being the distance between the embedded convective cores

and the wind farms. Downward strokes and LTUL from WT emanate from the vicinity of convective cores, whereas on the 16 November SIUL occurred far from the embedded cores of the precipitation system (50 km approx.).

4.6. Risk assessment

Since the availability of simultaneous observations of weather radar and LLS became available for the analysis of life-cycle of the thunderstorms, different studies have attempted to establish links between radar reflectivity, environmental temperature profiles and lightning. Lang and Rutledge (2011), summarizing on earlier studies, state that the general scope is that the existence of a 40 dBZ echo at or above the altitude of –10°C corresponds to a very high probability of lightning. The present analysis has shown that, as a general rule, LMA detections are limited to periods when the TOP–12 lies above the –10°C height. Moreover, VHF source's density showed a close relation with the height of the TOP–35. Surges in the number of sources detected by the LMA are usually observed shortly after the TOP–35 overtakes the –10°C height, and larger densities are collocated in time with greater heights of the TOP–35, which can reach the –40°C in the summer cases. In a similar way, lightning activity decreases as the TOP–35 losses height and ceases as the TOP–12 decays below the –10°C height. These conditions have been observed in all case studies, and therefore results suggest that they apply throughout the year. This pattern can be of utility in lightning hazard warning systems devoted to wind farms, considering that damage to WT is not solely linked to deep convection or severe weather conditions but also to low-intensity thunderstorms outside the main thunderstorm season.

On the other hand, whereas empirical formulas have been developed to estimate the number of downward flashes to a tall object, the majority of the strokes to modern turbines are expected to be UL. In this regard, it is worth recalling that upward leaders not followed by return strokes can go unnoticed by conventional LLS, and therefore the number of UL is being underestimated (e.g., March 2017). As Rachidi et al. (2008) pointed out, neglecting upward flashes, as done in practice nowadays, might result in an important underestimation of the actual number of strokes to WT. The present results provide evidence supporting this statement, as lightning that may pose a threat to wind turbines is linked to "out of season" low-intensity thunderstorms, which are not a significant contribution to the lightning climatology of the region, in terms of the amount of lightning and therefore the region's average flash density, which is the main lightning parameter used in risk assessment.

5. CONCLUDING REMARKS

The meteorological conditions and thunderstorm characteristics favouring lightning to wind turbines have been analysed in a series of episodes, by means of Lightning Mapping Array and weather radar data. The main takeaways of this study are summarized hereunder.

- As a general rule, lightning activity can be expected in cells where the radar TOP–12 product (height of the echo-tops >12 dBZ) is above the –10°C height. Besides, the TOP–35 reaching the –40°C is indicative of deep convection and large lightning intensities will follow. This rule of thumb applies throughout the year and may be useful to identify thundery conditions that can pose a threat to wind turbines outside the main thunderstorm season

- Lightning threats to wind turbines in the area of study do not occur during the main thunderstorm season, but during transitional periods (spring and autumn). Lightning activity in the area of study concentrates between June and October (85% of the year-round CGs) and especially during August and September (57% of CGs). However, all the analysed episodes with lightning from/to wind turbines occurred between November and April, months that account only for nine percent of the year-round lightning activity.

- Thunderstorms with downward lightning to wind turbines present a regular charge layer structure (tripole), but with particular features. The dominant charge layer is the lower positive one, which is, in turn, closer to the ground due to the environmental temperature. Besides, the reported downward CGs striking WT were mainly of negative polarity and with peak currents above the average.

- Conditions for self-initiated upward lightning from wind turbines were different, with a considerable stratiform region with a low cloud base, bearing a two-layer charge structure with positive over negative charge. Such characteristics are similar to those reported for upward lightning in winter thunderstorms in Japan and the US

- Although the thunderstorms involved in lightning incidence on wind turbines had no particular precipitation structure, downwards to wind turbines are related to convective cores embedded in a dominant stratiform region. This stratiform field may grow large enough to allow the necessary charge moment change to trigger upwards from the wind turbines.

- The particular conditions that lead to lightning strokes to wind turbines shall be taken into account in the lightning protection standards, which

currently seem to be underestimating the actual number of strokes to wind turbines.

6. ACKNOWLEDGEMENTS

The authors are grateful to the Meteorological Service of Catalonia for providing radar, lightning and radiosonde data. We thank Patricia Altube and the two anonymous reviewers for their comments, that led to further refinement of this study. This work was supported by research grants from the Spanish Ministry of Economy and Competitiveness (MINECO) and the European Regional Development Fund (FEDER): (MINECO) AYA2011-29936-C05-04; (MINECO/FEDER) ESP2013-48032-C5-3-R and (MINECO/FEDER) ESP2015-69909-C5-5-R; as well as by Fulgura S.L., the Meteorological Service of Catalonia and the Autonomous Government of Catalonia, under the framework of the Industrial Doctorate Programme.

7. REFERENCES

Abellán, E., Aran, M., Codina, B., Cunillera, J., 2011. Complex quality control of Barcelona radiosounding database. 6th European Conference on Severe Storms (ECSS) 2011, Palma de Mallorca, Spain.

Akita, M., Yoshida, S., Nakamura, Y., Morimoto, T., Ushio, T., Kawasaki, Z., Wang, D., 2011. Effects of charge distribution in thunderstorms on lightning propagation paths in Darwin, Australia. J. Atmos. Sci., 68, 719–726, doi.org/10.1175/2010JAS3597.1

Altaratz, O., Levin, Z., Yair, Y., 1999. Electrical and radar observation of thunderstorms in the eastern Mediterranean. Preprints, 11th Int. Conf. on Atmospheric Electricity, Guntersville, AL, ICAE, 468–471.

Altaratz, O., Levin, Z., Yair, Y., 2001. Winter Thunderstorms in Israel: A Study with Lightning Location Systems and Weather Radar. Mon. Weather Rev., 129, 1259–1266.

Argemí, O., Altube, P., Rigo, T., Ortiga, X., Pineda, N., Bech, J., 2014. Towards the improvement of monitoring and data quality assessment in the weather radar network of the Meteorological Service of Catalonia, 8th European Conference on Radar in Meteorology and Hydrology (ERAD), Garmisch-Partenkirchen, Germany, Sept. 2014

Bech, J., Vilaclara, E., Pineda, N., Rigo, T., López, J., O'Hora, F., Lorente, J., Sempere, D., Fàbregas, F.X., 2004. The weather radar network of the Catalan Meteorological Service: description and applications. Proceedings of the 3rd European Conference on Radar (ERAD 2004), Copernicus GmbH.

Berger, K., 1967. Novel observations on lightning discharges: Results of research on Mount San Salvatore, J. Franklin Inst., 283, 478–525, doi:10.1016/0016-0032(67)90598-4.

Betz, H.D., Schmidt, K., Oettinger, P., Wirz, M., 2004. Lightning detection with 3-D discrimination of intracloud and cloud-to-ground discharges. Geophys. Res. Lett., 31, L11108, doi:10.1029/2004GL019821.

Betz, H.D., Schmidt, K., Laroche, P., Blanchet, P., Oettinger, W.P., Defer, E., Dziewit, Z, Konarski, J., 2009a. Linet—An international lightning detection network in Europe. Atmos. Res., 91: 564 – 573. doi: https://doi.org/10.1016/j.atmosres.2008.06.012

Betz, H.D., Schmidt, K, Oettinger, W.P. 2009b. LINET: An international VLF/LF lightning detection network in Europe. Springer, 2009b. In: Betz, H.-D., Schumann, U., Laroche, P. (Eds.), Lightning: Principles, Instruments and Applications. Springer, Netherlands, pp. 115–140.

Braam, H., Rademakers, L.W.M.M., Wessels, H.R.A., Prins, R.K.N.J., Lok., R., Leunis, L., Ramakers, S.G.M., 2002. Lightning damage of OWECS Part 3: Case studies, published by ECN (www.ecn.nl), Netherlands

Buechler, D.E., Goodman, S.J., 1990. Echo Size and Asymmetry: Impact on NEXRAD Storm Identification. J. Appl. Meteor., 29, 962–969

Candela, A., Madsen, S.F., Nissim, M., Myers, J.D., Holboell, J., 2016. Lightning Damage to Wind Turbine Blades From Wind Farms in the U.S. IEEE Trans. Power Del., 31(3): 1043

Carey, L.D., Petersen, W.A.; Rutledge, S.A., 2003. Evolution of cloud-to-ground lightning and storm structure in the Spencer, South Dakota, Tornadic Supercell of 30 May 1998. Mon. Weather Rev. 131, 1811–1831.

Chan, M.-K., Chen, M., Du, Y-P., 2018. A macroscopic physical model for self-initiated upward leaders from tall grounded objects and its application. Atmos. Res., 200, 13–24.

Cummins, K.L., Murphy, M.J., 2009. An overview of lightning locating systems: history, techniques, and data uses, with an in-depth look at the U.S. NLDN. IEEE Trans. Electromagn. Compat. 51 (3), 499–518.

Clarence, N.D., Malan, D.J., 1957. Preliminary discharge processes in lightning flashes to ground, Q. J. R. Meteorol. Soc., 83, 161–172.

Cooray, V., Rakov, V., Theethayi, N., 2007. The lightning striking distance—Revisited. J. Electrostat. 65(5–6), 296–306. doi.org/10.1016/j.elstat.2006.09.008

Diendorfer, G., Pichler, H., Mair, M., 2009. Some parameters of negative upward-initiated lightning to the Gaisberg Tower (2000–2007). IEEE Trans. Electromagn. Compat. 51, 443–452.

Diendorfer, G., Pichler, H., Schulz, W., 2014. EUCLID Located Strokes to the Gaisberg Tower – Accuracy of Location and its assigned Confidence Ellipse. In: Int. Lightning Detection Conf. and Int. Lightning Meteorology Conf. (ILDC/ILMC), Tucson, 2014.

Diendorfer, G. 2017. Review of seasonal variations in occurrence and some current parameters of lightning measured at the Gaisberg Tower. 4th Int. Symposium on Winter Lightning (ISWL 2017), Joetsu, Japan.

Duda, J.D., Gallus, W.A., 2010. Spring and Summer Midwestern Severe Weather Reports in Supercells Compared to Other Morphologies. Wea. Forecasting, 25, 190–206.

Dye, J.E., Jones, J.J., Winn, W.P., Cerni, T.A., Gardiner, B., Lamb, D., Pitter, R.L., Hallett, J., Saunders, C.P.R., 1986. Early electrification and precipitation development in a small, isolated Montana cumulonimbus. J. Geophys. Res. 91, 1231–1247.

Eriksson, A. J., 1978. Lightning and tall structures, Trans. S. Afr. Inst. Electr. Eng., vol. 69, pp. 238–252.

Foley, A.M., Leahy, P.G., Marvuglia, A., McKeogh, E.J., 2012. Current Methods and Advances in Forecasting of Wind Power Generation. Renewable Energy, 37, 1-8.

Galanaki, E., Lagouvardos, K., Kotroni, V., Flaounas, E., Argiriou, A., 2018. Thunderstorm climatology in the Mediterranean using cloud-to-ground lightning observations, Atmos. Res., 207: 136-144

Golde, R. H., 1945. The frequency of occurrence and the distribution of lightning flashes to transmission lines. Electrical Engineering, 64(12): 902–910. doi.org/10.1109/EE.1945.6441405

Gremillion, M, Orville, R, 1999. Thunderstorm Characteristics of Cloud-to-Ground Lightning at the Kennedy Space Center, Florida: A Study of Lightning Initiation Signatures as Indicated by the WSR-88D. Amer. Meteor. Soc., 14, 640-649.

Hondl, K., Eilts, M., 1994. Doppler radar signatures of developing thunderstorms and their potential to indicate the onset of cloud-to-ground lightning. Mon. Weather Rev., 122, 1818-1836.

Honjo, N., 2015. Risk and its reduction measure for wind turbine against the winter lightning, in Proc. Asia-Pacific Intl. Conf. on Lightning, 2015, pp. 665-670.

IEC 61400-24, Wind Turbines – Part 24: Lightning Protection, 2010.

Jacobson, E.A., Krider, E.P., 1976. Electrostatic field Changes produced by Florida lightning, J. Atmos. Sci., 33, 103-117

Kotroni, V., Lagouvardos, K., 2016. Lightning in the Mediterranean and its relation with sea-surface temperature. Environ. Res. Lett. 11, 034006. http://dx.doi.org/10.1002/asl.685.

Krehbiel, P. R., 1986: The electrical structure of thunderstorms. In: The Earth's Electrical Environment, National Academies Press, 90–113.

Krehbiel, P.R., Brook, M., Khanna-Gupta, S., Lennon, C. L., Lhermitte, R., 1984. Some results concerning VHF lightning radiation from the real-time LDAR system at KSC, Florida. Proc. 7th Int. Conf. on Atmospheric Electricity, Boston, MA, Amer. Meteor. Soc., 388–393

Lang, T.J. Rutledge, S.A., 2011. A Framework for the Statistical Analysis of Large Radar and Lightning Datasets: Results from STEPS 2000. Mon. Weather. Rev., 139, 2536–2551

Lang, T.J., Lyons, W.A., Rutledge, S.A., Meyer, J.D., MacGorman, D.R., Cummer, S.A., 2010. Transient luminous events above two mesoscale convective systems: Storm structure and evolution, J. Geophys. Res., 115, A00E22, doi:10.1029/2009JA014500.

Lang, T.J., Li, J., Lyons, W.A., Cummer, S.A., Rutledge, S.A., MacGorman, D. R., 2011. Transient luminous events above two mesoscale convective systems: Charge moment change analysis, J. Geophys. Res., 116, A10306, doi:10.1029/2011JA016758.

Larsen, H.R., Stansbury, E.J., 1974. Association of lightning flashes with precipitation cores extending to height 7 km. J. Atmos. Terr. Phys. 36, 1547–1553.

Levin, Z., Yair, Y., Ziv, B., 1996: Positive cloud-to-ground flashes and wind shear in Tel-Aviv thunderstorms. Geophys. Res. Lett., 23, 2231–2234.

Love, E.R., 1973. Improvements on lightning stroke modeling and applications to the design of EHV and UHV transmission lines, University of Colorado.

Lund, N., and Coauthors, 2007. Relationship between lightning location and polarimetric radar signatures in an MCS. Proc. 13th Int. Conf. on Atmospheric Electricity, Beijing, China, ICAE, 557–560.

Lu, G., et al., 2013. Coordinated observations of sprites and in-cloud lightning flash structure, J. Geophys. Res. Atmos., 118, 6607–6632, doi:10.1002/jgrd.50459

Lyons, W.A., 1996. Sprite observations above the U.S. High Plains in relation to their parent thunderstorm systems, J. Geophys. Res., 101, 29,641–29,652, doi:10.1029/96JD01866.

Lyons, W.A., Williams, E. R., Cummer, S. A., Stanley, M. A., 2003. Characteristics of sprite-producing positive cloud-to-ground lightning during the 19 July 2000 STEPS mesoscale convective systems, Mon. Weather Rev., 131, 2417–2427.

Lyons, W.A., Cummer, S.A., Rutledge, S.A., Lang, T.J., Meyer, T., Warner, T.A., Samaras, T.A., 2011. TLEs and their parent lightning discharges, paper presented at 14th International Conference on Atmospheric Electricity (ICAE), Rio De Janeiro, Brazil, 7–12 Aug.

Lyons, W.A., et al., 2014. Meteorological Aspects of Two Modes of Lightning-Triggered Upward Lightning (LTUL) Events in Sprite-Producing MCS, 23rd Int. Lightning Detection Conf., 18-19 March 2014, Tucson, Arizona.

MacGorman, D.R., Rust, W.D.,1998. The Electrical Nature of Storms, 422 pp., Oxford Univ. Press, Oxford.

Manhardt, M., Heidler, F., Stimper, K., 2012. The electric field of negative upward lightning strikes at the Peissenberg tower, Germany. Int. Conf. on Lightning Protection (ICLP), 2012, IEEE, pp.1–9. 10.1109/ICLP.2012.6344205.

March, V., 2017. Key issues to define a method of lightning risk assessment for wind farms, Electr. Power Syst. Res., doi: 10.1016/j.epsr.2017.08.020

Marshall, T.C., Stolzenburg, M., 2002. Electrical energy constraints on lightning. J. Geophys. Res. 107 (D7). doi:10.1029/2000JD000024.

Matsudo, Y., Suzuki, T., Hayakawa, M., Yamashita, K., Ando, Y., Michimoto, K., Korepanov, V., 2007. Characteristics of Japanese winter sprites and their parents' lightning as estimated by VHF lightning and ELF transients, J. Atmos. Sol. Terr. Phys., 59, 1431–1446

Mazur, V., 2002. Physical processes during development of lightning flashes, C. R. Phys., 3, 1393–1409.

Mazur, V., Shao, X., Krehbiel, P.R., 1998. "Spider" lightning in intra-cloud and positive cloud-to-ground flashes, J. Geophys. Res., 103, 19,811–19,822, doi: 10.1029/98JD02003.

McEachron, K. B., 1939. Lightning to the Empire State Building, J. Franklin Inst., 227, 149–217, doi:10.1016/S0016-0032(39)90397-2.

Michimoto, K., 1991: A study of radar echoes and their relation to lightning discharge of thunderclouds in the Hokuriku district, Part 1: Observation and analysis of thunderclouds in summer and winter. J. Meteor. Soc. Japan, 69, 327–335.

Michimoto, K., 1993. A study of radar echoes and their relation to lightning discharge of thunderclouds in the Hokuriku district, Part 2: Observation and analysis of ''single flash'' thunderclouds in midwinter. J. Meteor. Soc. Japan, 71, 195–203.

Minowa, M, Minami, M, Yoda, M., 2006. Research into Lightning Damages and Protection Systems for Wind Power Plants in Japan. Proceedings of the 28th International Conference on Lightning Protection, Kanazawa, 2006; 1539–1544.

Montanyà, J., Pineda, N., March, V., Illa, A., Romero, D., Solà, G., 2006. Experimental evaluation of the Catalan Lightning Detection Network. 19th Int. Lightning Detection Conf., Tucson, Arizona.

Montanyà, J., Soula, S., Diendorfer, G., Solà, G., Romero, D., 2007. Analysis of altitude of isotherms and the electrical charge for flashes that struck the Gaisberg Tower. 13th International Conference on Atmospheric Electricity (ICAE), August 13-17 2007, Beijing, China.

Montanyà, J., van der Velde, O.A., March, V., Romero, D., Solà, G., Pineda, N., 2012. High-speed video of lightning and x-ray pulses during the 2009–2010 observation campaigns in north-eastern Spain. Atmos. Res. 117, 91–98.

Montanyà, J., 2014. Annual Report on the Performance of the Lightning Location System Operated by the Meteorological Service of Catalonia, Internal Technical Report, not Published.

Montanyà, J., van der Velde, O., Williams, E. R., 2014. Lightning discharges produced by wind turbines. J. Geophys. Res. Atmos., 119, 1455–1462, doi:10.1002/ 2013JD020225.

Montanyà, J., Fabró, F., van der Velde, O., March, V., Williams, E.R., Pineda, N., Romero, D., Solà, G., Freijo, M., 2016a. Global distribution of winter lightning: a threat to wind turbines and aircraft. Nat. Hazards Earth Syst. Sci., 16, 1465-1472

Montanyà, J., van der Velde, O., Domingo-Dalmau, A., Pineda, N., Argemí, O., Salvador, A., 2016b. Lightning mapping observations of downward lightning flashes to wind turbines. 33rd Int. Conf. Lightning Protection, Estoril, Portugal, 25-30 September 2016.

Murphy, M.J., Krider, E.P., Maier, M.W., 1996. Lightning charge analyses in small Convection and Precipitation Electrification (CaPE) experiment storms, J. Geophys. Res., 101(D23), 29615–29626, doi:10.1029/96JD01538.

Nag, A., Rakov V.A, 2009. Some inferences on the role of lower positive charge region in facilitating different types of lightning, Geophys. Res. Lett., 36, L05815, doi:10.1029/2008GL036783.

Nag, A., Murphy, M. J., Schulz, W., Cummins, K.L., 2015. Lightning locating systems: Insights on characteristics and validation techniques, Earth and Space Science, 2, 65–93, doi:10.1002/ 2014EA000051.

Neubert, T., Kuvvetli, I., Budtz-Jørgensen, C., Østgaard, N., Reglero, V. Arnold, N., 2006. The atmosphere-space interactions monitor (ASIM) for the international space station. ILWS Workshop 2006, GOA, February 19-24, 2006

Parker, M.D., Johnson, R.H., 2000. Organizational modes of mid-latitude mesoscale convective systems. Mon. Weather Rev.,128, 3413–3436

Pawar, S.D., Kamra, A.K., 2004. Evolution of lightning and the possible initiation/triggering of lightning discharges by the lower positive charge center in an isolated thundercloud in the tropics, J. Geophys. Res., 109, D02205, doi:10.1029/2003JD003735.

Pierce, E.T., 1971. Triggered Lightning and Some Unsuspected Lightning Hazards. Stanford Research Institute, Menlo Park, CA, 1971, pp. 20.

Pineda, N., Montanyà, J., 2009. Lightning detection in Spain: the particular case of Catalonia. In: Betz, H.-D., Schumann, U., Laroche, P. (Eds.), Lightning: Principles, Instruments and Applications. Springer, Netherlands, pp. 161–185.

Pineda, N., Soler, X., Vilaclara, E., 2011. Approximation to the Lightning Climatology in Catalonia. Technical Note nº 73. Meteorological Service of Catalonia: 71 p. Generalitat de Catalunya B-7024-2011 (in Catalan)

Poelman, D.R., Schulz, W., Diendorfer, G., Bernardi, M., 2016. The European lightning location system EUCLID – Part 2: Observations. Nat. Hazards Earth Syst. Sci., 16, 607–616, 2016. doi:10.5194/nhess-16-607-2016

Qie, X., Zhang, T., Chen, C., Zhang, G., Zhang, T., Wei, W., 2005. The lower positive charge center and its effect on lightning discharges on the Tibetan Plateau, Geophys. Res. Lett., 32, L05814, doi:10.1029/2004GL022162

Rachidi, F., Rubinstein, M., Montanyà, J., Bermudez, J.L., Rodriguez, R., Solà, G., Korovkin, N., 2008. A review of current issues in lightning protection of new generation wind turbine blades, IEEE Trans. Ind. Electron., vol. 55, no. 6, pp. 2489–2496, doi:10.1109/TIE.2007.896443.

Radicevic, R.M., Savic, M.S., Madsen S.F., Badea I., 2012. Impact of wind turbine blade rotation on the lightning strike incidence—A theoretical and experimental study using a reduced-size model, Energy, 45, 644–654.

Reynolds, S.E., Brook, M., 1956. Correlation of the initial electric field and the radar echo in thunderstorms. J. Meteor. , 13, 376-380.

Rizk, F.A.M. 1990. Modeling of transmission line exposure to direct lightning strokes, IEEE Trans. Power Del. 5 (4): 1983-1997

Rizk, F.A.M., 1994. Modelling of lightning incidence to tall structures, part I & II. IEEE Trans. Power Del. 9 (1): 162-193

Rison, W., Thomas, R.J., Krehbiel, P.R., Hamlin, T., Harlin J., 1999. A GPS-based three-dimensional lightning mapping system: Initial observations in central New Mexico, J. Geophys. Res., 26, 3573-3576.

Rivas Soriano, L. de Pablo F., Tomas, C., 2005. Ten-year study of cloud-to-ground lightning activity in the Iberian Peninsula. J. Atmos. Terr. Phys. 67: 1632–1639

Rakov, V.A., Uman, M.A., 2003. Lightning: Physics and Effects, Cambridge University Press, Cambridge.

Romero, C., Rachidi, F., Paolone, M., Rubinstein. M., 2013. Statistical Distributions of Lightning Currents Associated With Upward Negative Flashes Based on the Data Collected at the Säntis (EMC) Tower in 2010 and 2011. IEEE Trans. Power Del., 28(3)

Saunders, C.P.R., Bax-Norman, H., Emersic, C., Avila, E.E., Castellano, N.E., 2006. Laboratory studies of the effect of cloud conditions on graupel/ crystal charge transfer in thunderstorm electrification. Q. J. Roy. Met. Soc. 132, 2653–2673.

Schultz, C.J., Bruning, E.C., Carey, L.D., Petersen, W.A., Heckman, S., 2011. Total lightning within electrified snowfall using LMA, NLDN, and WTLN measurements. Eos. Trans. AGU, Fall Meet. Suppl.

Shao, X., Krehbiel, P., 1996. The spatial and temporal development of intracloud lightning, J. Geophys. Res., 101, 26,641–26,668, doi:10.1029/ 96JD01803

Shindo, T., Sekioka, S., Ishi, M., Shiraishi, H., Natsuno, D., 2012. Studies of lightning protection design for wind power generation systems in Japan, CIGRE 2012, C4 306.

Smorgonskiy, A., Tajalli, A., Rachidi, F., Rubinstein, M., Diendorfer, G., Pichler, H., 2015. An analysis of the initiation of upward flashes from tall towers with particular reference to Gaisberg and Säntis Towers, J. Atmos. Terr. Phys. 136(A): 46-51

Stackpole, J.D., 1967. Numerical analysis of atmospheric soundings. J. Appl. Meteor., 6, 464–467.

Suzuki, T., Hayakawa, M., Matsudo, Y., Michimoto, K. 2006, How do winter thundercloud systems generate sprite-inducing lightning in the Hokuriku area of Japan?, Geophys. Res. Lett., 33, L10806, doi:10.1029/2005GL025433.

Takahashi, T., 1978: Riming electrification as a charge generation mechanism in thunderstorms. J. Atmos. Sci., 35, 1536-1548.

Takahashi, Y., Miyasato, R., Adachi, T., Adachi, K., Sera, M., Uchida, U., Fukunishi, H., 2003. Activities of sprites and elves in the winter season, Japan, J. Atmos. Sol. Terr. Phys., 65: 551–560.

Thomas, R., Krehbiel, P.R., Rison, W., Hunyady, S.J., Winn, W.P., Hamlin, T., Harlin, J., 2004. Accuracy of the lightning mapping array. J. Geophys. Res. 109, D14207. doi:10.1029/2004JD004549

Tomine, K., Michimoto, K., Abe, S., 1986. Studies on thunderstorm in winter in the area surrounding Komatsu by radar (in Japanese). Tenki, 33, 445–452.

Tran, M.D., Rakov, V.A., 2015. When does the lightning attachment process actually begin? Journal of Geophysical Research: Atmospheres, 120, 6922–6936. doi.org/10.1002/2015JD023155

van der Velde, O.A., Montanyà, J., Romero, D., Pineda, N., Rico, R., Fabró, F., Solà, G., March, V., Soula, S., 2011. Results of the 2010-2011 lightning measurement campaigns in Spain, 6th European Conf. on Severe Storms, Palma de Mallorca, Spain, 3-7 October 2011

van der Velde, O.A., Montanyà, J., 2013. Asymmetries in bidirectional leader development of lightning flashes, J. Geophys. Res. Atmos., 118, doi:10.1002/2013JD020257.

van der Velde, O.A., J. Montanyà, S. Soula, N. Pineda, and J. Mlynarczyk, 2014. Bidirectional leader development in sprite-producing positive cloud-to-ground flashes: Origins and characteristics of positive and negative leaders, J. Geophys. Res. Atmos., 119, 12,755–12,779, doi:10.1002/2013JD021291.

Vincent, B.R, Carey L.D., Schneider, D., Keeter, K., Gonski, R., 2003. Using WSR-88D reflectivity data for the prediction of cloud-to-ground lightning: A North Carolina study. Nat. Wea. Digest, 27, 35-44.

Visacro, S., Guimaraes, M., Murta Vale, M.H., 2017. Striking distance determined from high-speed videos and measured currents in negative cloud-to-ground lightning. J. Geophys. Res. Atmos., 122, 13,356–13,369. doi.org/10.1002/2017JD027354

Wallace, J.M., Hobbs, P.V., 1973. Atmospheric Science, An Introductory Survey, International Geophysics, vol. 92, 2nd ed., 504 pp., Academic Press, New York.

Wang, D., Takagi, N., Watanabe, T., Sakurano, H., Hashimoto M., 2008. Observed characteristics of upward leaders that are initiated from a windmill and its lightning protection tower. Geophys. Res. Lett., 35, L02803, doi:10.1029/2007GL032136

Wang, D., Takagi, N., 2012. Characteristics of winter lightning that occurred on a windmill and its lightning protection tower in Japan, IEEJ Trans. Power Energy, 132(6), 568–572, doi:10.1541/ieejpes.132.568.

Wang, D., Takagi, N., Gamerota, W.R., Uman, M.A., Hill, J.D., Jordan, D.M., 2013. Initiation processes of return strokes in rocket-triggered lightning. Journal of Geophysical Research: Atmospheres, 118, 9880–9888. doi.org/10.1002/jgrd.50766

Wang, D., Wu, T., Takagi, N., 2017a. Charge structure of winter thunderstorm in Japan: a review and an update, 4th International Symposium on Winter Lightning, Japan, April 2017.

Wang, C., Zheng, D., Zhang, Y., Liu, L., 2017b. Relationship between lightning activity and vertical airflow characteristics in thunderstorms, Atmos. Res., 191, 2017, 12-19

Warner, T.A., Cummer, S.A., Lyons, W.A., Lang, T.J., Orville, R.E., 2011. Coordinated video and RF measurements of positive CGs inducing both sprites and upward tower discharges, paper presented at 5th Conference on Meteorological Applications of Lightning Data, Am. Meteor. Soc., Seattle, Wash.

Warner, T.A., Cummins, K.L., Orville, R.E., 2012a. Upward lightning observations from towers in Rapid City, South Dakota and comparison with National Lightning Detection Network data, 2004–2010, J. Geophys. Res., 117, D19109, doi:10.1029/2012JD018346.

Warner, T.A., Helsdon Jr., J.H. Bunkers, M.J., Saba, M.F., Orville, R.E., 2012b. UPLIGHTS: Upward lightning triggering study. Bull. Am. Meteorol. Soc., 94, 631 –635, doi:10.1175/BAMS-D-11-00252.1.

Williams, E.R., 1989. The tripole structure of thunderstorms. J. Geophys. Res. 94 (D11): 13,151–13,167.

Williams, E.R., 2001. The electrification of severe storms. Severe convective storms, meteor. Monogr., no. 50. Am. Meteorol. Soc. 527–561.

Williams, E.R., Zhang, R., Rydock, J., 1991. Mixed-Phase Microphysics and Cloud Electrification. J. Atmos. Sci., 48, 2195–2203

Williams, E.R., 2018. Lightning Activity in Winter Storms: A Meteorological and Cloud Microphysical Perspective. IEEJ Transactions on Power and Energy 138 (5): 364-373 doi:10.1541/ieejpes.138.364

Workman, E.J., Reynolds, S.E., 1949: Electrical activity as related to thunderstorm cell growth. Bull. Amer.Meteor. Soc., 30,142-149.

Yair, Y., Levin, Z., Altaratz, O., 1998. Lightning phenomenology in the Tel Aviv area from 1989 to 1996. J. Geophys. Res., 103, 9015–9025.

Yasuda, Y., Yokoyama, S., Minowa, M., Satoh, T., 2012. Classification of Lightning Damage to Wind Turbine Blades IEEJ Transactions on Electrical and Electronic Engineering: 559–566, doi:10.1002/tee.21773

Yeung, L.H.Y., Lai, E.S.T., Chiu, S.K.S., 2007. Lightning Initiation and Intensity Nowcasting Based on Isothermal Radar Reflectivity - A Conceptual Model. In: 33rd Int. Conf. on Radar Meteorology, Cairns, Australia, 6-10 August 2007

Yokoyama, S., 2013. Lightning protection of wind turbine blades. Electric Power Systems Research 94 (2013) 3– 9

Yuan, S., Jiang, R., Qie, X., Wang, D., Sun, Z., Liu, M., 2017. Characteristics of upward lightning on the Beijing 325 m meteorology tower and corresponding thunderstorm conditions. Journal of Geophysical Research: Atmospheres, 122. https://doi.org/10.1002/2017JD027198

Zhou, H., Theethayi, N., Diendorfer, G., Thottappillil, R., Rakov, V.A., 2010. On estimation of the effective height of towers on mountaintops in lightning incidence studies, Journal of Electrostatics 68: 415-418

Zhou, H., Diendorfer, G., Thottappillil, R., Pichler, H., Mair, M., 2012a. Measured current and close electric field changes associated with theinitiation of upward lightning from a tall tower, J. Geophys. Res., 117, D08102, doi:10.1029/2011JD017269.

Zhou, H., Diendorfer, G., Thottappillil, R., Pichler, H., Mair, M., 2012b. Characteristics of upward positive lightning flashes initiated from the Gaisberg Tower, J. Geophys. Res., 117, D06110, doi:10.1029/2011JD016903.

4 Conclusiones finales y perspectivas de futuro

4.1 Conclusiones

En el capítulo anterior se han destacado las conclusiones para cada uno de los artículos que conforman esta tesis. Este último capítulo aborda las conclusiones globales del trabajo realizado durante la tesis, así como sus principales aportaciones.

La actividad eléctrica atmosférica ha sido el eje principal de investigación de esta tesis. Pero más allá de las contribuciones que el trabajo realizado aportan al conocimiento del comportamiento del rayo, la vertiente práctica que ambiciona este proyecto de doctorado industrial ha proporcionado parámetros que indiquen la detección del inicio de actividad de rayos, así como la estructura eléctrica de las tormentas que la provoca, para que pueda ser implementada en sistemas de avisos, con el fin de mejorar la prevención y protección frente al rayo.

Con el objetivo principal de identificar las condiciones meteorológicas que favorecen la presencia de actividad de rayos durante todo el año, tanto desde el inicio de las primeras descargas de una nube de tormenta hasta las descargas nube-tierra, el primero de los artículos presenta una propuesta de posibles indicadores que determinen la presencia de actividad eléctrica sin aplicar, hasta el momento, ninguna diferenciación entre las descargas intra-nube y nube-tierra. Para tal fin, se ha realizado una climatología de las alturas de las isotermas de -40°C y -10°C (temperaturas directamente relacionadas con la estructura eléctrica de una tormenta), así como de alturas máximas de reflectividad radar de 12 dBZ y 35 dBZ para poder realizar una evaluación de todas ellas en la zona de estudio y, al mismo tiempo, poder realizar una evaluación de su variación a lo largo del año. Así, se propone el nivel de reflectividad radar de 35 dBZ superando la altura de la isoterma de -10°C como el mejor indicador con mayor probabilidad de detección y menor ratio de falsas alarmas a lo largo de todo el año. Junto con este indicador, se ha calcula una relación entre la intensidad de la actividad eléctrica y la altura de las tormentas para cada una de las estaciones del año, siendo para todas ellas una relación de una quinta potencia, reduciéndose a una tercera para el periodo invernal. Estos factores, junto con la evaluación de la evolución de la altura de la isoterma a lo largo del año, y con un enfoque especial hacia la baja altura de esta en invierno de 1.5-2.0 km, conforman una serie de parámetros útiles para los sistemas de alarma para que tengan en consideración las alturas detectadas de los niveles de reflectividad respecto a las alturas de las isotermas típicas de cada época del año. Esto es así debido a que típicamente las alturas de las tormentas han sido evaluadas por alturas constantes durante todo el año, típicamente referenciadas a las tormentas de verano con más actividad eléctrica, y motivamos a realzar la problemática que en periodos fuera de temporada, con tormentas que alcanzan alturas más bajas, pueden ocurrir situaciones con descargas hacia aerogeneradores que pudieran no haber sido advertidas.

El segundo de los artículos, a partir de la información extraída del primero, se aplica un nuevo filtro al estudio, dando un enfoque a la diferenciación entre las descargas intra-nube y las nube-tierra. Se destacan estas últimas debido al gran impacto humano y económico que supone para múltiples actividades que tienen lugar al aire libre, así como para los daños que suponen para la industria eólica la industria relacionada con los sistemas eléctricos, electrónicos y de telecomunicación en general. Para tal fin, se ha introducido al estudio el sistema de detección de rayos del LMA, que proporciona la localización tridimensional de las señales que conforman el rayo dentro de la nube de tormenta. Con esta información, se infiere la estructura eléctrica de la tormenta a partir de las detecciones de los inicios de cada rayo, y así poder analizar la evolución de la estructura eléctrica a lo largo de la tormenta y como esta influye en el tipo de descargas que son detectadas. Con el propósito de poder extrapolar la información que se extraiga a otras zonas de estudio, se introduce la red de detección de rayos LINET, con una cobertura a lo largo de Europa, para poder implementar la detección y clasificación de las descargas según si son rayos intra-nube o nube-tierra. Así, se presenta una metodología para la detección de la estructura eléctrica de la tormenta y que se categorizan tres estructuras eléctricas frecuentes: la estructura clásica tripolar (TriP), con una región de carga negativa dominante con dos regiones de carga positiva por encima y debajo de esta; la estructura de dipolo inferior (LwDip), diferenciándose de la anterior con una región de carga positiva inferior más dominante que la positiva superior; y una estructura de dipolo superior (UpDip), con la región de carga positiva superior más dominante que la positiva inferior. A partir de estas estructuras tipo, se detecta que las ratios de rayos nube-tierra son más elevados con situaciones de TriP y UpDip, reduciéndose en situaciones de LwDip, donde la región de carga positiva inferior dominante retiene parte de este tipo de descargas. Además, las alturas de las regiones de carga de la positiva superior tienen una dependencia directa con esta ratio, de igual forma que en el artículo anterior la altura de las tormentas influenciaba la intensidad de la actividad eléctrica. Por otro lado, es durante situaciones de LwDip cuando se detectan los rayos nube-tierra con picos de corriente más elevados, tanto positivos como negativos, por lo que se motiva la alerta frente a estas situaciones. Finalmente, se comparan las alturas detectadas de las regiones de carga con otros estudios, cuya concordancia permite la exportación de este estudio a otras zonas de especial interés.

El tercer y último artículo se ocupa de los aerogeneradores respecto a las descargas nube-tierra tanto descendentes como ascendentes. Inicialmente se presenta la problemática que presenta este sector a lo largo de todo el año, típicamente relacionada con los periodos de verano en que se detectan el 85% de descargas nube-tierra en el área de estudio, destacando que todas las descargas con final u origen en los aerogeneradores se han detectado en periodos fuera de temporada, de noviembre a abril, periodo que comprende el 9% de la actividad eléctrica anual. Esta casuística pretende dar énfasis a los episodios que ocurren en periodos que aparentemente no deberían presentar tanta afectación, destacando su peligrosidad y potencialidad de descarga eléctrica. A partir de estas consideraciones, se presentan nuevamente las estructuras que se detectan cuando ocurren este tipo de

descargas en distintos episodios de estudio. Así, se manifiesta la estructura clásica tripolar como la más frecuente en el caso de descargas descendentes, destacando la presencia de una región de carga positiva inferior dominante y cercana a la superficie. Estas descargas detectadas presentan mayormente polaridad negativa y un pico de corriente superior a la media. Por otro lado, la estructura con región de carga positiva superior dominante es la más frecuente en situaciones de descargas ascendentes desde los aerogeneradores. De forma general, se concluye que las tormentas que presentan núcleos convectivos en regiones estratiformes dominantes propician las descargas ascendentes, más propicias cuanto más crecimiento se detecte en el núcleo convectivo y la diferencia de carga entre regiones aumente. A partir de estas conclusiones, se motiva a los distintos interesados a introducir estas características a los respectivos sistemas de alarma, así como a su consideración a ser implementados en los estándares de protección frente al rayo.

4.2 Perspectivas de futuro

La presente tesis aporta nueva información que puede proporcionar una potencial utilidad visto desde distintas perspectivas. Por otro lado, se proponen nuevos enfoques de mejora que se pueden derivar del trabajo realizado, así como de ampliaciones hacia otros objetivos, fomentando la aplicabilidad de la información y características detectadas con los objetivos del doctorado industrial bajo el que se proyecta este trabajo de tesis.

Entre las propuestas de trabajos de futuro se listan las siguientes:

- **Mejora en el sistema de análisis**. Durante los análisis de episodios de estudio se ha trabajado sobre áreas de estudio de interés, pero algunos parámetros no han sido evaluados por tormentas individuales de forma automatizada, requiriendo una intervención para un análisis más detallado. Sistemas de *nowcasting* y traqueo de tormentas como los del SMC podrían intercambiar información con el presente estudio para la mejora de ambas partes, tanto en el seguimiento como la vigilancia.
- **Análisis de otros tipos de tormenta.** Este trabajo de investigación se ha centrado en las tormentas más frecuentes detectadas en la zona de estudio. No obstante, esta tesis presentaba en origen un especial interés en ampliar el estudio a tormentas con sistemas convectivos más complejos, o con estructuras eléctricas que presenten inversión de polaridad, etc., con lo que la ampliación de la investigación sería un factor de gran interés.
- **Ampliación a otros tipos de afectaciones.** La actividad del rayo muestra un elevado riesgo de provocar incidencias para los colectivos mencionados. El análisis de las tormentas con los datos de descargas eléctricas presenta potencialidad para detectar otros fenómenos meteorológicos que presentan tiempo adverso, como puede ser la caída de granizo y situaciones de precipitaciones especialmente intensas, entre otras.
- **Extrapolación de los datos extraídos de este estudio a otras zonas de especial interés, afectación y exposición.** Esta tesis se ha realizado bajo unas

condiciones geográficas y unos datos meteorológicos concretos. Aplicar los resultados y la metodología utilizada a otra área de estudio requeriría una adaptación para incluir las condiciones particulares de la zona y la información meteorológica disponible. Los datos usados por la red de descargas LINET de *nowcast GmbH*, con una amplia cobertura alrededor de Europa y otros lugares del mundo, favorece esta potencialidad.

- **Mejora de los criterios de análisis de estructura eléctrica**. Inferir la estructura eléctrica de una tormenta es una tarea compleja analizando los datos de descargas eléctricas. Múltiples estudios junto a este han presentado propuestas de análisis, pero su clasificación y su aplicabilidad en actuaciones operativas podrían ser mejoradas con la introducción de nuevas mediciones meteorológicas. Este modo podría ser extrapolado para, entre otros objetivos, una detección automática de las fases de las tormentas y el análisis de rayos para cada una de ellas.
- **Implementación y automatización**. Durante el desarrollo de la tesis se ha planteado realizar una herramienta propia y automatizada que integre las características mencionadas. Con los datos actualmente disponibles se podría realizar esta tarea y crear productos derivados.
- **Interés a clientes con especial afectación**. A lo largo de esta tesis se ha ido destacando la potencialidad de estas herramientas para el interés de distintos ámbitos empresariales, como son las industrias tecnológicas, de telecomunicaciones, y con un especial enfoque a la industria eólica. Empresas como Fulgura S.L. podrían desarrollar y mejorar las herramientas aquí presentadas y ofrecerlas a distintos potenciales clientes. Además, se promueve la valoración de este estudio para futuras implementaciones en los estándares de protección contra el rayo.

Bibliografía

Abellán, E., Aran, M., Codina, B., Cunillera, J., 2011. Complex quality control of Barcelona radiosounding database, in: Proceedings of the 6th European Conference on Severe Storms (ECSS), Palma de Mallorca, Spain, 3-7 October 2011.

Adler, R.F., Markus, M.J., Fenn, D.D., 1985. Detection of severe Midwest thunderstorms using geosynchronous satellite data (USA). Mon. Weather Rev. 113, 769–781. https://doi.org/10.1175/1520-0493(1985)113<0769:DOSMTU>2.0.CO;2

Ahrens, D.C., 2008. Essentials of Meteorology - Hurricanes, Essentials of Meteorology: And Invitation to the Atmosphere.

Akita, M., Yoshida, S., Nakamura, Y., Morimoto, T., Ushio, T., Kawasaki, Z., Wang, D., 2011. Effects of charge distribution in thunderstorms on lightning propagation paths in Darwin, Australia. J. Atmos. Sci. 68, 719–726. https://doi.org/10.1175/2010JAS3597.1

Altaratz, O., Levin, Z., Yair, Y., 2001. Winter thunderstorms in Israel: A study with lightning location systems and weather Radar. Mon. Weather Rev. 129, 1259–1266. https://doi.org/10.1175/1520-0493(2001)129<1259:WTIIAS>2.0.CO;2

Altaratz, O., Levin, Z., Yair, Y., 1999. Electrical and radar observation of thunderstorms in the eastern Mediterranean, in: Prepint in 11th International Conference on Atmospheric Electricity (ICAE), Guntersville, AL. pp. 468–471.

Altube, P., 2016. Procedures for improved weather radar data quality control. Ph.D. Thesis.

Altube, P., Bech, J., Argemí, O., Rigo, T., 2015. Quality control of antenna alignment and receiver calibration using the sun: Adaptation to midrange weather radar observations at low elevation angles. J. Atmos. Ocean. Technol. 32, 927–942. https://doi.org/10.1175/jtech-d-14-00116.1

Aran, M., Pineda, N., 2011. Convective instability indexes as thunderstorm predictors for Catalonia, in: Proceedings of the 6th European Conference on Severe Storms (ECSS), Palma de Mallorca, Spain, 3-7 October 2011.

Argemi, O., Altube, P., Rigo, T., Ortiga, X., Pineda, N., Bech, J., 2014. Towards the improvement of monitoring and data quality assessment in the weather radar network of the Meteorological Service of Catalonia (SMC) 8th European Conference on Radar in Meteorology and Hydrology (ERAD). Garmisch-Partenkirchen, Ger.

Bech, J., Vilaclara, E., Pineda, N., Rigo, T., Lorente, J., Sempere, D., 2004. The weather radar network of the Catalan Meteorological Service: description and applications. Proc. ERAD 416–420.

Bedka, K.M., 2011. Overshooting cloud top detections using MSG SEVIRI Infrared brightness temperatures and their relationship to severe weather over Europe. Atmos. Res. 99, 175–189. https://doi.org/10.1016/j.atmosres.2010.10.001

Berger, K., 1967. Novel observations on lightning discharges: Results of research on Mount San Salvatore. J. Franklin Inst. 283, 478–525. https://doi.org/10.1016/0016-0032(67)90598-4

Betz, H.D., Schmidt, K., Laroche, P., Blanchet, P., Oettinger, W.P., Defer, E., Dziewit, Z., Konarski, J., 2009a. LINET-An international lightning detection network in Europe. Atmos. Res. 91, 564–573. https://doi.org/10.1016/j.atmosres.2008.06.012

Betz, H.D., Schmidt, K., Oettinger, P., Wirz, M., 2004. Lightning detection with 3-D discrimination of intracloud and cloud-to-ground discharges. Geophys. Res. Lett. 31. https://doi.org/10.1029/2004GL019821

Betz, Hans D., Schmidt, K., Oettinger, W.P., 2009b. LINET-An international VLF/LF lightning detection network in Europe, in: Betz, Hans Dieter, Schumann, U., Laroche, P. (Eds.), Lightning: Principles, Instruments and Applications: Review of Modern Lightning Research. Springer Netherlands, Dordrecht, pp. 115–140. https://doi.org/10.1007/978-1-4020-9079-0_5

Biggerstaff, M.I., Zounes, Z., Addison Alford, A., Carrie, G.D., Pilkey, J.T., Uman, M.A., Jordan, D.M., 2017. Flash propagation and inferred charge structure relative to radar-observed ice alignment signatures in a small Florida mesoscale convective system. Geophys. Res. Lett. 44, 8027–8036. https://doi.org/10.1002/2017GL074610

Boccippio, D.J., 2002. Lightning scaling relations revisited. J. Atmos. Sci. 59, 1086–1104. https://doi.org/10.1175/1520-0469(2002)059<1086:LSRR>2.0.CO;2

Braam, H., Ramakers, S.G.M., Rademakers, L., Wessels, H., Prins, R.K.N.J., Lok, R., Leunis, L., 2002. Lightning Damage of OWECS Part 3: "Case Studies."

Brown, R.A., Kaufman, C.A., MacGorman, D.R., 2002. Cloud-to-ground lightning associated with the evolution of a multicell storm. J. Geophys. Res. Atmos. 107, ACL 13-1-ACL 13-13. https://doi.org/10.1029/2001JD000968

Bruning, E.C., Macgorman, D.R., 2013. Theory and observations of controls on lightning flash size spectra. J. Atmos. Sci. 70, 4012–4029. https://doi.org/10.1175/JAS-D-12-0289.1

Bruning, E.C., Rust, W.D., Macgorman, D.R., Biggerstaff, M.I., Schuur, T.J., 2010. Formation of charge structures in a supercell. Mon. Weather Rev. 138, 3740–3761. https://doi.org/10.1175/2010MWR3160.1

Bruning, E.C., Rust, W.D., Schuur, T.J., MacGorman, D.R., Krehbiel, P.R., Rison, W., 2007. Electrical and polarimetric radar observations of a multicell storm in TELEX. Mon. Weather Rev. 135, 2525–2544. https://doi.org/10.1175/MWR3421.1

Bruning, E.C., Weiss, S.A., Calhoun, K.M., 2014. Continuous variability in thunderstorm primary electrification and an evaluation of inverted-polarity terminology. Atmos. Res. 135–136, 274–284. https://doi.org/10.1016/j.atmosres.2012.10.009

Brunner, J.C., Ackerman, S.A., Bachmeier, A.S., Rabin, R.M., 2006. A quantitative analysis of the enhanced-V signature in relation to severe weather. 86th AMS Annu. Meet.

Buechler, D.E., Goodman, S.J., 1990. Echo size and asymmetry: impact on NEXRAD storm identification. J. Appl. Meteorol. 29, 962–969. https://doi.org/10.1175/1520-0450(1990)029<0962:ESAAIO>2.0.CO;2

Caicedo, J.A., Uman, M.A., Pilkey, J.T., 2018. Lightning Evolution In Two North Central Florida Summer Multicell Storms and Three Winter/Spring Frontal Storms. J. Geophys. Res. Atmos. 123, 1155–1178. https://doi.org/10.1002/2017JD026536

Carey, L.D., Murphy, M.J., McCormick, T.L., Demetriades, N.W.S., 2005. Lightning location relative to storm structure in a leading-line, trailing-stratiform mesoscale convective system. J. Geophys. Res. D Atmos. 110, 1–23. https://doi.org/10.1029/2003JD004371

Carey, L.D., Petersen, W.A., Rutledge, S.A., 2003. Evolution of cloud-to-ground lightning and storm

structure in the Spencer, South Dakota, tornadic supercell of 30 May 1998. Mon. Weather Rev. 131, 1811–1831. https://doi.org/10.1175//2566.1

Carey, L.D., Rutledge, S.A., 1996. A multiparameter radar case study of the microphysical and kinematic evolution of a lightning producing storm. Meteorol. Atmos. Phys. 59, 33–64. https://doi.org/10.1007/BF01032000

Carey, L.D., Schultz, E. V., Schultz, C.J., Deierling, W., Petersen, W.A., Bain, A.L., Pickering, K.E., 2019. An evaluation of relationships between radar-inferred kinematic and microphysical parameters and lightning flash rates in alabama storms. Atmosphere (Basel). 10. https://doi.org/10.3390/ATMOS10120796

Chan, M.K., Chen, M., Du, Y. ping, 2018. A macroscopic physical model for self-initiated upward leaders from tall grounded objects and its application. Atmos. Res. 200, 13–24. https://doi.org/10.1016/j.atmosres.2017.09.012

Clarence, N.D., Malan, D.J., 1957. Preliminary discharge processes in lightning flashes to ground. Q. J. R. Meteorol. Soc. 83, 161–172. https://doi.org/10.1002/qj.49708335603

Clulow, A.D., Strydom, S., Grant, B., Savage, M.J., Everson, C.S., 2018. Integration of a ground-based lightning warning system into a mining operation in the Democratic Republic of the Congo. Weather. Clim. Soc. 10, 899–912. https://doi.org/10.1175/wcas-d-18-0004.1

Coleman, L.M., Stolzenburg, M., Marshall, T.C., Stanley, M., 2008. Horizontal lightning propagation, preliminary breakdown, and electric potential in New Mexico thunderstorms. J. Geophys. Res. Atmos. 113. https://doi.org/10.1029/2007JD009459

Cooray, V., Cooray, G., Marshall, T., Arabshahi, S., Dwyer, J., Rassoul, H., 2014. Electromagnetic fields of a relativistic electron avalanche with special attention to the origin of lightning signatures known as narrow bipolar pulses. Atmos. Res. 149, 346–358. https://doi.org/10.1016/j.atmosres.2013.12.011

Cooray, V., Rakov, V., Theethayi, N., 2007. The lightning striking distance-Revisited. J. Electrostat. 65, 296–306. https://doi.org/10.1016/j.elstat.2006.09.008

Cummins, K.L., Krider, E.P., Malone, M.D., 1998a. The U.S. national lightning detection network™ and applications of cloud-to-ground lightning data by electric power utilities. IEEE Trans. Electromagn. Compat. 40, 465–480. https://doi.org/10.1109/15.736207

Cummins, K.L., Murphy, M.J., 2009. An overview of lightning locating systems: History, techniques, and data uses, with an in-depth look at the U.S. NLDN. IEEE Trans. Electromagn. Compat. 51, 499–518. https://doi.org/10.1109/TEMC.2009.2023450

Cummins, K.L., Murphy, M.J., Bardo, E.A., Hiscox, W.L., Pyle, R.B., Pifer, A.E., 1998b. A combined TOA/MDF technology upgrade of the US National Lightning Detection Network. J. Geophys. Res. Atmos. 103, 9035–9044. https://doi.org/10.1029/98JD00153

Curran, E.B., Holle, R.L., Lopez, R.E., 2000. Lightning casualties and damages in the United States from 1959 to 1994. J. Clim. 13, 3448–3464. https://doi.org/10.1175/1520-0442(2000)013<3448:LCADIT>2.0.CO;2

Dahl, J.M.L., Höller, H., Schumann, U., 2011. Modeling the flash rate of thunderstorms. Part I: Framework. Mon. Weather Rev. 139, 3093–3111. https://doi.org/10.1175/MWR-D-10-05031.1

Deierling, W., Latham, J., Petersen, W.A., Ellis, S.M., Christian, H.J., 2005. On the relationship of

thunderstorm ice hydrometeor characteristics and total lightning measurements. Atmos. Res. 76, 114–126. https://doi.org/10.1016/j.atmosres.2004.11.023

Deierling, W., Petersen, W.A., 2008. Total lightning activity as an indicator of updraft characteristics. J. Geophys. Res. Atmos. 113. https://doi.org/10.1029/2007JD009598

Deierling, W., Petersen, W.A., Latham, J., Ellis, S., Christian, H.J., 2008. The relationship between lightning activity and ice fluxes in thunderstorms. J. Geophys. Res. Atmos. 113. https://doi.org/10.1029/2007JD009700

Diendorfer, G., 2017. Review of seasonal variations in occurrence and some current parameters of lightning measured at the Gaisberg Tower. 4th Int. Symp. Winter Light. 1–6.

Diendorfer, G., Pichler, H., Mair, M., 2009. Some parameters of negative upward-initiated lightning to the gaisberg tower (2000-2007). IEEE Trans. Electromagn. Compat. 51, 443–452. https://doi.org/10.1109/TEMC.2009.2021616

Diendorfer, G., Pichler, H., Schulz, W., 2014. EUCLID Located Strokes to the Gaisberg Tower – Accuracy of Location and its assigned Confidence Ellipse. Int. Conf. Light. Detect.

Donaldson, R.J., Dyer, R.M., Kraus, M.J., 1975. An objective evaluation of techniques for predicting severe weather events. 9th Conf. Sev. Local Storms, Norman, Am. Meteorol. Soc. 321–326.

Doswell, C.A., Davies-Jones, R., Keller, D.L., 1990. On Summary Measures of Skill in Rare Event Forecasting Based on Contingency Tables. Weather Forecast. 5, 576–585. https://doi.org/10.1175/1520-0434(1990)005<0576:osmosi>2.0.co;2

Doswell III, C.A., 2007. Historical Overview of Severe Convective Storms Research. Electron. J. Sev. Storms Meteor 2, 1–25.

Doswell III, C.A., 2001. Severe Convective Storms. Sev. Convect. Storms. https://doi.org/10.1007/978-1-935704-06-5

Dotzek, N., Rabin, R.M., Carey, L.D., MacGorman, D.R., McCormick, T.L., Demetriades, N.W., Murphy, M.J., Holle, R.L., 2005. Lightning activity related to satellite and radar observations of a mesoscale convective system over Texas on 7-8 April 2002. Atmos. Res. 76, 127–166. https://doi.org/10.1016/j.atmosres.2004.11.020

Duda, J.D., Gallus, W.A., 2010. Spring and summer midwestern severe weather reports in supercells compared to other morphologies. Weather Forecast. 25, 190–206. https://doi.org/10.1175/2009WAF2222338.1

Dwyer, J., Uman, M., 2013. The physics of lightning. Phys. Rep. 534. https://doi.org/10.1016/j.physrep.2013.09.004

Dye, J.E., 1986. Early electrification and precipitation development in a small, isolated Montana cumulonimbus. J. Geophys. Res. 91, 1231–1247. https://doi.org/10.1029/JD091iD01p01231

Dye, J.E., Winn, W.P., Jones, J.J., Breed, D.W., 1989. The electrification of New Mexico thunderstorms. 1. Relationship between precipitation development and the onset of electrification. J. Geophys. Res. 94, 8643–8656. https://doi.org/10.1029/JD094iD06p08643

Elsom, D.M., Webb, J.D.C., 2014. Deaths and injuries from lightning in the UK, 1988-2012. Weather 69, 221–226. https://doi.org/10.1002/wea.2254

Eriksson, A.J., 1978. Lightning and Tall Structures. Trans S Afr Inst Electr Eng 69, 238–252.

https://doi.org/10.1049/piee.1978.0084

Farnell, C., Rigo, T., Pineda, N., 2017. Lightning jump as a nowcast predictor: Application to severe weather events in Catalonia. Atmos. Res. 183, 130–141. https://doi.org/10.1016/j.atmosres.2016.08.021

Figueras I Ventura, J., Pineda, N., Besic, N., Grazioli, J., Hering, A., Van Der Velde, O.A., Romero, D., Sunjerga, A., Mostajabi, A., Azadifar, M., Rubinstein, M., Montanyà, J., Germann, U., Rachidi, F., 2019. Polarimetric radar characteristics of lightning initiation and propagating channels. Atmos. Meas. Tech. 12, 2881–2911. https://doi.org/10.5194/amt-12-2881-2019

Foley, A.M., Leahy, P.G., Marvuglia, A., McKeogh, E.J., 2012. Current methods and advances in forecasting of wind power generation. Renew. Energy 37, 1–8. https://doi.org/10.1016/j.renene.2011.05.033

Fuchs, B.R., Rutledge, S.A., 2018. Investigation of Lightning Flash Locations in Isolated Convection Using LMA Observations. J. Geophys. Res. Atmos. 123, 6158–6174. https://doi.org/10.1002/2017JD027569

Fuchs, B.R., Rutledge, S.A., Bruning, E.C., Pierce, J.R., Kodros, J.K., Lang, T.J., MacGorman, D.R., Krehbiel, P.R., Rison, W., 2015. Environmental controls on storm intensity and charge structure in multiple regions of the continental United States. J. Geophys. Res. 120, 6575–6596. https://doi.org/10.1002/2015JD023271

Futyan, J.M., Del Genio, A.D., 2007. Relationships between lightning and properties of convective cloud clusters. Geophys. Res. Lett. 34. https://doi.org/10.1029/2007GL030227

Galanaki, E., Lagouvardos, K., Kotroni, V., Flaounas, E., Argiriou, A., 2018. Thunderstorm climatology in the Mediterranean using cloud-to-ground lightning observations. Atmos. Res. 207, 136–144. https://doi.org/10.1016/j.atmosres.2018.03.004

Garolera, A.C., Madsen, S.F., Nissim, M., Myers, J.D., Holboell, J., 2016. Lightning Damage to Wind Turbine Blades from Wind Farms in the U.S. IEEE Trans. Power Deliv. 31, 1043–1049. https://doi.org/10.1109/TPWRD.2014.2370682

Gatlin, P.N., Goodman, S.J., 2010. A total lightning trending algorithm to identify severe thunderstorms. J. Atmos. Ocean. Technol. 27, 3–22. https://doi.org/10.1175/2009JTECHA1286.1

Golde, R.H., 1945. The Frequency of Occurrence and the Distribution of Lightning Flashes to Transmission Lines. Trans. Am. Inst. Electr. Eng. 64, 902–910. https://doi.org/10.1109/T-AIEE.1945.5059060

Goodman, S.J., Buechler, D.E., Wright, P.D., Rust, W.D., 1988. Lightning and precipitation history of a microburst-producing storm. Geophys. Res. Lett. 15, 1185–1188. https://doi.org/10.1029/GL015i011p01185

Gremillion, M.S., Orville, R.E., 1999. Thunderstorm characteristics of cloud-to-ground lightning at the Kennedy Space Center, Florida: A study of lightning initiation signatures as indicated by the WSR-88D. Weather Forecast. 14, 640–649. https://doi.org/10.1175/1520-0434(1999)014<0640:TCOCTG>2.0.CO;2

Haklander, A.J., Van Delden, A., 2003. Thunderstorm predictors and their forecast skill for the Netherlands. Atmos. Res. 67–68, 273–299. https://doi.org/10.1016/S0169-8095(03)00056-5

Holle, R.L., 2016. A summary of recent national-Scale lightning fatality studies. Weather. Clim. Soc. 8, 35–42. https://doi.org/10.1175/WCAS-D-15-0032.1

Höller, H., Betz, H.D., Schmidt, K., Calheiros, R. V., May, P., Houngninou, E., Scialom, G., 2009. Lightning characteristics observed by a VLF/LF lightning detection network (LINET) in Brazil, Australia, Africa and Germany. Atmos. Chem. Phys. 9, 7795–7824. https://doi.org/10.5194/acp-9-7795-2009

Hondl, K.D., Eilts, M.D., 1994. Doppler radar signatures of developing thunderstorms and their potential to indicate the onset of cloud-to-ground lightning. Mon. Weather Rev. 122, 1818–1836. https://doi.org/10.1175/1520-0493(1994)122<1818:DRSODT>2.0.CO;2

Honjo, N., 2015. Risk and its Reduction Measure for Wind Turbine against the Winter Lightning. Apl2015 665–670.

International Electrotechnical Commission., 2010. Wind turbines. Part 24, Lightning protection.

Iudin, D.I., Rakov, V.A., Mareev, E.A., Iudin, F.D., Syssoev, A.A., Davydenko, S.S., 2017. Advanced numericalmodel of lightning development: Application to studying the role of LPCR in determining lightning type. J. Geophys. Res. 122, 6416–6430. https://doi.org/10.1002/2016JD026261

Jacobson, E.A., Krider, E.P., 1976. Electrostatic Field Changes Produced By Florida Lightning. J. Atmos. Sci. 33, 103–117. https://doi.org/10.1175/1520-0469(1976)033<0103:EFCPBF>2.0.CO;2

Jayaratne, E.R., Saunders, C.P.R., Hallett, J., 1983. Laboratory studies of the charging of soft-hail during ice crystal interactions. Q. J. R. Meteorol. Soc. 109, 609–630. https://doi.org/10.1002/qj.49710946111

Kaltenböck, R., Diendorfer, G., Dotzek, N., 2009. Evaluation of thunderstorm indices from ECMWF analyses, lightning data and severe storm reports. Atmos. Res. 93, 381–396. https://doi.org/10.1016/j.atmosres.2008.11.005

Karagiannidis, A., Lagouvardos, K., Kotroni, V., 2016. The use of lightning data and Meteosat infrared imagery for the nowcasting of lightning activity. Atmos. Res. 168, 57–69. https://doi.org/10.1016/j.atmosres.2015.08.011

Karagiannidis, A., Lagouvardos, K., Lykoudis, S., Kotroni, V., Giannaros, T., Betz, H.D., 2019. Modeling lightning density using cloud top parameters. Atmos. Res. 222, 163–171. https://doi.org/10.1016/j.atmosres.2019.02.013

Kasemir, H.W., 1960. A contribution to the electrostatic theory of a lightning discharge. J. Geophys. Res. 65, 1873–1878. https://doi.org/10.1029/jz065i007p01873

Kingfield, D.M., Calhoun, K.M., de Beurs, K.M., 2017. Antenna structures and cloud-to-ground lightning location: 1995–2015. Geophys. Res. Lett. 44, 5203–5212. https://doi.org/10.1002/2017GL073449

Kotroni, V., Lagouvardos, K., 2016. Lightning in the Mediterranean and its relation with sea-surface temperature. Environ. Res. Lett. 11. https://doi.org/10.1088/1748-9326/11/3/034006

Krausmann, E., Cozzani, V., Salzano, E., Renni, E., 2011. Industrial accidents triggered by natural hazards: An emerging risk issue. Nat. Hazards Earth Syst. Sci. 11, 921–929. https://doi.org/10.5194/nhess-11-921-2011

Krehbiel, P.R., 1986. The electrical structure of thunderstorms, in: Krider, E.P., Roble, R.G. (Eds.), The Earth's Electrical Environment. The National Academies Press, Washington D. C., pp. 90–113.

Krehbiel, P.R., Brook, M., Khanna-Gupta, S., Lennon, C.L., Lhermitte, R., 1984. Some Results Concerning Vhf Lightning Radiation From the Real-Time Ldar System At Ksc, Florida. 388–393.

Krehbiel, P.R., Riousset, J.A., Pasko, V.P., Thomas, R.J., Rison, W., Stanley, M.A., Edens, H.E., 2008. Upward electrical discharges from thunderstorms. Nat. Geosci. 1, 233–237. https://doi.org/10.1038/ngeo162

Krehbiel, P.R., Thomas, R.J., Rison, W., Hamlin, T., Harlin, J., Davis, M., 2000. GPS-based mapping system reveals lightning inside storms. Eos (Washington. DC). 81, 21–25. https://doi.org/10.1029/00EO00014

Kuhlman, K.M., MacGorman, D.R., Biggerstaff, M.I., Krehbiel, P.R., 2009. Lightning initiation in the anvils of two supercell storms. Geophys. Res. Lett. 36. https://doi.org/10.1029/2008GL036650

Kuhlman, K.M., Ziegler, C.L., Mansell, E.R., MacGorman, D.R., Straka, J.M., 2006. Numerically simulated electrification and lightning of the 29 June 2000 STEPS supercell storm. Mon. Weather Rev. 134, 2734–2757. https://doi.org/10.1175/MWR3217.1

Kumijan, M.R., 2013. Principles and Applications of Dual-Polarization Weather Radar. Part I: Description of the Polarimetric Radar Variables. J. Oper. Meteorol. 19, 226–242.

Laksen, H.R., Stansbury, E.J., 1974. Association of lightning flashes with precipitation cores extending to height 7 km. J. Atmos. Terr. Phys. 36. https://doi.org/10.1016/0021-9169(74)90232-3

Lang, T.J., Li, J., Lyons, W.A., Cummer, S.A., Rutledge, S.A., MacGorman, D.R., 2011. Transient luminous events above two mesoscale convective systems: Charge moment change analysis. J. Geophys. Res. Sp. Phys. 116. https://doi.org/10.1029/2011JA016758

Lang, T.J., Lyons, W.A., Rutledge, S.A., Meyer, J.D., MacGorman, D.R., Cummer, S.A., 2010. Transient luminous events above two mesoscale convective systems: Storm structure and evolution. J. Geophys. Res. Sp. Phys. 115. https://doi.org/10.1029/2009JA014500

Lang, T.J., Rutledge, S.A., 2011. A framework for the statistical analysis of large radar and lightning datasets: Results from steps 2000. Mon. Weather Rev. 139, 2536–2551. https://doi.org/10.1175/MWR-D-10-05000.1

Levin, Z., Yair, Y., Ziv, B., 1996. Positive cloud-to-ground flashes and wind shear in Tel-Aviv thunderstorms. Geophys. Res. Lett. 23, 2231–2234. https://doi.org/10.1029/96GL00709

Liu, C., Cecil, D.J., Zipser, E.J., Kronfeld, K., Robertson, R., 2012. Relationships between lightning flash rates and radar reflectivity vertical structures in thunderstorms over the tropics and subtropics. J. Geophys. Res. Atmos. 117. https://doi.org/10.1029/2011JD017123

Liu, C., Zipser, E.J., Nesbitt, S.W., 2007. Global distribution of tropical deep convection: Different perspectives from TRMM infrared and radar data. J. Clim. 20, 489–503. https://doi.org/10.1175/JCLI4023.1

Liu, F., Zhu, B., Lu, G., Lei, J., Shao, J., Chen, Y., Huang, A., Ma, M., Qin, Z., Zhong, J., Ren,

H., Wang, Z., Wan, Z., Liu, G., Peng, C., Peng, K., Zhou, H., 2021. Meteorological and Electrical Conditions of Two Mid-latitude Thunderstorms Producing Blue Discharges. J. Geophys. Res. Atmos. 126. https://doi.org/10.1029/2020jd033648

Lojou, J.-Y., Cummins, K.L., 2006. Total Lightning Mapping Using Both "VHF" Interferometry and Time of Arrival Techniques. Int. Light. Detect. Conf. Int. Light. Meteorol. Conf. 1–9.

López, J.A., Montanyà, J., van der Velde, O.A., Pineda, N., Salvador, A., Romero, D., Aranguren, D., Taborda, J., 2019. Charge Structure of Two Tropical Thunderstorms in Colombia. J. Geophys. Res. Atmos. 124, 5503–5515. https://doi.org/10.1029/2018JD029188

López, J.A., Pineda, N., Montanyà, J., Velde, O. van der, Fabró, F., Romero, D., 2017. Spatio-temporal dimension of lightning flashes based on three-dimensional Lightning Mapping Array. Atmos. Res. 197, 255–264. https://doi.org/10.1016/j.atmosres.2017.06.030

Love, E.R., 1973. Improvements in Lightning Stroke Modelling and Applications to the Design of EHV and UHV Transmission Lines. Tese M.Sc., Univ. Color. Denver, Color. United States Am.

Lu, G., Cummer, S.A., Li, J., Zigoneanu, L., Lyons, W.A., Stanley, M.A., Rison, W., Krehbiel, P.R., Edens, H.E., Thomas, R.J., Beasley, W.H., Weiss, S.A., Blakeslee, R.J., Bruning, E.C., MacGorman, D.R., Meyer, T.C., Palivec, K., Ashcraft, T., Samaras, T., 2013. Coordinated observations of sprites and in-cloud lightning flash structure. J. Geophys. Res. Atmos. 118, 6607–6632. https://doi.org/10.1002/jgrd.50459

Lund, N., Macgorman, D., Rust, D., Schuur, T., Krehbiel, P., Rison, W., Hamlin, T., Straka, J., 2007. Relationship Between Lightning Location and Polarimetric Radar Signatures in an MCS . 5–8.

Lund, N.R., Macgorman, D.R., Schuur, T.J., Biggerstaff, M.I., Rust, W.D., 2009. Relationships between lightning location and polarimetric radar signatures in a small mesoscale convective system. Mon. Weather Rev. 137, 4151–4170. https://doi.org/10.1175/2009MWR2860.1

Lyons, W., Cummer, S. a, Rutledge, S. a, Lang, T.J., Meyer, T., Warner, T. a, Samaras, T.M., 2011. TLEs and Their Parent Lightning Discharges. Proc. 14th Int. Conf. Atmos. Electr. - ICAE 6–9.

Lyons, W.A., 1996. Sprite observations above the U.S. High Plains in relation to their parent thunderstorm systems. J. Geophys. Res. Atmos. 101, 29641–29652. https://doi.org/10.1029/96jd01866

Lyons, W.A., Nelson, T.E., 2014. Meteorological Aspects of Two Modes of Lightning Triggered Upward Lightning (LTUL) Events in Sprite-Producing MCSs. 5th Intl. Light. Meteorol. Conf.

Lyons, W.A., Nelson, T.E., Williams, E.R., Cummer, S.A., Stanley, M.A., 2003. Characteristics of sprite-producing positive cloud-to-ground lightning during the 19 July 2000 STEPS mesoscale convective systems. Mon. Weather Rev. 131, 2417–2427. https://doi.org/10.1175/1520-0493(2003)131<2417:COSPCL>2.0.CO;2

MacGorman, D.R., Apostolakopoulos, I.R., Lund, N.R., Demetriades, N.W.S., Murphy, M.J., Krehbiel, P.R., 2011. The timing of cloud-to-ground lightning relative to total lightning activity. Mon. Weather Rev. 139, 3871–3886. https://doi.org/10.1175/MWR-D-11-00047.1

Macgorman, D.R., Burgess, D.W., Mazur, V., Rust, W.D., Taylor, W.L., Johnson, B.C., 1989. Lightning rates relative to tornadic storm evolution on 22 May 1981. J. Atmos. Sci. 46, 221–

250. https://doi.org/10.1175/1520-0469(1989)046<0221:lrrtts>2.0.co;2

MacGorman, D.R., David Rust, W., Schuur, T.J., Biggerstaff, M.I., Straka, J.M., Ziegler, C.L., Mansell, E.R., Bruning, E.C., Kuhlman, K.M., Lund, N.R., Biermann, N.S., Payne, C., Carey, L.D., Krehbiel, P.R., Rison, W., Eack, K.B., Beasley, W.H., 2008. TELEX The Thunderstorm Electrification and Lightning Experiment. Bull. Am. Meteorol. Soc. 89, 997–1013. https://doi.org/10.1175/2007BAMS2352.1

MacGorman, D.R., Rust, W.D., 1998. The Electrical Nature of Storms. Oxford University Press.

MacGorman, D.R., Straka, J.M., Ziegler, C.L., 2001. A lightning parameterization for numerical cloud models. J. Appl. Meteorol. 40, 459–478. https://doi.org/10.1175/1520-0450(2001)040<0459:ALPFNC>2.0.CO;2

Madsen, S.F., 2017. Design and Verification Methods for Wind Turbines, Ensuring Safe Operation During Lightning Exposure. 4th Int. Symp. Winter Light. 6.

Maggio, C., Coleman, L., Marshall, T., Stolzenburg, M., Stanley, M., Hamlin, T., Krehbiel, P., Rison, W., Thomas, R., 2005. Lightning-initiation locations as a remote sensing tool of large thunderstorm electric field vectors. J. Atmos. Ocean. Technol. 22, 1059–1068. https://doi.org/10.1175/JTECH1750.1

Manhardt, M., Heidler, F., Stimper, K., 2012. The electric field of negative upward lightning strikes at the Peissenberg tower, Germany. 2012 31st Int. Conf. Light. Prot. ICLP 2012. https://doi.org/10.1109/ICLP.2012.6344205

Mansell, E.R., MacGorman, D.R., Ziegler, C.L., Straka, J.M., 2005. Charge structure and lightning sensitivity in a simulated multicell thunderstorm. J. Geophys. Res. D Atmos. 110, 1–24. https://doi.org/10.1029/2004JD005287

Mansell, E.R., MacGorman, D.R., Ziegler, C.L., Straka, J.M., 2002. Simulated three-dimensional branched lightning in a numerical thunderstorm model. J. Geophys. Res. Atmos. 107, ACL 2-1-ACL 2-12. https://doi.org/10.1029/2000jd000244

Mansell, E.R., Ziegler, C.L., Bruning, E.C., 2010. Simulated electrification of a small thunderstorm with two-moment bulk microphysics. J. Atmos. Sci. 67, 171–194. https://doi.org/10.1175/2009JAS2965.1

March, V., 2018. Key issues to define a method of lightning risk assessment for wind farms. Electr. Power Syst. Res. 159, 50–57. https://doi.org/10.1016/j.epsr.2017.08.020

March, V., 2016. Lightning risk assessment to wind turbines: Methodology and guidelines. 2016 33rd Int. Conf. Light. Prot. ICLP 2016. https://doi.org/10.1109/ICLP.2016.7791381

March, V., 2015. Lightning Risk Assessment for direct lightning strikes to wind turbines in a wind farm – Recommendations to IEC 61400 - 24 517–522.

Market, P.S., Ebert-Cripe, R.L., Bodner, M., 2007. Case study of a longlived thundersnow event. Natl. Weather Dig. 31, 103–120.

Marshall, T.C., Rust, W.D., 1993. Two Types of Vertical Electrical Structures in Stratiform Precipitation Regions of Mesoscale Convective Systems. Bull. Am. Meteorol. Soc. 74, 2159–2170. https://doi.org/10.1175/1520-0477(1993)074<2159:ttoves>2.0.co;2

Marshall, T.C., Rust, W.D., 1991. Electric field soundings through thunderstorms. J. Geophys. Res. Atmos. 96, 22297–22306. https://doi.org/https://doi.org/10.1029/91JD02486

Marshall, T.C., Stolzenburg, M., 2002. Electrical energy constraints on lightning. J. Geophys. Res. Atmos. 107. https://doi.org/10.1029/2000jd000024

Marshall, T.C., Winn, W.P., 1982. Measurements of charged precipitation in a New Mexico thunderstorm: lower positive charge centers. J. Geophys. Res. 87, 7141–7157. https://doi.org/10.1029/JC087iC09p07141

Matsudo, Y., Suzuki, T., Hayakawa, M., Yamashita, K., Ando, Y., Michimoto, K., Korepanov, V., 2007. Characteristics of Japanese winter sprites and their parent lightning as estimated by VHF lightning and ELF transients. J. Atmos. Solar-Terrestrial Phys. 69, 1431–1446. https://doi.org/10.1016/j.jastp.2007.05.002

Mazarakis, N., Kotroni, V., Lagouvardos, K., Argiriou, A.A., 2009. The sensitivity of numerical forecasts to convective parameterization during the warm period and the use of lightning data as an indicator for convective occurrence. Atmos. Res. 94, 704–714. https://doi.org/10.1016/j.atmosres.2009.03.002

Mazur, V., 2002. Physical processes during development of lightning flashes. Comptes Rendus Phys. 3, 1393–1409. https://doi.org/10.1016/S1631-0705(02)01412-3

Mazur, V., 1989. A physical model of lightning initiation on aircraft in thunderstorms. J. Geophys. Res. Atmos. 94, 3326–3340. https://doi.org/10.1029/jd094id03p03326

Mazur, V., Ruhnke, L.H., 1993. Common physical processes in natural and artificially triggered lightning. J. Geophys. Res. Atmos. 98, 12913–12930. https://doi.org/https://doi.org/10.1029/93JD00626

Mazur, V., Shao, X.M., Krehbiel, P.R., 1998. "Spider" lightning in intracloud and positive cloud-to-ground flashes. J. Geophys. Res. Atmos. 103, 19811–19822. https://doi.org/10.1029/98JD02003

McCaul, E.W., Goodman, S.J., LaCasse, K.M., Cecil, D.J., 2009. Forecasting lightning threat using cloud-resolving model simulations. Weather Forecast. 24, 709–729. https://doi.org/10.1175/2008WAF2222152.1

McEachron, K.B., 1939. Lightning to the empire state building. J. Franklin Inst. 227, 149–217. https://doi.org/10.1016/S0016-0032(39)90397-2

Mecikalski, R.M., Bain, A.L., Carey, L.D., 2015. Radar and lightning observations of deep moist convection across Northern Alabama during DC3: 21 May 2012. Mon. Weather Rev. 143, 2774–2794. https://doi.org/10.1175/MWR-D-14-00250.1

Mecikalski, R.M., Carey, L.D., 2017. Lightning characteristics relative to radar, altitude and temperature for a multicell, MCS and supercell over northern Alabama. Atmos. Res. 191, 128–140. https://doi.org/10.1016/j.atmosres.2017.03.001

Meng, Q., Yao, W., Xu, L., 2019. Development of lightning nowcasting and warning technique and its application. Adv. Meteorol. 2019. https://doi.org/10.1155/2019/2405936

Mercader-Carbó, J., Codina, B., Sairouni, A., Cunillera, J., 2010. Results of the meteorological model WRF-ARW over Catalonia using diferent parametrizations of convection and cloud microphysics. Tethys J. Weather Clim. West. Mediterr. 7, 75–86. https://doi.org/10.3369/tethys.2010.7.07

Michimoto, K., 1993. A study of radar echoes and their relation to lightning discharges of

thunderclouds in the Hokuriku district PART II: Observation and analysis of "Single-Flash" thunderclouds in midwinter. J. Meteorol. Soc. Japan 71, 195–204. https://doi.org/10.2151/jmsj1965.71.2_195

Michimoto, K., 1991. A study of radar echoes and their relation to lightning discharge of thunderclouds in the Hokuriku district part I: Observation and analysis of thunderclouds in summer and winter. J. Meteorol. Soc. Japan 69, 327–336. https://doi.org/10.2151/jmsj1965.69.3_327

Minowa, M., Minami, M., Yoda, M., 2006. Research into Lightning Damages and Protection Systems for Wind Power Plants in Japan. Light. Prot. (ICLP), 2006 Int. Conf. 1539–1544.

Montanyà, J., 2014. Annual Report on the Performance of the Lightning Location System Operated by the Meteorological Service of Catalonia, Internal Technical Report (not published).

Montanya, J., Aranguren, D., Pineda, N., Sola, G., Romero, D., March, V., 2008. Total lightning, electrostatic field and meteorological radar applied to lightning hazard warning. 20th Int. Light. Detect. Conf. 4.

Montanyà, Joan, Fabró, F., Van Der Velde, O., March, V., Rolfe Williams, E., Pineda, N., Romero, D., Sol, G., Freijo, M., 2016. Global distribution of winter lightning: A threat to wind turbines and aircraft. Nat. Hazards Earth Syst. Sci. 16, 1465–1472. https://doi.org/10.5194/nhess-16-1465-2016

Montanyà, J., Pineda, N., March, V., Illa, A., Romero, D., Solà, G., 2006. Experimental Evaluation of the Catalan Lightning Detection Network. 19th Int. Light. Detect. Conf. Tucson 7.

Montanyà, J., Solà, S., Diendorfer, G., Romero, D., 2007. Analysis of the Altitude of the Isotherms and the Electrical Charge for Flashes that Struck the Gaisberg Tower. Int. Conf. Atmos. Electr. 2–5.

Montanyà, J., Van Der Velde, O., Domingo-Dalmau, A., Pineda, N., Argemí, O., Salvador, A., 2016. Lightning mapping observations of downward lightning flashes to wind turbines. 2016 33rd Int. Conf. Light. Prot. ICLP 2016. https://doi.org/10.1109/ICLP.2016.7791449

Montanyà, J., Van Der Velde, O., Romero, D., March, V., Solà, G., Pineda, N., Soula, S., Hermoso, B., 2012a. Two upward lightning at the Eagle Nest tower. 2012 31st Int. Conf. Light. Prot. ICLP 2012. https://doi.org/10.1109/ICLP.2012.6344373

Montanya, J., Van Der Velde, O., Williams, E.R., 2015. The start of lightning: Evidence of bidirectional lightning initiation. Sci. Rep. 5, 15180. https://doi.org/10.1038/srep15180

Montanyà, J., van der Velde, O., Williams, E.R., 2014. Lightning discharges produced by wind turbines. J. Geophys. Res. 119, 1455–1462. https://doi.org/10.1002/2013JD020225

Montanyà, J., van der Velde, O.A., March, V., Romero, D., Solà, G., Pineda, N., 2012b. High-speed video of lightning and x-ray pulses during the 2009-2010 observation campaigns in northeastern Spain. Atmos. Res. 117, 91–98. https://doi.org/10.1016/j.atmosres.2011.09.013

Murphy, A., Daan, H., 1985. Forecast Evaluation, in: Murphy, A.H., Katz, R.W. (Eds.), Probability, Statistics, And Decision Making In The Atmospheric Sciences. pp. 379–437.

Murphy, M.J., Krider, E.P., Maier, M.W., 1996. Lightning charge analyses in small Convection and Precipitation Electrification (CaPE) experiment storms. J. Geophys. Res. Atmos. 101, 29615–29626. https://doi.org/10.1029/96jd01538

Nag, A., Murphy, M.J., Schulz, W., Cummins, K.L., 2015. Lightning locating systems: Insights on characteristics and validation techniques. Earth Sp. Sci. 2, 65–93. https://doi.org/10.1002/2014EA000051

Nag, A., Rakov, V.A., 2009. Some inferences on the role of lower positive charge region in facilitating different types of lightning. Geophys. Res. Lett. 36. https://doi.org/10.1029/2008GL036783

Nesbitt, S.W., Zipser, E.J., 2000. A census of precipitation features in the tropics using TRMM: Radar, ice scattering, and lightning observations. J. Clim. 13, 4087–4106. https://doi.org/10.1175/1520-0442(2000)013<4087:ACOPFI>2.0.CO;2

Neubert, T., Kuvvetli, I., budtz-jørgensen, C., Ostgaard, N., Reglero, V., Arnold, N., 2006. The Atmosphere-Space Interactions Monitor (ASIM) for the International Space Station. AGU Fall Meet. Abstr. 2–5.

Neubert, T., Østgaard, N., Reglero, V., Blanc, E., Chanrion, O., Oxborrow, C.A., Orr, A., Tacconi, M., Hartnack, O., Bhanderi, D.D.V., 2019. The ASIM Mission on the International Space Station. Space Sci. Rev. 215, 26. https://doi.org/10.1007/s11214-019-0592-z

Pablo, F. De, Soriano, L.R., 2002. Relationship between cloud-to-ground lightning flashes over the Iberian Peninsula and sea surface temperature. Q. J. R. Meteorol. Soc. 128, 173–183. https://doi.org/https://doi.org/10.1256/00359000260498842

Panofsky, H.A., Brier, G., 1958. Some Applications of Statistics to Meteorology. Pennsylvania State University.

Parker, M.D., Johnson, R.H., 2000. Organizational modes of midlatitude mesoscale convective systems. Mon. Weather Rev. 128, 3413–3436. https://doi.org/10.1175/1520-0493(2001)129<3413:OMOMMC>2.0.CO;2

Pawar, S.D., Kamra, A.K., 2004. Evolution of lightning and the possible initiation/triggering of lightning discharges by the lower positive charge center in an isolated thundercloud in the tropics. J. Geophys. Res. Atmos. 109. https://doi.org/10.1029/2003jd003735

Pessi, A.T., Businger, S., 2009. Relationships among lightning, precipitation, and hydrometeor characteristics over the North Pacific Ocean. J. Appl. Meteorol. Climatol. 48, 833–848. https://doi.org/10.1175/2008JAMC1817.1

Petersen, W.A., Christian, H.J., Rutledge, S.A., 2005. TRMM observations of the global relationship between ice water content and lightning. Geophys. Res. Lett. 32, 1–4. https://doi.org/10.1029/2005GL023236

Petersen, W.A., Rutledge, S.A., Orville, R.E., 1996. Cloud-to-ground lightning observations from TOGA COARE: Selected results and lightning location algorithms. Mon. Weather Rev. 124, 602–620. https://doi.org/10.1175/1520-0493(1996)124<0602:CTGLOF>2.0.CO;2

Pierce, E.T., 1972. Triggered lightning and some unsuspected lightning hazards. Nav. Res. Rev. 14–28.

Pineda, N., Montanyà, J., 2009. Lightning detection in Spain: The particular case of Catalonia. Light. Princ. Instruments Appl. Rev. Mod. Light. Res. 161–185. https://doi.org/10.1007/978-1-4020-9079-0_7

Pineda, N., Montanyà, J., Salvador, A., van der Velde, O.A., López, J.A., 2018. Thunderstorm characteristics favouring downward and upward lightning to wind turbines. Atmos. Res. 214,

46–63. https://doi.org/10.1016/j.atmosres.2018.07.012

Pineda, N., Soler, X., Vilaclara, E., 2011. Aproximació a la climatologia de llamps a Catalunya : anàlisi de les dades de l'SMC per al període 2004-2008.

Poelman, D.R., Schulz, W., Diendorfer, G., Bernardi, M., 2016. The European lightning location system EUCLID - Part 2: Observations. Nat. Hazards Earth Syst. Sci. 16, 607–616. https://doi.org/10.5194/nhess-16-607-2016

Prentice, S.A., Mackerras, D., 1977. The Ratio of Cloud to Cloud-Ground Lightning Flashes in Thunderstorms. J. Appl. Meteorol. 16, 545–550. https://doi.org/10.1175/1520-0450(1977)016<0545:troctc>2.0.co;2

Price, C., Rind, D., 1994. Modeling global lightning distributions in a general circulation model. Mon. Weather Rev. 122, 1930–1939. https://doi.org/10.1175/1520-0493(1994)122<1930:MGLDIA>2.0.CO;2

Qie, X., Zhang, T.T., Chen, C., Zhang, G., Zhang, T.T., Wei, W., 2005. The lower positive charge center and its effect on lightning discharges on the Tibetan Plateau. Geophys. Res. Lett. 32. https://doi.org/https://doi.org/10.1029/2004GL022162

Rachidi, F., Rubinstein, M., Montanyà, J., Bermúdez, J.L., Sola, R.R., Solà, G., Korovkin, N., 2008. A review of current issues in lightning protection of new-generation wind-turbine blades. IEEE Trans. Ind. Electron. 55, 2489–2496. https://doi.org/10.1109/TIE.2007.896443

Radičević, B.M., Savić, M.S., Badea, I., 2012. Impact of wind turbine blade rotation on the lightning strike incidence. 2012 31st Int. Conf. Light. Prot. ICLP 2012. https://doi.org/10.1109/ICLP.2012.6344215

Rakov, V.A., Uman, M.A., 2003. Lightning: Physics and Effects. Cambridge University Press.

Rauber, R.M., Wegman, J., Plummer, D.M., Rosenow, A.A., Peterson, M., McFarquhar, G.M., Jewett, B.F., Leon, D., Market, P.S., Knupp, K.R., Keeler, J.M., Battaglia, S.M., 2014. Stability and charging characteristics of the comma head region of continental winter cyclones. J. Atmos. Sci. 71, 1559–1582. https://doi.org/10.1175/JAS-D-13-0253.1

Reynolds, S.E., Brook, M., 1956. Correlation of the Initial Electric Field and the Radar Echo in Thunderstorms. J. Meteorol. 13, 376–380. https://doi.org/10.1175/1520-0469(1956)013<0376:cotief>2.0.co;2

Rigo, T., Berenguer, M., Llasat, M. del C., 2019. An improved analysis of mesoscale convective systems in the western Mediterranean using weather radar. Atmos. Res. 227, 147–156. https://doi.org/10.1016/j.atmosres.2019.05.001

Rigo, T., Pineda, N., Bech, J., 2010. Analysis of warm season thunderstorms using an object-oriented tracking method based on radar and total lightning data. Nat. Hazards Earth Syst. Sci. 10, 1881–1893. https://doi.org/10.5194/nhess-10-1881-2010

Rison, W., Thomas, R.J., Krehbiel, P.R., Hamlin, T., Harlin, J., 1999. A GPS-based three-dimensional lightning mapping system: Initial observations in central New Mexico. Geophys. Res. Lett. 26, 3573–3576. https://doi.org/10.1029/1999GL010856

Rivas Soriano, L., de Pablo, F., Tomas, C., 2005. Ten-year study of cloud-to-ground lightning activity in the Iberian Peninsula. J. Atmos. Solar-Terrestrial Phys. 67, 1632–1639. https://doi.org/10.1016/j.jastp.2005.08.019

Rizk, F.A.M., 1994a. Modeling of Lightning Incidence to Tall Structures Part I: Theory. IEEE Trans. Power Deliv. 9, 162–171. https://doi.org/10.1109/61.277673

Rizk, F.A.M., 1994b. Modeling of Lightning Incidence to Tall Structures Part II: Application. IEEE Trans. Power Deliv. 9, 162–171. https://doi.org/10.1109/61.277690

Rizk, F.A.M., 1990. Modeling of transmission line exposure to direct lightning strokes. IEEE Trans. Power Deliv. 5, 1983–1997. https://doi.org/10.1109/61.103694

Romero, C., Rachidi, F., Paolone, M., Rubinstein, M., 2013. Statistical distributions of lightning currents associated with upward negative flashes based on the data collected at the Säntis (EMC) Tower in 2010 and 2011. IEEE Trans. Power Deliv. 28, 1804–1812. https://doi.org/10.1109/TPWRD.2013.2254727

Rosenfeld, D., Wolff, D.B., Atlas, D., 1993. General probability-matched relations between radar reflectivity and rain rate. J. Appl. Meteorol. 32, 50–72. https://doi.org/10.1175/1520-0450(1993)032<0050:GPMRBR>2.0.CO;2

Rust, W.D., MacGorman, D.R., Bruning, E.C., Weiss, S.A., Krehbiel, P.R., Thomas, R.J., Rison, W., Hamlin, T., Harlin, J., 2005. Inverted-polarity electrical structures in thunderstorms in the Severe Thunderstorm Electrification and Precipitation Study (STEPS). Atmos. Res. 76, 247–271. https://doi.org/10.1016/j.atmosres.2004.11.029

Rutledge, S.A., Williams, E.R., Keenan, T.D., 1992. The Down Under Doppler and Electricity Experiment (DUNDEE): overview and preliminary results. Bull. - Am. Meteorol. Soc. 73, 3–16. https://doi.org/10.1175/1520-0477(1992)073<0003:tdudae>2.0.co;2

Salvador, A., Pineda, N., Montanyà, J., Solà, G., 2020. Seasonal variations on the conditions required for the lightning production. Atmos. Res. 243, 104981. https://doi.org/10.1016/j.atmosres.2020.104981

San Segundo, H., López, J.A., Pineda, N., Altube, P., Montanyà, J., 2020. Sensitivity analysis of lightning stroke-to-flash grouping criteria. Atmos. Res. 242, 105023. https://doi.org/10.1016/j.atmosres.2020.105023

Saunders, C.P.R., Bax-Norman, H., Emersic, C., Avila, E.E., Castellano, N.E., 2006. Laboratory studies of the effect of cloud conditions on graupel/crystal charge transfer in thunderstorm electrification. Q. J. R. Meteorol. Soc. 132, 2653–2673. https://doi.org/10.1256/qj.05.218

Saunders, C.P.R., Keith, W.D., Mitzeva, R.P., 1991. The effect of liquid water on thunderstorm charging. J. Geophys. Res. 96, 11007–11017. https://doi.org/10.1029/91jd00970

Saunders, C.P.R., Peck, S.L., 1998. Laboratory studies of the influence of the rime accretion rate on charge transfer during crystal/graupel collisions. J. Geophys. Res. Atmos. 103, 13949–13956. https://doi.org/10.1029/97JD02644

Schultz, C.J., Bruning, E.C., Carey, L.D., Petersen, W.A., Heckman, S.J., 2011a. Total Lightning within electrified snowfall using LMA, NLDN and WTLN measurements, in: Eos Trans. AGU, Fall Meet. Suppl., AE12A-03, American Geophysical Union.

Schultz, C.J., Carey, L.D., Schultz, E. V., Blakeslee, R.J., 2015. Insight into the kinematic and microphysical processes that control lightning jumps. Weather Forecast. 30, 1591–1621. https://doi.org/10.1175/WAF-D-14-00147.1

Schultz, C.J., Lang, T.J., Bruning, E.C., Calhoun, K.M., Harkema, S., Curtis, N., 2018.

Characteristics of Lightning Within Electrified Snowfall Events Using Lightning Mapping Arrays. J. Geophys. Res. Atmos. 123, 2347–2367. https://doi.org/10.1002/2017JD027821

Schultz, C.J., Petersen, W.A., Carey, L.D., 2011b. Lightning and severe weather: A comparison between total and cloud-to-ground lightning trends. Weather Forecast. 26, 744–755. https://doi.org/10.1175/WAF-D-10-05026.1

Schultz, D.M., 1999. Lake-effect snowstorms in Northern Utah and Western New York with and without lightning. Weather Forecast. 14, 1023–1031. https://doi.org/10.1175/1520-0434(1999)014<1023:lesinu>2.0.co;2

Shao, X.M., Krehbiel, P.R., 1996. The spatial and temporal development of intracloud lightning. J. Geophys. Res. Atmos. 101, 26641–26668. https://doi.org/10.1029/96jd01803

Shepherd, T.R., Rust, W.D., Marshall, T.C., 1996. Electric fields and charges near 0°C in stratiform clouds. Mon. Weather Rev. 124, 919–938. https://doi.org/10.1175/1520-0493(1996)124<0919:EFACNI>2.0.CO;2

Shindo, T., Miki, T., Saito, M., Asakawa, A., Motoyama, H., Ishii, M., Taguchi, H., Tajima, A., Fujisawa, A., 2015. Meteorological conditions and occurrence of upward lightning at high structures. IEEJ Trans. Power Energy 135, 417–418. https://doi.org/10.1541/ieejpes.135.417

Shindo, T., Sekioka, S., Ishii, M., Shiraishi, H., Natsuno, D., 2012. Studies of lightning protection design for wind power generation systems in Japan. 44th Int. Conf. Large High Volt. Electr. Syst. 2012.

Shindo, T., Suda, T., 2008. A study of lightning risk. IEEJ Trans. Electr. Electron. Eng. 3, 583–589. https://doi.org/10.1002/tee.20316

Skamarock, C., Klemp, B., Dudhia, J., Gill, O., Barker, D., Duda, G., Huang, X., Wang, W., Powers, G., 2008. A Description of the Advanced Research WRF Version 3.

Smorgonskiy, A., Tajalli, A., Rachidi, F., Rubinstein, M., Diendorfer, G., Pichler, H., 2015. An analysis of the initiation of upward flashes from tall towers with particular reference to Gaisberg and Säntis Towers. J. Atmos. Solar-Terrestrial Phys. 136, 46–51. https://doi.org/10.1016/j.jastp.2015.06.016

Soriano, L.R., De Pablo, F., Díez García, E., 2001. Relationship between convective precipitation and cloud-to-ground lightning in the Iberian Peninsula. Mon. Weather Rev. 129, 2998–3003. https://doi.org/10.1175/1520-0493(2001)129<2998:RBCPAC>2.0.CO;2

Soula, S., Seity, Y., Feral, L., Sauvageot, H., 2004. Cloud-to-ground lightning activity in hail-bearing storms. J. Geophys. Res. Atmos. 109. https://doi.org/10.1029/2003jd003669

Stackpole, J.D., 1967. Numerical Analysis of Atmospheric Soundings. J. Appl. Meteorol. 6, 464–467. https://doi.org/10.1175/1520-0450(1967)006<0464:naoas>2.0.co;2

Stolzenburg, M., Marshall, T.C., 2008. Charge Structure and Dynamics in Thunderstorms, in: Leblanc, F., Aplin, K.L., Yair, Y., Harrison, R.G., Lebreton, J.P., Blanc, M. (Eds.), Planetary Atmospheric Electricity. Springer New York, New York, NY, pp. 355–372. https://doi.org/10.1007/978-0-387-87664-1_23

Stolzenburg, M., Marshall, T.C., Rust, W.D., Smull, B.F., 1994. Horizontal distribution of electrical and meteorological conditions across the stratiform region of a mesoscale convective system. Mon. Weather Rev. 122, 1777–1797. https://doi.org/10.1175/1520-

0493(1994)122<1777:HDOEAM>2.0.CO;2

Stolzenburg, M., Rust, W.D., Smull, B.F., Marshall, T.C., 1998. Electrical structure in thunderstorm convective regions 1. Mesoscale convective systems. J. Geophys. Res. Atmos. 103, 14059–14078. https://doi.org/10.1029/97JD03546

Storch, H. von, Zwiers, F.W., 1999. Statistical Analysis in Climate Research. Cambridge University Press.

Straka, J.M., Zrnic, D.S., Ryzhkov, A. V., 2000. Bulk hydrometeor classification and quantification using polarimetric radar data: Synthesis of relations. J. Appl. Meteorol. 39, 1341–1372. https://doi.org/10.1175/1520-0450(2000)039<1341:BHCAQU>2.0.CO;2

Suzuki, T., Hayakawa, M., Matsudo, Y., Michimoto, K., 2006. How do winter thundercloud systems generate sprite-inducing lightning in the Hokuriku area of Japan? Geophys. Res. Lett. 33. https://doi.org/10.1029/2005GL025433

Takahashi, T., 1978. Riming Electrification as a Charge Generation Mechanism in Thunderstorms. J. Atmos. Sci. 35, 1536–1548. https://doi.org/10.1175/1520-0469(1978)035<1536:reaacg>2.0.co;2

Takahashi, T., Miyawaki, K., 2002. Reexamination of riming electrification in a wind tunnel. J. Atmos. Sci. 59, 1018–1025. https://doi.org/10.1175/1520-0469(2002)059<1018:ROREIA>2.0.CO;2

Takahashi, Y., Miyasato, R., Adachi, T., Adachi, K., Sera, M., Uchida, A., Fukunishi, H., 2003. Activities of sprites and elves in the winter season, Japan. J. Atmos. Solar-Terrestrial Phys. 65, 551–560. https://doi.org/10.1016/S1364-6826(02)00330-9

Tan, Y., Tao, S., Liang, Z., Zhu, B., 2014. Numerical study on relationship between lightning types and distribution of space charge and electric potential. J. Geophys. Res. 119, 1003–1014. https://doi.org/10.1002/2013JD019983

Tao, S., Tan, Y., Zhu, B., Ma, M., Lu, W., 2009. Fine-resolution simulation of cloud-to-ground lightning and thundercloud charge transfer. Atmos. Res. 91, 360–370. https://doi.org/10.1016/j.atmosres.2008.05.012

Tessendorf, S.A., 2009. Characteristics of lightning in supercells, in: Betz, H.D., Schumann, U., Laroche, P. (Eds.), Lightning: Principles, Instruments and Applications: Review of Modern Lightning Research. Springer Netherlands, Dordrecht, pp. 83–114. https://doi.org/10.1007/978-1-4020-9079-0_4

Tessendorf, S.A., Rutledge, S.A., Wiens, K.C., 2007. Radar and lightning observations of normal and inverted polarity multicellular storms from STEPS. Mon. Weather Rev. 135, 3682–3706. https://doi.org/10.1175/2007MWR1954.1

Thomas, R.J., Krehbiel, P.R., Hamlin, T., Harlin, J., Shown, D., 2001. Observations of VHF source powers radiated by lightning. Geophys. Res. Lett. 28, 143–146. https://doi.org/10.1029/2000GL011464

Thomas, R.J., Krehbiel, P.R., Rison, W., Hunyady, S.J., Winn, W.P., Hamlin, T., Harlin, J., 2004. Accuracy of the lightning mapping array. J. Geophys. Res. D Atmos. 109. https://doi.org/10.1029/2004JD004549

Tomine, K., Michimoto, K., Abe, S., 1986. studies on thunderstorm in winter in the area surrounding

Komatsu by radar. Tenki 33, 445–452.

Tovar, C., Aranguren, D., López, J., Inampués, J., Torres, H., 2014. Lightning risk assessment and thunderstorm warning systems. 2014 Int. Conf. Light. Prot. ICLP 2014 1870–1874. https://doi.org/10.1109/ICLP.2014.6973434

Tran, M.D., Rakov, V.A., 2015. When does the lightning attachment process actually begin? J. Geophys. Res. 120, 6922–6936. https://doi.org/10.1002/2015JD023155

Ushio, T., Heckman, S.J., Boccippio, D.J., Christian, H.J., Kawasaki, Z.I., 2001. A survey of thunderstorm flash rates compared to cloud top height using TRMM satellite data. J. Geophys. Res. Atmos. 106, 24089–24095. https://doi.org/10.1029/2001JD900233

Van Der Velde, O.A., Montanyà, J., 2013. Asymmetries in bidirectional leader development of lightning flashes. J. Geophys. Res. Atmos. 118, 13,504-13,519. https://doi.org/10.1002/2013JD020257

van der Velde, O.A., Montanyà, J., Romero, D., Pineda, N., Rico, R., Fabró, F., Solà, G., March, V., Soula, S., 2011. Results of the 2010-2011 lightning measurements campaigns in Spain, in: 6th European Conference on Severe Storms, Palma de Mallorca, Spain, 3-7 October 2011.

Van Der Velde, O.A., Montanyà, J., Soula, S., Pineda, N., Mlynarczyk, J., 2014. Bidirectional leader development in sprite-producing positive cloud-to-ground flashes: Origins and characteristics of positive and negative leaders. J. Geophys. Res. Atmos. 119, 12,755-12,779. https://doi.org/10.1002/2013JD021291

Vincent, B., Carey, L., Schneider, D., Keeter, K., Gonski, R., 2003. Using WSR-88D reflectivity data for the prediction of cloud-to-ground lightning: a North Carolina study. Natl. Weather Dig. 27.

Visacro, S., Guimaraes, M., Murta Vale, M.H., 2017. Striking Distance Determined From High-Speed Videos and Measured Currents in Negative Cloud-to-Ground Lightning. J. Geophys. Res. Atmos. 122, 13,356-13,369. https://doi.org/10.1002/2017JD027354

Wallace, J.M., Hobbs, P. V., 2006. Atmospheric Science: An Introductory Survey, 2nd Editio. ed. Academic Press.

Wang, C., Zheng, D., Zhang, Y., Liu, L., 2017. Relationship between lightning activity and vertical airflow characteristics in thunderstorms. Atmos. Res. 191, 12–19. https://doi.org/10.1016/j.atmosres.2017.03.003

Wang, D., Takagi, N., 2012. Characteristics of winter lightning that occurred on a windmill and its lightning protection tower in Japan. IEEJ Trans. Power Energy 132, 568–572. https://doi.org/10.1541/ieejpes.132.568

Wang, D., Takagi, N., Gamerota, W.R., Uman, M.A., Hill, J.D., Jordan, D.M., 2013. Initiation processes of return strokes in rocket-triggered lightning. J. Geophys. Res. Atmos. 118, 9880–9888. https://doi.org/10.1002/jgrd.50766

Wang, D., Takagi, N., Watanabe, T., Sakurano, H., Hashimoto, M., 2008. Observed characteristics of upward leaders that are initiated from a windmill and its lightning protection tower. Geophys. Res. Lett. 35. https://doi.org/10.1029/2007GL032136

Wang, D., Wu, T., Takagi, N., 2018. Charge structure of winter thunderstorm in Japan: A review and an update. IEEJ Trans. Power Energy 138, 310–314.

https://doi.org/10.1541/ieejpes.138.310

Wang, F., Zhang, Y., Liu, H., Yao, W., Meng, Q., 2016. Characteristics of cloud-to-ground lightning strikes in the stratiform regions of mesoscale convective systems. Atmos. Res. 178–179, 207–216. https://doi.org/10.1016/j.atmosres.2016.03.021

Wang, H., Guo, F., Zhao, T., Qin, M., Zhang, L., 2016. A numerical study of the positive cloud-to-ground flash from the forward flank of normal polarity thunderstorm. Atmos. Res. 169, 183–190. https://doi.org/10.1016/j.atmosres.2015.10.011

Warner, T.A., Cummer, S.A., Lyons, W.A., Lang, T.J., Orville, R.E., 2011. Coordinated video and RF measurements of positive CGs inducing both sprites and upward tower discharges, in: Paper Presented at 5th Conference on Meteorological Applications of Lightning Data, Am. Meteor. Soc., Seattle, Wash.

Warner, T.A., Cummins, K.L., Orville, R.E., 2012. Upward lightning observations from towers in Rapid City, South Dakota and comparison with National Lightning Detection Network data, 2004-2010. J. Geophys. Res. Atmos. 117. https://doi.org/10.1029/2012JD018346

Warner, T.A., Helsdon, J.H., Bunkers, M.J., Saba, M.M.F., Orville, R.E., 2013. Uplights: Upward lightning triggering study. Bull. Am. Meteorol. Soc. 94, 631–635. https://doi.org/10.1175/BAMS-D-11-00252.1

Warner, T.A., Lang, T.J., Lyons, W.A., 2014. Synoptic scale outbreak of self-initiated upward lightning (SIUL) from tall structures during the central U.S. blizzard of 1–2 February 2011. J. Geophys. Res. 119, 9530–9548. https://doi.org/10.1002/2014JD021691

Weiss, S.A., Macgorman, D.R., Calhoun, K.M., 2012. Lightning in the anvils of supercell thunderstorms. Mon. Weather Rev. 140, 2064–2079. https://doi.org/10.1175/MWR-D-11-00312.1

Wiens, K.C., Rutledge, S.A., Tessendorf, S.A., 2005. The 29 June 2000 supercell observed during STEPS. Part II: Lightning and charge structure. J. Atmos. Sci. 62, 4151–4177. https://doi.org/10.1175/JAS3615.1

Wilcox, L.J., Hoskins, B.J., Shine, K.P., 2012. A global blended tropopause based on ERA data. Part I: Climatology. Q. J. R. Meteorol. Soc. 138, 561–575. https://doi.org/10.1002/qj.951

Williams, E., 2018. Lightning activity in winter storms: A meteorological and cloud microphysical perspective. IEEJ Trans. Power Energy 138, 364–373. https://doi.org/10.1541/ieejpes.138.364

Williams, E., Mushtak, V., Rosenfeld, D., Goodman, S., Boccippio, D., 2005. Thermodynamic conditions favorable to superlative thunderstorm updraft, mixed phase microphysics and lightning flash rate. Atmos. Res. 76, 288–306. https://doi.org/10.1016/j.atmosres.2004.11.009

Williams, E.R., 2001. The Electrification of Severe Storms, in: Doswell, C.A. (Ed.), Severe Convective Storms. American Meteorological Society, Boston, MA, pp. 527–561. https://doi.org/10.1007/978-1-935704-06-5_13

Williams, E.R., 1989. The tripole structure of thunderstorms. J. Geophys. Res. 94, 13151–13167. https://doi.org/10.1029/jd094id11p13151

Williams, E.R., 1985. Large-Scale Charge Separation in Thunderclouds. J. Geophys. Res. 90, 6013–6025. https://doi.org/10.1029/jd090id04p06013

Williams, E.R., Cooke, C.M., Wright, K.A., 1985. Electrical discharge propagation in and around

space charge clouds. J. Geophys. Res. 90, 6059–6070. https://doi.org/10.1029/JD090iD04p06059

Williams, E.R., Weber, M.E., Orville, R.E., 1989. The relationship between lightning type and convective state of thunderclouds. J. Geophys. Res. 94, 13213–13220. https://doi.org/10.1029/jd094id11p13213

Williams, E.R., Zhang, R., Rydock, J., 1991. Mixed-phase microphysics and cloud electrification. J. Atmos. Sci. 48, 2195–2203. https://doi.org/10.1175/1520-0469(1991)048<2195:MPMACE>2.0.CO;2

Workman, E.J., Reynolds, S.E., 1949. Electrical activity as related to thunderstorm cell growth. Bull. Am. Meteorol. Soc. 30, 142–144.

World Meteorological Organization, 2011. Manual on Codes - International Codes, Volume I.1, Annex II to the WMO Technical Regulations: part A-Alphanumeric Codes, WMO Publ. 306.

Wu, T., Yoshida, S., Akiyama, Y., Stock, M., Ushio, T., Kawasaki, Z., 2015. Preliminary breakdown of intracloud lightning: Initiation altitude, propagation speed, pulse train characteristics, and step length estimation. J. Geophys. Res. 120, 9071–9086. https://doi.org/10.1002/2015JD023546

Yair, Y., Levin, Z., Altaratz, O., 1998. Lightning phenomenology in the Tel Aviv area from 1989 to 1996. J. Geophys. Res. Atmos. 103, 9015–9025. https://doi.org/10.1029/98JD00087

Yamamoto, K., Noda, T., Yokoyama, S., Ametani, A., 2009. Experimental and analytical studies of lightning overvoltages in wind turbine generator systems. Electr. Power Syst. Res. 79, 436–442. https://doi.org/10.1016/j.epsr.2008.09.002

Yang, Y.H., King, P., 2010. Investigating the potential of using radar Echo reflectivity to nowcast cloud-to-ground lightning initiation over southern Ontario. Weather Forecast. 25, 1235–1248. https://doi.org/10.1175/2010WAF2222387.1

Yasuda, Y., Yokoyama, S., Minowa, M., Satoh, T., 2012. Classification of lightning damage to wind turbine blades. IEEJ Trans. Electr. Electron. Eng. 7, 559–566. https://doi.org/10.1002/tee.21773

Yeung, L.H.Y., Lai, E.S.T., Chiu, S.K.S., 2007. Lightning Initiation and Intensity Nowcasting Based on Isothermal Radar Reflectivity-A Conceptual Model. 33rd Int. Conf. Radar Meteorol. 6–10.

Yokoyama, S., 2013. Lightning protection of wind turbine blades. Electr. Power Syst. Res. 94, 3–9. https://doi.org/10.1016/j.epsr.2012.07.017

Yokoyama, S., Hermoso, B., Cooray, V., D'Alessandro, F., Diendorfer, G., Duquerroy, P., Engmann, G., Erichsen, H., Galvan, A., Gockenbach, E., Havelka, M., Ishii, M., Kanashiro, A., Hernández, Y., Montanya, J., Paolone, M., Rachidi, F., Rousseau, A., Sekioka, S., Yasuda, Y., 2014. Lightning Protection of Wind Turbine blades.

Yoshida, S., Morimoto, T., Ushio, T., Kawasaki, Z.I., 2009. A fifth-power relationship for lightning activity from Tropical Rainfall Measuring Mission satellite observations. J. Geophys. Res. Atmos. 114. https://doi.org/10.1029/2008JD010370

Yuan, S., Jiang, R., Qie, X., Wang, D., Sun, Z., Liu, M., 2017. Characteristics of Upward Lightning on the Beijing 325 m Meteorology Tower and Corresponding Thunderstorm Conditions. J. Geophys. Res. Atmos. 122, 12,093-12,105. https://doi.org/10.1002/2017JD027198

Yuter, S.E., Houze, R.A., 1995. Three-Dimensional Kinematic and Microphysical Evolution of Florida Cumulonimbus. Part II: Frequency Distributions of Vertical Velocity, Reflectivity, and Differential Reflectivity. Mon. Weather Rev. 123, 1941–1963. https://doi.org/10.1175/1520-0493(1995)123<1941:tdkame>2.0.co;2

Zhang, Y., Zhang, W., Meng, Q., 2012. Lightning casualties and damages in China from 1997 to 2010. 2012 31st Int. Conf. Light. Prot. ICLP 2012. https://doi.org/10.1109/ICLP.2012.6344207

Zhang, Z., Zheng, D., Zhang, Y., Lu, G., 2017. Spatial–temporal characteristics of lightning flash size in a supercell storm. Atmos. Res. 197, 201–210. https://doi.org/10.1016/j.atmosres.2017.06.029

Zheng, D., Zhang, Y., Meng, Q., 2018. Properties of Negative Initial Leaders and Lightning Flash Size in a Cluster of Supercells. J. Geophys. Res. Atmos. 123, 12,857-12,876. https://doi.org/10.1029/2018JD028824

Zhou, H., Diendorfer, G., Thottappillil, R., Pichler, H., Mair, M., 2012a. Measured current and close electric field changes associated with the initiation of upward lightning from a tall tower. J. Geophys. Res. Atmos. 117. https://doi.org/10.1029/2011JD017269

Zhou, H., Diendorfer, G., Thottappillil, R., Pichler, H., Mair, M., 2012b. Characteristics of upward positive lightning flashes initiated from the Gaisberg Tower. J. Geophys. Res. Atmos. 117. https://doi.org/10.1029/2011JD016903

Zhou, H., Theethayi, N., Diendorfer, G., Thottappillil, R., Rakov, V.A., 2010. On estimation of the effective height of towers on mountaintops in lightning incidence studies. J. Electrostat. 68, 415–418. https://doi.org/10.1016/j.elstat.2010.05.014

Zhou, Y., Qie, X., Soula, S., 2002. A study of the relationship between cloud-to-ground lightning and precipitation in the convective weather system in China. Ann. Geophys. 20, 107–113. https://doi.org/10.5194/angeo-20-107-2002

Zipser, E.J., Lutz, K.R., 1994. The vertical profile of radar reflectivity of convective cells: a strong indicator of storm intensity and lightning probability? Mon. Weather Rev. 122, 1751–1759. https://doi.org/10.1175/1520-0493(1994)122<1751:TVPORR>2.0.CO;2

Apéndice

5 Otras contribuciones

En esta sección se listan los artículos, así como las participaciones en congresos científicos, tanto en forma de póster como de presentación oral, con contenido derivado y/o relacionado con el trabajo realizado durante mi periodo doctoral. Estos se presentan de forma cronológica. Los artículos que no forman parte del compendio presentan un resumen para facilitar una evaluación de su contenido. En las participaciones en congreso se destacan un resumen de su contenido de especial interés, de forma que contribuyan al contenido y contexto de esta tesis.

5.1 Artículos

- Pineda, N., Montanyà, J, **Salvador, A.**, van der Velde, O., López, J. A., 2018. Thunderstorm characteristics favouring downward and upward lightning to wind turbines. *Atmospheric Research*, 214, 46-63. doi: 10.1016/j.atmosres.2018.07.012.
- López, J. A., Montanyà, J., van der Velde, O., Pineda, N., **Salvador, A.**, Romero, D., Aranguren, D., Taborda, J., 2019. Charge Structure of Two Tropical Thunderstorms in Colombia. Journal of *Geophysical Research: Atmospheres*, 124, 5503– 5515. doi: 10.1029/2018JD029188.

Abstract:

Charge structure derived from lightning leader development of tropical thunderstorms comprising equatorial latitudes of less than ±10° has not been investigated yet. In this work, using a lightning mapping array installed in northern Colombia, the charge structure, lightning leader initiations, and the cloud-to-ground strokes rates of two thunderstorms have been analyzed. Additionally, radar information is also included. The identification of the charge regions has been obtained by analyzing the propagation of lightning leader developments. Flashes initiate between 4 and 15 km altitude. High initiation rates are different in the two storms. In one case the high rates are found between 8 and 13 km. In the other case, the initiation heights are found between 10 and 15 km. The storms show typical tripolar charge structure where the upper positive charge is present at 10 to ~15 km, the midlevel negative charge is found between 6 and 9 km, and the lower positive charge between 4 and 6 km altitude. Intracloud lightning flashes with inverted polarity have been identified for short period. In other periods, screening layer flashes have been detected at 14–15 km. The overall results show that the charge structures in the two Colombian storms are similar to the structures reported in North Central Florida, but with the significant difference that the flash initiation altitudes are 2 km higher in Colombia. The vertical configuration of the charge regions and the leader development of these thunderstorms may help explain the occurrence of terrestrial gamma-ray flashes in tropical thunderstorms.

Resumen:

Este artículo analiza la estructura eléctrica de las tormentas en Colombia con datos de un sistema LMA instalado en la zona. A partir de la detección de los inicios de cada rayo se infirió las regiones de carga neutra entre las distintas regiones de carga de polaridad opuesta entre ellas. A partir de la potencia de señal de las distintas descargas se deduce la polaridad de las distintas regiones de carga. Este proceso se realizó a lo largo de toda la tormenta para establecer la estructura eléctrica en cada momento de su ciclo de vida. A su vez, se comparó con otros parámetros meteorológicos como las alturas máximas de niveles de reflectividad, así como las intensidades de descargas nube-tierra, tanto positivas como negativas, la ratio de descargas de LMA y la altura de la tropopausa. El trabajo realizado durante este artículo fue clave para el desarrollo del segundo artículo del compendio de esta tesis, en el que se analizaron las estructuras eléctricas de las tormentas de múltiples episodios de interés.

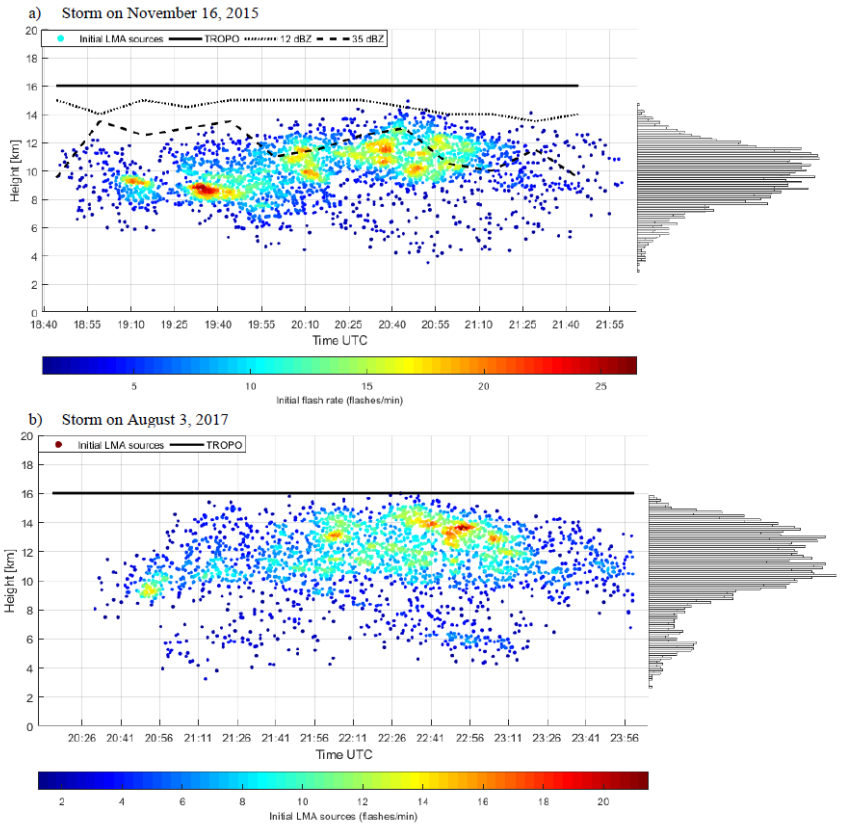

Spatial and temporal density of the lightning flash initiation. The histograms on the right show the frequency distribution of the initiation heights. TOP-12 dBZ (dotted line), TOP-35 dBZ (dashed line), Tropopause altitude (solid line). For the 16 November 2015 case, the height of the tropopause was deduced from the closest radiosonde. In the case of August 3, 2017, the height of the tropopause was determined from reanalysis.

- **Salvador, A.**, Pineda, N., Montanyà, J., Solà, G., 2020. Seasonal variations on the conditions required for the lightning production. *Atmospheric Research*, 243: 104981. doi: 10.1016/j.atmosres.2020.104981.
- **Salvador, A.**, Pineda, N., Montanyà, J., López, J. A., Solà, G., 2021. Thunderstorm charge structures favouring cloud-to-ground lightning. *Atmospheric Research*, 105577. doi: 10.1016/j.atmosres.2021.105577.

5.2 Participaciones en congresos

- Montanyà, J., van der Velde, O., Domingo-Dalmau, A., Pineda, N., Argemí, O., **Salvador, A.**, 2016. Lightning mapping observations of downward lightning flashes to wind turbines. *33rd International Conference on Lightning Protection (ICLP), Estoril, Portugal*, pp. 1-6. doi: 10.1109/ICLP.2016.7791449.

Abstract:

Negative downward leaders that produced lightning strokes to wind turbines are identified by means of the Lightning Mapping Array data of the Ebro Valley Laboratory (NE Spain). Four cases are analyzed together with weather radar imagery. All flashes hitting wind turbines were originated in small convective cells with moderate development. Notwithstanding the moderate convection, all cases occurred under what can be called "out of season conditions", where the ''charging zone'' is located closer to the ground and may favour downward leaders to tall structures. Cloud charge structures showed negative region from 3 km to more than 5 km with a low positive charge below (not always detectable).

Resumen:

Con la motivación de detectar características comunes en episodios de tormentas en que algunas turbinas eólicas han sufrido daños de descargas eléctricas, se analizan las imágenes del radar meteorológico, así como las descargas detectadas por el LMA. Este estudio permitió observar que en la zona de estudio cerca del delta del Ebro la mayoría de descargas a este tipo de infraestructuras ocurren en periodos más fríos, cuando hay un número de descargas muy pequeño respecto al total anual, con situaciones en que las regiones de carga de la nube de tormenta están situadas más cerca de la superficie, lo cual favorece la descarga hacia infraestructuras elevadas. Durante estos episodios, además, las tormentas no presentaban gran capacidad convectiva, siendo la mayoría con un nivel convectivo moderado, con niveles de reflectividad de 35 dBZ que difícilmente alcanzaban los 7 km.

a)

b)

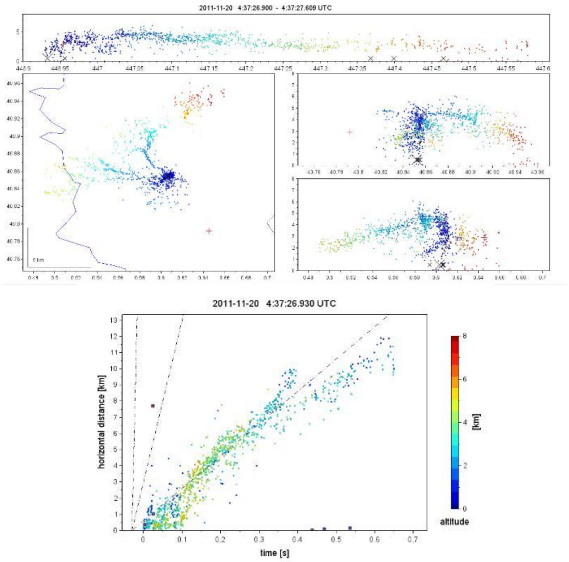

LMA views of the detected sources. Upper graph corresponds to height vs. time and under it the top (LAT vs. LON) and side views (LAT and LON vs. height). Lower graph corresponds to time vs. distance from the beginning of the lightning

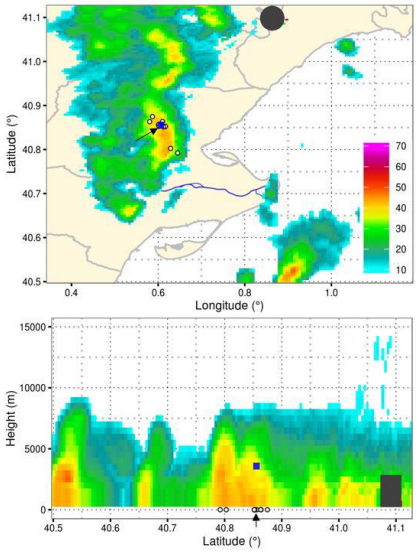

Maximum radar reflectivity (in dBZ) plot. The blue square corresponds to the LMA initial point (intracloud breakdown). White dots are the CG LINET strokes. Arrow points to the wind turbines. In grey, the radar location.

- Montanyà, J., van der Velde, O., March, V., **Salvador, A.**, Pineda, N., 2016. Lightning threats to wind turbines. *XXII Jornades de Meteorologia Eduard Fontseré*, p. 1. https://static-m.meteo.cat/wordpressweb/wp-content/uploads/2017/09/21085220/MONTANYA_WIND_v1.pdf

Abstract:

Under thunderstorm conditions, man-made structures that are much higher than their surroundings (100 m or more) are exposed to strong local electric fields and are prone to initiate upward lightning leaders. Multi-megawatt wind turbines are a particular sort of such tall structures as the rotating blades encompass almost 40% of the total turbine height. Moreover, the extensive presence of composite materials on the blades (such as glass fiber and carbonreinforced plastics) combined with the high exposure to lightning attachments can end in severe damage, even in a collapse of the blades after a lightning protection failure. In fact, lightning threats to wind turbines are present all year-round. During the warm season, when the majority of lightning occurs at mid-latitudes, wind turbines have a higher probability of being struck by normal negative cloudto-ground lightning than their surroundings. During the cold season, despite the rather low lightning activity, low cloudbase thunderstorms present favorable conditions for the initiation of upward lightning flashes from tall structures such as wind turbines. Recent research reported that these off-season storms can produce very energetic lightning events and a large amount of damage. Nowadays the wind energy industry is migrating toward the installation of offshore windfarms, where winter lightning damage on turbines may be enhanced. Therefore, it has become even more necessary to gain deeper in-sight into the understanding of the initiation and development of lightning flashes triggered by complex rotating structures. In this presentation we summarize the recent activity of the Lightning Research Group from the Technical University of Catalonia regarding lightning threats to wind turbines.

Resumen:

La presentación muestra un estado del arte de las posibles afectaciones que las descargas eléctricas atmosféricas pueden causar a infraestructuras elevadas, con un especial enfoque hacia los aerogeneradores. Para ello, presenta los resultados de distintos estudios realizados por el *Lightning Research Group* de la Universidad Politècnica de Catalunya, en que se muestran análisis de rayos producidos por las mismas turbinas eólicas, así como las originadas en la misma nube de tormenta y con impacto final en estas infraestructuras. A partir de la motivación causada por la observación de que la mayoría de este tipo de descargas se detectan en periodos fríos, se presentan también mapas de impactos de rayos y de días de tormenta, con enfoque en todo el mundo, para resaltar la principal afectación de esta problemática en regiones extratropicales. Finalmente se presentan los estándares de protección de los aerogeneradores frente al rayo, destacando las características propias de la zona de instalación, así como de las características intrínsecas de los aerogeneradores que influyen en la exposición frente al rayo de este tipo de infraestructuras.

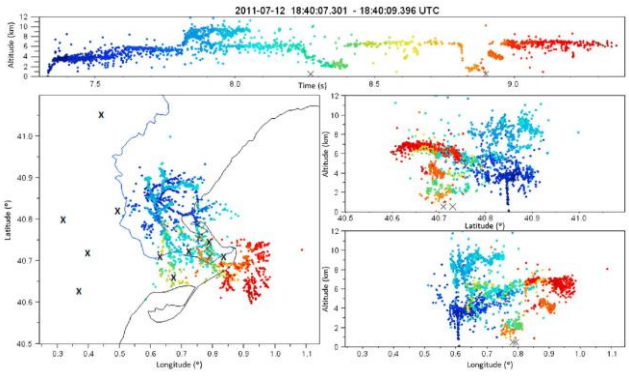

LMA sources of an upward flash originated on a wind turbine and terminating at ground. Cross symbols indicate ground strokes, crosses (bold) in the plan view correspond to the locations of the ELMA stations ground-to-cloud-to-ground flash

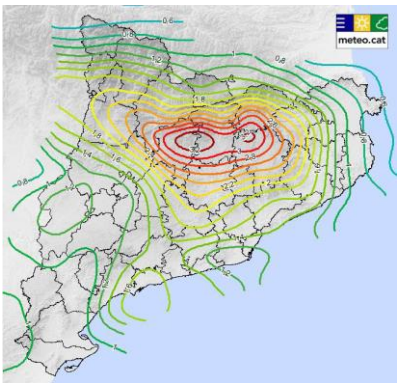

Lightning flash density [Ng] (CG flash km-2 year-1)

- **Salvador, A.**, Montanyà, J., Pineda, N., Solà, G., van der Velde, O., 2017. Potential of the lightning mapping array for the nowcasting of severe weather. *2nd European Nowcasting Conference (ENC), Offenbach am Main, Alemania*, pp. 7-8.

Abstract:

The electrical activity within a convective cell is related to the strength of its updraft, and thus, to its potential severity. The trends in the lightning activity may help to diagnose the severe weather potential of a thunderstorm. Observational evidence suggests that the trends of the intracloud fraction of the total lightning activity may be a more robust indicator, compared to some characteristics of the cloud-to-ground fraction (e.g., positive polarity dominance). The present study takes advantage of the three-dimensional lightning mapping system (Lightning Mapping Array, LMA) to analyze severe weather episodes occurred in Catalonia (NE Iberian Peninsula). The main objective is to investigate the potential of the LMA to detect trends that can be useful as nowcast predictors (e.g., trends in the total flash rate, changes in the height of the charge layers, polarity reversal). Complementary data includes radar reflectivity to detect convective cores, temperature profiles from NWP and complementary LINET lightning data.

Resumen:

A partir del análisis de un episodio de tiempo adverso con precipitación en forma sólida en Catalunya, en esta presentación se presentaron algunos resultados en la detección de patrones utilizando los datos del LMA, como por ejemplo un incremento súbito del número de descargas detectadas, así como la determinación de la estructura eléctrica de la tormenta. Se identificaron las alturas de las isotermas de 0°C, −10°C, −40°C y la tropopausa a partir del radiosondeo más próximo, y se compararon resultados con el sistema LINET instalado en la zona, con especial interés de las ratios de descargas y las alturas de los IC detectados.

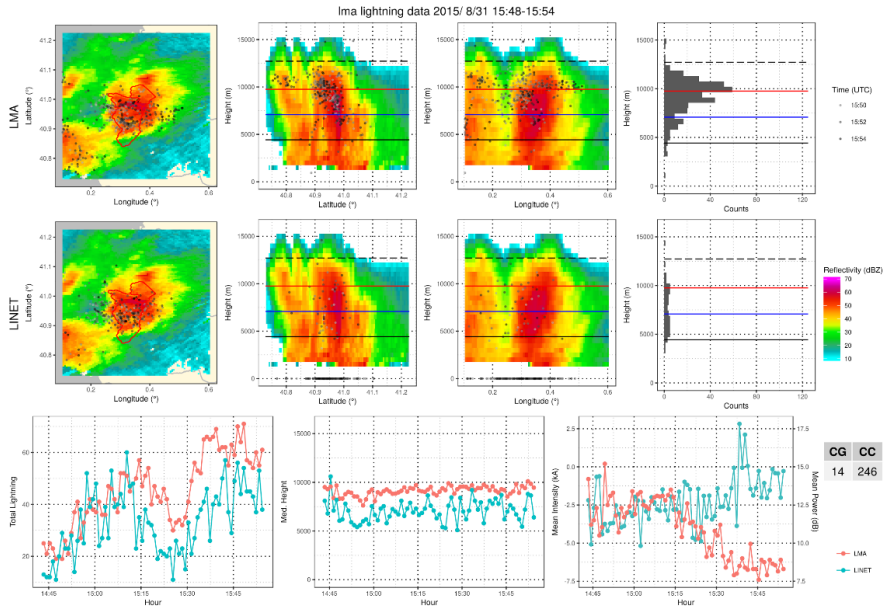

Representación de la comparativa de una tormenta seguida por el sistema LMA y LINET. Las dos filas superiores muestran un instante de la tormenta, con representaciones (de izquierda a derecha) en LAT vs. LON, LAT vs. altitud, LON vs. Altitud y un histograma de alturas de las señales de (arriba) LMA y (medio) LINET. En la fila inferior se representa la evolución del (de izquierda a derecha) número total de rayos, altura de estos y picos de corriente y potencia de los dos sistemas de detección.

- Montanyà, J., **Salvador, A.**, van der Velde, O., Pineda, N., Fabró, F., Williams, E., López, J. A., 2017. Winter, moderate and deep convection thunderstorms in northeastern Spain: Favorable conditions for the triggering of upward lightning from wind turbines. *4th International Symposium on Winter Lightning (ISWL), Joetsu, Japón*, pp. 1-5.

Abstract:

This study presents electrical characteristics of thunderstorms occurring in the cold season inferred by the Lightning Mapping Array and meteorological radar in northeastern Spain. Examples of the conditions of upward lightning associated with wind turbines are provided. We found that storms fulfilling the assumed criteria of winter thunderstorms present very low CG activity, low electrical active cores (< 4 km) and low cloud tops (12 dBZ @ < 6 km). Those storms that present slightly warmer temperatures at 700 hPa show much more vertical development. The data support the view that upward discharges can be triggered under a lowered negative charged region and absent lower positive region, a situation which occurs during the cool season with advection of cold air of maritime arctic origins from the north.

Resumen:

En la presentación se enseñaron más evidencias sobre las características propias de las tormentas de invierno que causan rayos ascendentes de los aerogeneradores, con actividad de CG muy baja, así como alturas bajas de las regiones de carga más activas (< 4 km) y las alturas de las tormentas, no superiores a los 6 km. Además, este tipo de rayos son favorecidos mayormente por una región de carga negativa baja en altura, y con una región de carga positiva inferior ausente, típicamente durante los mencionados meses más fríos. Se mostraron distintas fotografías de estructuras elevadas en zonas de especial afectación, así como algunos ejemplos añadidos de rayos ascendentes.

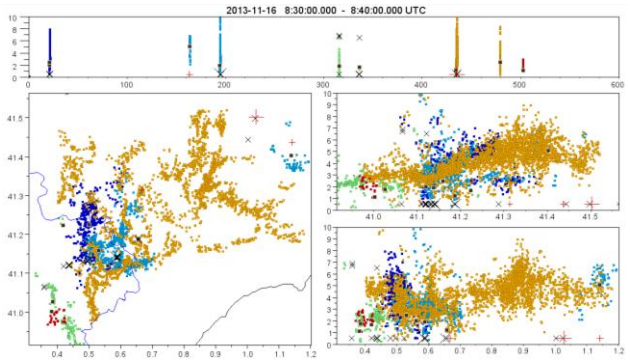

Ten minutes of LMA sources where it can be seen a few lightning in the area (2013/11/16).

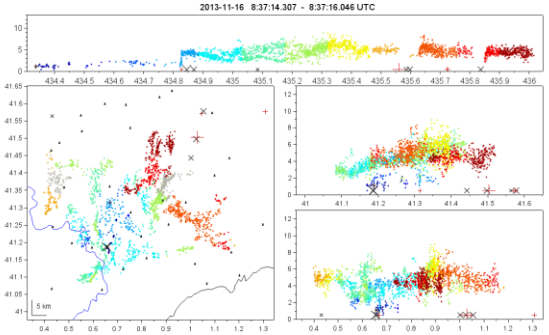

Upward flash initiated by a wind turbine on 2013/11/16

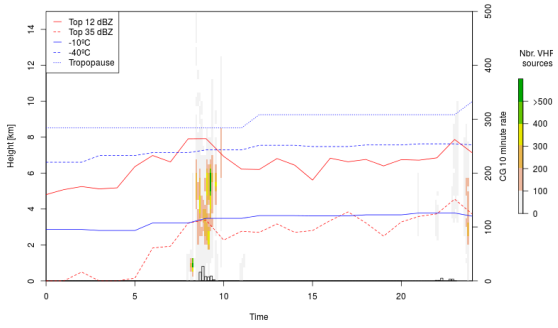

LMA sources, isotherms and radar reflectivity for the 2013/11/16.

- **Salvador, A.**, Pineda, N., Montanyà, J., van der Velde, O., 2017. Exploring thunderstorm patterns related to severe weather with Lightning Mapping Array data. *9th European Conference on Severe Storms (ECSS), Pula, Croacia.* https://meetingorganizer.copernicus.org/ECSS2017/ECSS2017-108.pdf

Abstract:

It is well-known that the use of lightning data, mixed with radar observations, is a useful indicator on the short-term forecasting of severe weather. The electrical activity is highly related to the strength of the updraft of the storms, and a detailed analysis of the behaviour of lightning throughout the storm life-cycle can reveal some patterns linked to the severe weather hazard. In this study, we take advantage of the large capabilities of the Lightning Mapping Array to analyze some classical patterns related to severity (e.g., IC/CG rate, positive anomalies, lightning jump). Furthermore, we analyzed also some less-known patterns (e.g., lightning holes, lightning bubbles) as well as changes in mean peak current, electric charge layer mean altitude, structures with inverted polarity, etc.; all in all, seeking to establish which patterns can be good predictors of severe weather phenomena. The data used in this study comes form the first Lightning Mapping Array system deployed in Europe, installed in the Ebro's River Delta in Catalonia (NE Iberian Peninsula). Complementary data includes lightning from LINET, as well as weather data from the Meteorological Service of Catalonia.

Resumen:

El objetivo de esta presentación se enfocó en detectar patrones en las señales del LMA para la detección de episodios de tiempo severo. A partir de unos episodios de interés con precipitación en forma sólida, se detectaron algunos patrones como el *lightning jump* (aumento súbito del número de descargas), un descenso generalizado de las alturas, así como un *lightning hole* (región de una tormenta donde, debido a un muy intenso corriente ascendente, las condiciones no son favorables para la separación de cargas y se produce un "agujero" de detección de señales). Patrones a partir de la detección radar como los *bow-echo* también han sido detectados en algunos episodios.

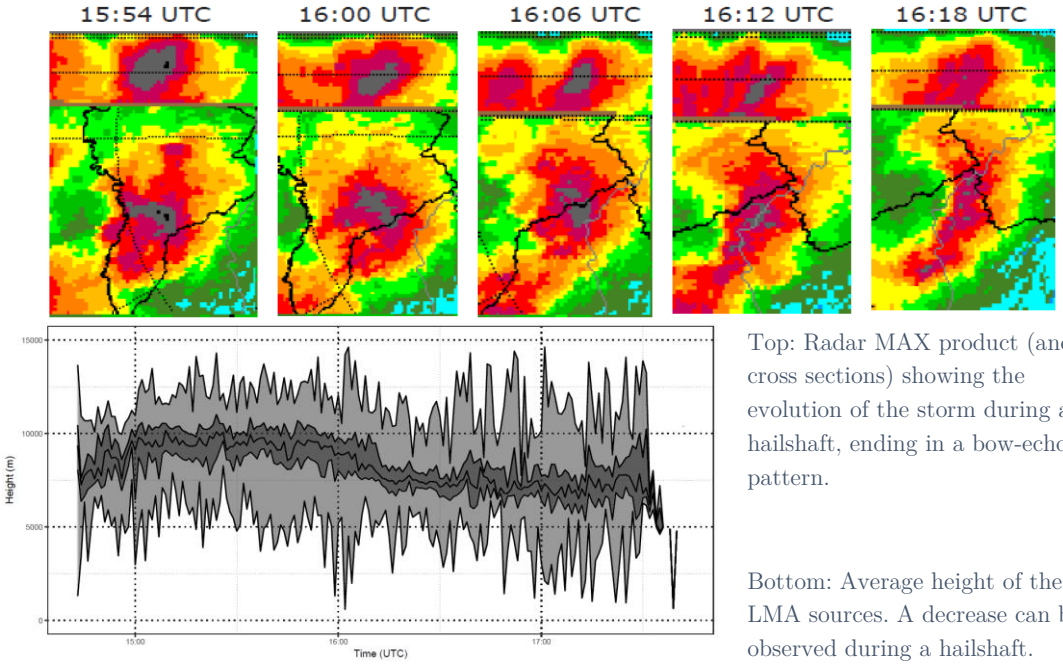

Top: Radar MAX product (and cross sections) showing the evolution of the storm during a hailshaft, ending in a bow-echo pattern.

Bottom: Average height of the LMA sources. A decrease can be observed during a hailshaft.

- **Salvador, A.**, Pineda, N., Montanyà, J., Solà, G., van der Velde, O., 2018. Thunderstorm patterns that may be useful to warn about lightning threats to wind turbines and other tall structures. *XVI International Conference on Atmospheric Electricity (ICAE), Nara, Japón.*

Abstract:

Lightning activity in convective storms is highly related to the strength of its updraft. Thus, the characterization of the vertical electrical structure of the storm and its evolution throughout its life cycle can be useful to infer the phase of the storm and its potential to become severe. Patterns related to changes in the lightning intensity like the lightning jump are known to be effective in the warning of imminent severe weather, but other patterns like inverted charge layers are more difficult to infer from conventional lightning location systems (LLS). Three-dimensional lightning mapping systems, such as the Lightning Mapping Array (LMA), are able to detect the fine structure of the in-cloud lightning channels. Moreover, they allow inferring the vertical structure of the charge layers, as the located sources are mainly coming from negative leaders moving through regions of positively charged cloud particles, and typically weaker sources from positive leader move inside the negative charge region. Monitoring the heights and trends of the charge layer structure may be useful to warn about potential threats, not only sev ere weather but also lightning damage to tall structures like wind turbines in low base charge layer thunderstorms. These tall structures are known to be very sensitive to the interaction with lightning, for downward and also upward discharges. These occur throughout the year, paying particular attention to winter lightning due the low altitude of the cloud charge structure, making possible that wind turbines can self initiate lightning flashes. In the analysis of such a lightning threat, to complement LMA data, weather radar data and vertical temperature profiles from radiosonde have been taken into account. Accordingly, this study presents some LMA derived patterns that may be indicative of lightning threats to tall structures such as wind turbines. Likewise, information from the LINET LLS, widely deployed around the world, is used to make comparisons with the LMA system to detect similar patterns, so these patterns information could be extrapolated to other areas of interest.

Resumen:

Esta presentación presentaba los primeros resultados encontrados entre las alturas de las descargas detectadas por el LMA, en que se inició a inferir su estructura a partir de las alturas con más concentración de inicios de descarga, con un especial enfoque hacia las situaciones de LPCR. Además, se planteó la potencialidad de la utilización de las alturas de las descargas en altura detectadas con la red de detección LINET para la determinación de esta estructura. Se introdujeron datos de evolución del número de descargas nube-tierra detectadas, identificando por separado las de polaridad positiva y negativa, indicando los instantes en que los primeros dominaban sobre los segundos, con posibles situaciones de inversión de polaridad de la tormenta. También se analizaron episodios en qué se habían detectado incrementos súbitos de ratios de descargas, llamados *lightning jumps*, indicador de potencial tiempo adverso.

Se analizaron unos episodios de especial interés, como aquellos en los que en la zona de estudio habían sido detectados fenómenos adversos de precipitación en forma de granizo, así como de descargas en aerogeneradores. Para los primeros, se detectó que se habían detectado situaciones de granizo bajo condiciones de estructura eléctrica inversa, así como descenso en altura de las regiones de carga, así como una situación sostenida de inversión de polaridad. Para el episodio de descargas

a aerogeneradores, se habían detectado las regiones de carga a muy baja actitud, por debajo de los 5 km, propiciando la descarga hacia las palas de distintos aerogeneradores, propiciando la motivación a analizar estos casos para el interés de las industrias eólicas.

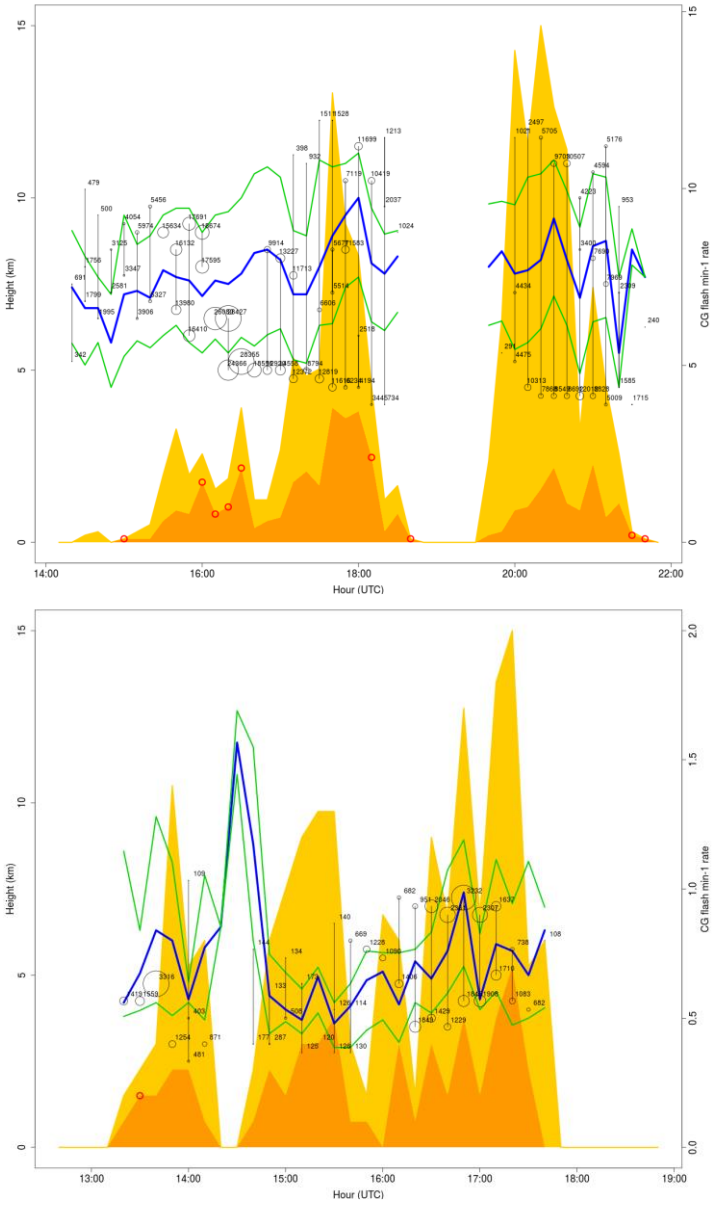

Evolutions of the vertical structure of the thunderstorms occurring in the area of study for different days. Time–height LMA is represented through the centers of positive charge (upper and lower). The vertical line indicates the distance between the two positive charge centers; the numbers at each end correspond to the number of sources. The amount of sources is also represented by a circle, the radius is indicative of the number of sources. LINET CG flash rate is represented on the background with two colored areas, the total CG flash rate in yellow, the positive CG fraction in orange. Positive anomalies (+CG > -CG) are highlighted with a red circle. The green-blue-green lines indicate the p25-p50-p75 altitudes of LINET IC.

Top: 2015/08/31

- Hail episode
- Inverted electrical structure
- Dominant LPCR
- Positive anomaly

Bottom: 2016/09/14

- Downward to wind turbine
- Charge centers at low altitude

- Pineda, N., Altube, P., Rigo, T., Farnell, C., Montanyà, J., van der Velde, O., **Salvador, A.**, Bech, J., Rodríguez, O., 2019. Severe weather patterns of a tornadic event associated to a squall line in the western Mediterranean region. *10th European Conference on Severe Storms, Cracovia, Polonia.* European Severe Storms Laboratory. https://meetingorganizer.copernicus.org/ECSS2019/ECSS2019-114.pdf

Abstract:

In this study, an attempt is made to identify severe weather patterns that may be useful for the recognition of tornados embedded in mesoscale convective systems or squall lines. Weak tornados are frequent in southern Europe and near the Mediterranean coastal regions in particular, mostly during late summer and early autumn. In particular, the analysis focuses on a storm occurred on the 18 October 2017 that affected the city of Valls (Catalonia), causing several injuries and damaging hundreds of trees, traffic signal and lamp posts. A field damage survey indicated a 6 km linear path with EF1 estimated damage. The tornado was associated to a squall line, which formed perpendicular to the coast and moved from SW to NE, crossing all Catalonia. The region of study is in the area of coverage of one of the two Lightning Mapping Array (LMA) currently operating in Europe, which provides detailed 3D mapping of the cloud lightning channels. Besides, the Lightning Location System of the Meteorological Service of Catalonia (SMC) provided IC and CG lightning data. The study also benefits from the network of C-band Doppler weather radars operated by the SMC. Regarding the case study, the "lightning jump" algorithm of the SMC provided a warning of severe weather for the squall line with a lead time of 20 min. Preliminary results on the LMA data analysis show a "lightning hole", a lightning-free region immediately above the tornado track.

Resumen:

A partir de un episodio de especial interés en que se detectó un tornado en la ciudad de Valls (Tarragona), se evaluó la posibilidad de identificar este proceso de tiempo adverso con el sistema de detección de rayos LMA localizado en el delta del Ebro. Debido a la gran concentración de observaciones de tornados en la zona, existe un gran interés en poder detectar patrones que puedan anticipar este evento. Después de un análisis de las condiciones meteorológicas previas al suceso con información de radiosondeo, reanálisis y de radar, y posterior evaluación de los daños causados, se motivó la introducción de los sistemas de detección de rayos en la observación del suceso. Tras un cálculo de la sensibilidad del sistema LMA en la región de estudio, se analizaron las señales detectadas para detectar posibles patrones que indicaran tiempo severo. Entre ellos, se destacan algunos de estos indicadores, como situaciones de *lightning jump*, con un aumento súbito del número de descargas minutos previos al suceso, así como la detección de actividad eléctrica continua durante todo el periodo de tiempo adverso.

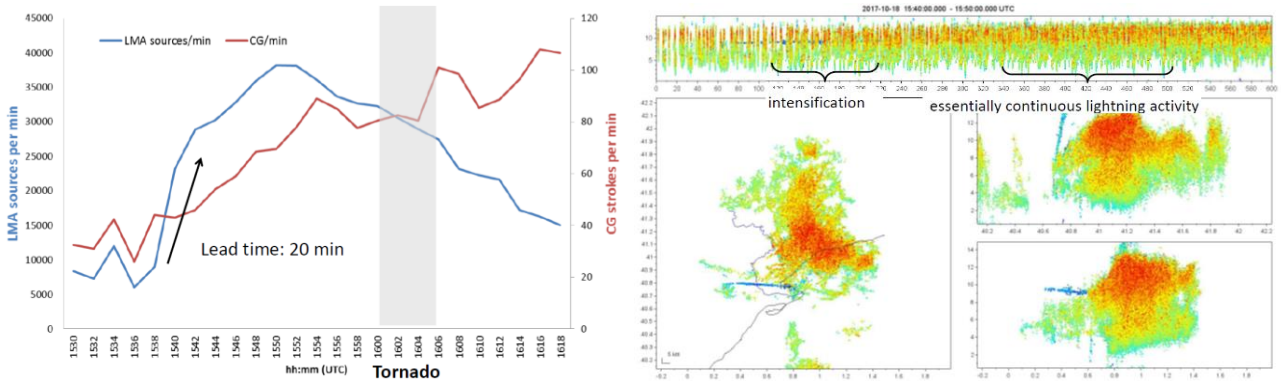

Left: Detection of a Lightning Jump event 20 minutes before tornado detection. Right: 10 minutes of LMA sources evolution. Continuous lightning activity can be seen during the tornado event.

6 Contribuciones durante el Doctorado Industrial

6.1 Presentación

Este doctorado forma parte del Programa de Doctorats Industrials (PDI), gestionado por la Agència de Gestió d'Ajuts Universitaris i de Recerca (AGAUR) de la Generalitat de Catalunya. Dentro del proyecto, la motivación intrínseca de transferencia de tecnologías y, del mismo modo, de los conocimientos hacia un entorno productivo refuerza los vínculos entre el mundo universitario e investigación con el mundo empresarial. Así, la colaboración añadida con MINECO y del Fondo Europeo del Desarrollo Regional (FEDER) ha permitido disponer de herramientas de investigación como el LMA durante la realización de la tesis doctoral, lo cual ha sido de inestimable ayuda para la evolución de los estudios realizados.

Este factor determinante ha contribuido a que parte de mi formación durante el doctorado se haya realizado dentro de un entorno empresarial, el cual ha permitido aplicarle una visión distinta al contenido de los estudios realizados, realizando aplicaciones orientadas a los intereses del mercado y de la industria, entre otros.

Dicho esto, no quisiera finalizar esta tesis sin describir algunos de los proyectos que se han llevado a cabo durante este proyecto que quedan ligeramente fuera del contenido propio de la tesis aquí presentada, pero dan valor añadido a los estudios que se han ido realizando en paralelo a estos, y su contenido ha permitido transmitir datos, información y, sobre todo, formación, entre las distintas facetas de este doctorado industrial.

6.2 Organismos y empresas colaboradoras

En el doctorado industrial han participado distintos organismos, los cuales han aportado sus conocimientos y herramientas a sus respectivos entornos académicos y empresariales. Desde el entorno de formación universitaria el principal organismo ha sido la UPC, dentro del grupo LRG del Departament d'Enginyeria Elèctrica. Por otro lado, el SMC ha participado de forma muy estrecha y activa en el entorno de la formación universitaria, visto especialmente como un elemento clave en la investigación del contenido de esta tesis, además de proporcionar muchos de los datos de los sistemas de detección, destacando los de teledetección como la información de rayos del XDDE, el radar de la XRAD y el radiosondeo de Barcelona, sin la cual esté doctorado no se habría podido llevar a cabo.

Dejando de lado el punto de vista universitario y pasando al entorno empresarial, distintas empresas han participado de forma colaborativa en este proyecto para proporcionar el enfoque de sus necesidades activas de mejora, así como de los requerimientos en cuanto a proporcionar información y valor al cliente final.

La empresa Fulgura S.L., localizada en Terrassa (Barcelona), es una empresa *spin-off* de la UPC con experiencia en el sector del rayo, tanto desde el punto de vista de la prevención, como protección e investigación. Entre sus funciones, se ofrecen servicios especializados para compañías eléctricas, eólicas y servicios meteorológicos, entre otros. Juntamente con la empresa Dena Desarrollos S.L., bajo la marca comercial INGESCO, se han desarrollado distintos aplicativos que han sido utilizados de forma operativa, los cuales la información del rayo ha sido siempre protagonista.

Por último, la empresa *nowcast GmbH*, con localización en Múnich (Alemania), ha sido también parte integrante de este doctorado industrial. Fundada en el año 2002, esta empresa decidió crearse a partir de la investigación del Prof. Dr. Hans-Dieter Betz en la Universidad de Múnich, de la cual se derivó la red de detección de rayos LINET. Esta ha sido muy utilizada durante todo el doctorado industrial gracias a su amplia distribución a lo largo de Europa, destacando también sus zonas de estudio a lo largo del mundo, como por ejemplo Sudamérica, Asia, África y Australia, entre otros.

6.3 Actividades realizadas

La colaboración entre las distintas empresas ha sido estrecha a lo largo del periodo en que se ha realizado el doctorado industrial. Muchas de las actividades aquí descritas han sido fruto de la actividad y frecuente colaboración entre Fulgura S.L. e INGESCO, las cuales han ocupado gran parte del tiempo dentro del ámbito empresarial.

Entre estas actividades, desde el punto de vista de colaboración entre Fulgura S.L. e INGESCO se destacan las siguientes:

- Sincronización en tiempo real de la base de datos de rayos provenientes de la red de detección de rayos LINET con la base de datos locales de INGESCO, a partir del convenio de colaboración con *nowcast GmbH*, y su posterior mantenimiento.
- Elaboración de un estudio de mercado con los distintos sistemas de detección de descargas eléctricas, detección de tormentas y de tiempo adverso, las herramientas disponibles para su visualización, y de las compañías que subministran estos sistemas y herramientas. Igualmente, se destacan algunas empresas dedicadas al sector y se realiza un perfil del cliente objetivo.
- Programación desarrollada para la realización de mapas en tiempo real con las descargas de rayos detectadas por la red LINET en toda la península ibérica, las islas Baleares, y sus inmediaciones. Actualmente se puede consultar en directo en la página web de INGESCO (https://www.ingesco.com/es/mapa-rayos-tiempo-real). Un ejemplo de estos mapas se puede encontrar en la Figura 18.

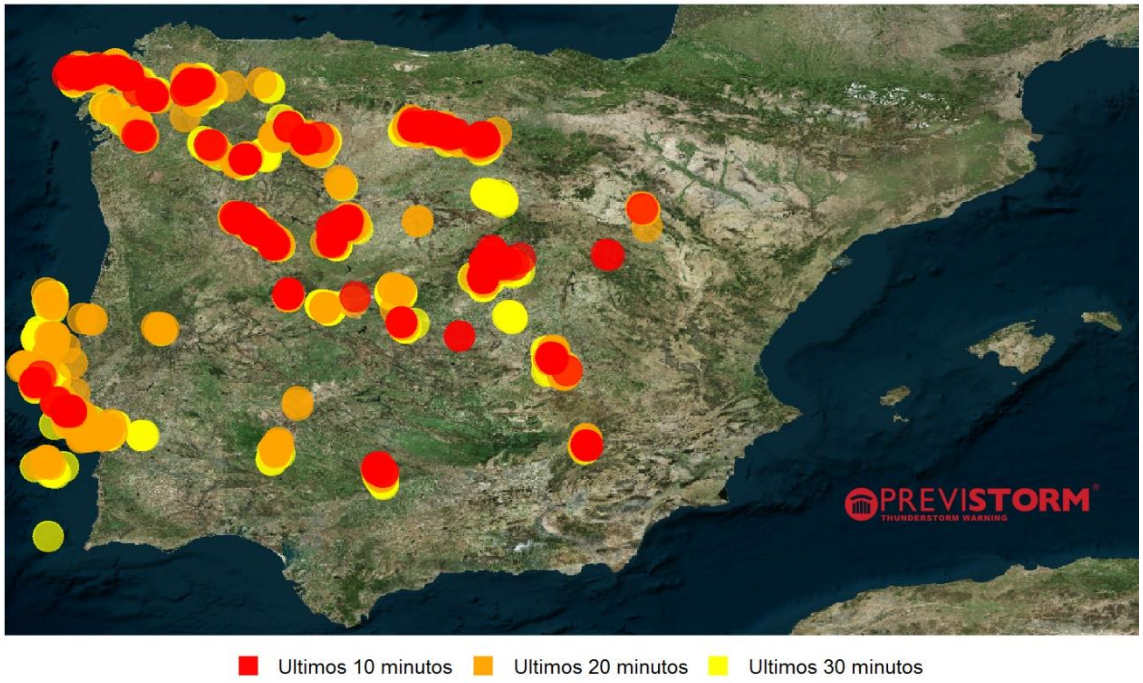

Figura 18. Representación de un mapa con las zonas de la península ibérica, con una escala de colores, afectadas por actividad de rayos por tramos de 10 minutos. Para más consultas, visitar la página web de INGESCO (https://www.ingesco.com/es/mapa-rayos-tiempo-real).

- Creación de un sistema de alarmas mediante correo electrónico. Bajo una base de datos de clientes en que se proporcionaba una dirección electrónica y las coordenadas de interés para emitir avisos, y a partir de la actualización en tiempo real de la base de datos de LINET, se emitieron corres electrónicos informativos de cercanía de tormentas a las zonas potencialmente afectadas. Además, se creó una interfaz web para analizar el número de avisos que se le hacían llegar a cada cliente, entre otros parámetros.
- Realización de cálculos de datos de impactos de rayos en una línea eléctrica para la elaboración de un informe posterior con análisis histórico para posterior distribución al cliente.
- Elaboración de webs de consultas históricas de actividad de rayos con la base de datos de LINET. A falta de una herramienta que fuera de fácil acceso, se creó una interfaz web para realizar consultas de descargas de rayos a petición del técnico, introduciendo información básica como la fecha, las coordenadas, y el radio de afectación a analizar. Posteriormente, evolucionó con la implementación de nuevas características, como archivos exportables con los metadatos de los rayos, y elaboración automática de informes con la información de interés y mapas con indicaciones de las zonas afectadas, entre otros.
- Informes meteorológicos para distintos periodos de estudio, analizando las situaciones de temperatura, precipitaciones, humedad e intensidad y dirección del viento en una zona de interés a petición de un cliente.

- Publicación en tiempo real en el perfil de Twitter de INGESCO de la actividad de rayos de la península ibérica detectados por la red de descargas LINET, separándola en cinco zonas de análisis, y proporcionando información cuantitativa y representación gráfica de la actividad eléctrica de la zona. En el momento de escribir estas líneas se pueden observar actualizaciones en el perfil de Twitter indicado (https://twitter.com/INGESCO).

De manera regular a lo largo del doctorado se han realizado visitas a las instalaciones de *nowcast GmbH* en Múnich, y una última visita a las instalaciones de Ubimet, Viena. En ellas se han ido realizando actualizaciones del trabajo realizado, así como distintos informes sobre las características del sistema de detección LINET, así como sus puntos débiles y de mejora. Seguidamente se listan las actividades registradas más destacadas:

- Realización de informe de evaluación de la red LINET instalada en el País Vasco y gestionado por Euskalmet. Se realizaron ejemplos de detección de episodios de interés, así como de análisis de distintos parámetros. Finalmente, de simularon unos mapas de eficiencia de detección en la zona.
- Análisis comparativo entre la red LINET y LMA en la zona cercana al delta del Ebro. Se evaluaban las señales detectadas por la red LINET intentando establecer parejas con las señales de LMA, detectando puntos comunes y discrepancias en la salida de las soluciones de ambos sistemas.
- Estudio de las señales CG de LINET para mejorar el algoritmo que determina la solución de la señal recibida. El objetivo reside en la mejora de la discriminación entre las descargas CG e IC. Para ello se detectaron unos patrones y situaciones recurrentes, circunstancia que provocó una nueva propuesta en el enfoque para mejorar la salida de estas señales.
- Evaluación de las señales detectadas por el sistema LINET en la zona de Alemania. Se realizaron análisis de distribución de amplitudes de carga y alturas máximas detectadas a lo largo del territorio, comparativos con la orografía y a las posiciones de los detectores. Resolución de problemas en la detección de amplitud de carga en Australia debido a ciertas discrepancias en el análisis de la zona de estudio.